Steel Braces with Intentional Eccentricity (BIEs) – Application and Seismic Performance

by

ANDRÉS GONZÁLEZ UREÑA

Department of Civil Engineering

McGill University

Montréal, Québec, Canada

July 2021

A thesis submitted to McGill University in partial fulfillment of the requirements of the degree of

Doctor of Philosophy

Dedication:

To Julia, whose love, company, and support made this adventure achievable

ABSTRACT

Concentrically Braced Frames (CBFs) with Hollow Structural Sections (HSSs) as the bracing members are one of the most popular structural steel Seismic Force Resisting Systems (SFRSs), widely used in mid- and low-rise buildings. However, they present significant shortcomings that pose limits to their potential. These are related primarily to their invariably high elastic stiffness, to their minimal post-yielding stiffness, to the susceptibility of HSS braces to local buckling and consequent low cycle fatigue induced fracture, and to the overstrength that results from the observance of the design code limits on the local and global slenderness.

Braces with Intentional Eccentricity (BIEs), otherwise traditional braces with their longitudinal axis offset with respect to the forces' line of action, have been proposed by Skalomenos et al. to overcome these limitations of CBFs. As they are subject to bending moment accompanying the axial force, both under tension and compression loading, BIEs are naturally more flexible than traditional concentric braces. In tension, they present a high post-yielding stiffness. In compression, their response is not affected by a marked loss of strength due to overall buckling; further, the more even distribution of strain demands along the length of the brace member delays the onset of local buckling. Moreover, the strength and stiffness of BIEs can be regulated by adjusting the eccentricity, granting the designer better control over the structure's dynamic response, and reducing the overstrength. Skalomenos et al. performed tests on round HSS BIEs, which demonstrated a response to loading consistent with the above described behaviour; however, neither the application of BIEs to buildings nor their implementation in a global design approach were addressed.

In this thesis, the seismic performance of square HSS BIEs and their application as the energy dissipating elements of SFRSs is addressed. It includes the characterization, through numerical models and the physical testing of full-scale specimens, of their response to cyclic and monotonic load, and the development of a displacement-based seismic design procedure for Frames with Intentionally Eccentric Braces (FIEBs) that accounts for the particularities of BIEs and modern code philosophy. This procedure is used in the design of hypothetical multi-storey buildings, allowing for the assessment of their seismic performance by means of Non-Linear Response-History Analysis (NLRHA), and a comparison with that of traditional CBFs. In the design of the FIEBs, and in the numerical models and physical tests, a simple and cost-effective plate assembly was considered for the introduction of the eccentricity.

The results show that square HSS BIEs exhibit the benefits of the intentional eccentricity as described above, and that the seismic performance of FIEBs designed with the proposed procedure is satisfactory and on par with the objectives of modern design codes. What is more, FIEBs presented lower maximum and residual storey drifts than CBFs and required less material in many cases. As such, FIEBs may constitute an advantageous alternative to traditional CBFs as the SFRS of buildings in regions of high seismic hazard. However, the results from physical testing shed light on the vulnerability of the bracing member's ends to premature fracturing under some conditions, limiting the deformation capacity of BIEs in certain cases, a topic that will need to be addressed in further research.

RÉSUMÉ

Les cadres à contreventements concentriques (CCC) avec des profilés tubulaires HSS pour diagonales sont l'un des Systèmes de Reprise des Charges Latérales (SRCL) en acier les plus populaires, amplement utilisés dans des bâtiments de faible et moyenne hauteur. Cependant, ils possèdent des faiblesses qui posent limite à leur potentiel. Celles-ci sont issues principalement de leur rigidité élastique invariablement haute, de leur rigidité post-plastification presque nulle, de la susceptibilité des profilés HSS au voilement local et à la fracture par fatigue à bas cyclage qui en suit, et de la sur-résistance qui découle du respect des limites imposées par les normes de conception à l'élancement des diagonales et de ses parois.

Les Diagonales à Excentricité Intentionnelle (DEI), des diagonales par ailleurs ordinaires dont l'axe longitudinal est décalé par rapport à la ligne d'action des charges, ont été proposées par Skalomenos et al. comme alternative aux diagonales concentriques conventionnelles (DCC) capable de surmonter les limitations de celles-ci. Par l'effet de l'excentricité, à l'effort axial se joint l'effort de flexion. Ainsi, les DEI sont d'emblée plus flexibles que les DCC. De plus, en traction, elles bénéficient d'une rigidité post-plastification considérable et, en compression, leur réponse flexionnelle n'est pas marquée par une perte significative de résistance due au flambement global et la distribution plus uniforme des demandes en déformation au long de la membrure entraîne un retard de l'apparition du voilement local. En outre, la résistance et la rigidité des DEI peuvent être réglées en modifiant l'excentricité, ce qui concède au concepteur un meilleur contrôle sur la réponse dynamique de la structure et réduit la sur-résistance involontaire. Skalomenos et al. ont effectué sur des spécimens de DEI fabriquées avec un HSS de section ronde des essais dont les résultats sont en accord avec le comportement décrit plus haut. Cependant, ni l'application des

DEI à des bâtiments, ni leur implémentation dans une approche globale de conception n'ont été abordées.

La performance des DEI à membrure HSS de section carrée et leur emploi comme éléments dissipateurs de SRCL sont abordés dans cette thèse. Ce travail inclut la description, basée sur d'analyses numériques et sur d'essais sur des spécimens grandeur nature, de la réponse de ces DEI sous chargements monotoniques et cycliques et la mise au point d'une méthode basée sur les déplacements pour la conception parasismique de Cadres Contreventés à Diagonales Intentionnellement Excentrées (CCDIE) prenant compte des spécificités des DEI et des exigences des normes de conception modernes. Cette méthode est ensuite appliquée à la conception de CCDIE hypothétiques à plusieurs étages, permettant ainsi la comparaison de leur performance avec celle de CCC traditionnels au moyen d'analyses dynamiques non linéaires (NLRHA). Dans la conception des CCDIE et pour les analyses numériques et essais expérimentaux, un assemblage de plaques d'acier économique et simple à fabriquer a été employé pour introduire l'excentricité.

Les résultats montrent que les DEI à membrure HSS carrée bénéficient des avantages liés à l'excentricité intentionnelle tels que décrits ici, et que la performance des CCDIE aux charges sismiques est convenable et en accord avec les objectifs des normes de conception modernes. De plus, les CCDIE ont présenté des rapports de déplacement inter-étages maximaux et résiduels plus bas que ceux des CCC, tout en requérant d'une moindre quantité de matériel. Ainsi, les CCDIE pourraient représenter une alternative avantageuse aux CCC pour le SRCL de bâtiments dans des zones à fort aléa sismique. Cependant, les essais sur des DEI ont dévoilé un point faible aux extrémités de la membrure HSS qui, sous certaines conditions, peuvent se fracturer prématurément, réduisant la capacité de déformation de la diagonale et soulevant le besoin de plus de recherche à son sujet.

ACKNOWLEDGMENTS

I would like to extend my deepest gratitude to Professor Colin Rogers for his outstanding patience and generosity, and for his constant guidance and support over these years. I am also immensely grateful to Professor Robert Tremblay for proposing such an exciting research program, and for obligingly and constructively sharing his knowledge and experience throughout.

I would also like to acknowledge Constructions Proco and Atlas Tube, whose generous contribution made the laboratory testing program possible. Equally appreciated is the kind collaboration from the technicians and engineers at Polytechnique Montréal's Structures Laboratory, and from the many graduate and undergraduate research assistants from McGill University and Polytechnique Montréal who participated in the study. I also thank DPHV Structural Consultants and ADF Group Inc. for their generous technical and financial support, as well as the Natural Sciences and Engineering Research Council of Canada (NSERC), the Fonds de Recherche du Québec – Nature et Technologies (FRQ-NT), and the Centre d'Études Interuniversitare des Structures sous Charges Extrêmes (CEISCE).

Finally, I express my appreciation to the Universidad de Costa Rica (UCR) for financing my doctoral studies, and in particular to the staff at the Oficina de Asuntos Internacionales y Cooperación Externa (OAICE) and at the Escuela de Ingeniería Civil (EIC) for their steady backing and assistance.

PREFACE

This thesis is presented in a manuscript-based format in accordance with the Thesis Guidelines from Graduate and Postdoctoral Studies, McGill University. It comprises two journal and two conference paper manuscripts, in addition to the chapters corresponding to the Introduction and Conclusions. The contributions of the authors to the herein included manuscripts are as follows.

Chapter 2:

A. González Ureña, R. Tremblay, and C. A. Rogers, "Earthquake-resistant design of steel frames with intentionally eccentric braces," *Journal of Constructional Steel Research,* vol. 178, p. 106483, 2021/03/01/ 2021, doi: https://doi.org/10.1016/j.jcsr.2020.106483.

- A. González Ureña developed the proposed design procedure, conducted the numerical analyses, analyzed the resulting data and wrote the manuscript.
- R. Tremblay assisted in developing of the design procedure and the selection and scaling of ground motion records, and edited the manuscript.
- C. A. Rogers supervised the research and edited the manuscript.

Chapter 3:

A. González Ureña, R. Tremblay, and C. A. Rogers, "Numerical investigation of the seismic response of square HSS Braces with Intentional Eccentricity," presented at the 17th World Conference on Earthquake Engineering, Sendai, Japan, 2020, C000832.

- A. González Ureña conducted the numerical analyses, analyzed the resulting data and wrote the manuscript.
- R. Tremblay and C. A. Rogers supervised the research and edited the manuscript.

Chapter 4:

A. González Ureña, R. Tremblay, and C. A. Rogers, "Design and performance of Frames with Intentionally Eccentric Braces " presented at the 17th World Conference on Earthquake Engineering, Sendai, Japan, 2020, C000830.

- A. González Ureña developed the proposed design procedure, conducted the numerical analyses, analyzed the resulting data, and wrote the manuscript.
- R. Tremblay provided the selected scaled ground motion records and edited the manuscript.
- C. A. Rogers assisted in the development of the design procedure, supervised the research, and edited the manuscript.

Chapter 5:

A. González Ureña, R. Tremblay, and C. A. Rogers, "Experimental and Numerical Study of Square HSS BIEs under Cyclic Loading," Submitted to *Engineering Structures*.

- A. González Ureña designed the test specimens, conducted the laboratory tests and numerical analyses, and wrote the manuscript.
- R. Tremblay coordinated the fabrication of the test specimens and the allocation of the laboratory's human and material resources, assisted in the design of the experimental program, supervised the research, and edited the manuscript.
- C. A. Rogers assisted in the design of the test specimens and experimental program, and in the test specimen fabrication coordination, supervised the research, and edited the manuscript.

The main distinct original contributions to knowledge contained in this thesis are the following:

- Investigation of the response to monotonic and cyclic loading of square HSS Braces with Intentional Eccentricity
- Design of a cost effective and practical plate assembly for the introduction of the eccentricity in rectangular HSS Braces with Intentional Eccentricity
- Development of a mathematical formula to predict the fracture life of square HSS Braces with Intentional Eccentricity
- Development of a procedure for the seismic design of Frames with Intentionally Eccentric Braces
- Design of multi-storey Frames with Intentionally Eccentric Braces and evaluation of their seismic performance and cost, in comparison to that of traditional concentrically braced frames
- Experimental evaluation of the performance of full-scale ASTM A1085 square HSS Brace with Intentional Eccentricity specimens subjected to cyclic loading

TABLE OF CONTENTS

LIST OF FIGURES

LIST OF TABLES

CHAPTER 1: INTRODUCTION

1.1. BACKGROUND

Concentrically Braced Frames (CBFs) are one of the most widely used structural steel Seismic-Force-Resisting Systems (SFRSs) in low- and mid-rise buildings in regions with high seismic hazard. Their popularity, besides being due to their relative cost-effectiveness, benefited from the shortcomings of moment frames that events such as the 1994 Northridge and 1995 Kobe earthquakes evidenced [1-3]. Hollow Structural Sections (HSSs) are frequently selected for the bracing members in CBFs, owing to their efficiency in compression, the relative simplicity of the detailing of their connections to the braced bent, and their aesthetic appeal.

In essence, CBFs are vertically oriented cantilevered trusses in which the diagonal bracing members provide the lateral strength and stiffness. The global lateral loads are thus carried to the ground by the braces as tensile and compressive axial forces. As illustrated in Figure 1.1, under seismic action the braces alternate between yielding in tension and buckling in compression. Although the yielding of braces in tension provides most of the energy dissipation and ductility, substantial energy dissipation can also be provided by their inelastic buckling and subsequent straightening, depending on their slenderness [4, 5]. The energy dissipation capacity of CBFs allows that their braces be designed for storey shears lower than those that would occur were the system intended to respond elastically. However, this exploit requires that the braces be able to develop sufficient ductility under cyclic loading, and that the non-dissipating components of the SFRS, namely the connections, beams, columns, and foundations, be designed so that they withstand, relatively undamaged, the probable demands arising from the inelastic response of the

braces. This design approach, to which adhere the seismic design provisions of most modern design codes, is known as Capacity-Based Design.

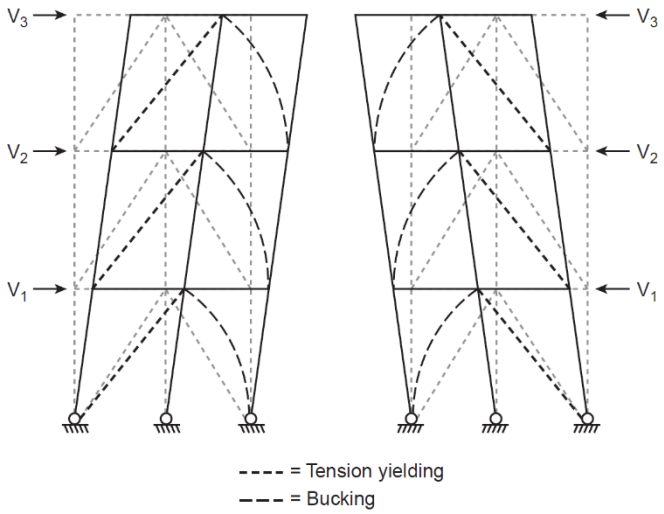

Figure 1.1: Schematic of CBF inelastic behaviour (from [6])

Notwithstanding their advantages, CBFs present significant shortcomings that pose limits to their potential. To begin with, due to their inherently high elastic stiffness, the natural period of vibration of CBFs tends to be very short and typically lies within the plateau of the design acceleration spectra, resulting in high seismic design forces for the bracing members. Combined with the compression strength governing the dimensioning of the bracing members, this derives in the need of specifying relatively heavy sections for those and, consequentially, in high capacity-based design forces for the non-dissipating elements of the SFRS and its foundations, which translate into a considerable portion of the final cost of the structure.

A particular drawback of HSS concentric braces, is that they are especially susceptible to low-cycle fatigue failure following the onset of local buckling in the mid-length plastic hinge region that develops in compression. Photographs showing the typical progression of this failure mode are presented in Figure 1.2. Once local buckling in compression manifests under cyclic loading, fracture is likely to occur in a subsequent tension excursion. Thus, seismic design provisions, such

as the CSA S16-14 [7], impose stringent limits to the local and global slenderness of HSS braces with the intent of reducing the probability of local buckling developing under the effects of the anticipated seismic demands, so that the system may offer sufficient ductility and energy dissipation. The limits proscribe the use of overly stocky braces and locally slender sections, as it has been found in research that these exhibit the most limited fracture life [4, 5, 8, 9].

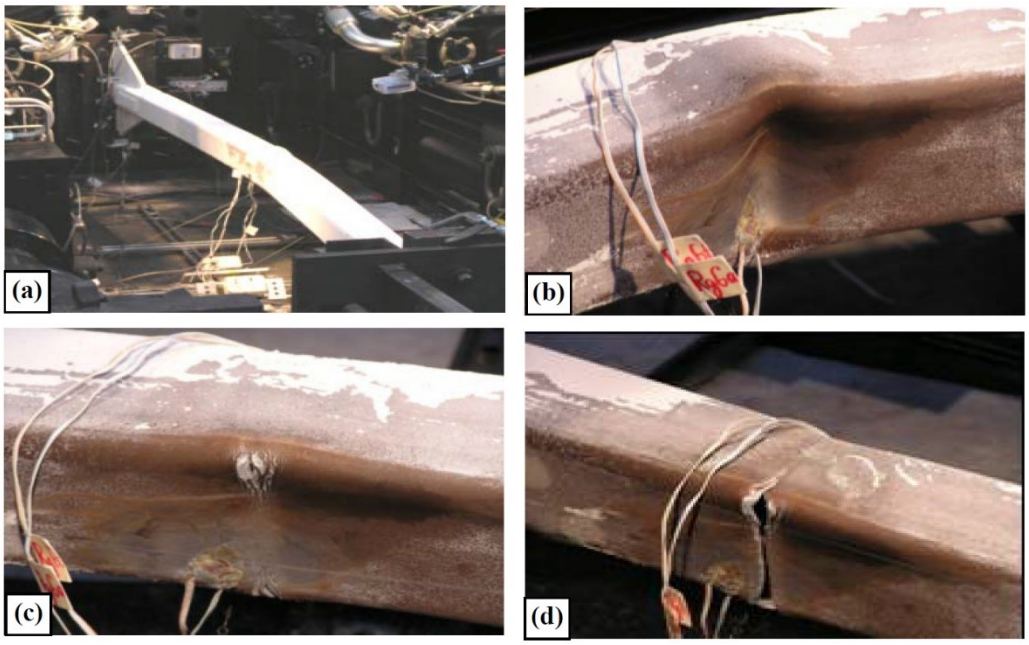

Figure 1.2: Typical progression of brace specimen damage (a) Global buckling, (b) Local buckling, (c) Fracture initiation and (d) Loss of tensile strength (from [1])

Observing these limits, however, reduces the array of allowable HSSs that one could select in designing a CBF. This may produce additional overstrength, because the final sections for the bracing members of particular storeys might possess significantly higher strength than that required to satisfy the seismic demands on them. Further, this may result in the concentration of the displacement demands in storeys with lower strength to capacity ratios [10].

Moreover, the intentional energy dissipation mechanism of CBFs implies that when a storey engages in inelastic action, its stiffness reduces to a minimum, as the brace in tension yields while the brace in compression is buckled. This can entail large displacement demands and possibly

compromise the stability of the structure by triggering a soft-storey mechanism [11]. To reduce the probability of soft-storey mechanisms, the design codes specify lower ductility-related force modification factors for CBFs than for other systems such as moment frames, limit their maximum height, and require special detailing for the columns in braced bents. These factors further contribute to limiting the cost-effectiveness of CBFs and their range of applications in regions of high seismic hazard.

Skalomenos et al. [12, 13] proposed a variation of traditional concentric braces that would offer an improved seismic performance and potentially overcome their shortcomings listed above. The Brace with Intentional Eccentricity (BIE), is a brace member whose axis is offset with respect to the line of action of the forces acting through it. An overview of the proposed brace, as presented by Skalomenos et al. [13], is reproduced in Figure 1.3. Because of the eccentricity, the brace is subjected to flexure in addition to the axial load, which modifies fundamentally its response and produces an initial stiffness lower than that of a concentrically loaded brace of the same section.

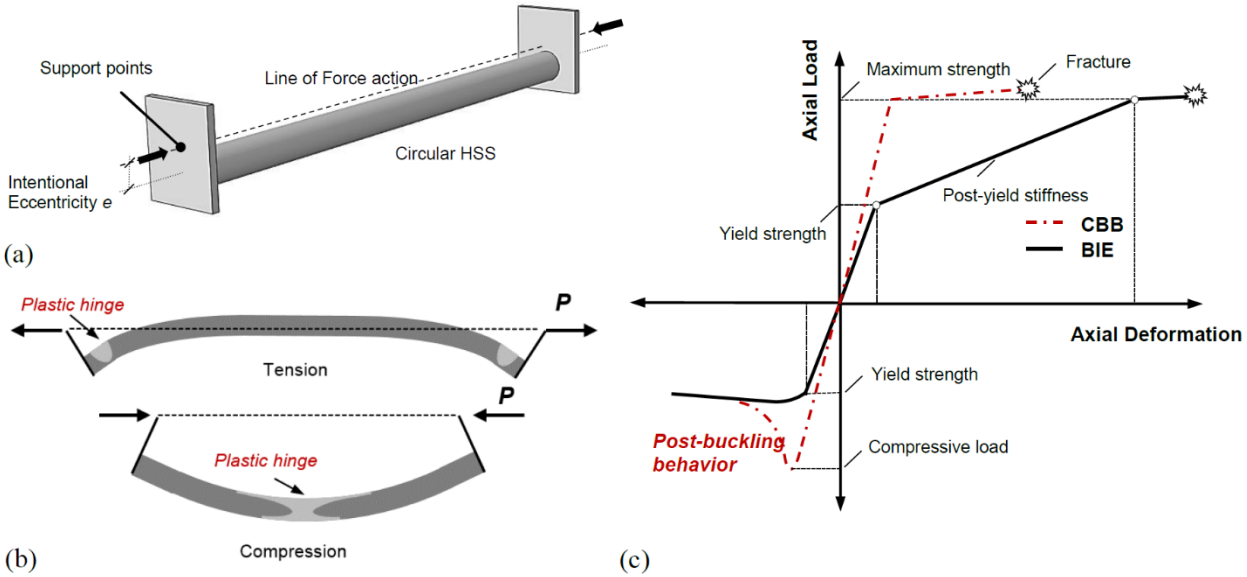

Figure 1.3: Overview of proposed steel brace: (a) BIE configuration; (b) deformed shape under tension and compression; and (c) backbone curves of traditional concentric brace (Conventional Buckling Brace or CBB in [12, 13]) and BIE (from [13])

Under tension, the brace bends toward the line of action of the forces as it elongates, and the BIE remains fully elastic until the extreme fibre in tension reaches the yielding stress. If loading is continued beyond that point, the BIE displays a significant post-yielding stiffness, as the plasticisation progresses through the section, until it is fully yielded and reaches the same maximum strength as if it were a traditional concentric brace, although at a significantly larger displacement. As such, in contrast with the nearly elastic-perfectly plastic behaviour of a concentrically loaded brace, the BIE exhibits a tri-linear response to loading in tension, as presented in Figure 1.3 (c). Kinematically, loading in tension entails a progressive reduction of the effective eccentricity and, in theory, the BIE can only attain its maximum tensile strength when the eccentricity is effectively annulled, i.e. when the brace is under pure tension. To reach this stage, the bracing member's ends must rotate considerably, which implies the development of plastic hinges at those locations (Figure 1.3 (b)).

Under compression, the BIE displays a smooth flexural response, with the bracing member bending away from the line of actions of the forces (Figure 1.3 (b)). As such, the response of the BIE is markedly distinct to that of a concentrically loaded brace in that there is no global buckling involved. Instead, the force-deformation curve transitions seamlessly from the elastic to the post-buckling regimes, devoid of sharp peaks such as those found for concentrically loaded braces. (Figure 1.3 (c)). Moreover, the plastic hinge that inevitably develops at mid-length if the compression loading is continued, does so at larger displacement levels than in the case of concentrically loaded braces, as the strain demands are distributed over the length of the BIE due to bending, instead of concentrating at the centre of the span.

Presumably, these characteristics of the response of BIEs allow them to moderate the limitations of concentrically loaded braces and CBFs discussed above. Firstly, due to their combined axial

and flexural response, BIEs are inherently less stiff, which results in longer periods of vibration and thus in lower force and acceleration demands. Secondly, the introduction of the eccentricity purportedly delays the formation of the mid-length plastic hinge in compression, associated with the onset of local buckling, resulting in an extended fracture life under cyclic loading. Also, the significant post-yielding stiffness of BIEs can help in controlling excessive displacements in multi-storey buildings. Finally, the possibility of controlling the stiffness and strength of BIEs by adjusting the eccentricity is expected to grant the designer a more comprehensive control over the dynamic response of the structure, besides allowing for the reduction of unwanted overstrength in particular storeys and its associated costs.

In their research, Skalomenos et al. performed tests under cyclic loading on five half-scale BIE specimens based on a single round HSS, as well on a concentrically loaded brace with the same section as reference. Their published results [12, 13] were consistent with the behaviour described above and augured the benefits of employing BIEs as the dissipative elements of SFRSs However, their study did not bring about the application of these eccentrically loaded braces in buildings, nor did it address their implementation in a global design approach.

1.2. RESEARCH OBJECTIVES

This study aims to generate information on the seismic performance of square HSS Braces with Intentional Eccentricity, both at the cross-section and member levels, and on the seismic response of buildings designed with BIEs as the dissipating elements of their SFRS. It intends to shed light on the question whether Frames with Intentionally Eccentric Braces (FIEBs) may constitute a competent SFRS, consistent with contemporary seismic design philosophy. To achieve this purpose, the following objectives were established.

1.2.1. Main objective

- To evaluate the performance and suitability of BIEs as the energy dissipating components of SFRSs of buildings designed for high seismic hazard, in the scope of modern earthquake design philosophy

1.2.2. Specific objectives

- To characterise, through numerical models, and through the physical testing of full-scale specimens, the response to reversed cyclic and monotonic load of square HSS BIEs
- To study the effects of the magnitude of the eccentricity and local and global slenderness on the performance and failure life of BIEs
- To develop a preliminary procedure for the seismic design of FIEBs that accounts for the specificities of the force-deformation response of BIEs, and current code requirements and performance objectives
- To compare the performance of FIEBs to that of traditional CBFs, considering both structural response and costs

1.3. SCOPE AND METHODOLOGY

The study spanned three main phases or stages, as described below. It must be noted, however, that these did not occur chronologically, as there was significant overlap and reciprocal feedback between the three.

1.3.1. Numerical study on BIEs

In the first phase of the study, being that BIEs are a newly proposed type of brace, it was necessary to address and identify which variables affected the response of BIEs under monotonic and cyclic

loading, and to investigate qualitatively and quantitatively how those variables exerted their influence. Thus, the beginning of the study consisted of exploratory inquiries based on numerical models in OpenSees [14] and Abaqus [15], with the intent of understanding the influence of variables such as the length of the BIE, the magnitude of the eccentricity, the length of the rigid assemblies that accommodated the eccentricity, the cross-section, the material properties, the type of supports (i.e. whether pinned, fixed, or other type of end restraints were considered), among others, on the response of BIEs. In the preparation of the models, the data published by Skalomenos et al. [12, 13], was used for calibration to ensure that they were indeed capable of reproducing with reasonable accuracy the behaviour of BIEs. A sample of the base code of the OpenSees BIE models is included in Appendix A: OpenSees code samples for reference.

It was identified that the variables that affected most the occurrence in BIEs of local buckling at mid-length under cyclic loading were the global slenderness, the local slenderness, and the magnitude of the eccentricity. In the second part of the first phase of the research, a parametric study based on 243 FE models in Abaqus was conducted in order to derive an equation to use in design to estimate the equivalent drift ratio at which a BIE would develop local buckling as a function of these variables.

After the physical testing of the BIE specimens, described in Section 1.3.3, was completed, an additional round of analysis of finite elements models in Abaqus was conducted, in an effort to provide additional data to complement and expand upon the experimental results.

1.3.2. Development and evaluation of a design procedure for FIEBs

In order to evaluate the performance of FIEBs as SFRSs, it was necessary first to establish a practical method or procedure to design such structures in accordance with modern seismic design

code rationale and performance objectives. Due to their particular force-deformation behaviour in tension, the conventional force-based design procedure used with CBFs and other systems is not suitable for use with BIEs. For traditional concentrically loaded braces, the force-deformation behaviour is idealised as elastic-perfectly plastic, and the braces can then be dimensioned by equating their yield strength to the seismic demand resulting from an elastic analysis, in which the force level is reduced to account for ductile response and overstrength. In the case of BIEs, the maximum capacity is attained at deformation levels that depend on the eccentricity and that might be too large to be compatible with the maximum allowable inelastic drift ratios (e.g. 2.5% in [16]). Furthermore, their post-yield stiffness is significant and varies with the section properties, the member slenderness and the eccentricity, making both an elastic-perfectly plastic idealisation and the use of a ductility reduction factor, unfitting.

Given these considerations, the development of a displacement-based design procedure, consistent with the approach described by Priestley et al. [17], appeared as a reasonable choice, adaptable to the BIEs distinct-force deformation curve. The appropriateness of the displacement-based approach for the design of traditional CBFs had already been demonstrated in research [18, 19], and the present study intended to verify its applicability to FIEBs.

The development of the proposed design procedure consisted of an adaptation of the basic Direct Displacement-Based design method [17], incorporating some specific aspects of North American design codes [7, 16, 20, 21], with the aim of producing a comprehensive set of steps that would result in outcomes consistent with the Codes' philosophy and performance objectives. The procedure used the equation derived from the parametric study on local buckling to estimate the fracture life of BIEs, allowing for the selection of braces compatible with the selected target drift ratios. The process was iterative, as significant trials were required to identify and select adequate

models to estimate the target displacement vector and the equivalent damping ratio, and to control the P-Δ effects.

The validation of the design method relied on the verification of the appropriateness of the design assumptions (i.e. target displacement vector and equivalent damping) and fulfillment of the performance objectives, by subjecting building models, designed with the procedure, to Non-Linear Response-History Analyses (NLRHA), and assessing whether their response was consistent with that intended in design. To construct and analyse the models, fibre-based models of FIEBs in OpenSees were employed. In these, the modelling of the brace elements was based on the data collected from the numerical analyses described above. A sample of the OpenSees code employed for the NLRHA of FIEBs in included in Appendix A: OpenSees code samples for reference.

During the study, model buildings were designed and analysed considering different locations with moderate and high seismic hazard, including Los Angeles in California, USA, and Montréal and Vancouver in Canada. For each particular location, the design procedure was adjusted to reflect specific requirements of the design code of reference in the region. The ground motion records used in the NLRHA were specifically selected and scaled to adequately represent the seismic hazard of the particular location, as per [21] and [16]. The version of the design procedure applied for the design of the buildings in Canada included provisions to consider wind loading and to reflect explicitly performance objectives associated with Service-Level ground motions.

1.3.3. Physical testing of full-scale BIE specimens

Prior to this study, the only experimental data on BIEs came from the tests by Skalomenos et al. [12, 13] on half-scale round HSS specimens. As such, no published information existed on full-scale square HSS BIE specimens. In conducting this study, it was considered of great relevance to

perform physical tests on BIE specimens as they permit the observation of phenomena not necessarily accounted for in the numerical models, such as fracture and unforeseen local effects.

The experimental program was carried out in the Structural Engineering Laboratory at Polytechnique Montréal. It included four BIE specimens and one reference concentrically loaded specimen, made from square ASTM 1085 HSS sections, for which the cross-sections and eccentricities were selected with the intention of comparing the response of braces both complying with or exceeding the limits to the global and local slenderness given in [7]. The design of the specimens was based on the assumption of their hypothetical use in a braced bent 4 m tall by 6 m wide, as these dimensions were compatible with the existing testing frame and equipment available in the laboratory, and are representative of dimensions typically encountered in CBFs. A configuration of side plates connecting the HSS to a knife plate in which a clearance was provided, intended to yield in bending under low levels of axial loading, was selected to accommodate the eccentricity, in account for its cost-effectiveness and simplicity. This detail corresponded as well to that used in all the numerical analyses, both of isolated BIEs and of FIEBs.

1.4. THESIS OUTLINE

The most relevant results of the study are presented in five chapters, in addition to this introduction. A summary of the contents of each chapter follows.

In Chapter 2, a comprehensive report on the basic characteristics of BIEs, their response to monotonic and cyclic loading, and the influence of the different variables involved, is presented, followed by a detailed step-by-step description of a proposed displacement-based design procedure for FIEBs. Finally, the seismic performance of 4-, 8- and 12-storey FIEBs designed in Los Angeles, California, USA, as per the proposed procedure for two levels of target drift ratio, is

discussed and contrasted to that of Special CBFs [20, 21], based on NLRHA analyses of models in OpenSees.

In Chapter 3, a numerical investigation on the fracture life of square HSS BIEs, based on a parametric study of finite element models of BIEs considering a wide range of global and local slenderness ratios and eccentricity ratios, is presented in detail. The investigation leads to the proposal of an equation for use in design to predict the drift ratio at which a BIE under cyclic loading develops local buckling. Information on the energy dissipation and damping properties of BIEs is also provided.

In Chapter 4, an updated version of the design procedure for FIEBs is presented, including provisions to consider in design wind loading and to address explicitly the performance of the structure under the action of frequent, or "Service-Level", earthquakes. The revised design procedure is put to use in the design of 4-, 8-, and 12-storey FIEBs for target drift ratios of 2.5% and 1.5%, located in Vancouver, British Columbia, and Montréal, Québec, to represent conditions of high and moderate seismic hazard, respectively. The cost of the resulting structures is compared to that of Moderately Ductile (Type MD) and Low Ductility (Type LD) CBFs [7, 16] designed for the same conditions.

In Chapter 5, a description of the experimental test program preparation and a summary of its results are provided. The laboratory test results are further expanded with the analyses of finite element models of BIEs, selected to complement and expand upon the experimental data. The implications on the design of FIEBs of the physical testing and numerical modelling findings are discussed.

Finally, in Chapter 6, a summary and discussion of the main conclusions of the study is presented, and a list of recommendations for future research on BIEs and FIEBs is proposed.

1.5. LITERATURE REVIEW

BIEs are a very recently proposed type of steel brace. As such, research on them is incipient. Notwithstanding, a review of the published literature on BIEs, as well as on related systems that rely on the eccentric loading of braces and their asymmetric response to tension and compression loading to offer an improved performance over traditional concentrically loaded braces, is presented herein.

1.5.1. Braces with Intentional Eccentricity (BIEs)

Skalomenos et al. introduced the concept of the Brace with Intentional Eccentricity and presented the results of the testing under cyclic loading of five half-scale round HSS BIE specimens, and one reference concentrically loaded brace specimen [12, 13]. In all specimens the same round HSS, with a diameter of 114.3 mm and a thickness of 3.5 mm, was employed. What varied were the eccentricity, the type of connection, and whether the ends of the HSS were reinforced with rib stiffeners, as reported in Table 1.1. The total, or hinge-to hinge, length was 2131 mm, and the free length of the bracing member, equal to the total length minus the length of the rigid assemblies used to introduce the eccentricity, was 1575 mm for all six specimens. Details of the employed gusset plate connection and the loading frame configuration are shown in Figure 1.4.

Table 1.1: Specimens tested by Skalomenos et al. [12, 13]

Specimen	Eccentricity (mm)	Type of connection	Stiffeners at bracing member ends
G1-OoP-60	60	Gusset plate, out-of-plane bending	No
G1-OoP-30	30	Gusset plate, out-of-plane bending	No
G1-OoP-0	0	Gusset plate, out-of-plane bending	No
G2-OoP-60	60	Gusset plate, out-of-plane bending	Yes
G2-InP-60	60	Gusset plate, in-plane bending	Yes
P-InP-60	60	Pin, in-plane bending	No

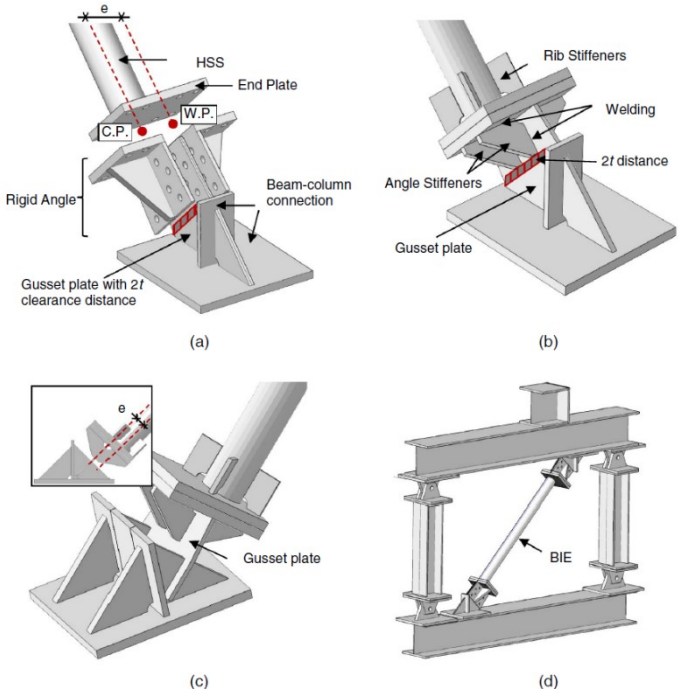

Figure 1.4: Typical details of Skalomenos et al. test specimens: (a) Out-of-plane end plate connection; (b) out-of-plane end plate connection with stiffeners; (c) in-plane end plate connection with stiffeners; (d) Specimen G1-OoP-60 connected to the loading frame (from [12])

The results of the tests showed that, in comparison with the concentric brace, the eccentric braces presented lower initial stiffness and a significantly larger post-yielding stiffness in tension. The magnitudes of these stiffnesses decreased as the eccentricity increased. In compression, the BIEs exhibited a more stable behaviour, devoid of marked loss of strength due to global buckling. The data also showed that the onset of local buckling at mid-length was delayed, in terms of equivalent

storey drift, by the eccentricity favouring a more even distribution of the strains in compression along the length of the brace. Low-cycle fatigue-induced fracture at the mid-length plastic hinge following the onset of local buckling was the failure mode observed in all specimens except for G1-OoP-60, for which a tensile fracture occurred at the brace end. With the intent to prevent this failure mode, rib stiffeners were applied to the brace end of specimens G2-OoP-60 and G2-InP-60, which had the same eccentricity and did not present this type of fracture. Specimen P-InP-60 was identical to Specimen G1-OoP-60 except in that its connection was pinned and oriented to bend in the plane of the frame. It displayed a behaviour almost identical to that of the latter, in terms of strength and stiffness, except that it did fail by fracture at mid-length. In general, the results showed that the gusset plate connections provided no significant restraint to the free rotation of the brace ends and, as such, did not behave differently from the pinned connection. Although no damage was observed in the gusset plates, which were detailed with a clearance twice as long as their thickness, it was noted that these were subjected to rotations when the braces were in tension, as they were in compression, unlike the gusset of the concentric specimen which did not exhibit significant rotation under tension. The energy dissipation capacity of the BIEs was also compared to that of the concentrically loaded brace. BIEs presented the same maximum equivalent viscous damping ratio, however they attained it at larger displacement levels depending on the eccentricity. Moreover, for the lower eccentricity (30 mm), the BIEs started dissipating energy at lower displacements than the concentrically loaded brace because they reached first-yielding at less overall displacement. In [12], a mathematical formulation to estimate the backbone curve of BIEs as a function of their geometry and yielding stress was presented; it could approximate the behaviour of the BIEs tested in the study with fair accuracy. The hysteresis curves of test specimens G1-Oop-60 and G1-OoP-0 are reproduced in Figure 1.5.

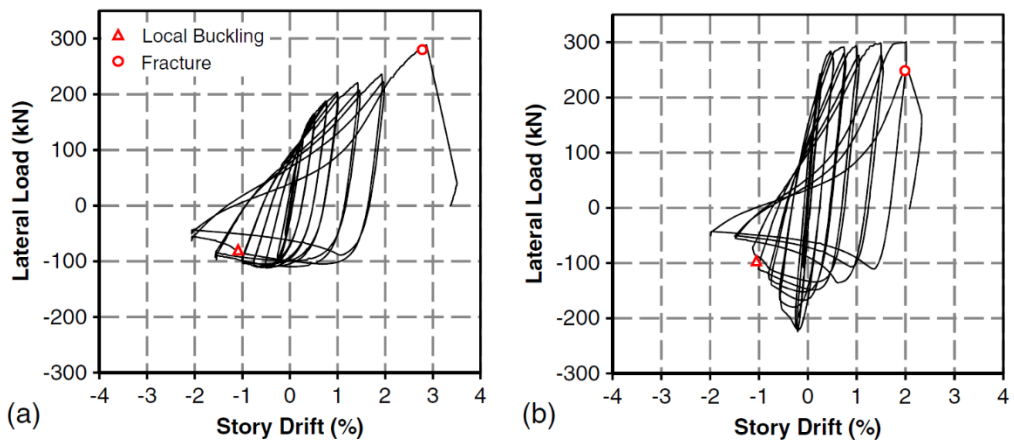

Figure 1.5: Hysteresis curves of test specimens: (a) G1-OoP-60; (b) G1-OoP-0 (from [12])

1.5.2. Naturally Buckling Braces (NBBs)

Naturally Buckling Braces (NBBs), proposed and studied by Inamasu et al. [22-24], are braces which, in addition to being installed with an intentional eccentricity, have the two halves of their cross-section composed of steels with different mechanical properties. As shown in Figure 1.6, in NBBs, the half of the bracing member closest to the line of action of the forces, which when the brace is under tension is subjected to tension stresses due to bending in addition to the axial load, is made from a steel with a low yield strength and high ductility, while the opposed half is made from a high strength steel with significantly lower ductility. In the research presented in [22], the two halves are bound together by welded battens, in the continuation of the study presented in [23] and [24], bolts were also employed as an alternative fastening solution. The intent of such configuration is that the low yielding steel provides energy dissipation at low displacement levels, while the high strength steel grants high stiffness and remains undamaged until large displacement levels. Hence, NBBs aim to enhance the benefits of the eccentric loading by relying on the contrast in behaviour between the two materials.

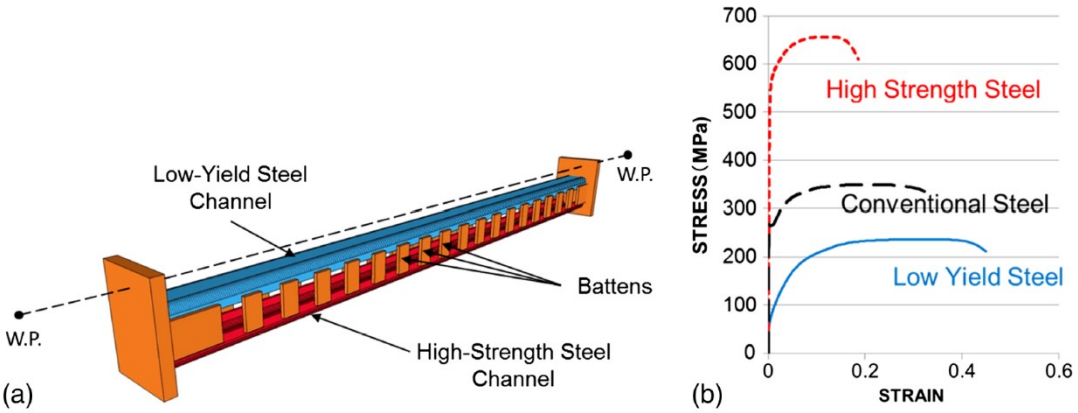

Figure 1.6: Naturally buckling brace (NBB): (a) composition of the brace (WP = work point); (b) material properties of the adopted high performance steels based on tensile tests (from [22])

In [22], the test results of 6 specimens with configurations as presented in Figure 1.7 were reported. The specimens were selected to compare the responses of specimens made with the combination of different steel grades, as described above, to that of specimens made with conventional steel exclusively, and to study the effects of the eccentricity and the cross-section radius of gyration. Thus, all specimens had the same length and cross-sectional area, and relied on the same pinned connection to the testing frame. Specimens HLS-D20-E0, -E60, and -E80 were fabricated with the low yield and high strength steels, and differed in their eccentricities: 0, 60 mm, and 80 mm, respectively. Specimens CS-D20-E0 and – E60 were geometrically identical to Specimens HLS-D20-E0 and -E60, but fabricated with conventional steel only. Finally, Specimen HLD-D60-E60 was identical to Specimen HLS-D20-E60, except that it had a larger separation between the two halves of its cross-section. The results showed the same effects due to the introduction of the eccentricity as in [12] and [13], namely a significant post-yielding stiffness, a stable flexural response in compression and a delay in the onset of local buckling. The use of a combination of the low yield and high strength steels resulted in earlier yielding and engagement in energy dissipation, and in a further delay of the onset of local buckling, thus considerably increasing the overall ductility.

In [23] and [24], the study was continued to investigate the effects of different ways to connect the two halves of the cross-section and to introduce the eccentricity, as shown in Figure 1.8, as well as those of the use of gusset plate connections instead of the pinned connections used in [22]. Four specimens were tested with identical cross-sections and length; of those, three were based on the configurations from Figure 1.8 and the fourth incorporated the same end plate configuration from the previous study. It was found that the proposed revised configurations for the introduction of the eccentricity were adequate to achieve the desired behaviour, consistent with that of the specimens from the previous study. As well, the gusset plate provided a nearly unrestrained rotation capacity, producing a response very similar to that of the pinned connection.

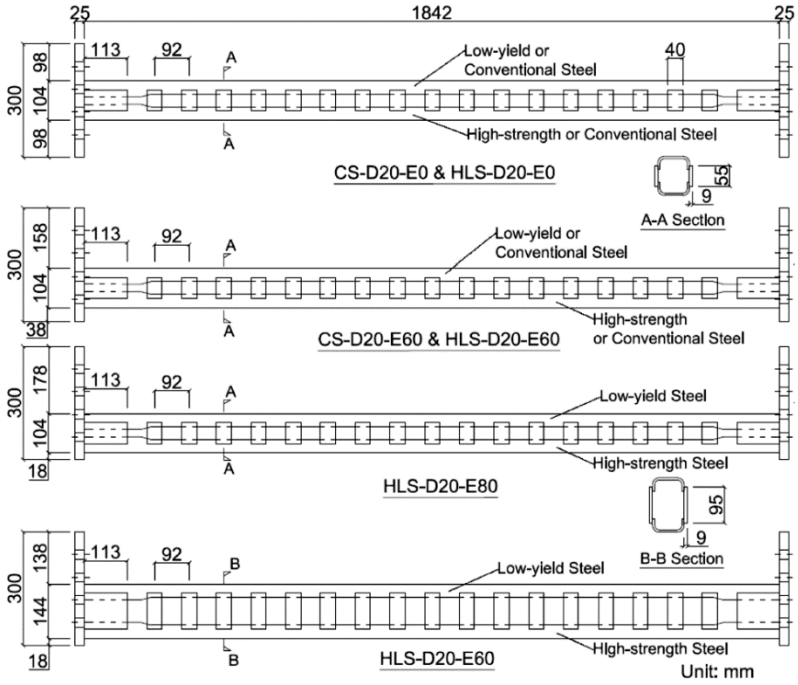

Figure 1.7: Dimension details of test specimens (from [22])

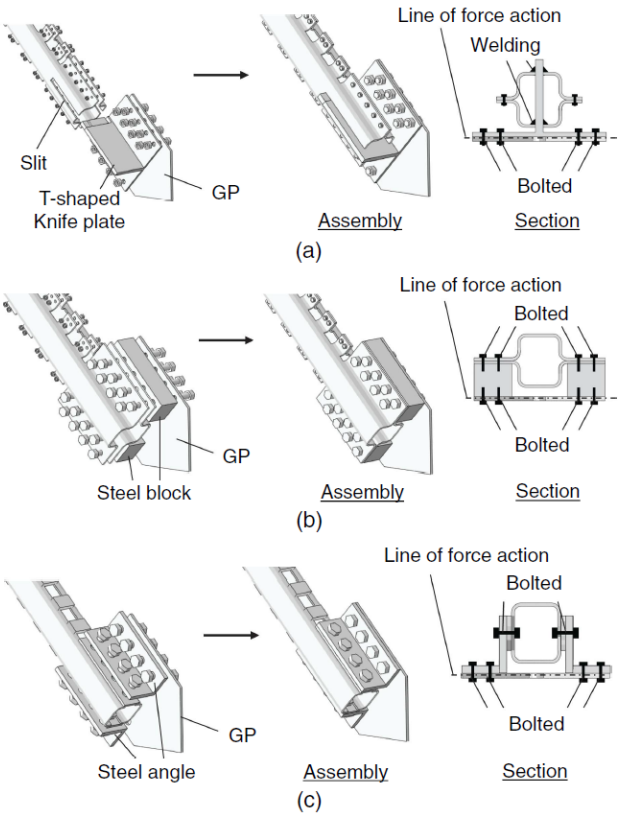

Figure 1.8: Configurations of proposed connections: (a) knife plate type; (b) steel block type; (c) steel angle type (from [24]).

1.5.3. BIEs with induction-heat treatment

In [25] and [26], Skalomenos et al. studied a modification to their BIE concept, consisting of the application of an induction heat treatment to the half of the cross section farther away from the line of force action, to increase its yield stress and to achieve a brace with characteristics similar to those of the Naturally Buckling Brace. In Figure 1.9, a concept schematic for the proposed brace is presented, along with a detail of how the treatment is applied to the brace, and the theoretical backbone curves of the brace and kinematic behaviour. As can be noted from Figure 1.9 (c), the resulting backbone curves are similar to that of a regular BIE, except that the ultimate strength and post-yielding stiffness of the brace are significantly higher.

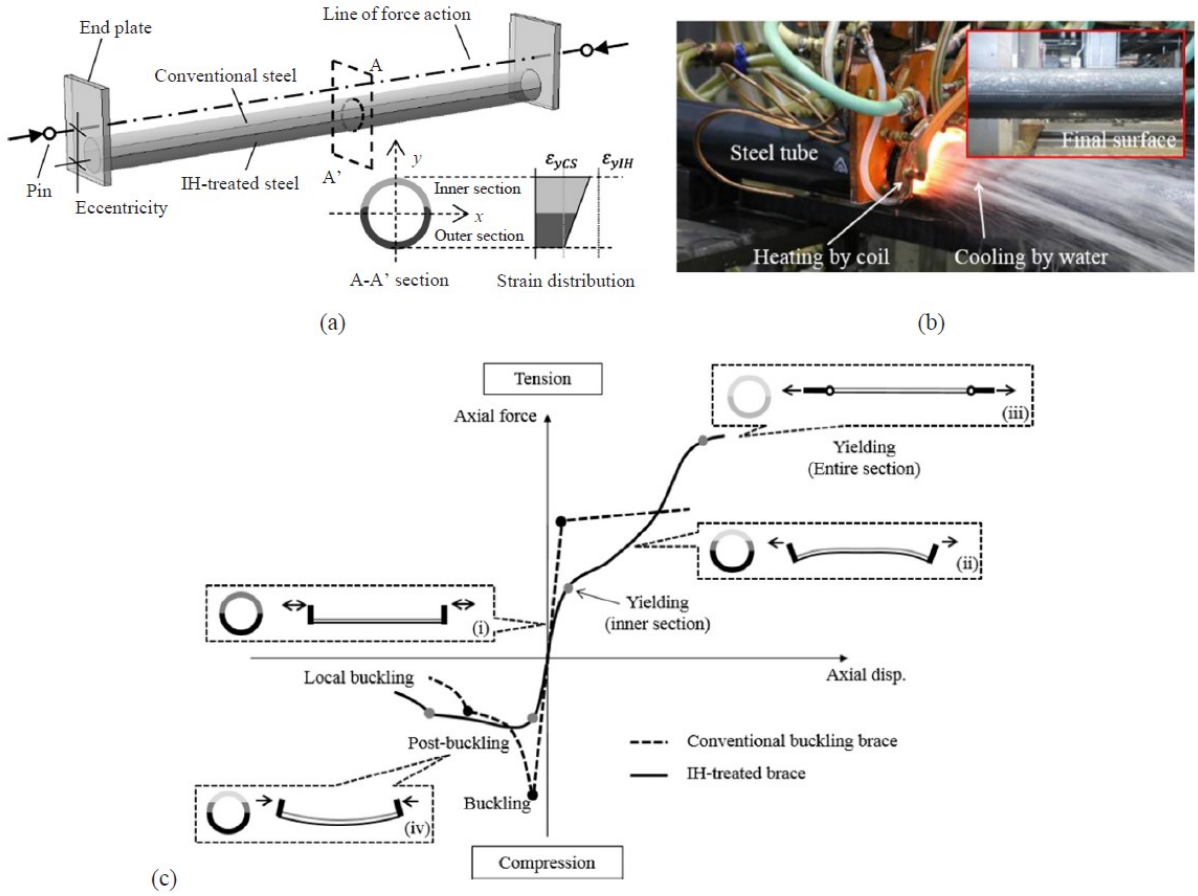

Figure 1.9: Induction heat-treated steel brace: (a) concept; (b) manufacturing process; and (c) backbone curves (from [26])

In [26], test results from 4 induction heat-treated BIEs under cyclic loading were presented and compared to those from Specimen G1-OoP-60 from [12], with which they shared all dimensions and the 60 mm eccentricity, as shown in Figure 1.10. In these 4 specimens, the variable was the extent of the region on which the heat treatment was applied: In Specimen IHBIE-0D-R1, the treatment was applied to the total length of the external half, with respect to the eccentricity; in Specimen IHBIE-0D-N, in addition to the external half, the complete perimeter of the HSS within a distance corresponding with two diameters measured from the connecting end plate was treated; and in Specimen IHBIE-2D-R1, no treatment whatsoever was applied to the ends of the bracing member. The fifth Specimen, IHBIE-0D-R2, not included in the figure, was identical to Specimen

IHBIE-0D-R1, expect that its connections were modified to produce in-plane, instead of out-of-plane, bending. Except for Specimen IHBIE-0D-N, rib stiffeners were used in all specimens.

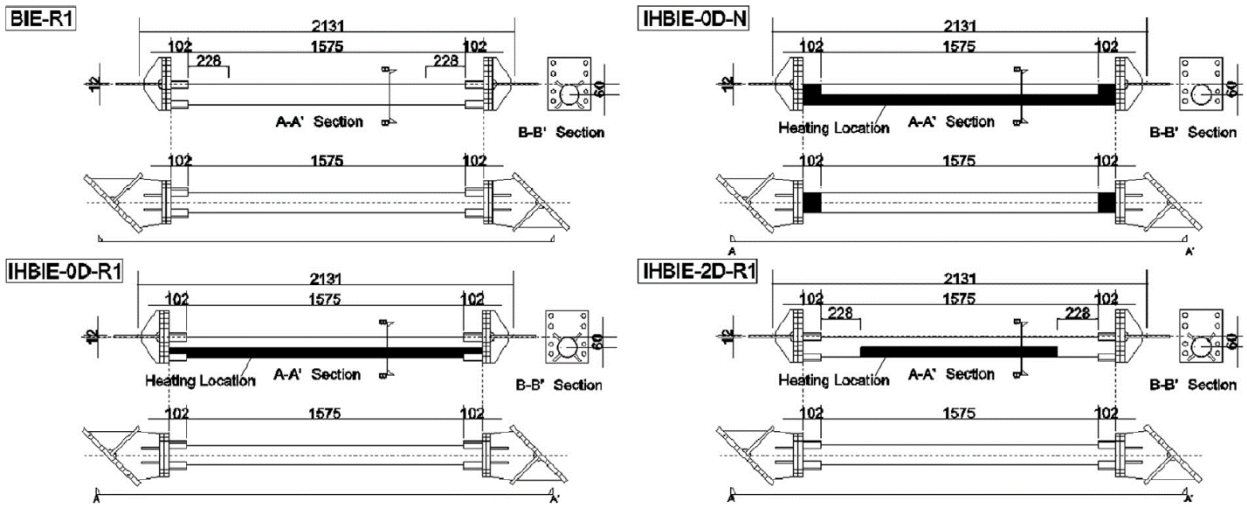

Figure 1.10: Dimensions and configuration details of test specimens (from [26])

The results were consistent with the theoretical behaviour described above. However, it was found that, in comparison with the non-treated BIE, applying the heat treatment at the bracing member's ends, especially when the whole perimeter was involved, reduced the overall ductility by favouring a tension fracture at that location, even when rib stiffeners were employed. Specimen, IHBIE-2D-R1, whose ends did not receive the treatment, achieved a ductility on par with that of the reference BIE, with its failure mode consisting of fracture at mid-length following the onset of local buckling, while exhibiting significantly higher tensile strength and post-yielding stiffness. The study in [26] included as well the results from finite element model analyses investigating the effects of increasing further the yield strength of the treated half of the HSS. According to these, besides increasing the post-yielding stiffness and tensile strength of the BIE, this would allow for the onset of local buckling to be delayed, although only by a small margin.

1.5.4. Curved steel knee brace

Zhou et al. [27, 28] published research on curved steel knee braces (CSKBs). Although these were proposed as knee braces, instead of full diagonal braces, their behaviour at the member level presents similarities to that of BIEs and they could, presumably, be employed as full diagonal braces. The basic configuration of a CSKB is shown in Figure 1.11. The CSKB is composed of a built-up H section curved about its minor axis, and is connected to the rest of the structure by pins that pass through ear plates welded to end plates placed at the ends of the curved part of the brace.

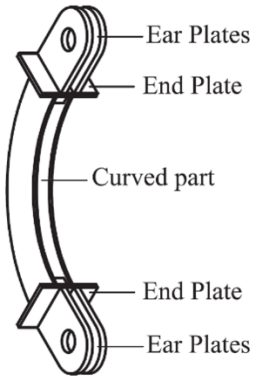

Figure 1.11: Configuration of Curved steel knee brace (from [27])

As presented in Figure 1.12, the monotonic response of CSKBs encompasses a reduced elastic stiffness and a significant post-yielding in tension, and an almost elastic-perfectly plastic flexural response in compression, much like BIEs. Analogously to the eccentricity in BIEs, by adjusting the curvature of the brace for a given cross-section and length, its stiffness and strength can be modified. However, the kinematic response of CSKBs is fundamentally different to that of BIEs, especially in tension, as shown in Figure 1.13. Due to their curvature, and to the lack of an effective eccentricity at the brace's ends, the most severe stress and strain demands in tension occur at mid-length, where a plastic hinge eventually develops. In BIEs, as the initial eccentricity is constant along the length, it is at the brace's ends where the demands are higher and where plastic hinges develop.

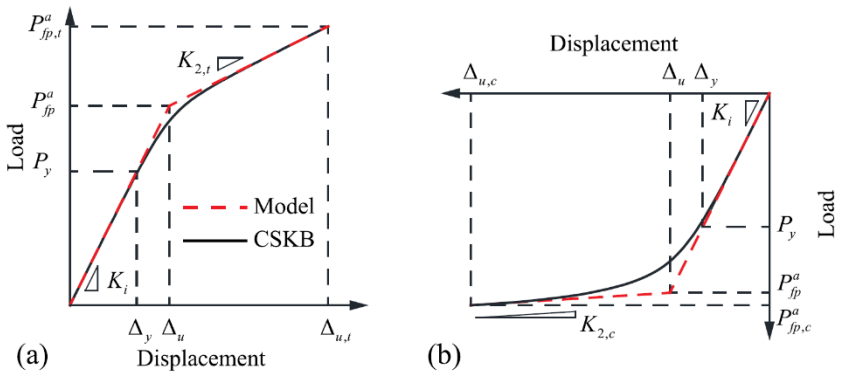

Figure 1.12: Backbone curves of CSKB: (a) in tension; (b) in compression (from [28])

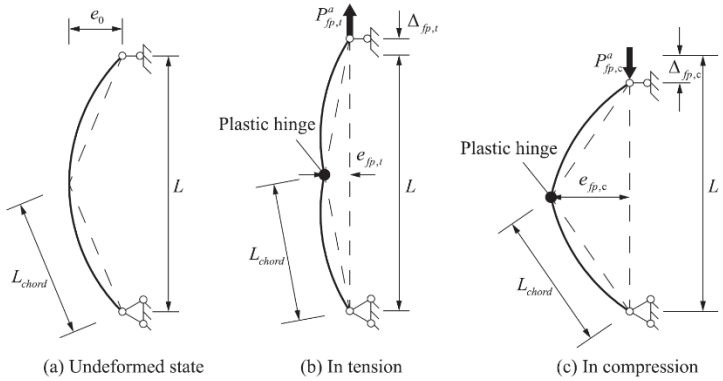

Figure 1.13: Kinematic response of CSKB and plastic hinges (from [28])

Zhou et al. presented the results of testing of CSKB specimens under monotonic and under cyclic loading in [27] and [28], respectively. These showed that by varying the curvature of the brace, its strength and stiffness could be adjusted, that the ductility of the braces increased with the curvature, and that under cyclic loading the braces displayed a stable hysteretic force-deformation behaviour with high equivalent damping capacity. The equivalent damping ratio was found to increase with the curvature, as the differences between the tension and compression behaviour became less marked due to the reduction in the post-yielding stiffness.

1.5.5. Steel A-brace

The application of a curved steel dissipating element, similar to the CSKB, to an alternative type of brace, named the 'A-brace', has been proposed by Hsu and Halim [29, 30]. In this system, the brace is composed of two articulated brace segments and an additional steel curved damper,

forming the shape of an ‘A’, as shown in Figure 1.14. Given the eccentricity that results between the frame diagonal and the pin connections of the curved damper to the brace segments, the forces and deformations on this element are amplified, which allows it to dissipate energy from very low storey displacements. The global behaviour of the proposed A-brace is consistent with that of the CSKB described in Section 1.5.4, exhibiting a significant post-yielding stiffness in tension, an almost elastic-perfectly plastic force-displacement relation in compression, and a stable hysteretic force-deformation response under cyclic loading up to high displacement levels. Another advantage of the configuration is that only the relatively small curved damper would require replacement after a seismic event in the case of permanent damage.

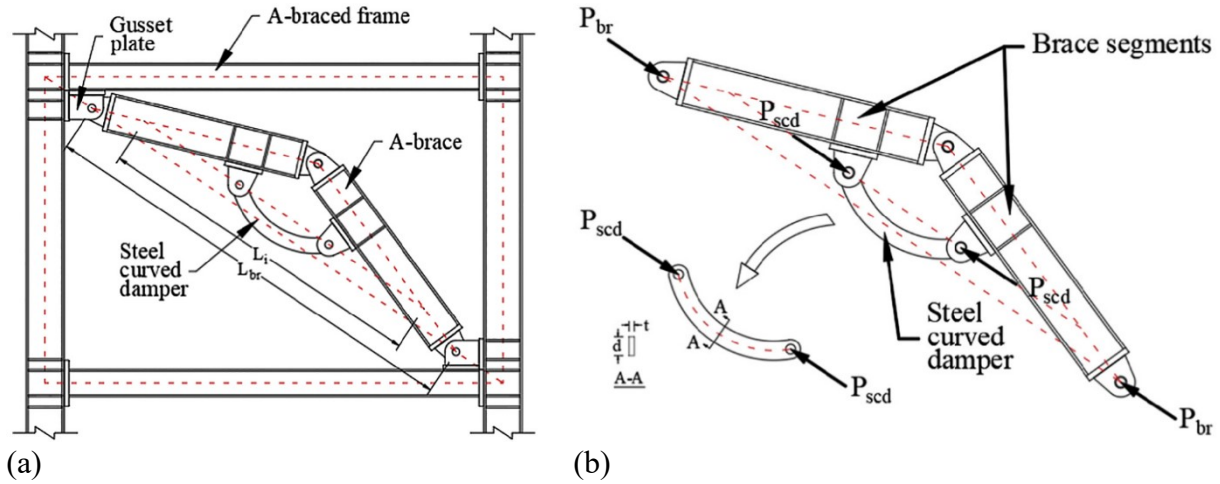

Figure 1.14: A-brace: (a) configuration; (b) load transmission mechanism (from [30])

The A-braces studied by Hsu and Halim relied on a steel curved damper with a rectangular cross-section, as shown in Figure 1.14. In [29], the results from a series of tests under cyclic loading, both of the steel dampers alone and of whole A-braces were presented. It was confirmed that the system provided high ductility and energy dissipation capacity, especially if dampers with a plate depth to thickness ratio lower than 4 were employed, as these could reach equivalent storey drifts larger than 5% without buckling in compression. In [30], the authors presented experimental results from the testing of steel moment resisting frames upgraded with A-braces, and results from

non-linear response-history analyses of numerical models of multi-storey moment frames reinforced with A-braces. The results showed that the proposed system was successful in reducing considerably the base shears and storey drifts of the reinforced frames and in preventing the development of plastic hinges in beams and columns.

1.5.6. Summary

As laid out in the above presented review, several brace systems that take advantage of eccentric loading and combined axial and flexural response to offer improved seismic performance over traditional concentrically loaded braces have been proposed recently and produced promising results. The performance of tests on BIEs [12, 13], otherwise traditional braces with their longitudinal axis offset to produce a combined axial and flexural response, has shed light on the ability to overcome some of the most notorious shortcomings of CBFs by relying on the eccentric loading of the braces. Further, research on NBBs [22-24] and IHBIEs [25, 26] showcased the beneficial effects of accentuating further the asymmetric nature of eccentrically loaded braces by using materials with different strength and ductility properties of opposed sides of the bracing member's cross-section. Finally, it has been shown that the use of curved bracing members, such as the CSKB [27, 28], can achieve an asymmetric force-deformation response that resembles considerably that of eccentric braces, offering therefore similar advantages. The energy dissipation capacity of these curved braces can further be exploited by their integration in a system that amplifies the displacements applied to them, such as the A-brace [29, 30]

None of the listed novel brace types have been fully developed for use in practice. However, in the author's opinion plain BIEs remain the most straightforward and easily implementable among these systems, and possess a considerable potential worthy of further investigation. Although the research by Skalomenos et al. indicates that, at the member level, BIEs offer clear advantages over

traditional concentrically loaded braces, the question whether their incorporation as the energy dissipating members of braced frames may constitute an efficient and practical alternative to CBFs remains. Equally important is how to achieve this from a design perspective reconciling the untraditional force-deformation response of BIEs and contemporary design philosophy.

REFERENCES

[1] B. Fell, A. Kanvinde, and G. Deierlein, *Large-scale testing and simulation of earthquake-induced ultra low cycle fatigue in bracing members subjected to cyclic inelastic buckling*. Stanford, CA: John A. Blume Earthquake Engineering Center, 2010.

[2] S. Santagati, D. Bolognini, and R. Nascimbene, "Strain life analysis at low-cycle fatigue on concentrically braced steel structures with RHS shape braces," *Journal of earthquake engineering,* vol. 16, no. sup1, pp. 107-137, 2012.

[3] P. Uriz and S. A. Mahin, "Toward earthquake-resistant design of concentrically braced steel-frame structures," Pacific Earthquake Engineering Research Center (PEER), University of California, Berkeley, 2008.

[4] K. Lee and M. Bruneau, "Energy dissipation of compression members in concentrically braced frames: Review of experimental data," *Journal of structural engineering,* vol. 131, no. 4, pp. 552-559, 2005.

[5] R. Tremblay, M. H. Archambault, and A. Filiatrault, "Seismic response of concentrically braced steel frames made with rectangular hollow bracing members," *Journal of Structural Engineering,* vol. 129, no. 12, pp. 1626-1636, 2003.

[6] M. Bruneau, C. M. Uang, and R. Sabelli, *Ductile design of steel structures*, 2nd ed. New York: McGraw-Hill, 2011, pp. xxi, 905 p.

[7] *CSA. S16-14: Design of steel structures*, Canadian Standards Association (CSA), Toronto, ON, 2014.

[8] B. V. Fell, *Large-scale testing and simulation of earthquake-induced ultra low cycle fatigue in bracing members subjected to cyclic inelastic buckling*. University of California, Davis, 2008.

[9] X. Tang and S. C. Goel, "Brace fractures and analysis of Phase I Structure," *Journal of Structural Engineering,* vol. 115, no. 8, pp. 1960-1976, 1989, doi: 10.1061/(ASCE)0733-9445(1989)115:8(1960).

[10] S. Costanzo, M. D'Aniello, and R. Landolfo, "Proposal of design rules for ductile X-CBFS in the framework of EUROCODE 8," *Earthquake Engineering & Structural Dynamics,* vol. 48, no. 1, pp. 124-151, 2019, doi: 10.1002/eqe.3128.

[11] R. Tremblay, "Achieving a stable inelastic seismic response for concentrically braced steel frames," *Engineering Journal, AISC,* vol. 40(2), pp. 111-129, 2003.

[12] K. A. Skalomenos, H. Inamasu, H. Shimada, and M. Nakashima, "Development of a steel Brace with Intentional Eccentricity and experimental validation," *Journal of Structural Engineering,* vol. 143, no. 8, p. 04017072, 2017, doi: 10.1061/(ASCE)ST.1943-541X.0001809.

[13] K. A. Skalomenos, H. Inamasu, H. Shimada, M. Kurata, and M. Nakashima, "Experimental investigation of steel braces installed with intentional eccentricity using gusset plate connections," Proceedings of the *16th World Conference on Earthquake Engineering*, 2017, vol. 188.

[14] F. T. McKenna, "Object-oriented finite element programming: Frameworks for analysis, algorithms and parallel computing," Ph.D. Thesis, Civil Engineering, University of California, Berkeley, 1997.

[15] *Dassault Systèmes, Abaqus/CAE 2019*. (2018). Dassault Systèmes Simulia Corp., Providence, RI.

[16] *National Building Code of Canada 2015, 14th ed.* , National Research Council of Canada (NRCC), Ottawa, ON, 2015.

[17] M. J. N. Priestley, G. M. Calvi, and M. J. Kowalsky, *Displacement-based seismic design of structures*. Pavia, Italy: IUSS Press 2007, pp. xvii, 721 p.

[18] G. O'Reilly, J. Goggins, and S. Mahin, "Performance-based design of a self-centering concentrically braced frame using the direct displacement-based design procedure," Proceedings of the *15th World Conference on Earthquake Engineering*, Lisbon, Portugal, 2012.

[19] K. K. Wijesundara and P. Rajeev, "Direct displacement-based seismic design of steel concentric braced frame structures," *Australian Journal of Structural Engineering,* vol. 13, no. 3, pp. 243-257, 2012.

[20] *ANSI/AISC 341-16: Seismic provisions for structural steel buildings*, American Institute for Steel Construction (AISC), Chicago, IL, 2016.

[21] *ASCE/SEI 7-16: Minimum design loads and associated criteria for buildings and other structures*, American Society of Civil Engineers (ASCE), Reston, VA, 2017. [Online]. Available: https://ascelibrary.org/doi/abs/10.1061/9780784414248

[22] P. C. Hsiao, K. Hayashi, H. Inamasu, Y. B. Luo, and M. Nakashima, "Development and testing of naturally buckling steel braces," *Journal of Structural Engineering,* vol. 142, no. 1, p. 04015077, 2016, doi: 10.1061/(ASCE)ST.1943-541X.0001319.

[23] H. Inamasu, K. A. Skalomenos, P. C. Hsiao, K. Hayashi, M. Kurata, and M. Nakashima, "Experimental investigation of bolt-configured naturally buckling braces with gusset plate connections," Proceedings of the *16th World Conference on Earthquake Engineering (16WCEE)*, 2017, vol. 619.

[24] H. Inamasu, K. A. Skalomenos, P. C. Hsiao, K. Hayashi, M. Kurata, and M. Nakashima, "Gusset plate connections for Naturally Buckling Braces," *Journal of Structural Engineering,* vol. 143, no. 8, p. 04017065, 2017, doi: 10.1061/(ASCE)ST.1943-541X.0001794.

[25] K. A. Skalomenos, M. Kurata, H. Shimada, and M. Nishiyama, "Use of induction-heating in steel structures: material properties and novel brace design," *Journal of Constructional Steel Research,* vol. 148, pp. 112-123, 2018, doi: https://doi.org/10.1016/j.jcsr.2018.05.016.

[26] K. A. Skalomenos, M. Kurata, and M. Nishiyama, "Induction-heat treated steel Braces with Intentional Eccentricity," *Engineering Structures,* vol. 211, p. 110461, 2020.

[27] Z. Zhou, B. Ye, and Y. Chen, "Experimental investigation on monotonic performance of steel curved knee braces for weld-free beam-to-column connections," Proceedings of the *2017 World Congress on Advances in Structural Engineering and Mechanics (ASEM17)*, Ilsan, South Korea, 2017.

[28] Z. Zhou, B. Ye, and Y. Chen, "Experimental investigation of curved steel knee braces with adjustable yield displacements," *Journal of Constructional Steel Research,* vol. 161, pp. 17-30, 2019, doi: https://doi.org/10.1016/j.jcsr.2019.06.011.

[29] H. L. Hsu and H. Halim, "Brace performance with steel curved dampers and amplified deformation mechanisms," *Engineering Structures,* vol. 175, pp. 628-644, 2018, doi: https://doi.org/10.1016/j.engstruct.2018.08.052.

[30] H. Halim and H. L. Hsu, "Steel A-braced frame upgrade performance under various load characteristics," *Journal of Constructional Steel Research,* vol. 175, p. 106303, 2020.

FOREWORD TO CHAPTER 2

As described in Chapter 1:, the main objective of the research presented in this thesis is to evaluate the performance and suitability of BIEs as the energy dissipating components of SFRSs of buildings designed for high seismic hazard, in the scope of modern earthquake design philosophy. As such, Chapter 2 was prepared as an exploratory investigation on the seismic design and performance of Frames with Intentionally Eccentric Braces (FIEBs). It begins with a comprehensive overview of the basic characteristics of Braces with Intentional Eccentricity, including their geometric configuration and components, the influence of the different variables involved, their response to monotonic and cyclic loading, and considerations regarding their numerical modelling, among others. This is followed with the detailed presentation of a displacement-based procedure specially developed for the seismic design of FIEBs. Finally, the performance of model 4-, 8- and 12-storey FIEBs designed with said procedure in Los Angeles, CA, for two levels of target drift ratio is studied, and compared to that of Special Concentrically Braced Frames (SCBFs) using Non Linear Response-History Analysis (NLRHA).

CHAPTER 2: EARTHQUAKE-RESISTANT DESIGN OF STEEL FRAMES WITH INTENTIONALLY ECCENTRIC BRACES

Published in Journal of Constructional Steel Research, Volume 178, March 2021, https://doi.org/10.1016/j.jcsr.2020.106483

Andrés González Ureña, Robert Tremblay, Colin A. Rogers

ABSTRACT

Braces with Intentional Eccentricity (BIEs) have been proposed to overcome some of the shortcomings of Concentrically Braced Frames (CBFs), namely the implications of their inherently stiff nature, their limited post-yielding stiffness and the susceptibility of Hollow Structural Sections (HSSs) to premature local buckling and fracture, and the excessive overstrength that may result from the design codes limits on the local and global slenderness. However, the application of BIEs for use in buildings has not yet been attempted, nor has their implementation in a global design approach yet been addressed. In this paper, a procedure based on the Direct Displacement Based Design (DDBD) method is employed in the seismic design of Frames with Intentionally Eccentric Braces (FIEBs). Buildings of 4, 8 and 12 storeys are designed as FIEBs with HSS brace members, with target drift ratios of 1.5% and 2.5%, and as Special CBFs for comparison purposes. The performance of the resulting buildings is assessed through Non-Linear Response-History Analysis. The results show that the employed design procedure is well suited to FIEBs, that their

seismic performance is satisfactory and complies with the proposed performance objectives, and that they can constitute an economically advantageous alternative to conventional CBFs.

Keywords: steel braced frames; eccentric braces; earthquake-resistant design; displacement-based design

2.1. INTRODUCTION

Concentrically Braced Frames (CBFs) with Hollow Structural Sections (HSSs) as the brace members are widely used as the seismic-force-resisting system (SFRS) of low- and mid-rise buildings. Despite their popularity, these structures present significant drawbacks that hinder their convenience. Firstly, the ductility and the energy dissipation capacity of the braced frame is limited by the susceptibility of HSS braces to low cycle fatigue induced fracture at the plastic hinge region [1, 2]. Secondly, due to their invariably stiff nature, CBFs are constrained to low fundamental periods of vibration and, thus, to high acceleration and force demands, which, in combination with the overstrength that originates from the compression resistance governing the sizing of the brace members, result in high design forces for the capacity protected components of the structure and its foundations, weighing significantly on the total cost of construction. Additionally, Conventional Concentric Braces (CCBs) possess nearly no post-yielding stiffness, potentially resulting in large deformation demands and stability issues. Furthermore, although the design codes prescribe limits to the local and global slenderness of the bracing members in CBFs aiming to ensure that they provide an adequate response and sufficient ductility, the need to comply with these often results in unintentional excessive overstrength in particular storeys, favouring the concentration of drift demands in storeys with a lower capacity to demand ratio [3]. The propensity of CBFs to develop a soft-storey seismic response is mitigated by the modest force modification factors and stringent building height limits specified in the codes, further hindering their cost-effectiveness and range of application in seismically active regions.

To overcome these shortcomings of CCBs, Skalomenos et al. [4] proposed the use of Braces with Intentional Eccentricity (BIEs) as an alternative lateral load carrying system. A BIE is, straightforwardly, an otherwise conventional brace with its longitudinal axis offset with respect to

the working points (i.e. the frame diagonal). As, due to this eccentricity, they are subjected to bending moment and axial force simultaneously under seismic action, BIEs are naturally more flexible than CCBs and are characterised by a pseudo-trilinear force-displacement behaviour in tension, with an early initiation of inelastic response and significant post-yielding stiffness, and a smooth flexural response in compression devoid of sharp peaks and loss of stiffness due to sudden buckling. Moreover, their pre- and post-yielding stiffness can be controlled by varying the prescribed eccentricity, enabling a better control over the dynamic response of the structure. These characteristics of BIEs presumably auspice an earlier and better distributed engagement of dissipative action. In addition to this, the onset of local buckling at the mid-length, which precedes fracture, is delayed in terms of axial displacements because the strain demand is more evenly distributed along the brace length. In their research, Skalomenos et al. performed cyclic load tests on five half-scale BIE specimens with two eccentricity values and one CCB, all made from the same circular HSS, and obtained results consistent with the behaviour described above. However, their published works did not address the application of these braces in buildings nor did they speak to the implementation of BIEs in a global design approach. These steps are necessary to determine whether BIEs would indeed produce SFRSs with advantages, in terms of cost or structural performance, over conventional CBFs.

In this paper, an exploratory investigation on the seismic design and performance of Frames with Intentionally Eccentric Braces (FIEBs) made of square HSSs is presented. Given the particular force-deformation behaviour of BIEs, which, as is herein described, sets them apart from conventional dissipating elements, an alternative design approach addressing explicitly the characteristics of the BIEs, namely one based on the Direct Displacement-Based Design procedure, was developed. Prototype buildings based on a common plan configuration and with

number of storeys of 4, 8 and 12, were designed using the proposed design procedure for two target maximum drift ratios: 2.5% and 1.5%. To consider a relatively high seismic hazard, the buildings were supposed located in Los Angeles, CA, on a class C site, resulting in seismic design category D, according to ASCE/SEI 7-16 [5]. The braces were designed to bend in the plane of the frame using a knife-plate to gusset-plate connection. The eccentricity was achieved by means of side-plated assemblies linking the bracing members to their connections to the frame beam-to-column joints, designed following constructive and cost-effectiveness criteria. To allow for the comparison of costs and structural performance, conventional Special CBFs were also designed for the same conditions. The performance of all resulting frames under seismic action was assessed numerically through Non-Linear Response-History Analyses (NLRHA) on fiber-based models in OpenSees [6].

2.2. CHARACTERIZATION OF BIES

2.2.1. Components of BIEs

The essential components of a nonspecific BIE are presented schematically in Figure 2.1. The eccentricity, e, is defined as the parallel offset between the axis of the bracing member and the line connecting the frame's working points, which would normally coincide with the frame diagonal. The eccentricity is introduced by assemblies that transfer rigidly the axial loads between the working points and the bracing member, hereon designated as *eccentering* assemblies. Beyond their length, L_{ea} , the specific design of the *eccentering* assemblies does not have a significant effect on the response of the BIE provided that they can be assumed to behave as rigid bodies linking the bracing member to its connection to the rest of the structure. Examples of *eccentering* assemblies are those tested by Skalomenos et al. and the ones considered in this research, which are described further below. The total, or hinge to hinge, length of the BIE is L.

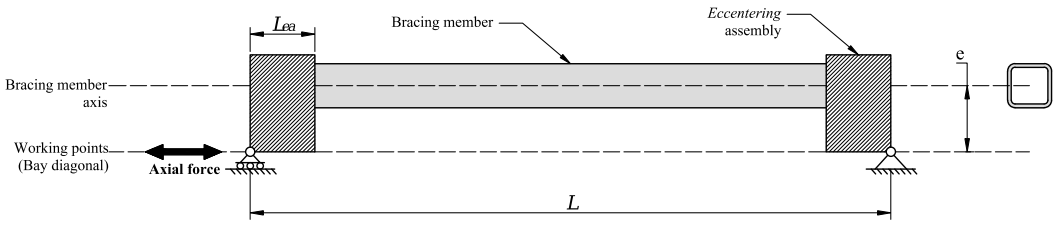

Figure 2.1: Schematic drawing of a nonspecific BIE and its components

2.2.2. Modelling of BIE response

In this research, the OpenSees platform is the main resource used to model BIEs and to study their response and the effects of the different variables involved. OpenSees allows for the construction of fiber-based finite element frame objects incorporating the specified material stress-strain curve and force-deformation hysteretic parameters at the fiber level and, as such, allows for the explicit representation of distributed plasticity. The software is also capable of handling geometric nonlinearity and is therefore well suited to reproduce the global response of steel frames with elements under flexural compression, including buckling of braces. OpenSees has been used extensively in research on steel frame structures and its suitability for these purposes has been demonstrated in many publications [7, 8]. Since the published data on the numerical modelling of BIEs is scarce, the authors verified the applicability of OpenSees for BIEs by programming models of the tests described in Skalomenos et al. and verifying that the numerical results were in reasonable agreement with the published test results.

Fiber-based finite element models, however, possess the limitation of being unable to capture localized phenomena such as local buckling, which is of great relevance as an indicator of the imminent failure of HSS brace members. Therefore, the OpenSees analyses are complemented in this research with shell-based finite element models in the commercial software Abaqus [9] when there is need to explicitly capture the onset of local buckling, as is explained in Section 2.2.7. The suitability of Abaqus for this purpose has also been demonstrated in the literature [10].

2.2.3. Monotonic force-deformation behaviour of BIEs

The kinematic response of BIEs, which was described in Skalomenos et al., and is here anew summarized, relies on the assumption that the connections at the ends of the *eccentering* assemblies behave as pins. In practice, this can be reasonably approximated by employing ductile connections detailed to yield in flexure at low levels of axial load such as those commonly used in CBFs. The idealised general behaviour of BIEs under tensile (a) and compressive (b) monotonic load, compared to that of CCBs, is presented in Figure 2.2. Due to the eccentric loading, bending moments develop at its ends with initial magnitude equal to the product of the force and the prescribed eccentricity. Under tensile load, the BIE bends toward the working point axis as it elongates and, since the moment arm across the brace length decreases as the loading progresses, the effective stiffness increases with the axial deformation until the outermost fiber in tension attains the yielding stress, F_y. The corresponding point on the curve, $T_y - \Delta_y$, marks a discontinuity on the force-deformation response, and is designated as the "first yield" point. As loading is continued beyond this stage, the plasticity extends through the cross-section and the BIE responds with a lower stiffness that, however, increases as the effective eccentricity keeps decreasing. The maximum tensile force developed by the BIE, T_u, is attained when the effective eccentricity where the bracing member meets the *eccentering* assembly reaches zero, thus allowing the full cross-section to yield in tension. Nearing this stage, depending on the magnitudes of e and L_{ea}, plastic hinges may develop where the brace ends meet the *eccentering* assemblies because bending of the HSS compensates the rotation of the *eccentering* assemblies in order to maintain the parallelism between the bracing member's axis and the frame diagonal. The maximum rotation demand on the HSS at that location, θ_{t_u}, can be estimated as $tan^{-1}(e/L_{ea})$. As shown in Figure 2.2 (a), the force-deformation backbone curve of BIEs in tension can be approximated with a tri-

linear model, as proposed in Skalomenos et al. An initial, or elastic, portion with stiffness K_i extends up to the "first yield" point, T_y, followed by a post-"first yield" portion, with secondary stiffness K_s, limited by the ultimate yield point, T_u. This is trailed by a final segment, comprising the fully yielded section, that extends until the brace eventually fractures.

When compressive load is applied, the BIE bends away from the working point axis and the increment of the brace deflection entails a progressive reduction of the stiffness, as the effective eccentricity at the brace mid-length increases. As proposed by Skalomenos et al., the maximum force developed in compression, C', can be approximated by the load corresponding to the elastic limit state of a column subjected to eccentric axial load, using, Equation (2.1) where P_{cr} is Euler's buckling load, A is the cross-section's area and S is the section modulus.

$$C' = \frac{F_y A}{1 + \dfrac{eA}{S\cos\left(\dfrac{\pi}{2}\sqrt{\dfrac{C'}{P_{cr}}}\right)}} \tag{2.1}$$

In contrast with CCBs, in BIEs the maximum force in compression does not manifest as a sharp peak in the force-deformation curve. Instead, their response transitions smoothly from elastic to inelastic post-buckling behaviour. As such, the backbone curve of BIE response in compression can be idealised as elastic-perfectly plastic, with initial stiffness K_i and maximum force C' as shown in Figure 2.2 (b). As the deformation progresses, a plastic hinge develops at the brace-mid-length where the strain demand concentrates. As it will be explained, the set composed by T_y, T_u, C', K_i, and K_s comprises the relevant parameters used for design, which depend on the length, cross section and eccentricity of the BIE.

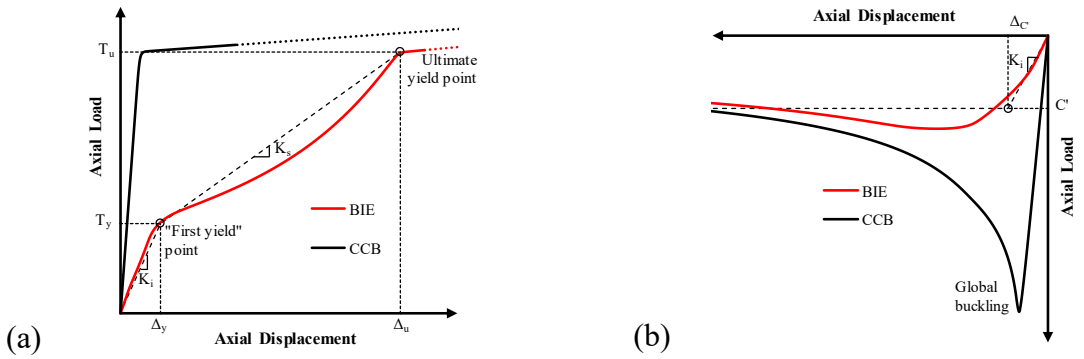

Figure 2.2: Compared BIE and CCB idealised monotonic force-deformation behaviour: tension (a) and compression (b) (not to scale)

The effects of the eccentricity magnitude on the BIE's monotonic response can be observed in Figure 2.3, which, as an example, presents the results of analyses carried out in OpenSees on models of BIEs of an ASTM A1085 HSS 178×178×16 for different levels of eccentricity under monotonic tensile (a) and compressive (b) loading. The length of the BIE for these models was 5408 mm, including *eccentering* assemblies modelled as 360 mm long rigid links. The end connections were modelled as 38.1 mm thick plates with a width of 360 mm and a clearance of 77 mm to allow for unrestrained plastic rotation and to resist the force associated with the probable brace resistance in tension. The design is consistent with that of a BIE intended for a 6 m wide by 4 m tall braced bay considering a knife plate to gusset plate end connection producing in-plane bending of the BIEs, as is discussed below. A nominal yield stress of 345 MPa was considered both for the plates and the HSS for these analyses. Referring to the idealized models of BIE response described above, the relevant values for design, i.e. T_y, T_u, C', K_i, and K_s can be obtained from such analyses. Table 2.1 presents this set of parameters, as obtained from the curves shown in Figure 2.3. In general, for a given section BIE, T_y, C', K_i, and K_s will decrease as a function of the eccentricity, resulting in an increase of the deformations associated with "first yield" and ultimate yield. The ultimate yield force, T_u, does not depend on the eccentricity, as it is a function of the section's gross area and material yield stress.

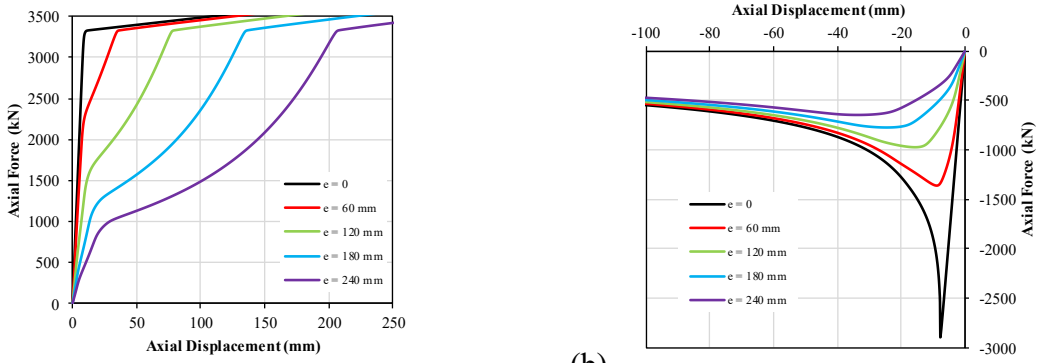

Figure 2.3: Influence of eccentricity on the force deformation of HSS 178×178×16 BIEs with L=5408 mm and L_{ea}=360 mm: tension (a) and compression (b)

Table 2.1: Example of relevant design values as a function of eccentricity for HSS 178×178×16 BIEs with L=5408 mm and L_{ea}=360 mm

Eccentricity, e, (mm)	"First yield" force, T_y, (kN)	Ultimate yield force, T_U, (kN)	Compressive resistance, C', (kN)	Initial stiffness, K_i, (kN/mm)	Secondary stiffness, K_s, (kN/mm)
0	-	3325.8	1788.3	356.5	-
60	2088.1	3325.8	1032.7	271.2	44.8
120	1471.2	3325.8	716.1	136.2	27.6
180	1135.8	3325.8	554.9	69.7	18.4
240	926.2	3325.8	454.9	39.4	13.1

Taking the horizontal components of the axial forces obtained for the analyses shown in Figure 2.3 and summing them, one obtains the storey shear force that two contiguous braced frames with bracing members such as described above acting in opposite directions would produce when subjected to horizontal displacement at the top, as presented in Figure 2.4. Note that in contrast with the CCBs (i.e. e = 0), the storey shear response of the BIEs with significant eccentricities working in pairs increases continuously with the displacement; there is no peak corresponding to buckling of the compression brace and subsequent drop in storey shear capacity. As is discussed below, the eccentricity to bracing member section depth ratios (e/H) that commonly result from the use of the design procedure herein described are larger than 0.66, and therefore the shear – deformation stiffness of the BIE pairs is continuously positive.

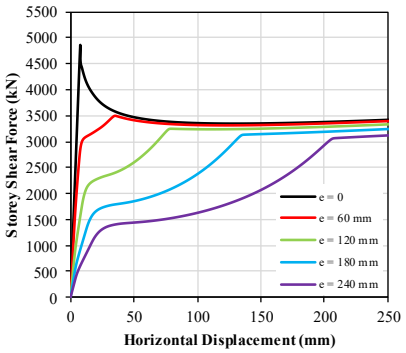

Figure 2.4: Influence of eccentricity on the storey shear vs. top displacement response for two contiguous 6 m by 4 m bays with HSS 178×178×16 BIEs acting in opposite directions.

2.2.4. Influence of the *eccentering* assemblies' length

The length of the *eccentering* assemblies, L_{ea}, plays a significant role on the force-deformation response of BIEs in tension, and should thus be incorporated explicitly in any BIE model. Firstly, the bending moments that develop on the bracing members' ends and how they evolve as the brace elongates and bends toward the working point axis depend on the dimensions of the *eccentering* assemblies. For a given eccentricity, an increase of L_{ea} implies a reduction of the maximum rotation demand, θ_{t_u}, thus decreasing the displacement required to annul the eccentricity and reach the ultimate yield point. Also, supposing that the total length, L, remains unchanged, an increase of L_{ea} results in a reduction of the length of the deformable bracing member, and therefore in an increase of the axial stiffness of the BIE. An example of this can be observed in Figure 2.5 (a), which presents the monotonic force-deformation curves in tension for a set of BIE models with varying L_{ea}. The values of K_i and K_s, and hence the "first yield" and ultimate yield deformations, depend on the length of the *eccentering* assemblies. The response in compression, however, is not significantly affected by the magnitude of L_{ea}, as Figure 2.5 (b) shows, presumably because the stiffness of the compression response mainly depends on the rotational rigidity of the mid-length region and the end connections.

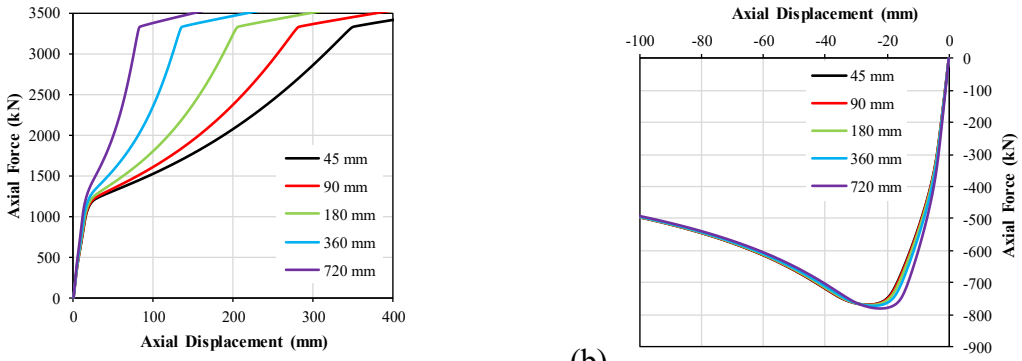

Figure 2.5: Influence of L_{ea} on the force-displacement response of HSS 178×178×16 BIEs with L=5408 mm and e=180 mm: tension (a) and compression (b)

2.2.5. Influence of residual stresses and in section variation of F_y of BIEs

Due to their fabrication process, which involves rolling and cold working, HSSs contain residual stresses and present a variation of the yield stress, F_y, across their cross section. Koval [11] presents a thorough review of the available research on the topic and proposes a model of the distribution of the residual stresses and yield stress gradient over the thickness and the perimeter of rectangular HSSs, applicable to fiber elements models in OpenSees. A comparison of the monotonic force-deformation response of an OpenSees BIE model that neglects the residual stresses and yield stress gradient against one that includes these effects using Koval's model is presented in Figure 2.6. In the latter, only the variation of the residual stresses across the thickness was considered, as it was shown by Koval that the variation across the perimeter exerts no significant influence on an HSS's force-deformation response. Considering the nominal value for F_y of 345 MPa, the net yield stress on the model with the effects was uniformly scaled so that both models had an equal ultimate tensile strength. As can be seen, the effects of the residual stresses and yield stress gradient do not modify considerably the response in monotonic tension, producing only slight changes to the shape of the curve and to the displacements corresponding to "first yield" and ultimate yield. In

compression, the inclusion of the effects results in an even smoother transition from the elastic to the post-buckling regimes.

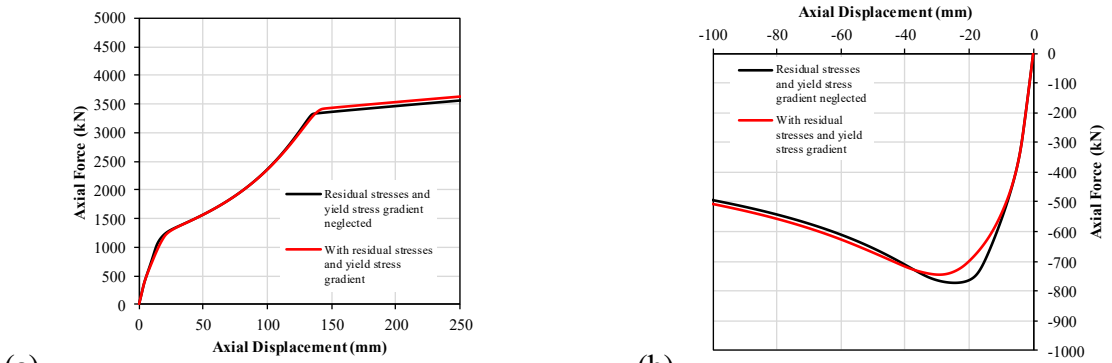

(a) (b)

Figure 2.6: Influence of yield stress gradient and residual stresses on the force-displacement response of HSS 178×178×16 BIEs with L=5408 mm and e=180 mm: tension (a) and compression (b)

2.2.6. Response of BIEs to cyclic loading

The axial force vs. lateral drift hysteretic plots of an ASTM A1085 HSS 178×178×16 BIE with an eccentricity of 180 mm, and a CCB of the same section, are presented in Figure 2.7 (a). The resulting storey shear vs. lateral drift plots that would result from pairs of such braces acting in opposing directions in adjacent bays are shown in Figure 2.7 (b). The data were obtained from OpenSees analyses where the brace dimensions and components were, again, defined assuming a 6 m wide by 4 m tall braced bay. A loading protocol with symmetrical cycles of increasing equivalent storey drift amplitude of 0.1, 0.25, 0.75, 1.0, 1.5, 2 and 3% was followed. In Figure 2.7 (a), it can be noted how, in contrast with the CCB, the BIE exhibits a significant secondary (post "first yield") stiffness in tension with the maximum load increasing at each cycle, while in compression the maximum load stabilizes at the post-buckling force level. These properties are conserved when two braces act jointly, as seen in Figure 2.7 (b).

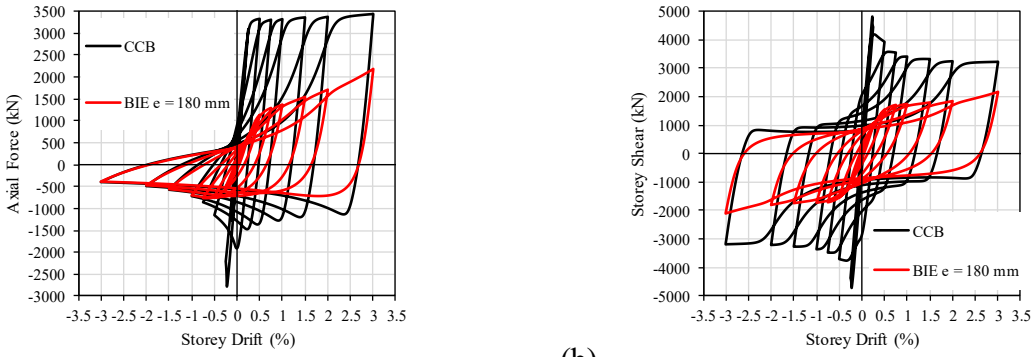

(a) (b)

Figure 2.7: Single brace axial force vs. lateral drift (a) and storey shear vs. lateral drift (b) for HSS 178×178×16 CCBs and BIEs with e = 180 mm under cyclic load.

2.2.7. Fracture life of BIEs

As for conventional braces, low-cycle fatigue fracture, triggered by local buckling, presumably governs the failure mode of HSS BIEs. However, the physical tests by Skalomenos et al. showed that the introduction of eccentricity delays the onset of local buckling at the brace mid-length in terms of axial displacement or equivalent inter-storey drift ratio. This is explained by the strain demands being more evenly distributed along the brace length due to the presence of bending from the onset of loading. To generalize these findings to BIEs made with square HSSs commonly used in North America, i.e. ASTM A1085 HSSs, the authors performed a parametric study based on 243 individual finite element BIE models in Abaqus based on standard commercially available sections and dimensioned assuming the use of the braces in a 6 m by 4 m braced bay. The considered variables were the global (L/r) and local (b/t) slenderness ratios and the eccentricity ratio, defined as the specified eccentricity divided by the section height, $e_0 = \frac{e}{H}$. Given the lack of available data necessary to adequately calibrate a material damage model to capture low-cycle fatigue fracture in BIEs, the onset of local buckling at the brace mid-length was regarded as an indicator of imminent failure. It has been shown in previous research on HSS braces [1, 2, 12] that once local buckling occurs, the brace will likely fracture in the subsequent tension excursion. The BIE models in the study were subjected to reversed cyclic loading with increasing displacement

amplitude; the drift ratio of the cycle with maximum amplitude that the BIE could sustain before developing local buckling was reported as the maximum allowable drift ratio, θ_{md}. The maximum drift ratio amplitude in the load protocol was 5%; this value was reported for the models that did not show local buckling during the analyses. As expected, the results illustrate that the fracture life of BIEs increases with the eccentricity, the global slenderness and the stockiness of the section. A multiple regression analysis was then applied to obtain an expression to estimate θ_{md} as a function of e_0 and a combined slenderness ratio: $\lambda_0 = \frac{Lt}{rb}$, given in Equation (2.2). The data point scatter and the surface corresponding to the obtained function are shown in Figure 2.8. It must be noted, however, that the appropriateness of the proposed equation is yet to be validated by contrasting the drift ratios at the onset of local buckling it predicts, against actual results from physical testing of BIE specimens.

$$\theta_{md} = -0.4312 + 0.1943\lambda_0 + 0.6704e_0 - 0.001319\lambda_0^2 - 0.01833\lambda_0 e_0 + 0.241e_0^2 \qquad (2.2)$$

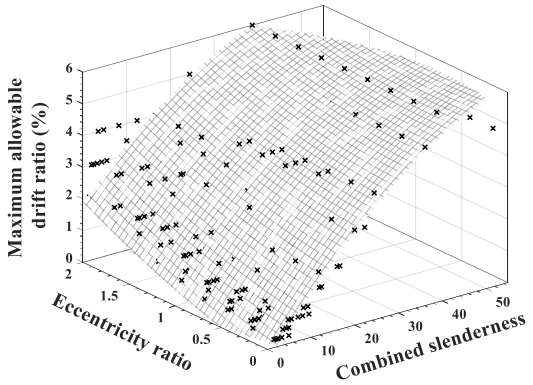

Figure 2.8: Maximum allowable drift ratio vs. eccentricity ratio and combined slenderness

2.2.8. Energy dissipation capacity of BIEs

In comparison with CCBs, a larger amount of energy is required to reach the tensile yield strength of BIEs. This is due to the additional energy required to straighten the bracing member and annul the eccentricity. In Figure 2.9, the total energy required to attain T_u, disaggregated into its axial

and flexural components, is presented for an ASTM A1085 HSS 152×152×13 BIE with different levels of eccentricity. To construct this plot, first the energy required to attain T_u for a perfectly straight brace was obtained from an analysis under monotonic load in OpenSees. This energy is thus associated with the axial elongation of the brace (blue part of the bars in Figure 2.9). Then, the analysis was replicated for increasing e/H ratios, and the difference in the total energy with respect to the concentric model is assumed to be associated with bending (red part of the bars). As expected, the flexural energy increases with the eccentricity, whereas the axial energy does not vary. However, as the eccentricity is increased, the displacement required to reach T_u increases accordingly. As such, although it would be impractical to fully benefit from the maximum theoretical energy dissipation capacity of BIEs in design, as the displacement involved could be excessive. However, one could still benefit from part of the additional energy dissipation by performing a design oriented towards the BIEs attaining a predetermined and practical, drift or displacement target under seismic action. The energy dissipation capacity at the target displacement could then be exploited in design through an equivalent damping ratio.

The equivalent damping ratio, ξ_{eq}, quantifies the net damping capacity of a dissipative system under cyclic loading for a given loading cycle accounting for all the energy-dissipating mechanisms involved [13]. ξ_{eq} can be obtained from Equation (2.3), where E_d is the area enclosed by the force-deformation curve for the cycle of interest, and F_m and Δ_m are respectively the maximum force in the cycle and the displacement amplitude.

$$\xi_{eq} = \frac{E_d}{2\pi F_m \Delta_m} \tag{2.3}$$

Skalomenos et al. presented the equivalent damping ratios, ξ_{eq}, obtained for their test specimens at each drift level. It was shown that although the maximum values of ξ_{eq} were not significantly

affected by the eccentricity, the drift ratio at which they occurred varied notably as the yield displacement changed with the eccentricity. Preliminary data collected from numerical analyses performed by the researchers on BIEs have shown that, indeed, there is no clear correlation between the eccentricity and the net energy dissipation capacity. Further, the eccentricity has no notable effect on the equivalent damping ratio as a function of the ductility demand. The ductility demand is defined as the ratio between the cycle amplitude and the drift corresponding to the "first yield" point of the BIE. An example of this behaviour is presented in Figure 2.10 for ASTM A1085 HSS 152×152×13 BIEs, in which it can be observed that for eccentricity ratios equal to 1.0 or larger, the maximum value for ξ_{eq} and the associated ductility demand are practically constant.

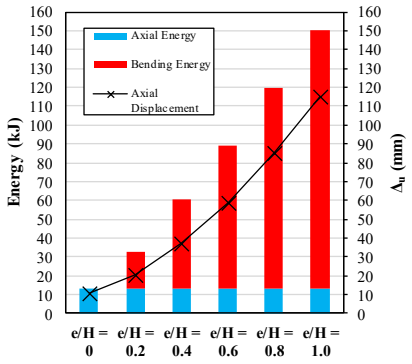

Figure 2.9: Energy input and axial displacement required to reach T_u under monotonic loading for HSS 152×152×13 BIEs with L=5408 mm and L_{ea}=305 mm

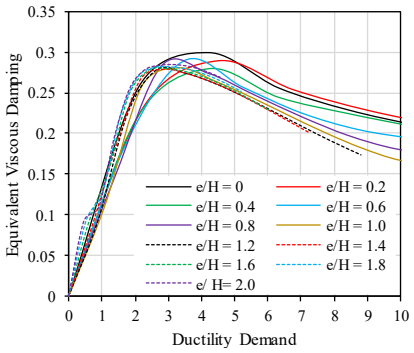

Figure 2.10: ξ_{eq} vs. ductility demand for HSS 152×152×13 BIEs with L=5408 mm and L_{ea}=305 mm

2.2.9. Sensitivity to member out-of-straightness

While in CCBs the member out-of-straightness plays an important role on the brace buckling strength, in BIEs, given that their responses in compression and in tension encompass an inherent flexural component, the effect of the member imperfection is overshadowed by that of the eccentricity. Depending on whether the out-of-straightness increases (positive out-of-straightness) or decreases (negative out-of-straightness) the effective eccentricity, it may entail an increment or decrement in the BIE strength and stiffness. As positive out-of-straightness increases, the effective

eccentricity at mid-length, the values of K_i, K_s, C', and T_y decrease accordingly. Conversely, with negative out-of-straightness those values increase. Numerical analyses carried out by the authors to study the influence of member out-of-straightness on the monotonic and cyclic response of BIEs indicate that the effects of out-of-straightness smaller than $\pm$ $L/1000$, the fabrication tolerance in North American codes [14, 15], are negligible. Figure 2.11 presents the change of the compressive strength of BIEs as a function of the out-of-straightness with respect to the compressive strength of a perfectly straight BIE, C'_0, as obtained from OpenSees models of BIEs with different global slenderness and eccentricities. The results show that the influence of the out-of-straightness is greater for smaller eccentricities and larger slenderness; however, for out-of-straightness within the $\pm$ $L/1000$ tolerance, which corresponds with the region highlighted in gray in Figure 2.11, the differences are within ± 5%.

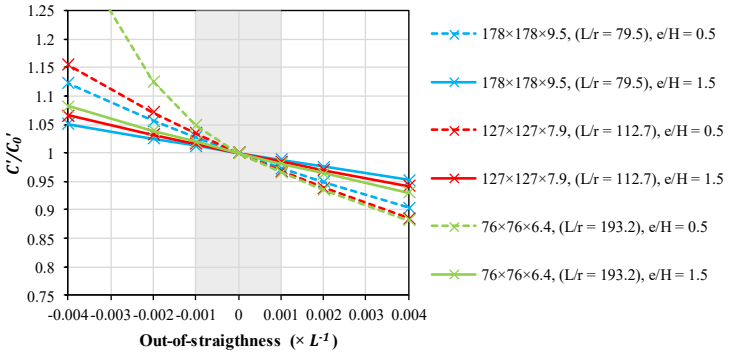

Figure 2.11: Change of the compressive strength of BIEs as a function of the out-of-straightness, with respect to the compressive strength of a perfectly straight BIE

2.3. DESIGN PROCEDURE FOR FIEBs

As shown in the previous section, BIEs present a particular force-deformation behaviour that makes them stand out from traditional dissipative elements used in SFRSs, such as CCBs, moment frame connections or eccentrically braced frame links, among others. The monotonic response of common SFRSs can be reasonably approximated by elastic-perfectly plastic models; they respond

elastically until they reach their yield resistance, at a relatively low displacement or rotation, and then, if the loading is continued, they deform plastically with the force or moment remaining at an essentially constant level until fracture. Considering this, traditional dissipative elements are well suited for the force-based design methods that most modern design codes wield; they can be dimensioned by equating their yield strength to the seismic demand resulting from an elastic analysis, in which the force level is reduced to account for ductile response and overstrength. In the case of BIEs, however, the maximum capacity in tension is attained at variable deformation levels that depend on the eccentricity and that might even be larger than the maximum inter-storey drift ratios allowed by the design codes, e.g. 2.0% in ASCE/SEI 7-16 for buildings over 4 storeys high and 2.5% for buildings with 4 or fewer storeys. Furthermore, BIEs' secondary stiffness is significant and also varies with the eccentricity, the section properties and the brace geometry, making both the elastic-perfectly plastic idealisation and the use of a ductility related seismic force reduction factor unfitting.

Given these considerations, the use of a displacement-based design method, allowing for the explicit consideration of the force the BIEs develop as a function of the axial displacement, appears as a rational course of action. Specifically, an adaptation of the Direct Displacement-Based Design method (DDBD) [16], is here employed. In past research, the appropriateness of the DDBD approach for the seismic design of multiple types of structures, including CBFs [17, 18], has been demonstrated; the results presented in this paper can be considered a verification of its applicability to FIEBs. In the following sections, a description is given of the steps of the adapted design procedure as used in this research. For general information on the DDBD method, refer to [16].

2.3.1. Selection of design target storey drift and displacement vector and calculation of associated equivalent mass and equivalent displacement

In DDBD, the target displacement vector generally corresponds to the inelastic first mode shape of the structure and, as such, is specific for the structural system and the height of the building. It is important to note this target displacement vector is a design assumption that does not necessarily reflect the distribution of anticipated maximum storey displacements, as it does not account for the effects of higher modes or the reversing nature of earthquake demands. Expressions are available to approximate the inelastic first mode shape of various traditional structural systems, but in the case of FIEBs, none are yet available as the research on the new structural system is incipient. Moreover, the formal calibration of such expressions requires a considerable amount of data and work which, in the authors' opinion, will be justified at a later stage once the potential of the new system will have been established.

In this research, the inelastic first mode shape proposed by Priestley et al. [16] for moment frames, given in Equation (2.4) is used. Although expressions developed for CBFs exist, such as the one presented by Al-Mashaykhi et al. [19], and arguably that system bears more similarities to the proposed system than moment frames, analyses by the authors have shown that the inelastic first mode shape of FIEBs is in fact closer to the shape obtained with Equation (2.4) than to that obtained with the expressions for CBFs. An example of this is presented in Figure 2.12. A proposed explanation for this observation is that, given that BIEs are naturally less stiff than CCBs, the displacement profile of FIEBs is closer to that of an ideal shear building, in contrast with CBFs where the contribution to the deformed shape of the axial deformations of the columns in more significant. In Equation (2.4), n is the number of storeys, H_i and H_n are the elevations of the ith and top storeys and δ_i is the normalised lateral displacement of the ith storey.

$$n \leq 4: \qquad \delta_i = \frac{H_i}{H_n}$$
$$n > 4: \qquad \delta_i = \frac{4H_i}{3H_n}\left(1 - \frac{H_i}{4H_n}\right) \tag{2.4}$$

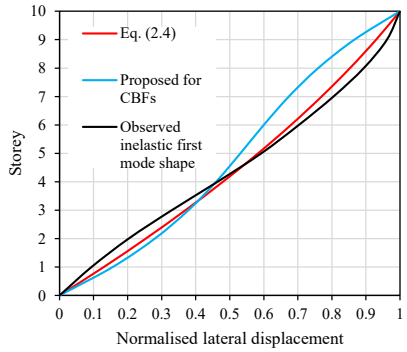

Figure 2.12: Observed inelastic first mode shape of a 10 storey FIEB, compared with predicted inelastic first mode shapes for moment frames and CBFs

The normalised displacement vector obtained with Equation (2.4) is then scaled to produce the selected lateral design drift of the critical storey, which is the first storey for buildings 5 storeys and taller, to obtain the storey design displacements, d_i, which, along with the storey masses, m_i, are used in the calculation of the displacement (Equation (2.5)) and mass (Equation (2.6)) of the equivalent Single Degree of Freedom System (SDOF) at the design level.

$$\Delta_{eq} = \frac{\sum d_i^2 m_i}{\sum d_i m_i} \tag{2.5}$$

$$M_{eq} = \frac{\sum d_i m_i}{\Delta_{eq}} \tag{2.6}$$

2.3.2. Determination of equivalent damping ratio and target period

The target period, T_{eq}, is obtained from the damped displacement design spectrum by reading the ordinate corresponding to Δ_{eq}. To do so, however, the equivalent viscous damping ratio, ξ_{eq}, used to reduce the displacement spectrum must first be defined. In the same manner as for the

displacement vector, no models exist yet for the estimation of the equivalent viscous damping of FIEBs in the context of DDBD. The formal development of such models remains for the moment out of the scope of this exploratory investigation. In lieu of that, the models proposed by Wijesundara et al. [20] for the equivalent damping ratio of CCBs as a function of the member's non dimensional slenderness, λ, and the ductility demand, μ, given by Equation (2.7) are used. This approach is considered acceptable since, as is explained in the previous section, for BIEs, ξ_{eq} as a function of μ is not sensibly affected by the variation of the eccentricity level and because, as is shown below, the results obtained using this approach are satisfactory.

$$\begin{aligned} \mu \leq 2: \qquad & \xi_{eq} = 0.03 + \left(0.23 - \frac{\lambda}{15}\right)(\mu - 1) \\ \mu > 2: \qquad & \xi_{eq} = 0.03 + \left(0.23 - \frac{\lambda}{15}\right) \\ & \lambda = \frac{L}{r}\sqrt{\frac{F_y}{\pi^2 E}} \end{aligned} \tag{2.7}$$

Equation. (2.7) gives ξ_{eq} for a pair of identical braces acting together in opposite direction. Thus, assuming that only one type of BIE is used per storey, the average value from all storeys is used to obtain the design ξ_{eq} of the FIEB, which is then used to reduce the base displacement spectrum through the damping correction factor, R_ξ. In this research, the damping correction factor recommended by Eurocode 8 [21], given by Equation (2.8) is used. The base design displacement spectrum, S_d, is obtained by applying Equation (2.9) to the 5% damping elastic design acceleration spectrum, S_a.

$$R_\xi = \sqrt{\frac{0.1}{0.05 + \xi_{eq}}} \tag{2.8}$$

$$S_d = S_a \frac{T^2}{4\pi^2} \tag{2.9}$$

2.3.3. Calculation of target "primary" target secant stiffness, associated base shear and equivalent static force vector

Having obtained T_{eq}, the target "primary" secant stiffness, K_{eq}, can be calculated with Equation (2.10). The authors refer to this stiffness as "primary" since it is directly associated with the target spectral displacement of the equivalent SDOF system. Additional "auxiliary" stiffness might also need to be provided to the FIEB to comply with stability and regularity criteria, as explained below. The primary base shear, V_{eq}, is obtained by multiplying K_{eq} by Δ_{eq} (Equation (2.11)), and subsequently can be distributed as the corresponding storey lateral forces, F_i. In this research, the distribution of storey forces is performed as per Clause 12.8.3 of ASCE/SEI 7-16 (Equations (2.12) and (2.13)); however, instead of the initial period, T_{eq} is used to compute the exponent k in acknowledgment of the structure's anticipated condition at the design level. In Equation (2.13), for structures with T_{eq} < 0.5 s, k = 1; for structures with T_{eq} >2.5 s, k = 2; and for structures with T_{eq} between these two values, k is interpolated linearly.

$$K_{eq} = 4\pi^2 \frac{M_{eq}}{T_{eq}} \tag{2.10}$$

$$V_{eq} = K_{eq}\Delta_{eq} \tag{2.11}$$

$$F_{eq,i} = C_{vi}V_{eq} \tag{2.12}$$

$$C_{vi} = \frac{W_i h_i^k}{\sum_{i=1}^{n} W_i h_i^k} \tag{2.13}$$

2.3.4. Selection of BIEs for each storey, providing capacity equal to the *design shear* at the design displacement level and complying with regularity and stability criteria

At each storey, the BIEs, in terms of a section-eccentricity pair (e.g. HSS 178×178×16 – e = 230 mm) are selected such that the storey shear capacity they provide at the target storey displacement, d_i, is equal to the *design shear*. The storey *design shear*, $v_{d,i}$, given by Equation (2.14), is defined as the sum of the equivalent primary storey shear, $v_{eq,i}$ (i.e. the cumulated effects of the forces $F_{eq,i}$ above storey i obtained from step 3), and the notional loads, $v_{n,i}$, amplified by a factor accounting for the P-Δ effects which, given that FIEBs are relatively flexible structures, if not addressed in the design might induce a reduction of the effective stiffness of the structure as it evolves toward the design displacement. In this paper, the magnitude of the notional loads applied corresponds to 0.002 times the factored gravitational loads, $C_{f,i}$, as per clause C2.J.2b of ANSI/AISC 360-16 [14]. The amplification factor used to account for the P-Δ effects at the design level, $U_{2,i}$, is based on that of CSA S16-14 Clause 27.1.8.2 [15], given by Equation (2.15), where v_i^* is the storey shear capacity of the chosen section-eccentricity pair at the design displacement level. This amplification factor is preferred over that given by clause 12.8.7 of ASCE/SEI 7 as it compensates the loss of storey shear resistance due to P-Δ effects at the expected displacement.

$$v_{d,i} = U_{2,i}(v_{eq,i} + v_{n,i}) \tag{2.14}$$

$$U_{2,i} = 1 + \left(\frac{C_{f,i} d_i}{v_i^* h_i}\right) \tag{2.15}$$

The selection of the BIE section-pairs can rely on simplified models of the monotonic behaviour of the BIEs in tension and compression, such as those described in Section 2.3 (cf. Table 2.1).

These can be obtained from numerical analyses under monotonic load performed on fiber-element models based on the design properties of the material (i.e. F_y), and considering the actual dimensions the BIE will have in the braced bent, in particular its total length, L, and the length of the *eccentering* assemblies, L_{ea}. To ensure that the resulting FIEB indeed attains safely the intended displacement levels, the fracture life of the selected section-eccentricity pairs needs to be considered. This can be performed by verifying that the allowable drift, calculated with Equation (2.2), is at least 50% higher than the design drift to include a safety margin.

In addition to providing sufficient capacity to satisfy the *design shear*, the BIEs shall also comply in each storey with minimum stability and regularity criteria to favour an adequate response of the structure. To prevent geometric instability, the ratio of effective lateral stiffness to counterbalancing geometric stiffness at the design displacement level should be at least 1.5, as through several preliminary evaluations, the authors have found that satisfying this limit reduces the probability of collapse due to geometric instability. Similarly, it was found that, to avoid soft-storey mechanisms and concentrations of shear demands in particular storeys, a smooth variation of the storey stiffness over the height of the building is required. To achieve this, the vertical stiffness criteria of the National Building of Canada 2015 [22] is observed; the lateral stiffness at any storey is no less than 70% of any adjacent storey or 80% of the average stiffness of the three storeys above or below.

2.3.5. Design of the protected members of the FIEB to withstand elastically the probable forces imposed by the action of the BIEs

To ensure the conditions for the BIEs to fully develop their intended axial force vs. deformation hysteretic response at the design level and beyond, Capacity-Based Design principles are observed. Thus, the non-dissipating members of the FIEBs, i.e. beams, columns, connections and

foundations are treated as protected members. As such, they are provided with enough resistance to respond elastically to the forces imposed by the inelastic action of the BIEs. Given that the forces developed by the braces depend on the storey drift level, the probable forces are calculated assuming storey drifts 50% higher than the design drift in anticipation of ground motions more intense than those associated with the design level. To consider the probable difference between nominal and real material properties, the brace forces are further augmented by the R_y factor corresponding to the brace member's expected material strength. In the case of ASTM A1085 HSS members, R_y = 1.25 as per ANSI/AISC 341-16 [23]. As it was shown in Section 2.2.3, since the force-displacement behaviour of BIEs in compression can be approximated with an elastic-perfectly plastic model, there is no need to distinguish between buckling and post-buckling cases when analysing the forces imposed by the BIEs on the rest of the structure, as is the case for CCBs.

2.3.6. Assessment of the performance of the resulting design

To verify that the performance objectives are fulfilled, the seismic performance of the resulting building should be assessed employing a detailed analysis such as NLRHA. Also, the designer should verify that the structure satisfies service level states and all other relevant ultimate limit states, such as those including wind loading.

2.4. SEISMIC PERFORMANCE OF MULTI-STOREY FIEBs

To study the seismic performance of FIEBs and to verify the validity of the design procedure, 4-, 8-, and 12-storey prototype buildings based on the plan configuration shown in Figure 2.13 (a) were designed for target maximum drift ratios, θ_d, of 2.5% and 1.5%. The buildings were also designed as Special Concentrically Braced Frames (SCBFs) following ANSI/AISC 341-16 for the purpose of comparison with traditional braced frame systems. A braced frame configuration with

pairs of single diagonals acting in opposite directions in contiguous bays, as shown in Figure 2.13 (b) was selected. The braced frame designed and analysed corresponds to one of those situated along the longest dimension of the building. The columns' orientation was chosen so that in-plane deformations of the frame produced bending about their weak axis. The foundation restraints were considered as pins.

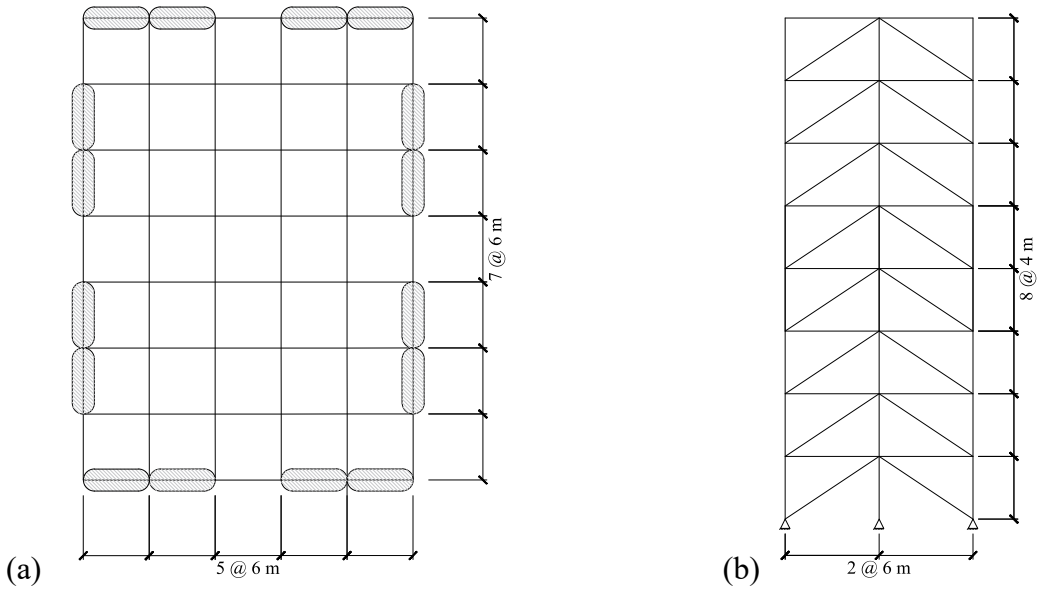

Figure 2.13: Plan configuration of considered prototype building (a), with highlighted regions indicating braced bents and vertical configuration of considered SFRS (b) (8-storey frame shown)

2.4.1. General design criteria

The buildings were located in downtown Los Angeles, CA, (34º05'N, 118º26'W) on a site class C. The general and seismic design criteria and requirements are those from ASCE/SEI 7-16 and the resulting seismic design category is D. The design of the FIEBs was performed following the procedure described above, while for the design of the SCBFs the Equivalent Lateral Force Procedure was employed, with a Response Modification Coefficient, *R*, of 6. The design seismic ground motion values were taken from the SEAOC/OSHPD Seismic Design Maps online tool (www.seismicmaps.org). The resulting Maximum Considered Earthquake (MCE_R) and Design-Level Earthquake (DE) acceleration response spectra along with their associated non-reduced

displacement response spectra, obtained with Equation (2.9), are presented in Figure 2.14. In consistency with the seismic design criteria of ASCE/SEI 7-16 (2017), the buildings were designed for the demands corresponding to the Design-Level Earthquake. To account for accidental eccentricity, a 10% increment to the acceleration spectra was applied based on the plan configuration of the building. The dead and live loads considered in the design, as well as the storey seismic masses, are given in Table 2.2. It was also assumed that the floor slabs present a 0.25 m overhang along the perimeter of the building and that the weight of the exterior wall was 1.5 kPa. Only dead, live and seismic loads were considered, wind loads were not included in this study. For the design of the beams and columns, the requirements for SCBFs from ANSI/AISC 341-16 were observed both for FIEBs and for SCBFs. It was defined that for all buildings the column section would change every three storeys (two in the case of the 4 storey buildings or the topmost storeys of the 8 storey buildings), while the lightest complying beam would be selected at each storey. Formal design of connections, optimization of sections regarding constructability, and assessment of the performance of the buildings under service-level earthquake loads were left out of the scope of the paper.

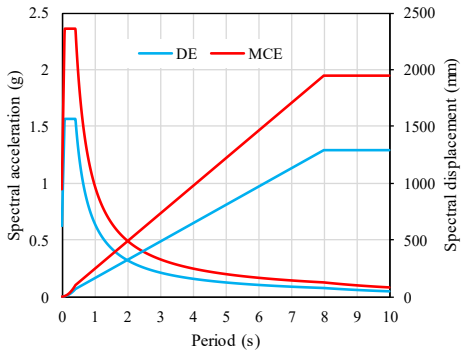

Figure 2.14: Acceleration and displacement design response spectra for the prototype buildings

Table 2.2: Design loads and seismic masses for prototype buildings

Storey	Dead load (kPa)	Live load (kPa)	Seismic mass (kN)
Roof	1.4	0.9	2188
All other storeys	4.1	2.4	6191

2.4.2. Bracing member design considerations

Given that, as explained previously, the BIE force-deformation models used in design need to correspond to the actual dimensions of the bracing member, it was defined that the total length of the bracing members would be 75% of the frame diagonal's length (i.e. 5408 mm). This dimension was selected and fixed at the beginning of the design process because the resulting free space was deemed sufficient to accommodate the final dimensions of the columns, beams, and connections that would result from the process. The connections to the frames consist of bolted gusset- and knife-plate arrangements designed to produce in-plane bending of the brace. The introduction of the eccentricity is achieved by means of two side-plates that link the HSS to the knife plate. The pin-like behaviour is assured by including a clearance of twice the knife-plate's thickness between the end of the *eccentering* assembly and its connection to the gusset plate. This configuration was adopted on account of its simplicity and to prevent the storey drifts from imposing in-plane bending moments on the BIEs other than those arising from the eccentricity, thus favouring a simpler and more predictable force-deformation hysteretic behaviour. It was also defined that both the length of the *eccentering* assemblies, L_{ea}, (i.e. the side plates) and the width of the knife-plates would be roughly twice the HSS height, rounded to the closest higher multiple of 5 mm. These dimensions were selected considering that L_{ea} should be such to allow the probable tensile force and moment produced at the bracing member's end to be transmitted through reasonably sized welds, first to the side plates and then to the knife-plate, and that the width of the knife plate should

be such that a reasonable plate thickness would result in order to grant a tension capacity at least equal to the probable tensile force, while having relatively low flexural stiffness. An example of the considered connection and *eccentering* assembly is shown in Figure 2.15. The behaviour and performance of the proposed arrangement, including whether the HSS can withstand the cyclic rotational demands it is subjected to, is to be investigated in a later stage of the research program and remains out of the scope of the present paper. In the case of CCBs, an analogous solution was considered but with the knife-plate slotted into the bracing member.

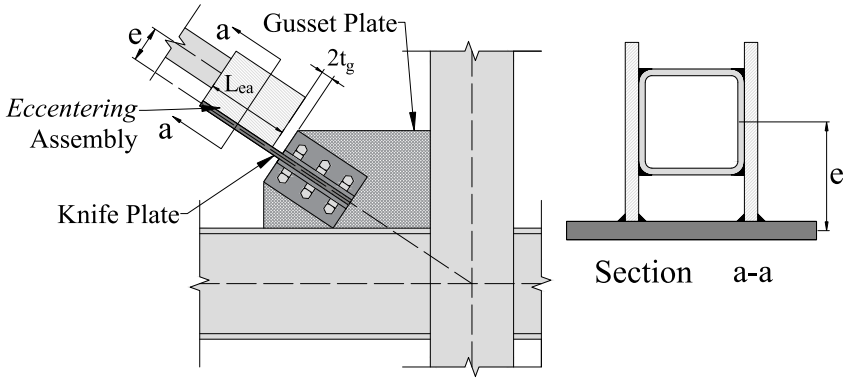

Figure 2.15: Example of considered BIE to frame joint connection and *eccentering* assembly

To make the section-eccentricity pair selection process described in Step 4 of the design procedure more efficient, a database containing the relevant design parameters for BIEs made from a wide array of commercially available HSSs was created. The database was prepared using OpenSees models based on the material's nominal mechanical properties (i.e. F_y = 345 MPa) and considering eccentricities ranging from null to three times the section height in 10 mm increments and the brace/*eccentering* assembly dimensions described above.

2.4.3. Resulting design

The resulting bracing members, beams and columns for all buildings are presented in Figure 2.16 through Figure 2.18. It can be noted for the FIEBs that the proposed design procedure, together with the intention of using the lightest allowable sections, favoured that instead of recurring to

frequent section changes along the building height for the bracing members, a gradually increasing eccentricity for a constant section would be preferred. In addition, the design procedure necessitated that identical section-eccentricity pairs be selected for several adjacent storeys to comply with all the proposed stiffness requirements, indicating that possibly it would have been beneficial to consider a smaller eccentricity increment, such as 5 mm, when preparing the design properties database. However, it is questionable whether such a small resolution in the specified eccentricity would be practical in a realistic fabrication context, considering workmanship and section production tolerances. It can be noted as well that the observed e_0 ratios do not present a wide variation with building height for a given drift ratio. In the buildings with θ_d=2.5%, the average e/H value varies between 1.07 and 1.28 while in the buildings with θ_d=1.5%, the observed values are between 0.71 and 0.99. As commented in Section 2.2.3, for these eccentricity ratios it is expected that the storey shear-deformation stiffness of the BIE pairs will be continuously positive.

The approximate steel tonnage is given in Table 2.3, broken down by beams and columns and bracing members. For all three building heights, the FIEBs with θ_d=2.5% present a lower tonnage than the equivalent SCBF, with the difference increasing with the building height. Although the net weight of the bracing members is slightly higher, the reduction in the protected members given the lower capacity-based design forces compensates and produces an overall lower weight. If design of the foundations had also been included, the difference between the two systems would be even greater. The FIEBs with θ_d=1.5%, however, were heavier than the SCBFs, with the difference becoming more significant at lower heights.

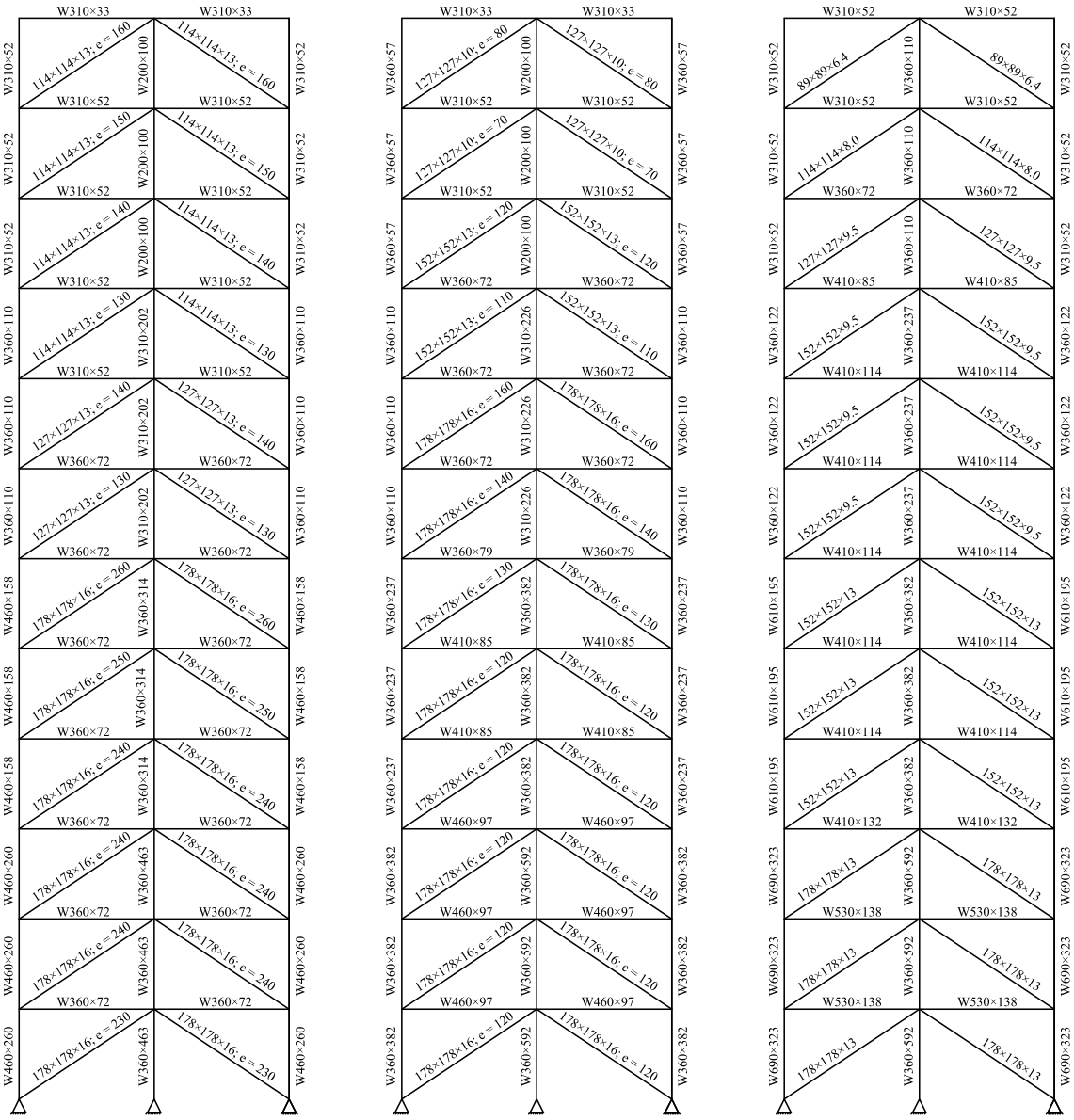

Figure 2.16: Resulting design for 12 storey buildings

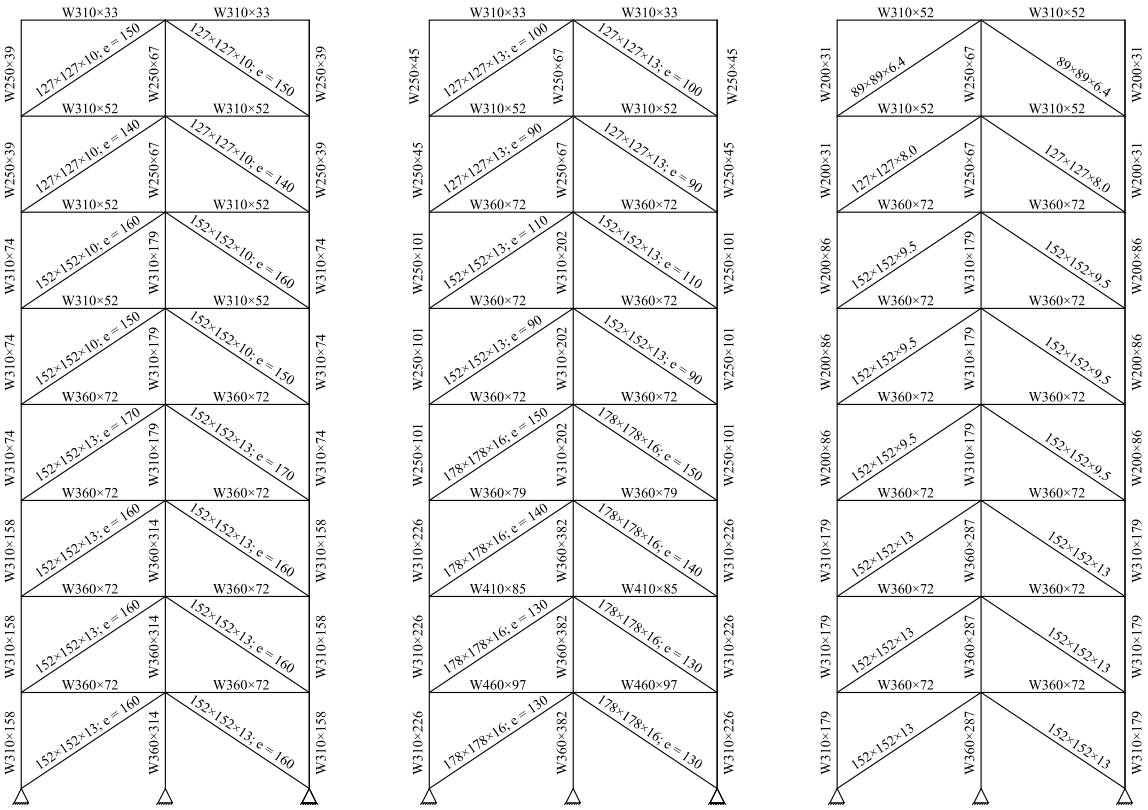

Figure 2.17: Resulting design for 8 storey buildings

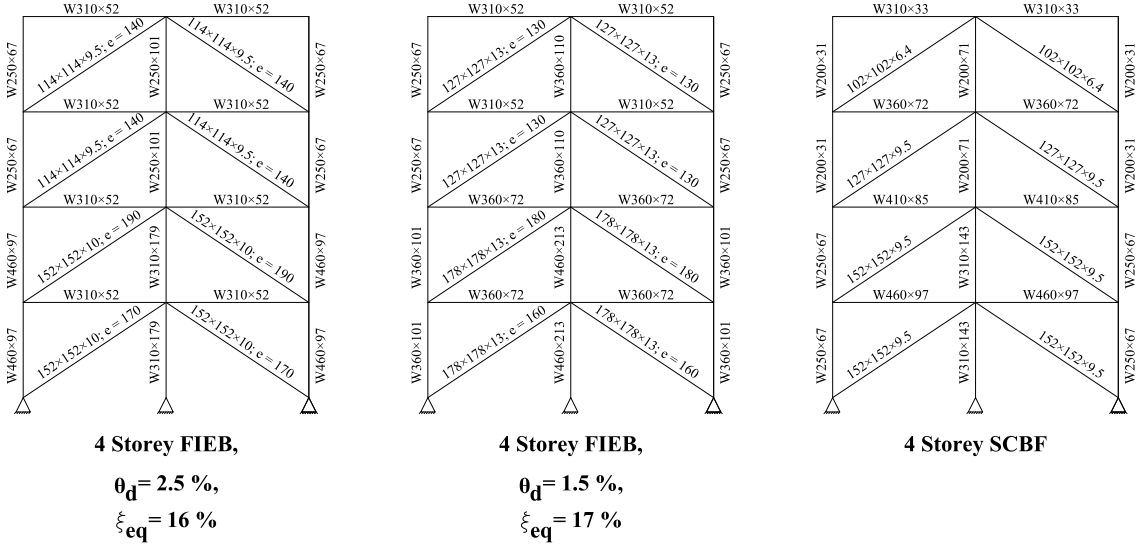

Figure 2.18: Resulting design for 4 storey buildings

Table 2.3: Steel tonnage per braced frame for the resulting designs

Building type	Beams and columns (t)	Bracing members (t)	Total weight (t)
12 Storey SCBF	47.33	7.76	55.09
12 Storey FIEB - θ_d= 2.5%	35.81	9.92	45.73
12 Storey FIEB - θ_d= 1.5%	45.18	11.20	56.38
8 Storey SCBF	19.42	4.67	24.09
8 Storey FIEB - θ_d= 2.5%	18.37	5.16	23.53
8 Storey FIEB - θ_d= 1.5%	22.86	7.1	29.96
4 Storey SCBF	5.08	1.92	7.01
4 Storey FIEB - θ_d= 2.5%	4.93	2.03	6.96
4 Storey FIEB - θ_d= 1.5%	5.61	3.03	8.64

The fundamental and target periods of the structures are shown in Table 2.4, along with the equivalent damping ratios that were used in the design, as per Step 2 of the design procedure. As expected, the FIEBs are significantly softer structures than the CBFs, especially those designed for the higher target drift ratio, and therefore the anticipated force and acceleration demands are lower. The design equivalent damping ratios showed little variation, ranging between 16% and 18% for all 6 FIEBs designed, and not showing any particular trend regarding the building's height or design drift ratio.

Table 2.4: Fundamental and target periods and design damping ratios for the resulting designs

Building type	Fundamental period (s)	Target period (s)	Design ξ_{eq} (%)
12 Storey SCBF	1.55	-	-
12 Storey FIEB - θ_d= 2.5%	2.59	5.48	18
12 Storey FIEB - θ_d= 1.5%	1.75	3.14	16
8 Storey SCBF	0.93	-	-
8 Storey FIEB - θ_d= 2.5%	1.55	3.61	17
8 Storey FIEB - θ_d= 1.5%	1.15	2.16	17
4 Storey SCBF	0.49	-	-
4 Storey FIEB - θ_d= 2.5%	0.94	2.15	16
4 Storey FIEB - θ_d= 1.5%	0.72	1.32	17

Table 2.5 presents the rotation demands on the HSSs where they meet the *eccentering* assembly at 1.5 times the target displacement for the 12 storey FIEB with θ_d=2.5%. The values resulting from

the design of this building range from 0.27 rad to 0.43 rad and are similar to those obtained for the other 5 FIEBs. Although not included in the scope of the preliminary study presented in this paper, it is planned to address in a subsequent stage of the research program whether the connections and the HSSs themselves are capable of sustaining such levels of rotation under combined tension force and bending.

Table 2.5: Rotation demand at the HSS and *eccentering* assembly interface at 1.5 times the target displacement for the 12 storey FIEB with θ_d=2.5%

Storey	BIE	Rotation demand at 1.5 times the target displacement (rad)
12	114×114×13 – e = 160 mm	0.27
11	114×114×13 – e = 150 mm	0.31
10	114×114×13 – e = 140 mm	0.34
9	114×114×13 – e = 130 mm	0.39
8	127×127×13 – e = 140 mm	0.38
7	127×127×13 – e = 130 mm	0.43
6	178×178×16 – e = 260 mm	0.26
5	178×178×16 – e = 250 mm	0.29
4	178×178×16 – e = 240 mm	0.31
3	178×178×16 – e = 240 mm	0.33
2	178×178×16 – e = 240 mm	0.34
1	178×178×16 – e = 230 mm	0.37

2.4.4. Non-Linear Response-History Analysis

The NLRHA method was used to assess the performance of the 9 designed frames subjected to seismic demands, both at the DE and at the MCE_R levels, to verify whether the proposed design procedure effectively allows control of the peak storey drifts at the design level and to obtain information about the structural system's response at the maximum considered earthquake level.

2.4.4.1. Selection and scaling of ground motions

For the analyses, 21 out the 22 records that compose the Far-Field Record Set proposed in FEMA P695 [24] were selected. The record of the Cape Mendocino earthquake at Rio Dell Overpass (record sequence number 829) was not included as it is no longer available in the PEER-NGA West2 database [25], from where all records were obtained. Thus, the employed set comprised 42 individual horizontal components obtained from 13 crustal events with magnitudes ranging from 6.5 to 7.6, including 7 that occurred in California, recorded on class C or D sites at an average distance of 16.4 km from the source. The initial scaling of the records was performed using the online tool of the PEER-NGA West2 database, based on the maximum-direction (RotD100) response spectra, using the DBE spectrum as target. A second, common, scaling factor was then applied to all ground motions so that the mean suite spectrum was equal or larger than 90% of the target spectrum at all periods over the period range of interest. For the MCE_R analyses, a subsequent scaling factor of 1.5 was applied to all records. For scaling purposes, a period range of interest for each building height was selected, with the lower bound corresponding to 0.2 times the shortest fundamental period of the group of structures (e.g. 0.1 s for the 4-storey SCBF) and the higher bound corresponding to the target period of the most flexible structure in the group (i.e. the FIEB with θ_d = 2.5%). Instead of specific period ranges of interest for each particular building, the use of a common period range for each group with equal number of storeys was preferred as it enables the direct comparison of the buildings' response to identical seismic demands. Thus, the period ranges of interest were from 0.31 s to 5.48 s for the 12-storey buildings, from 0.19 s to 3.61 s for the 8-storey buildings, and from 0.1 s to 2.15 s for the 4-storey buildings. Figure 2.19 presents the spectra of the scaled employed ground motion suite, the period ranges of interest and the target DE spectrum.

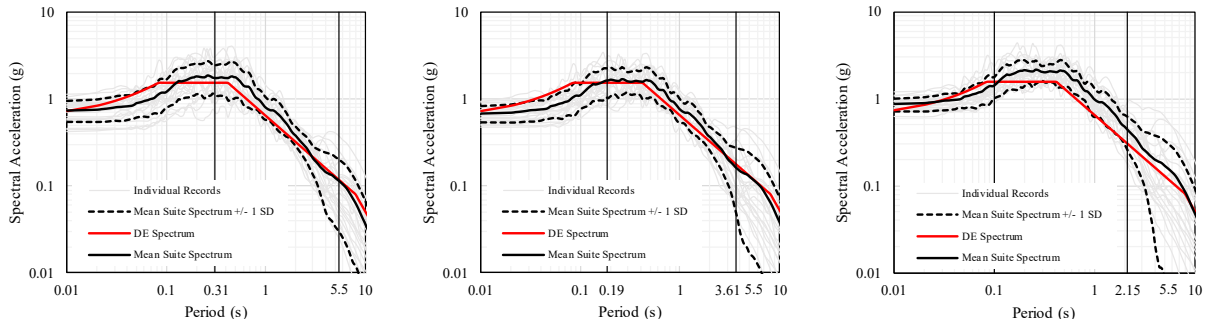

Figure 2.19: Mean Spectra of the employed scaled ground motion suite, period ranges of interest, and target DE spectrum: (a) 12-storey buildings ; (b) 8-storey buildings; (c) 4-storey buildings

2.4.4.2. Modelling considerations

Plane models of the designed frames were created using fiber-based elements in OpenSees. Probable material resistances were considered: R_yF_y=431 MPa for the HSSs and R_yF_y=380 MPa for the beams, columns, and plates. An initial out-of-straightness of a thousandth of the element length was applied to all frame elements, which corresponds to the fabrication tolerance in North American codes [14, 15]. For the braces, the imperfection was introduced such that it increased the effective eccentricity, thus reducing their stiffness and strength. The gravitational loads applied were 100% of the dead loads plus 50% of the live loads as per Clause 16.3.2 of ASCE/SEI 7-16. The knife-plates and *eccentering* assemblies were explicitly modelled, while the rest of the connections to the frame joints were modelled as rigid links. At each storey, the mass was introduced lumped in the central node, and diaphragm constraints were applied. Rayleigh damping of 2.5% was considered for the structures, and P-Δ effects were included in the models using the leaning column approach. In the analyses, an additional factor of 1.1 was applied to the ground motion records to ensure consistency between demand and capacity as braced frame strength was increased by 10% to account for accidental torsion effects in design. Numerical tests were performed to verify that the residual stresses and in-section variation of F_y across the HSSs

produced no significant influence on the response of the FIEBs; these effects were therefore not included in the final analyses.

2.4.4.3. Results and discussion

To determine whether the proposed design procedure allows one to effectively anticipate the storey drift ratios that the buildings will develop under seismic action at the design earthquake level, the mean values of the peak storey drifts under the DE level ground motions are plotted for all 6 FIEBs, as shown in Figure 2.20. For each structure, the mean of the peak values, and the differences with respect to the target are reported in Table 2.6. For the 12- and 8-storey FIEBs designed for θ_d = 2.5%, the mean peak storey drifts in the Table are lower than the design limit, which can be considered satisfactory, although the difference, in particular for the 12-storey building, can be in part interpreted as a consequence of the design procedure not considering the effects of higher modes of vibration in the selection of the target displaced shape. In the case of the 4-storey building with θ_d = 2.5%, however, the difference of 25.6% indicates that the design procedure did not control the drift as intended. As for the buildings designed for θ_d = 1.5%, the 12- and 8- storey buildings present mean peak storey drift values remarkably close to the design target, while the 4-storey FIEB developed peak storey drifts on average 66.7% larger than the target level. The higher than anticipated storey drifts concerning the 4-storey buildings can be explained by the mean suite response spectrum being on average 40% higher than the design spectrum between 0.1 s and 2.15 s, as can be observed in Figure 2.19 (c). This is a consequence of the requirement for the mean suite response spectrum not to be inferior by more than 10% to the target spectrum over the period range of interest.

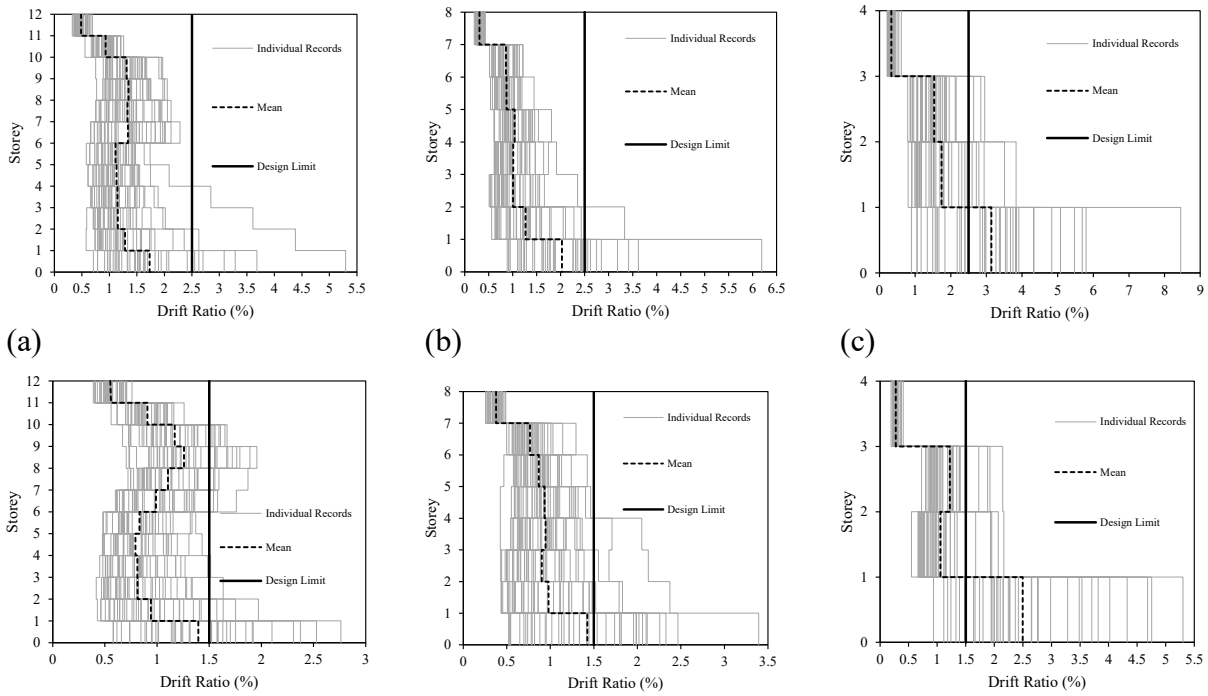

Figure 2.20: Peak storey drifts at DE level for FIEBs: (a) 12-storey with θ_d= 2.5%; (b) 8-storey with θ_d = 2.5%; (c) 4-storey with θ_d = 2.5%; (d) 12-storey with θ_d = 1.5%; (e) 8-storey with θ_d = 1.5%; (f) 4-storey with θ_d= 1.5%

Table 2.6: Mean peak storey drifts at DE level compared with design targets

Building type	Mean Peak Storey Drift (%)	Difference (%)
12 Storey FIEB - θ_d= 2.5%	1.73	-30.7
8 Storey FIEB - θ_d= 2.5%	2.02	-19.2
4 Storey FIEB - θ_d= 2.5%	3.14	25.6
12 Storey FIEB - θ_d= 1.5%	1.40	-6.67
8 Storey FIEB - θ_d= 1.5%	1.43	-4.67
4 Storey FIEB - θ_d= 1.5%	2.50	66.7

The effectiveness of the capacity-based protection measures included in the proposed design procedure is evaluated by comparing the peak storey shears that developed in the FIEBs under the MCE_R level ground motions with those used to design the protected FIEB elements, i.e. storey shears determined at 1.5 times the storey drifts expected at the DE level, as presented in Figure 2.21. For all FIEBs but one, the mean of the peak storey shears is lower than the capacity-based design shear used to dimension the beams and columns. In the case of the 4-Storey FIEB designed

for θ_d = 1.5%, the mean peak storey shears are in practical terms equal to the design forces, being higher by less than 1.0%. This indicates that the drift-based amplification contained in the design procedure could adequately reduce the probability of excessive demand on the protected elements at the MCE_R level, and thus of the occurrence of an unwanted failure mechanism. However, for all buildings there were ground motion records for which the capacity-based design storey shear was exceeded; which is attributed to the fact that the peak drifts surpassed the assumed 1.5 times the design level in several cases, which is not surprising given the number and variability of the records considered. To effectively annul the possibility for a ground motion to produce storey shears larger than the design storey shear, it would be necessary either to calculate the design storey shears based on the ultimate tension force that can be developed by the bracing members (i.e. $R_y F_y A_g$), or to implement a fuse-like device in the brace connections that would pose a cap to the maximum forces transmitted to the protected elements. As the first option would eliminate one of the purported benefits of FIEBs over CBFs, to reduce the costs by limiting the design forces on the protected elements, the second option could represent a reasonable alternative to be investigated in a subsequent stage of the research program.

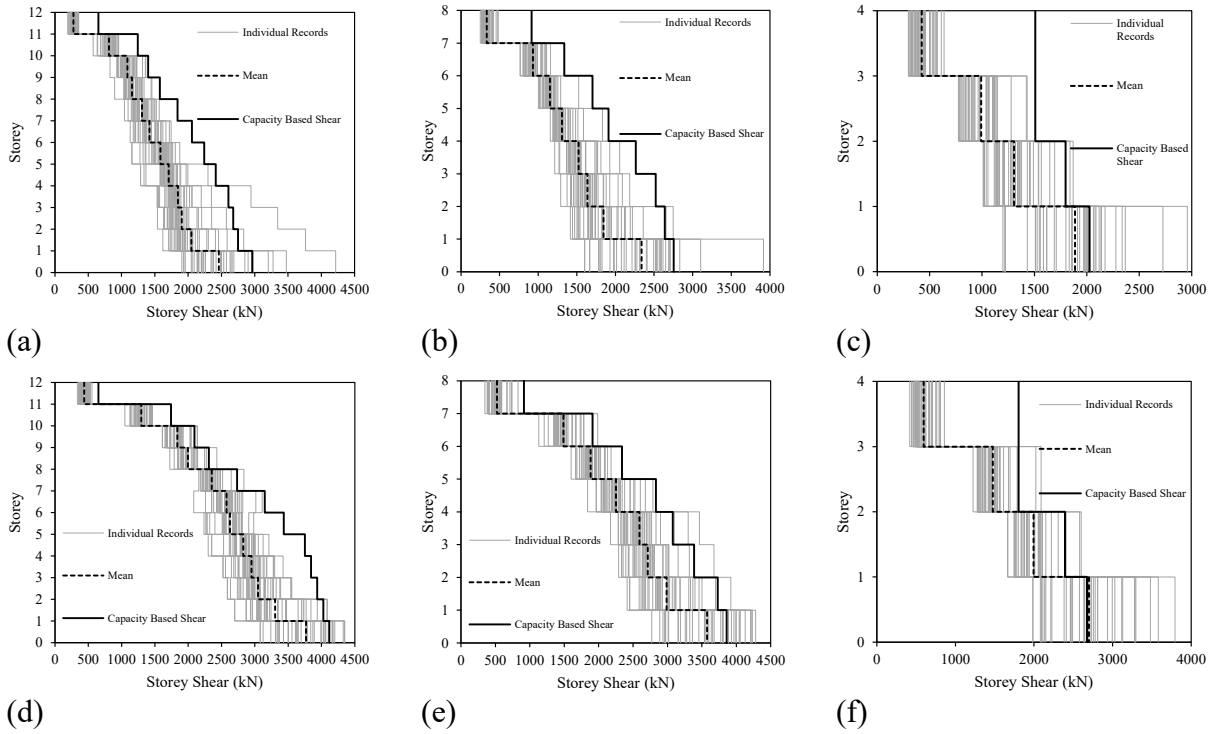

Figure 2.21: Maximum storey shears at MCE_R level for FIEBs: (a) 12-storey with θ_d=2.5%; (b) 8-storey with θ_d=2.5%; (c) 4-storey with θ_d=2.5%; (d) 12-storey with θ_d=1.5%; (e) 8-storey with θ_d=1.5%; (f) 4-storey with θ_d=1.5%

The number of ground motions at the MCE_R level causing unacceptable storey drifts for each structure is reported in Table 2.7. In this study, storey drifts of 5% and 30% were arbitrarily set as the thresholds for unacceptable response and structural collapse, respectively. No collapses were observed in the frames studied according to this criterion. As shown, the SCBFs presented worse overall performance at the MCE_R level than the FIEBs, in terms of unacceptable responses. Finite element analysis of the BIEs at the first storey was performed to verify that these braces could sustain the seismic drift demand without developing local buckling. In the FE analyses, shell-element models of the BIEs in Abaqus were subjected to the displacement histories recorded from the OpenSees analyses that produced maximum drifts close to 5%. In Figure 2.22, an example of the resulting axial force vs. storey drifts plots resulting from these analyses is shown, along with the deformed shape of the BIE model at the point of maximum compression. The analyses showed that the BIEs could withstand that drift level without developing local buckling, indicating that the

unacceptable response threshold could be larger than 5% storey drifts in terms of brace inelastic response. The mean peak and residual storey drifts under the MCE_R level ground motions for the SCBFs and FIEBs are compared in Figure 2.23 and Figure 2.24, respectively. As expected, storey drifts for the FIEBs designed with 1.5% target drift are consistently lower than those sustained by the FIEBs designed using a target drift of 2.5%. Compared to the FIEBs, the SCBFs exhibited markedly larger peak and residual drifts at the first storey at the MCE_R level. Conversely, the FIEBs presented larger drifts for most other storeys, showing that the system can produce a more even distribution of the drift demand over the building height. Although not shown here, similar differences were observed at the DE level; the SCBFs experienced mean peak storey drifts smaller than both FIEBs for the 12-storey buildings, and larger than the FIEBs with θ_d = 1.5% for the 8- and 4-storey buildings.

Table 2.7: Number of unacceptable responses for MCE_R NLRHA

Building type	Unacceptable results (θ_{max} > 5%)
12 Storey SCBF	3
12 Storey FIEB - θ_d= 2.5%	1
12 Storey FIEB - θ_d= 1.5%	2
8 Storey SCBF	11
8 Storey FIEB - θ_d= 2.5%	2
8 Storey FIEB - θ_d= 1.5%	0
4 Storey SCBF	22
4 Storey FIEB - θ_d= 2.5%	18
4 Storey FIEB - θ_d= 1.5%	10

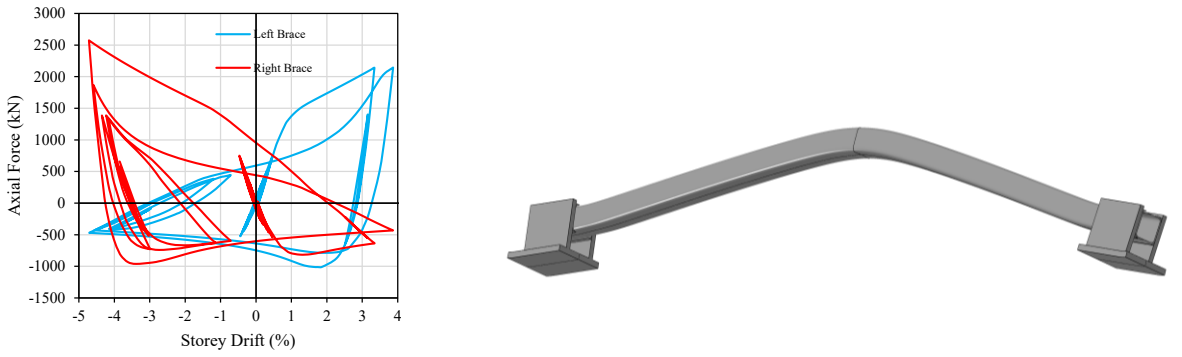

(a) (b)

Figure 2.22: Response of first storey braces of the 12-storey FIEB with θ_d = 2.5% for a ground motion that produced maximum drift close to 5%: (a) axial force vs. storey drift; (b) deformed shape at maximum drift for right brace finite element model

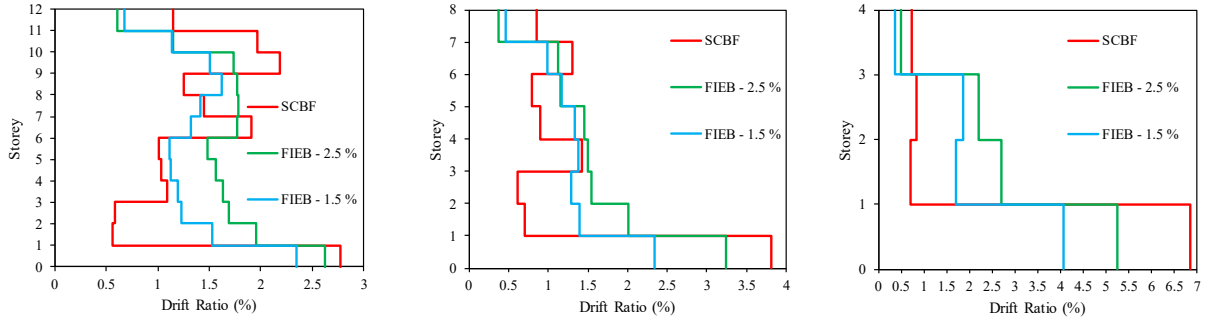

(a) (b) (c)

Figure 2.23: Comparison of mean peak storey drifts at MCE_R level: (a) 12-storey buildings; (b) 8-storey buildings; (c) 4-storey buildings

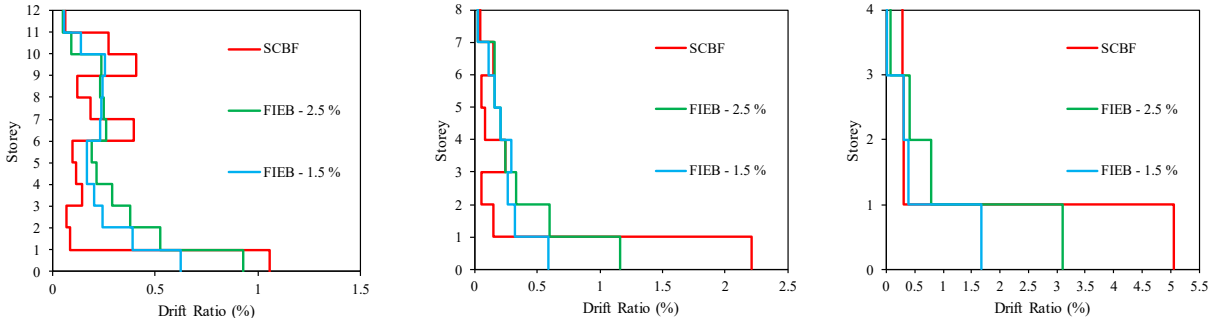

(a) (b) (c)

Figure 2.24: Comparison of mean residual storey drifts at MCE_R level: (a) 12-storey buildings; (b) 8-storey buildings; (c) 4-storey buildings

The difference in the observed peak and residual drifts in SCBFs and FIEBs can be explained by the essentially distinct post-yielding stiffness that each system possesses. While the conventional concentrically braced frame boasts a nearly null stiffness after yielding of the tension brace, thus

opposing no resistance to further displacement demand, the frame with intentionally eccentric braces benefits from a significant post-yielding stiffness that is not reduced until very large deformations, counterbalancing large displacement pulses. This is evident from the comparison of the first storey shear vs. drift history plots of SCBFs and FIEBs for some of the ground motions, which produced unacceptable response from the SCBFs, while the FIEBs performed remarkably well. One of such examples is presented in Figure 2.25, for the ground motion record with sequence number 721 in PEER NGA West 2 database, 90º component, and scale factor of 2.59 for MCE_R including 10% increase for accidental torsion.

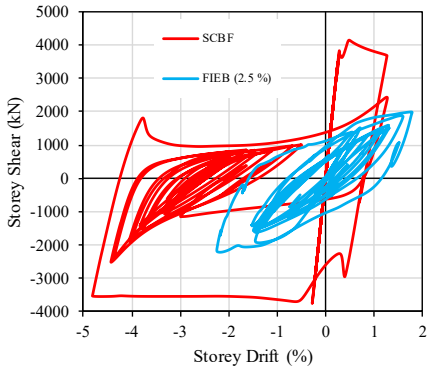

Figure 2.25: First storey shear vs. drift history plot for 12-storey SCBF and FIEB with θ_d = 2.5% for ground motion number 721, 90º component at MCE_R level

2.5. CONCLUSIONS

It was shown that the characteristics of BIEs potentially enable this recently proposed type of brace to overcome some of the most prominent drawbacks of traditional CCBs; notably, those associated with their high inherent stiffness, their susceptibility to local buckling and subsequent low-cycle fatigue-induced fracture, and their propension to concentrate drift demands in a limited number of storeys. A seismic design procedure based on the Direct Displacement Based Design approach was proposed in an effort to explicitly account for the particular force-displacement response of BIEs.

The proposed procedure was employed in the design of hypothetical buildings located in a high seismic hazard region. The performance of the resulting structures was assessed through Non-Linear Response-History Analysis, using an established ground motion record suite. It was verified, albeit preliminarily, that the proposed design procedure could be considered adequate for the design of Frames with Intentionally Eccentric Braces as it produces buildings that, on average, comply with the selected target maximum drifts and performance objectives. Although the maximum storey drifts were larger than the design targets for the FIEBs with shorter periods, the results can be regarded as auspicious, considering that the scaled ground motion record suite used in the analysis produced demands larger than those anticipated in the design. Moreover, the forces in the capacity-protected elements did not surpass, on average, the threshold considered in design. Furthermore, the results obtained showed that FIEBs may present a safer response to severe ground motions than SCBFs, because the maximum and residual storey drifts were significantly lower, owing to the substantial secondary stiffness of BIEs. Also, it was shown that FIEBs designed for relatively high target drift ratios can result in economic advantages over SCBFs.

Further studies, however, are required to refine the equivalent damping ratios and design displacement vectors used in the design procedure, and to address an effective way of controlling or capping the maximum storey shears in anticipation of ground motions more severe than expected. Research is also necessary to evaluate the performance of the proposed *eccentering* assembly and connections, and to validate or refute the preliminary fracture life equation herein proposed.

ACKNOWLEDGEMENTS

The first author wishes to thank Universidad de Costa Rica for financing the undertaking of his doctoral studies. The authors would also like to acknowledge DPHV Structural Consultants and

ADF Group Inc. for their generous technical and financial support, as well as the Natural Sciences and Engineering Research Council of Canada (NSERC), the Fonds de Recherche du Québec – Nature et Technologies (FRQ-NT) and the Centre d'Études Interuniversitaire des Structures sous Charges Extrêmes (CEISCE).

REFERENCES

[1] X. Tang and S. C. Goel, "Brace fractures and analysis of Phase I Structure," *Journal of Structural Engineering,* vol. 115, no. 8, pp. 1960-1976, 1989, doi: 10.1061/(ASCE)0733-9445(1989)115:8(1960).

[2] R. Tremblay, "Inelastic seismic response of steel bracing members," *Journal of Constructional Steel Research,* vol. 58, no. 5-8, pp. 665-701, 2002, doi: 10.1016/S0143-974X(01)00104-3.

[3] S. Costanzo, M. D'Aniello, and R. Landolfo, "Proposal of design rules for ductile X-CBFS in the framework of EUROCODE 8," *Earthquake Engineering & Structural Dynamics,* vol. 48, no. 1, pp. 124-151, 2019, doi: 10.1002/eqe.3128.

[4] K. A. Skalomenos, H. Inamasu, H. Shimada, and M. Nakashima, "Development of a steel Brace with Intentional Eccentricity and experimental validation," *Journal of Structural Engineering,* vol. 143, no. 8, p. 04017072, 2017, doi: 10.1061/(ASCE)ST.1943-541X.0001809.

[5] *ASCE/SEI 7-16: Minimum design loads and associated criteria for buildings and other structures*, American Society of Civil Engineers (ASCE), Reston, VA, 2017. [Online]. Available: https://ascelibrary.org/doi/abs/10.1061/9780784414248

[6] F. T. McKenna, "Object-oriented finite element programming: Frameworks for analysis, algorithms and parallel computing," Ph.D. Thesis, Civil Engineering, University of California, Berkeley, 1997.

[7] A. Agüero, C. Izvernari, and R. Tremblay, "Modelling of the seismic response of concentrically braced steel frames using the OpenSees analysis environment," *International Journal of Advanced Steel Construction,* vol. 2, no. 3, pp. 242-274, 2006.

[8] P. Uriz, F. C. Filippou, and S. A. Mahin, "Model for cyclic inelastic buckling of steel braces," *Journal of structural engineering,* vol. 134, no. 4, pp. 619-628, 2008.

[9] *Dassault Systèmes, Abaqus/CAE 2019*. (2018). Dassault Systèmes Simulia Corp., Providence, RI.

[10] B. Fell, A. Kanvinde, and G. Deierlein, *Large-scale testing and simulation of earthquake-induced ultra low cycle fatigue in bracing members subjected to cyclic inelastic buckling*. Stanford, CA: John A. Blume Earthquake Engineering Center, 2010.

[11] I. Koval, "Accounting for cold working and residual stress effects on the axial strength of HSS bracing members," M. Eng. Thesis, Civil, Geological, and Mining Engineering, École Polytechnique de Montréal, 2018.

[12] R. Tremblay, M. H. Archambault, and A. Filiatrault, "Seismic response of concentrically braced steel frames made with rectangular hollow bracing members," *Journal of Structural Engineering,* vol. 129, no. 12, pp. 1626-1636, 2003.

[13] A. K. Chopra, *Dynamics of structures: theory and applications to earthquake engineering*, 4th ed. Upper Saddle River, N.J.: Prentice Hall, 2012, pp. xxxiii, 944 p.

[14] *ANSI/AISC 360-16: Specification for structural steel buildings* American Institute for Steel Construction (AISC), Chicago, IL, 2016.

[15] *CSA. S16-14: Design of steel structures*, Canadian Standards Association (CSA), Toronto, ON, 2014.

[16] M. J. N. Priestley, G. M. Calvi, and M. J. Kowalsky, *Displacement-based seismic design of structures*. Pavia, Italy: IUSS Press 2007, pp. xvii, 721 p.

[17] K. K. Wijesundara and P. Rajeev, "Direct displacement-based seismic design of steel concentric braced frame structures," *Australian Journal of Structural Engineering,* vol. 13, no. 3, pp. 243-257, 2012.

[18] G. O'Reilly, J. Goggins, and S. Mahin, "Performance-based design of a self-centering concentrically braced frame using the direct displacement-based design procedure," Proceedings of the *15th World Conference on Earthquake Engineering*, Lisbon, Portugal, 2012.

[19] M. Al-Mashaykhi, P. Rajeev, K. Wijesundara, and M. Hashemi, "Displacement profile for displacement based seismic design of concentric braced frames," *Journal of Constructional Steel Research,* vol. 155, pp. 233-248, 2019.

[20] K. Wijesundara, R. Nascimbene, and T. J. Sullivan, "Equivalent viscous damping for steel concentrically braced frame structures," *Bulletin of Earthquake Engineering,* vol. 9, no. 5, pp. 1535-1558, 2011, doi: 10.1007/s10518-011-9272-4.

[21] *EN 1998-1:2004 Eurocode 8: Design of structures for earthquake resistance - Part 1: general rules, seimic action and rules for buildings*, European Committee for Standardization (CEN), Brussels, Belgium, 2004.

[22] *National Building Code of Canada 2015, 14th ed.* , National Research Council of Canada (NRCC), Ottawa, ON, 2015.

[23] *ANSI/AISC 341-16: Seismic provisions for structural steel buildings*, American Institute for Steel Construction (AISC), Chicago, IL, 2016.

[24] FEMA, "Quantification of building seismic performance factors, FEMA P695," Federal Emergency Management Agency (FEMA),, Redwood City, CA 2009.

[25] PEER. The PEER ground motion selection web application [Online] Available: http://ngawest2.berkeley.edu/

FOREWORD TO CHAPTER 3

Chapter 3 presents in detail the numerical parametric study that resulted in an equation to predict the fracture life of BIEs included as part of the proposed design procedure discussed in Chapter 2. The proposed equation expresses the maximum equivalent ratio that a BIE can withstand under reversed cyclic loading before local buckling occurs at its mid-length as a function of the eccentricity to HSS depth (e/H) ratio, selected to characterise non-dimensionally the eccentricity, and a parameter combining the global and local slenderness: $\lambda_0 = (L/r)/(b_{el}/t)$. Supposing that, as for traditional concentrically loaded braces, the susceptibility to local buckling of BIEs will decrease as the global slenderness (L/r) grows and as the local slenderness (b_{el}/t) diminishes, the λ_0 parameter was selected to produce a non-dimensional variable combining the complementary effects of the global and local slenderness of the HSS bracing member on its fracture life. The study was designed to include a wide array of commercially available square HSSs and practicable eccentricity ratios, considering the introduction of the eccentricity by means of *eccentering* assemblies which are cost-effective, easy to fabricate, and straightforward to model. The material properties employed in the study were based on coupon data from past research on CSA G40.20-21 Class C HSS bracing members conducted at McGill University. In addition to the data on the fracture life of BIEs, the study provided information on their energy dissipation and equivalent damping capacity, which was important in defining the equivalent damping ratio model to incorporate in the design procedure.

.

CHAPTER 3: NUMERICAL INVESTIGATION OF THE SEISMIC RESPONSE OF SQUARE HSS BRACES WITH INTENTIONAL ECCENTRICITY

Conference paper, published in the Proceedings of the 17th World Conference on Earthquake Engineering, Sendai, Japan (http://www.17wcee.jp/links.php – paper nºC000832). Oral presentation postponed due to the COVID-19 pandemic.

Andrés González Ureña, Robert Tremblay, Colin A. Rogers

ABSTRACT

Concentrically Braced Frames (CBFs) comprising Hollow Structural Section (HSS) bracing members possess high stiffness and are susceptible to premature local buckling at the plastic hinge region, leading to low-cycle fatigue induced fracture. Intentionally offsetting the axis of otherwise conventional steel braces with respect to the working points has been proposed to overcome these shortcomings. Braces with Intentional Eccentricity (BIEs), the novel type of brace proposed by researchers in Japan, are subject to bending moment in addition to axial force under seismic action and, as such, inherently possess lower axial stiffness than Conventional Concentric Braces (CCBs). Their pre- and post-yielding stiffness can be adjusted by varying the eccentricity, allowing for better control of the structure's dynamic response to ground motion excitations. A single experimental study has been performed on BIEs, with results indicating that, in comparison with

CCBs, local buckling and fracture occurred in BIEs at significantly higher drift ratios due to the strain demand being more evenly distributed along the brace length.

A numerical investigation has been undertaken to verify the generalisation of this behaviour to square HSS BIEs with different global and local slenderness ratios and to shed light on the range of imposed axial deformation these braces are able to sustain safely, as function of the eccentricity and their global and local slenderness. The investigation consists of a parametric study of finite element models of BIEs considering global slenderness ratios (L/r) ranging from 50 to 200, local slenderness ratios (b/t) between 4 and 36 and eccentricity ratios (e/H) from 0 (i.e. that of a CCB) to 2. Based on cost-effectiveness from a constructive point of view, and since the study is planned to be continued by the physical testing of full-scale BIE specimens, the BIE models were designed considering that the eccentricity is introduced by an assembly consisting of welded side plates linking the bracing members to the end connections. It was observed that the introduction of the eccentricity does delay, in terms of axial displacement, or imposed drift ratio, the onset of local buckling and thus, presumably, the fracturing of the brace. The article presents the numerical study and discusses the results and their implications for the design of Frames with Intentionally Eccentric Braces (FIEBs). An equation for predicting the deformation capacity of BIEs is proposed. Recommendations regarding the equivalent damping properties of BIEs for their use in the context of a Displacement-Based Design approach are also provided.

Keywords: steel braced frames; braces with intentional eccentricity; frames with intentionally eccentric braces; numerical investigation; earthquake-resistant design

3.1. INTRODUCTION

Concentrically Braced Frames (CBFs) constitute an often-favoured choice for the Seismic-Force-Resisting System (SFRS) of low- to mid-rise buildings in earthquake-prone regions due to their cost-effectiveness. In these, Hollow Structural Sections (HSSs) are frequently selected as the bracing members, owing to their efficiency in compression over other section shapes, and to their aesthetic appeal. However, CBFs with HSS bracing members bear significant drawbacks that limit their advantages. Primarily, it has been demonstrated in research [1, 2] that HSSs are susceptible to low-cycle fatigue fracturing as a result from the large concentration of strains in the mid-length plastic hinge after the onset of local buckling. Additionally, as Conventional Concentric Braces (CCBs) possess negligible post-yielding stiffness, large deformation demands, potentially triggering instability, are a concern. Finally, as an implication of their inherently high stiffness, CBFs are confined to low fundamental vibration periods, and therefore to larger spectral acceleration demands than in other, more flexible, systems, which, in combination with the overstrength ensuing from the difference between the tensile and compressive capacities of the braces, entails high capacity-based design forces for the non-dissipating members of the SFRS and its foundations, reverberating in the cost of the structure.

Recently, the concept of Braces with Intentional Eccentricity (BIEs) has been proposed by Skalomenos et al. [3] as an alternative to CCBs that overcomes the deficiencies listed above. Simply put, a BIE is an otherwise conventional bracing member, with its longitudinal axis offset perpendicularly with respect to the working points, or braced frame diagonal. Being subject to bending moment in addition to axial force under earthquake loading, BIEs are substantially more flexible than CCBs and exhibit a distinct force-deformation response that sets them apart from CCBs and other traditional dissipative elements. Under monotonic tension, BIEs present a pseudo

tri-linear response, with a significant post-yielding stiffness that depends on the prescribed eccentricity, while in compression, they show a steady flexural behaviour, devoid of salient peaks corresponding to buckling. In their study, Skalomenos et al. performed physical tests of reduced scale BIE specimens under cyclic loading, and their results confirmed the behaviour described above. They also showed that, in comparison with CCBs, BIEs benefit from a longer fracture life, in terms of allowable imposed drift ratio under cyclic loading, as due to the eccentricity, the strain demand is more evenly distributed along the brace length, thus delaying the onset of local buckling at the central plastic hinge region.

Considering their particular force-deformation behaviour, the authors of this article advocate a Displacement-Based Design based procedure as being appropriate in the design of Frames with Intentionally Eccentric Braces (FIEBs). This is expanded upon in a paper companion to the present one [4]. In the proposed design procedure, the predicted fracture life of BIEs and the equivalent damping ratio associated to them, constitute essential inputs: the former defines the maximum target displacements that the designer can specify, and on the latter depends the scaling factor to apply to the design displacement spectrum. In this paper, results from a numerical parametric study are presented aiming to shed light on the range of imposed cyclic axial deformation, or storey drifts, that square HSS BIEs can safely sustain before the onset of local buckling, as a function of the prescribed eccentricity and the global and local slenderness ratios. Information is also provided regarding the energy dissipation and equivalent damping properties of BIEs.

3.2. PROPERTIES OF BIEs

The components of a nonspecific BIE are presented in Figure 3.1. The eccentricity, e, is defined as the parallel offset between the bracing member's longitudinal axis and the line of action of the

forces transmitted by the frame, or working points' axis. The eccentricity is introduced by the *eccentering* assemblies, which in general can be any arrangement of plates designed to accommodate the eccentricity, while linking rigidly the bracing member to its end connections and subsequently to the frame members. In the figure, the connections are shown as pins, however, in a realistic scenario, a free rotation condition of the BIE's end would be approximated by detailing the connection such that it yields in flexure for low levels of force, as is done often for CCBs. The force-deformation behaviour of a BIE depends on the bracing member's cross section and its material, the prescribed eccentricity, e, the hinge-to-hinge length, L, and the *eccentering* assemblies' length, L_{ea}.

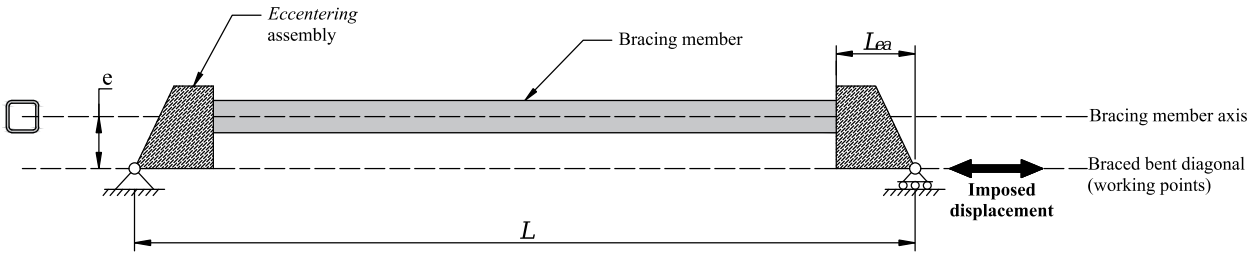

Figure 3.1: Schematic drawing of a general BIE and its components

The typical force-deformation behaviour of BIEs under monotonic tensile (a) and compressive (b) loading is presented in Figure 3.2. In contrast with CCBs, whose behaviour in tension is close to elastic-perfectly plastic, the BIEs show a response in tension that can be idealised as tri-linear. For low levels of tensile load or imposed displacement, the BIE responds elastically in combined flexure and axial load and the brace bends toward the working points axis. When the outermost fiber in tension attains the yielding stress, the BIE is said to have reached its "first yield point" (T_y, δ_y) and the force-deformation curve transitions from the initial, or elastic, regime into the secondary, or post-yielding regime, which presents a markedly lower, although significant, stiffness. As the displacement increases, the effective eccentricity decreases, entailing a gradual

increment of the stiffness while the yielding of the cross-section progresses. As the full cross-section yields, the BIE attains its "ultimate yield point" (T_u, δ_u), whose load level is the same as the yield tensile strength of a CCB of the same section, but at a significantly greater displacement. The force-deformation of BIEs in tension can thus be approximated by a tri-linear model: a starting segment with initial, or elastic, stiffness, K_i, that extends to the first yield point, followed by a second segment with secondary, or post-yielding stiffness, K_s, until the ultimate yield point is attained, and a third, fully yielded, segment with negligible stiffness. In compression, BIEs present a smooth flexural response. As the compressive loading increases, the brace bends away from the axis connecting its working points, and hence its stiffness reduces progressively. Opposed to the characteristic response of CCBs in compression, which presents a prominent peak corresponding to overall buckling, the BIEs transition seamlessly from the elastic to the post-buckling regimes. It is proposed that the response of BIEs in compression be approximated with an elastic-perfectly plastic model, with initial stiffness K_i, and with maximum compressive load, C', calculated as the elastic limit state of a column under eccentric axial load, as proposed in [3].

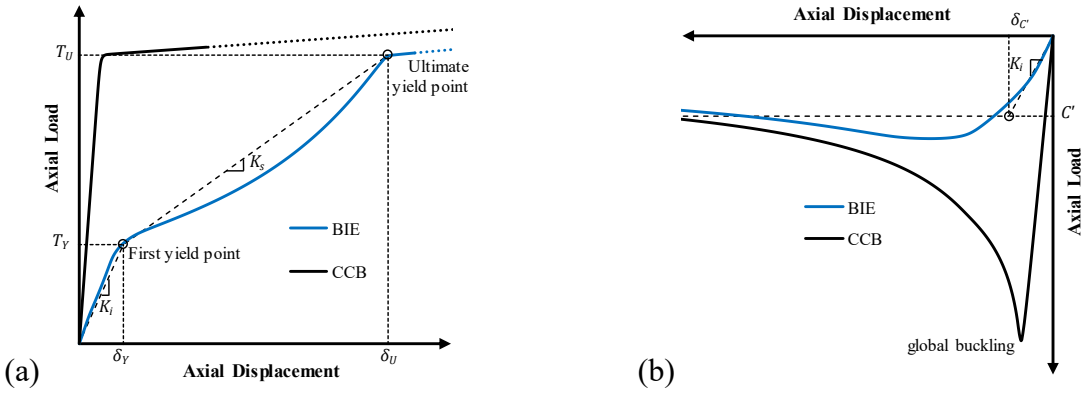

Figure 3.2: Idealised force-deformation behaviour of BIEs and CCBs: tension, (a), and compression, (b)

The influence of the eccentricity on the values of K_i, K_s, and T_Y can be observed in Figure 3.3, which was constructed using results of fiber models of 178×178×16 HSS BIEs in OpenSees [5].

In these models, all parameters were kept constant, except for the eccentricity to showcase, its effects on the tensile response of BIEs. The overall length, L, was 5408 mm and the *eccentering* assemblies were represented by rigid links with length, L_{ea}, of 360 mm. The end connections were modelled as rectangular plates with thickness of 38.1 mm and width of 360 mm, and a free length of 77 mm intended to yield in flexure under low levels of force, thus approximating the desired pin-like behaviour. The yield stress was taken as 345 MPa both for the plates and the HSS.

The particularities of the BIEs' force-deformation response translate also to cyclic loading, as shown in Figure 3.4, which compares the force-deformation hysteresis plots of CCBs and BIEs of the same section, under cyclic load with increasing displacement amplitude, obtained from OpenSees analyses based on dimensions consistent with a 6 m by 4 m braced bay. In spite of being capable of opposing, in net terms, less resistance and dissipating less energy than the CCBs, the BIE's response shows promising features such as the lack of peaks due to buckling, a positive post-yielding stiffness and an increment of the maximum load at each cycle. The failure mode of BIEs is likely to be in most cases the same as for CCBs: low-cycle fatigue induced fracturing at the mid-length after the onset of local buckling. However, as the results of Skalomenos et al. [3] indicate, the introduction of the eccentricity can delay, in terms of imposed displacement or drift ratio, the onset of local buckling and subsequent fracture.

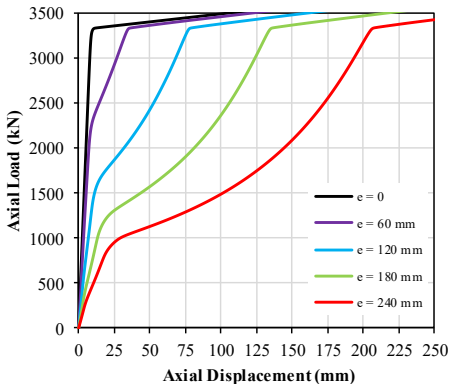

Figure 3.3: Influence of eccentricity in the tension force-displacement behaviour of 178×178×16 HSS BIEs

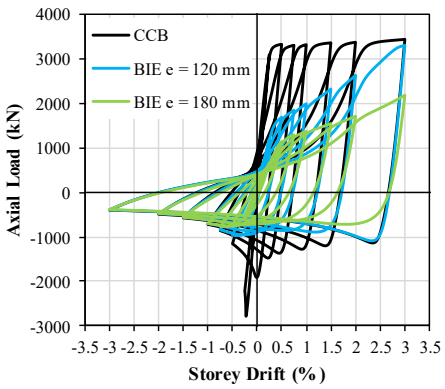

Figure 3.4: Axial force vs. storey drift for 178×178×16 HSS BIEs and CCBs under cyclic load

As can be inferred from the behaviour described in the preceding lines, the conventional force-based seismic design procedures of many modern design codes, such as the National Building Code of Canada [6], are not well-suited for use with BIEs. These procedures assume that the dissipating elements of the SFRS behave in an elastic-perfectly plastic manner, and, as such, can be sized by equating their yield strength to the expected seismic demands, scaled-down accounting for the system's ductility and overstrength. BIEs, however, present a response dissimilar to an elastic-perfectly plastic model and attain their maximum resistance at displacement levels that depend on the eccentricity and that might be too large to comply with serviceability limit states. Furthermore, the resistance they provide varies constantly with the imposed displacement, rendering the use of ductility-based seismic force reduction factors inappropriate. For these reasons, the authors propose a displacement-based procedure for the design of FIEBs, which is presented in detail in [4].

However, a displacement-based design procedure is ineffectual if the resulting structure is not able to attain the selected displacement levels. Thus, for their use in a displacement-based procedure, it is fundamental to be able to estimate what magnitude of displacement, or storey drift, a given

BIE can safely sustain under cyclic loading, i.e. without being affected by local buckling, as it is the precursor of fracture.

3.3. DEFINITION OF PARAMETRIC STUDY AND MODELLING CONSIDERATIONS

With the objective of obtaining an empirical equation that would allow one to estimate a square HSS BIE's fracture life as a function of its global and local slenderness, and the eccentricity, a parametric study based on finite element model analyses in Abaqus [7] was undertaken. It was defined that the variables to consider would be the eccentricity to section height ratio, e/H, the global slenderness parameter, L/r, and the local slenderness ratio, b_{el}/t (H is the section's outside height, r its radius of gyration, t its wall thickness and b_{el} the width of the flat faces of the HSS, taken as $H - 4t$).

Given that the actual calibration of a fracture model requires extensive information which, for the moment, is not available for BIEs, the threshold of imminent failure is determined by the onset of plastic local buckling. The suitability of Abaqus to simulate local buckling has previously been established in the literature, e.g. [8].

The concept of the connections and *eccentering* assemblies considered in the development of the models is shown in Figure 3.5. It is the same configuration considered for the design of buildings presented in [4]. It was selected accounting for its simplicity and cost-effectiveness, and also to produce the in-frame-plane bending of the BIE. It consists of a gusset- and knife- plate assembly, connected by bolted angles. The eccentricity is introduced by side plates that tie rigidly the HSS to the knife plate. Flare-bevel welds at the HSS's corners provide its connection to the side plates.

The knife plate is detailed using a clearance with a length of twice the plate's thickness, t_g, to allow for the unrestrained rotation of the BIE's ends.

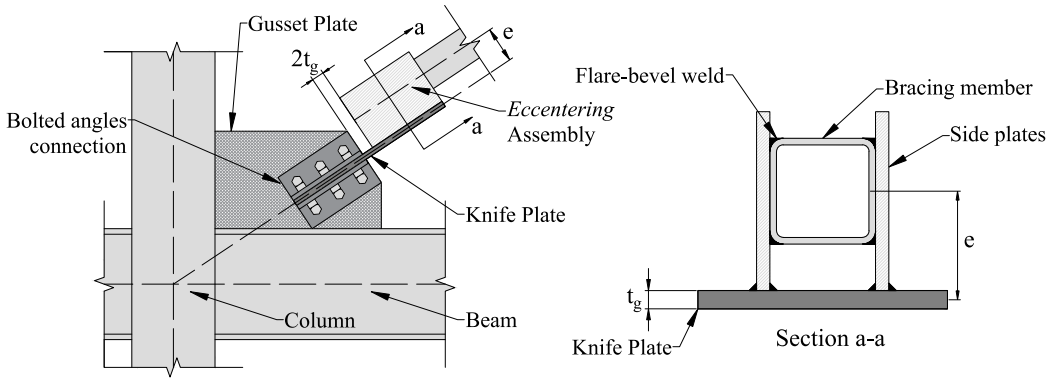

Figure 3.5: Example of the considered BIE to frame connection and *eccentering* assembly

In the numerical models, however, the bolted angles connection is not explicitly modelled, instead, a fixed end condition is enforced at the end of the knife plate clearance, as shown in Figure 3.6. All plates and the HSS are modelled using shell elements (S4R) with 11 integration points through the thickness. The flare-bevel welds were modelled using solid elements to more realistically represent the interaction between the connected elements. The typical seed size of the shell elements varied from 2 mm to 6 mm as a function of the overall model's dimensions. Symmetry was used so that only a quarter of the actual BIE had to be modelled, reducing the computational expense. As is explained later, a model employing the same principles, but based on the published results in [3], was first constructed and analysed to validate the modelling considerations.

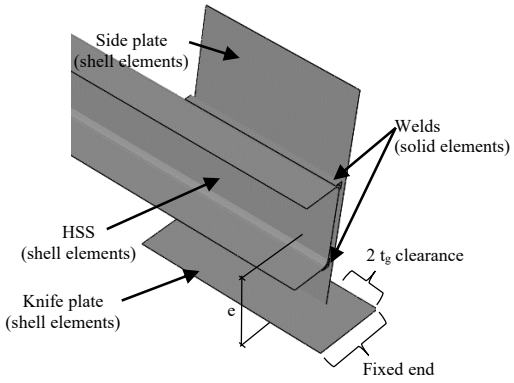

Figure 3.6: Detail of typical modelled *eccentering* assembly and connection

Table 3.1 presents the selected sections for the parametric study and the thickness of their side- (t_s) and knife-plates (t_g) and the length of the knife plate clearance (L_g). The thicknesses were defined so that the plates had sufficient strength to resist the maximum probable force that the HSS could develop in tension, i.e. $A_g R_y F_y$, with A_g being the gross area of the cross-section and $R_y F_y$ taken as 460 MPa, as per [9]. In all the models the hinge to hinge length was taken as 5470 mm, and both the side plated *eccentering* assembly's length and the knife plate's width were taken as 300 mm. These dimensions are within the expected range for a BIE in a 6 m by 4 m bay, considering the size of the columns, beams and gusset plate and bolted angle connections. Recognising that for all commercially available square HSS sections with the same outside height, the value of r is approximately constant, five groups of sections with constant height were selected to provide five approximate values for the L/r variable: 55, 80, 115, 150 and 200. Within each group, all six or five commercially available thicknesses were included in the study, as can be observed in Table 3.1. The Table also indicates whether the selected sections comply with the global and local slenderness limits of [9] for HSSs employed in CBFs (the global slenderness must be between 70 and 200). Finally, for each section, nine levels of e/H were considered: 0 (CCB), 0.25, 0.5, 0.75, 1, 1.25, 1.5, 1.75 and 2, for a total of 243 individual analyses.

Table 3.1: Selected sections and model dimensions

Section	H (mm)	L/r	b_{el}/t	Limiting b_{el}/t (CSA S16-14)	Complies with slenderness limits?	t_s (mm)	t_g (mm)	L_g (mm)
254×254×16	254.0	56.9	12.0	17.8	No	32.0	76.0	152.0
254×254×13	254.0	56.0	16.0	17.8	No	51.0	64.0	128.0
254×254×9.5	254.0	55.2	22.7	17.8	No	38.0	51.0	102.0
254×254×8.0	254.0	54.8	27.9	17.8	No	32.0	38.0	76.0
254×254×6.4	254.0	54.2	36.0	17.8	No	25.0	32.0	64.0
178×178×16	177.8	84.3	7.2	17.8	Yes	38.0	51.0	102.0
178×178×13	177.8	82.3	10.0	17.8	Yes	32.0	44.0	88.0
178×178×9.5	177.8	80.4	14.7	17.8	Yes	25.0	32.0	64.0
178×178×8.0	177.8	79.5	18.4	17.8	No	22.0	32.0	64.0
178×178×6.4	177.8	78.6	24.0	17.8	No	16.0	22.0	44.0
178×178×4.8	177.8	77.8	33.2	17.8	No	13.0	19.0	38.0
127×127×13	127.0	119.7	6.0	18.7	Yes	22.0	32.0	64.0
127×127×9.5	127.0	115.6	9.3	18.5	Yes	16.0	22.0	44.0
127×127×8.0	127.0	114.0	12.0	18.4	Yes	16.0	22.0	44.0
127×127×6.4	127.0	112.1	16.0	18.4	Yes	13.0	16.0	32.0
127×127×4.8	127.0	110.3	22.6	18.3	No	10.0	13.0	26.0
102×102×13	101.6	155.0	4.0	20.4	Yes	16.0	22.0	44.0
102×102×9.5	101.6	148.2	6.7	20.1	Yes	13.0	19.0	38.0
102×102×8.0	101.6	145.5	8.8	20.0	Yes	13.0	16.0	32.0
102×102×6.4	101.6	142.4	12.0	19.8	Yes	10.0	13.0	26.0
102×102×4.8	101.6	139.5	17.3	19.7	Yes	8.0	10.0	20.0
102×102×3.2	101.6	136.8	27.9	19.5	No	6.0	8.0	16.0
76×76×9.5	76.2	206.4	4.0	22.6	No	10.0	13.0	26.0
76×76×8.0	76.2	201.1	5.6	22.6	No	8.0	10.0	20.0
76×76×6.4	76.2	195.4	8.0	22.4	Yes	8.0	10.0	20.0
76×76×4.8	76.2	189.9	11.9	22.1	Yes	5.0	8.0	16.0
76×76×3.2	76.2	184.8	20.0	21.9	Yes	5.0	5.0	10.0

All models were subjected to the same loading protocol, which consisted of cycles of imposed equivalent drift ratio of increasing magnitude: ± 0.1, ± 0.25, ± 0.5, ± 0.75, ± 1, ± 1.5, ±2, ± 3, ± 4 and ± 5%, each imposed for two cycles, as shown in Figure 3.7. This load protocol is the same

used in the tests presented in [3], although in this case the cycles initiate with the loading in compression instead of tension.

Regarding the material properties, a true stress-true strain curve based on real coupon data (specimen HS 152 from reference [10]) from a square HSS, scaled so that its yield stress, F_y, was equal to the probable yield strength of HSSs according to [9], $R_y F_y$=460 MPa, was input into the software. The selected true stress-true strain curve is presented in Figure 3.8. A combined hardening model, considering both isotropic and kinematic hardening, computed by the software based on the stress-strain curve was employed. For the plates, an elastic-perfectly plastic material with F_y=385 MPa was employed. The welds were modelled as elastic. No residual stresses were considered.

Both global imperfection of the BIE and local imperfection of the HSS were included in the models. Examples of the global and local buckled shapes considered in the models are shown in Figure 3.9 and Figure 3.10, respectively. The global buckled shape was scaled so that the maximum initial imperfection at the center of the brace was equal to 1/500 times the hinge to hinge length, and the local buckled shape was scaled to produce a local change of 1% on the initial minimum distance across opposite faces of the HSS.

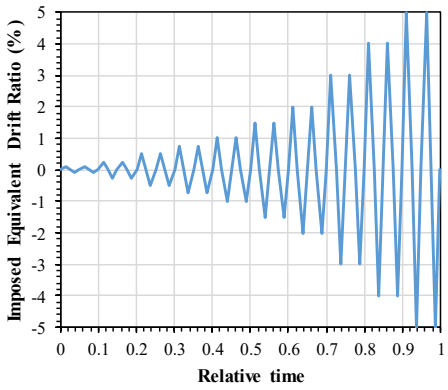

Figure 3.7: Loading protocol

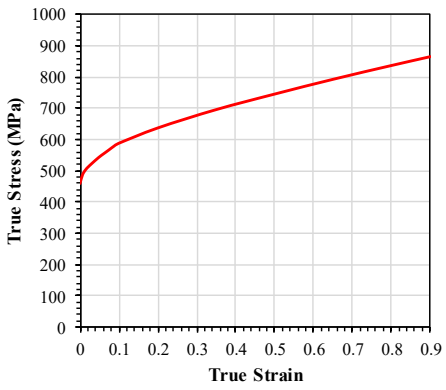

Figure 3.8: True stress-true strain curve for the HSS material (inelastic portion)

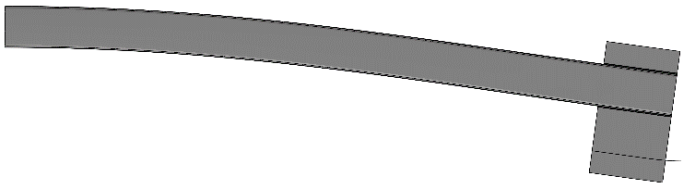

Figure 3.9: Example of deformed shape for global buckling imperfection

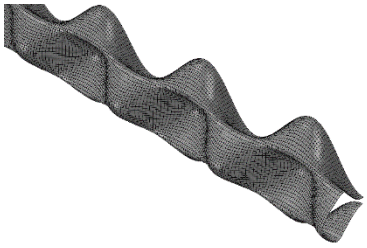

Figure 3.10: Example of deformed shape for local buckling imperfection

3.4. VALIDATION OF MODELLING APPROACH

To verify the appropriateness of the modelling considerations described above, a model of one of the specimens tested by Skalomenos et al. [3], specimen G1-Oop-60, was constructed and analysed in Abaqus, using the information provided in [3]. Both the HSS and the gusset plate were modelled using shell elements, which was not possible for the *eccentering* assembly's elements due to their geometry. The initial imperfections were consistent with what is described in the previous section, and the material with the curve in Figure 3.8, which was again scaled down to match the F_y and F_u values reported in [3].

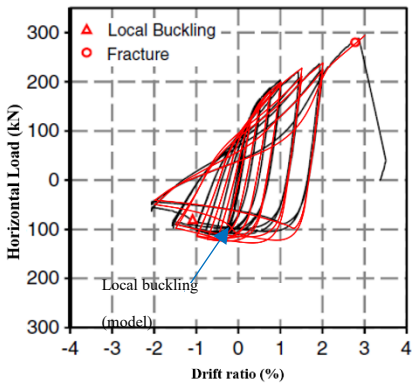

Figure 3.11: Comparison of results from Abaqus validation model with experimental results for specimen G1-Oop-60 from reference [3]

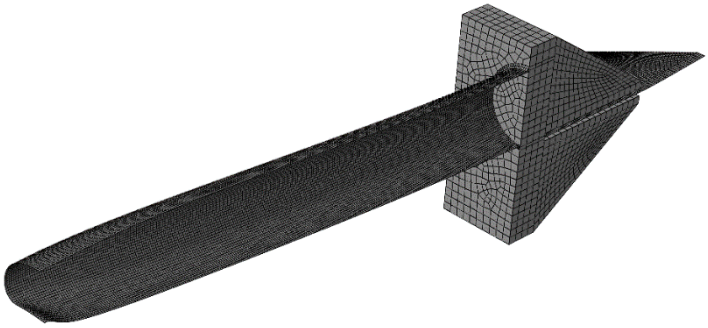

Figure 3.12: Abaqus validation model at onset of local buckling

Figure 3.11 presents the results from the so defined validation model, superimposed on the experimental force-drift hysteresis curve reported for specimen G1-Oop-60 in [3]. As can be noted, the proposed modelling approach produced a result that matches satisfactorily the experimental results, even though the actual stress-strain information for the materials involved was not available. The onset of local buckling was predicted within the same cycle as it occurred in the test, although slightly earlier. Figure 3.12 shows the deformed shape of the validation model at the onset of local buckling.

3.5. RESULTS

For the 243 individual numerical analyses, force-drift hysteresis plots were obtained and the drift amplitude of the cycle in which the BIE developed local buckling, θ_{md}, was reported. As the precise occurrence of local buckling is not always evident in the hysteresis plots, it was identified by inspecting the animation of the deformation history of the models. 6% was reported as the maximum drift ratio for the specimens for which local buckling was not observed, as the testing protocol had a maximum amplitude of 5%. Figure 3.13 presents an example of the resulting force-

drift hysteretic curve, including an indicator for the onset of local buckling. Figure 3.14 shows the deformed state of the same BIE's mid-length at the onset of local buckling.

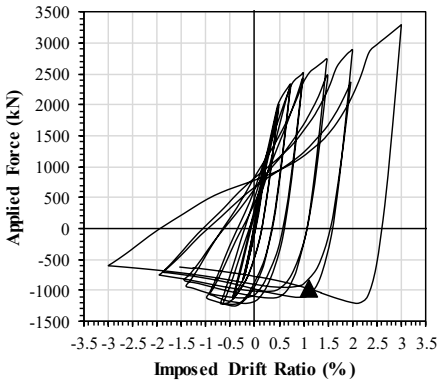

Figure 3.13: Example of obtained force – drift hysteretic curve for HSS 178×178×16 model with e/H=0.75, with indication for observed onset of local buckling

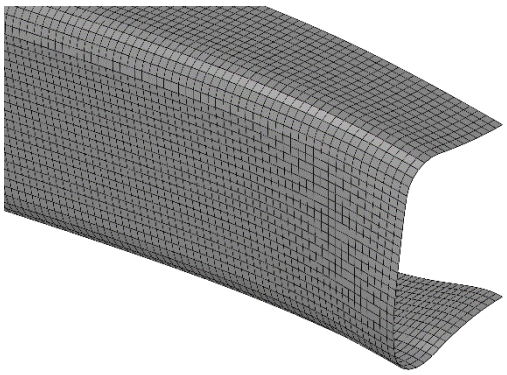

Figure 3.14: Incipient local buckling at mid-length of HSS 178×178×16 model with e/H=0.75

The results show that, as expected, the fracture life increases with the eccentricity, with the section compactness and with the global slenderness. In the majority of cases, local buckling occurred at the expected location, but in some particular cases, such as for the 254×254×6.4 for e/H ratios larger than 1.5, it was observed that local buckling occurred in the top of the BIE toward the ends of the braces instead of at the bottom at the mid-length. This is presumably due to the formation of plastic hinges when the brace is loaded in tension, and this aspect will be further investigated at later stages of the research program, although preliminarily sections with such a large local slenderness do not seem to have much potential to be employed as BIEs. In Figure 3.15 and Figure 3.16 the observed maximum drift ratios for the HSS 102×102 and the HSS 178×178 models are presented. Note that according to these results, very compact sections would be able to sustain very large drift ratios without being affected by local buckling, and therefore be very well suited to be employed in FIEBs with large target deformation levels.

A non-dimensional combined slenderness parameter, $\lambda_0 = (L/r)/(b_{el}/t)$ was defined to group together both slenderness parameters and analyse the relation of θ_{md} to λ_0 and e/H. Thus, it was possible, after eliminating outlier results, to obtain through multiple regression an expression that allows one to estimate the maximum allowable drift ratio as a function of the combined slenderness parameter and the eccentricity ratio. The obtained expression is given in Equation (3.1). The so obtained regression model presents an adjusted R-square value of 0.98 and a root mean square error (RMSE) of 0.345. Figure 3.17 presents a scatter plot with the obtained point data, and the surface obtained with Equation (3.1), Figure 3.18 compares the observed values of θ_{md} with those resulting from the use of Equation (3.1).

$$\theta_{md} = -0.4312 + 0.1943\lambda_0 + 0.6704e_0 - 0.001319\lambda_0^2 - 0.01833\lambda_0 e_0 + 0.241e_0^2 \qquad (3.1)$$

It is recommended that when considered a given BIE for its use in a FIEB, its expected fracture life be estimated employing Equation (3.1), considering a safety margin. Further research, however, including physical testing is required to obtain more information on the fracture life of BIEs and to further refine the proposed model.

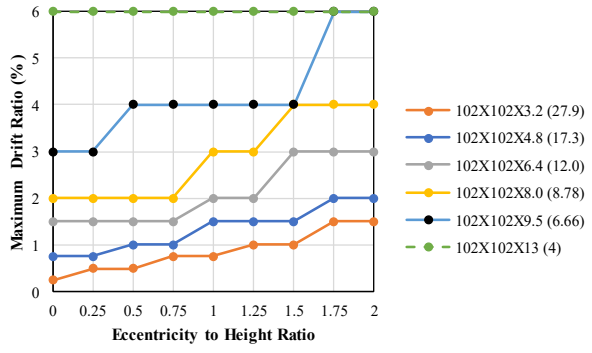

Figure 3.15: Observed maximum drift ratios for HSS 102×102 models (L/r ≈ 150)

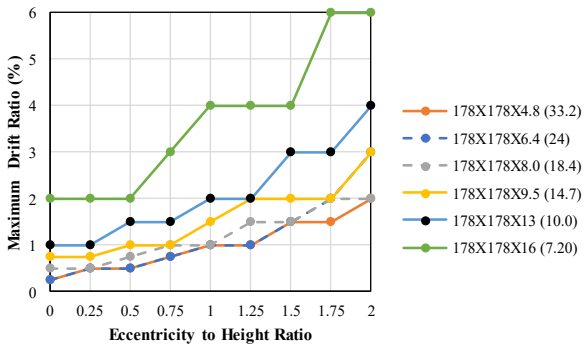

Figure 3.16: Observed maximum drift ratios for HSS 178×178 models (L/r ≈ 90)

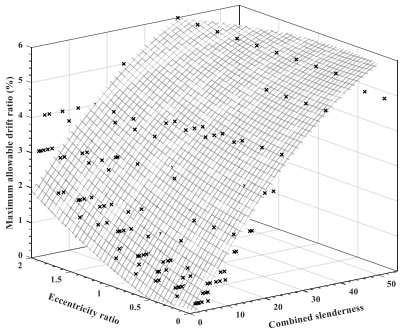

Figure 3.17: Maximum allowable drift ratio vs. combined slenderness and eccentricity ratio

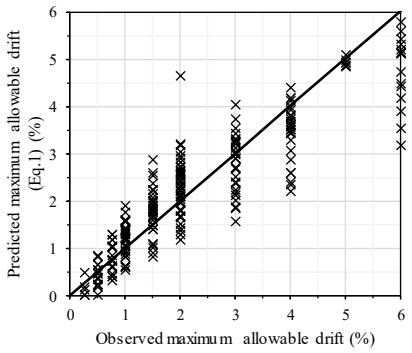

Figure 3.18: Maximum allowable drift ratios – observed vs. predicted by Eq. (3.1)

In addition to θ_{md}, the total dissipated energy by the BIEs before the onset of local buckling was also calculated. Figure 3.19 and Figure 3.20, present the total energy dissipated by the HSS 102×102 and the HSS 178×178 models, as a function of the eccentricity. As can be observed, there is no clear correlation between the eccentricity and the energy dissipation capacity of the BIEs. Instead, the results suggest that the energy dissipation capacity is a property of the section itself. The downward trend of the curve for the HSS 102×102×13 model occurred because no local buckling was observed during the entire load protocol, therefore, because of the increasing eccentricity, the total amount of energy dissipated during the test decreased.

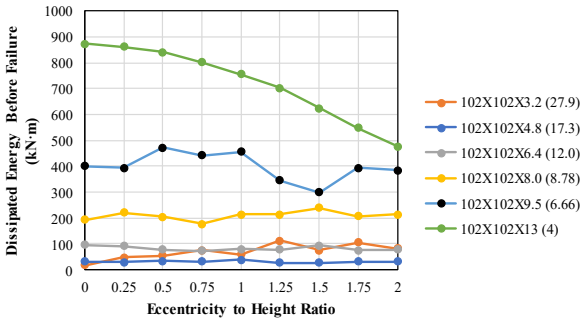

Figure 3.19: Dissipated energy prior to the onset of local buckling for HSS 102×102 models (L/r ≈ 150)

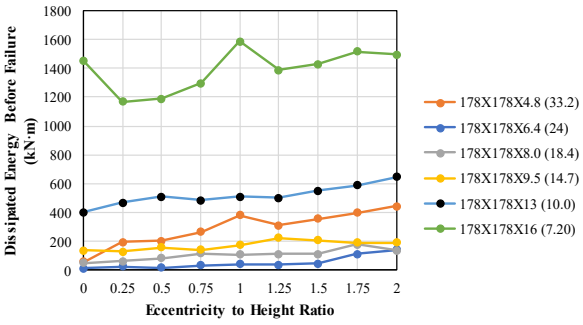

Figure 3.20: Dissipated energy prior to the onset of local buckling for HSS 178×178 models (L/r ≈ 90)

To obtain a better estimate of the actual damping that the BIEs would produce in a FIEB, the equivalent viscous damping ratio, ξ_{eq}, was calculated for each cycle based on its definition given

in [11], using Equation (3.2), where E_d is the energy dissipated during a complete cycle, F_m is the maximum force attained in the cycle and δ_m the displacement amplitude of the cycle.

$$\xi_{eq} = \frac{E_d}{2\pi F_m \delta_m} \tag{3.2}$$

The results of this calculation obtained for the Abaqus models of the HSS 178×178×16 are presented in Figure 3.21 as an example. It can be noted that, for eccentricity ratios higher than 1.0, the maximum value of ξ_{eq} seems not to present much variation. However, it must be noted that neither the spacing of the cycle's amplitude nor the amount of data points that were registered in the analysis runs in Abaqus were fine enough to adequately obtain these results as, initially, it was not planned that the parametric study would be used to provide this information. For this reason, additional analyses were performed in OpenSees, with a higher resolution of data points and a finer increment of the displacement amplitude (cycles were defined in increments of 0.25% equivalent drift ratio), in order to obtain more reliable information regarding the equivalent damping ratio of BIEs.

The results of these second set of analyses showed that although the maximum value of the equivalent damping ratio shows very little variation for a given section as a function of the eccentricity ratio, the displacement at which this maximum value of ξ_{eq} is attained did show a correlation with the eccentricity ratio. However, by having ξ_{eq} expressed instead as a function of the ductility demand, calculated with respect to the displacement of the first yield point obtained from tests under monotonic load, it was found that for BIEs with eccentricity ratios larger than 0.8, the maximum value for ξ_{eq} and the associated ductility demand are approximately constant. An example of these results is shown in Figure 3.22 for BIEs of HSS 152×152×13.

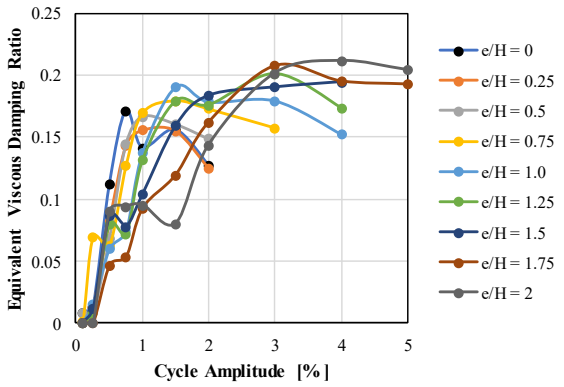

Figure 3.21: Equivalent viscous damping vs. cycle amplitude from Abaqus models for HSS 178×178×16

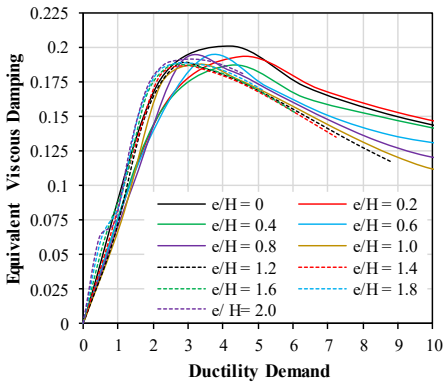

Figure 3.22: Equivalent viscous damping vs. ductility demand from OpenSees models for HSS 152×152×13

A formal model to estimate the values of ξ_{eq} of BIEs to be used in displacement-based design is yet to be developed. The values obtained in this research provide only an estimate of those, as actual values employable for design would require further calibration to ensure that they would provide adequate results under the effects of actual ground motions. The formal creation of these models was not considered in the scope of this research. However, considering that the maximum value of ξ_{eq} as a function of the ductility demand, μ, is nearly constant for a given section, and that it is not affected by the eccentricity, the use on BIEs of the models developed by Wijesundara et al. [12] for the equivalent damping of CCBs, given by Equation (3.3), is considered appropriate in the interim. Their use as part of the design procedure developed by the authors [4] has so far yielded acceptable results.

$$\begin{aligned} \mu \leq 2: \quad & \xi_{eq} = 0.03 + \left(0.23 - \frac{\lambda}{15}\right)(\mu - 1) \\ \mu > 2: \quad & \xi_{eq} = 0.03 + \left(0.23 - \frac{\lambda}{15}\right) \\ & \lambda = \frac{L}{r}\sqrt{\frac{F_Y}{\pi^2 E}} \end{aligned} \tag{3.3}$$

3.6. CONCLUSIONS

BIEs appear as innovative dissipative elements whose use in seismic-force-resisting systems has the potential to overcome some of the major shortcomings of conventional concentric braces, specifically those related to their invariably high stiffness and their propensity to premature failure due to low-cycle fatigue fracture, as the introduction of the eccentricity is expected to delay the onset of local buckling. However, due to their particular force-deformation behaviour they are better suited to displacement-based design procedures instead of force-based ones. For this reason, it is of great relevance to estimate the displacement level that a given BIE would be able to sustain safely under cyclic loading.

With the intent of doing so, a numeric parametric study was undertaken for square HSSs, treating the eccentricity ratio, the global slenderness ratio and the local slenderness ratio as variables. As expected, the results showed that the fracture life increases with the eccentricity ratio, the section compactness, and overall slenderness. Using the results from the 243 individual analyses, a prediction equation based on multiple regression was obtained to estimate the maximum allowable drift ratio for BIEs as a function of the eccentricity ratio and a combined slenderness parameter that encompasses both local and global slenderness. Through a validation model that approximated well the experimental results presented by Skalomenos et al. in their seminal paper on BIEs [3], it was verified that the modelling approach used in the parametric study was able to simulate the response of BIEs, in particular the onset of local buckling.

Additionally, information was gathered regarding the energy dissipation capacity of BIEs and the equivalent damping ratio associated with it. It was found that the net energy dissipation capacity previous to the onset of local buckling does not depend on the eccentricity; it seems instead to be a function of the geometry of the bracing member and its material. As well, it was determined that

neither the maximum equivalent damping ratio nor the ductility demand at which it occurs for a given BIE depend on the eccentricity. Thus, until properly calibrated methods specifically for BIEs are presented, it is suggested that the relations developed by Wijesundara et al. for estimating the equivalent damping ratio of concentric braces be used to approximate the equivalent damping ratio of BIEs in a displacement-based design scenario.

All the results presented herein are to be considered as preliminary, given that so far, no test results have been published for BIEs made of square HSSs or employing the *eccentering* assembly here considered. Further stages of the ongoing research program include the physical testing of BIEs such as those considered in this study. The data obtained will shed additional light on the actual behaviour and failure mode of BIEs and will be used to validate, refine or refute the proposed model.

ACKNOWLEDGEMENTS

The authors would like to thank DPHV Structural Consultants, ADF Group Inc. and Constructions Proco for their generous technical and financial support, as well as the Natural Sciences and Engineering Research Council (NSERC) of Canada, the Fonds de Recherche du Québec – Nature et Technologies (FRQ-NT) and the Centre d'Études Interuniversitaire des Structures sous Charges Extrêmes (CEISCE). The first author also wishes to acknowledge Universidad de Costa Rica for financing the undertaking of his doctoral studies.

REFERENCES

[1] X. Tang and S. C. Goel, "Brace fractures and analysis of Phase I Structure," *Journal of Structural Engineering,* vol. 115, no. 8, pp. 1960-1976, 1989, doi: 10.1061/(ASCE)0733-9445(1989)115:8(1960).

[2] R. Tremblay, "Inelastic seismic response of steel bracing members," *Journal of Constructional Steel Research,* vol. 58, no. 5-8, pp. 665-701, 2002, doi: 10.1016/S0143-974X(01)00104-3.

[3] K. A. Skalomenos, H. Inamasu, H. Shimada, and M. Nakashima, "Development of a steel Brace with Intentional Eccentricity and experimental validation," *Journal of Structural Engineering,* vol. 143, no. 8, p. 04017072, 2017, doi: 10.1061/(ASCE)ST.1943-541X.0001809.

[4] A. González Ureña, R. Tremblay, and C. A. Rogers, "Design and performance of Frames with Intentionally Eccentric Braces " Proceedings of the *17th World Conference on Earthquake Engineering*, Sendai, Japan, 2020. Paper no. C000830.

[5] F. T. McKenna, "Object-oriented finite element programming: Frameworks for analysis, algorithms and parallel computing," Ph.D. Thesis, Civil Engineering, University of California, Berkeley, 1997.

[6] *National Building Code of Canada 2015, 14th ed.* , National Research Council of Canada (NRCC), Ottawa, ON, 2015.

[7] *Dassault Systèmes, Abaqus/CAE 2019*. (2018). Dassault Systèmes Simulia Corp., Providence, RI.

[8] B. Fell, A. Kanvinde, and G. Deierlein, *Large-scale testing and simulation of earthquake-induced ultra low cycle fatigue in bracing members subjected to cyclic inelastic buckling*. Stanford, CA: John A. Blume Earthquake Engineering Center, 2010.

[9] *CSA. S16-14: Design of steel structures*, Canadian Standards Association (CSA), Toronto, ON, 2014.

[10] R. Moreau, "Evaluation of the "Modified-Hidden-Gap" connection for square HSS brace members," M. Eng. Thesis, Civil Engineering and Applied Mechanics, McGill University 2014.

[11] A. K. Chopra, *Dynamics of structures: theory and applications to earthquake engineering*, 4th ed. Upper Saddle River, N.J.: Prentice Hall, 2012, pp. xxxiii, 944 p.

[12] K. Wijesundara, R. Nascimbene, and T. J. Sullivan, "Equivalent viscous damping for steel concentrically braced frame structures," *Bulletin of Earthquake Engineering,* vol. 9, no. 5, pp. 1535-1558, 2011, doi: 10.1007/s10518-011-9272-4.

FOREWORD TO CHAPTER 4

In Chapter 4, an updated version of the design procedure found in Chapter 2 is described. The procedure was revised for its application in Canada; thus, some specific points were modified to reflect the requirements of the National Building Code of Canada and the CSA S16-14 standard. Additionally, provisions were incorporated aiming to minimize the damage in the structure produced by frequent, or service level, earthquakes, and to consider wind loading explicitly. Although there is a significant overlap between the contents of Chapter 4 and Chapter 2, its inclusion in this thesis was deemed pertinent as it showcases the versatility of the proposed design procedure, demonstrates the applicability of Frames with Intentionally Eccentric Braces in regions with different levels of seismic hazard, sheds light on their performance for ground motions with various types of seismic sources, provides information on the expected damage due to frequent earthquakes, and identifies the conditions under which they are most advantageous in comparison with traditional concentrically braced frames.

CHAPTER 4: DESIGN AND PERFORMANCE OF FRAMES WITH INTENTIONALLY ECCENTRIC BRACES

Conference paper, published in the Proceedings of the 17th World Conference on Earthquake Engineering, Sendai, Japan (http://www.17wcee.jp/links.php – paper nºC000830). Oral presentation postponed due to the COVID-19 pandemic.

Andrés González Ureña, Robert Tremblay, Colin A. Rogers

ABSTRACT

Concentrically Braced Frames (CBFs) with Hollow Structural Sections (HSSs) as the bracing members present significant shortcomings that pose limits to their convenience. Due to their inherently stiff nature, CBFs are usually constrained to low fundamental periods of vibration and, thus, high acceleration and force demands, which, in conjunction with the intrinsic overstrength that derives from the compression resistance controlling the dimensioning of the bracing members, results in high design forces for the capacity-protected components of the structure and its foundations. Furthermore, their ductility and energy dissipation capacity are hindered by the susceptibility of HSSs to low-cycle fatigue induced premature fracturing at the plastic hinge region after the onset of local buckling. To address these shortcomings of Conventional Concentric Braces (CCBs), researchers from Japan recently proposed the use of Braces with Intentional Eccentricity (BIEs). Being subject to both flexural and axial deformations under axial loading, BIEs are inherently less stiff than CCBs. Moreover, their axial stiffness can be adjusted by varying

the eccentricity to obtain the desired frame response. Also, initiation of local buckling occurs at larger axial displacements because the strain demand is more evenly distributed over the brace length. However, BIEs are not well suited for standard force-based design procedures given that the force they develop varies continuously with their axial deformation, and that they attain their maximum capacity at large deformation values that depend on the eccentricity. For this reason, the use of BIEs compels the use of an alternative design approach that handles explicitly their particular response to loading.

This article presents a Direct Displacement-Based Design (DDBD) procedure for the seismic design of Frames with Intentionally Eccentric Braces (FIEBs). The proposed procedure includes provisions aiming to control the performance of the structure when subjected to design level earthquakes and to minimize its damage under frequent earthquakes. The method is applied to prototype buildings of 4, 8 and 12 storeys, with square HSS bracing members, and considering two levels of target drift ratio. The structures are designed for a region of high seismic hazard and for a region of moderate seismic hazard, both within Canada. The performance of the so designed buildings is then evaluated through Non-Linear Response-History Analysis (NLRHA). The results show that the seismic performance of FIEBs is satisfactory and on par with the performance objectives incorporated in the procedure and those of the National Building Code of Canada. Furthermore, the resulting tonnage of the FIEB buildings is compared to that of traditional Moderately Ductile and Limited Ductility CBFs designed for identical conditions, showing that FIEBs may constitute an economically advantageous alternative to conventional CBFs, specially in the case of moderately tall buildings located in regions of high seismic hazard.

Keywords: steel braced frames; eccentric braces; earthquake-resistant design; displacement-based design

4.1. INTRODUCTION

Despite their popularity as Seismic-Force Resisting Systems (SFRSs) for low- and mid-rise buildings in seismic regions, due to their efficiency and aesthetic appeal, Concentrically Braced Frames (CBFs) with Hollow Structural Sections (HSSs) as the bracing members bear notable shortcomings that weigh on their overall convenience. To begin with, due to their intrinsic stiffness, CBFs generally possess low fundamental vibration periods, and are thus subjected to high spectral acceleration demands, which, in combination with the considerable overstrength that originates from the compression resistance governing the sizing of the bracing members, leads to large capacity-based design forces for the protected components of the SFRS and foundations, increasing the cost of the structure. In addition to this, HSSs have been proven to be prone to low-cycle fatigue induced fracturing in the mid-length plastic hinge region following the onset of local buckling [1, 2], diminishing their ductility under cyclic loading and their energy dissipation capacity. Lastly, because of the nearly null post-yielding stiffness of Conventional Concentric Braces (CCBs), CBFs are at risk of becoming unstable when subjected to ground motions inducing very large displacement demands or ratcheting.

In 2017, Skalomenos et al. [3] proposed to introduce an intentional eccentricity to otherwise conventional bracing members, addressing the drawbacks stated above by modifying the force-deformation response of the lateral load carrying system. The proposed Braces with Intentional Eccentricity (BIEs) are otherwise regular CCBs, with their longitudinal axis translated with respect to the working points. In contrast with CCBs, BIEs are naturally less stiff as they are subjected to bending moment in combination with axial force. Under tension, they display a pseudo tri-linear force-deformation response with considerable post-yielding stiffness. Under compression, they exhibit a smooth flexural response in which the brace transitions from the elastic to the post-

buckling regime without showing sharp peaks due to buckling. Moreover, by adjusting the magnitude of the eccentricity, the pre- and post-yielding stiffness of the BIE can be controlled. Skalomenos et al. performed physical tests under cyclic loading on reduced scale round HSS BIE specimens with two levels of eccentricity. In addition to confirming the behaviour described above, their results showed that, compared to a CCB made from the same HSS, BIEs develop local buckling at the mid-length plastic hinge region at higher imposed drift ratios, thus delaying fracture.

In an effort to reconcile the Capacity-Based Design philosophy that prevails in many modern design codes, such as the National Building Code of Canada [4], and the distinct force-deformation response of BIEs, which sets them apart not only from CCBs, but from most other traditional ductile dissipative elements, the authors of this article propose a design procedure for Frames with Intentionally Eccentric Braces (FIEBs) based on the Direct Displacement-Based Design (DDBD) method. This design approach addresses explicitly the particularities of BIEs, and incorporates provisions aiming to guarantee that the components of the SFRS, other than the braces proper, withstand undamaged the demands arising from the inelastic response of the latter. This paper includes a brief overview of the characteristics of BIEs and their implications on building design, a delineation of the proposed design procedure, and the assessment, through Non-Linear Response-History Analysis (NLRHA), of the performance of twelve example buildings with square HSS BIEs, designed using such procedure.

In a companion paper [5], the authors present results from a numerical parametric study on BIEs, in which some of the herein proposed design procedure's considerations, regarding fracture life and equivalent damping ratios of BIEs, are based.

4.2. BIEs AND THEIR FORCE-DEFORMATION RESPONSE

The components of a nonspecific BIE are presented schematically in Figure 4.1. The prescribed eccentricity, e, is the offset between the working points, which generally would coincide with the braced bent diagonal, and the bracing member's axis. The eccentric condition of the brace is achieved by means of *eccentering* assemblies, that is, any sort of plate assembly conceived to transfer rigidly the forces between the bracing member and its connections to the frame, while accommodating the eccentricity. Assuming that the connections at the ends of the BIE behave as pins, its force-deformation response depends on the geometry of the cross-section, the total length, L, the *eccentering* assembly's length, L_{ea}, and the eccentricity.

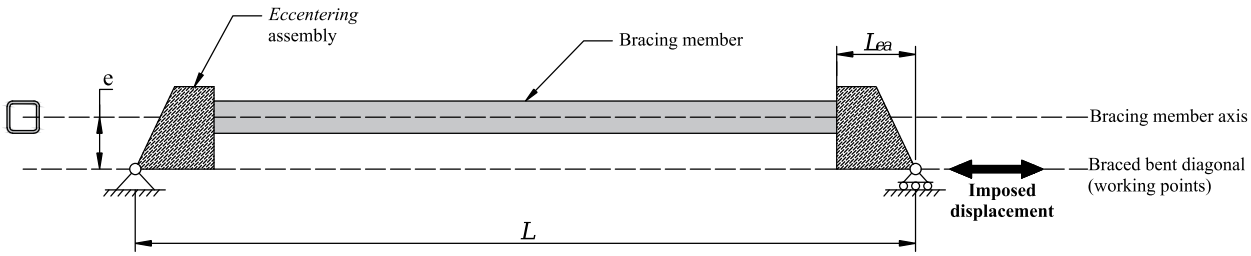

Figure 4.1: Schematic drawing of a general BIE and its components

In Figure 4.2, the idealised force-deformation behaviour of BIEs under tensile and compressive loads is presented and compared to that of CCBs. Under tensile load, as the BIE elongates it is also subjected to moment and thus bends toward the working point axis. When the outermost fiber in tension reaches the yield stress, the BIE attains the *first yield point*, (T_y, δ_y), marking the transition from the elastic to the post-yielding stages, and a net reduction of the stiffness. As loading progresses beyond this point, plastification of the cross-section progresses gradually. However, since the net eccentricity reduces in the deformed configuration of the brace, this stage is characterised by a continuously increasing stiffness. When the complete cross-section reaches yielding, the BIE attains its *ultimate yield point*, (T_u, δ_u), at a force level equal to the yield tensile

strength of a CCB. As shown in Figure 4.2-(a), the force-deformation behaviour of BIEs in tension can be approximated by a tri-linear model, with an initial, or elastic, stiffness K_i, a secondary, or post-yielding stiffness K_s, and finally, a negligible fully-yielded stiffness.

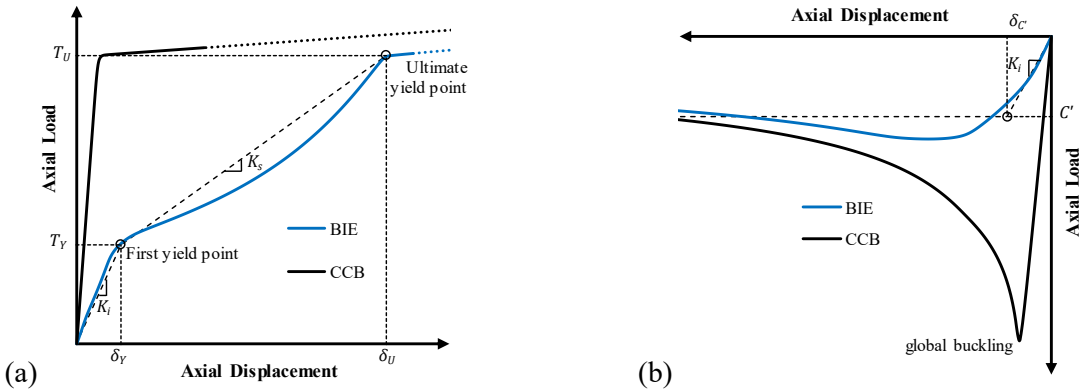

Figure 4.2: Idealised force-deformation behaviour of BIEs and CCBs: tension, (a), and compression, (b)

Under compressive load, the BIE bends away from the working points axis, producing a progressive increment of the net eccentricity and, therefore, a reduction of the stiffness, transitioning seamlessly from the elastic to the post-buckling regime (Figure 4.2-(b)). It is proposed that the response of BIEs in compression be approximated with an elastic-perfectly plastic model, with initial stiffness K_i and maximum force, C'. The compressive resistance of the BIE, C', can be estimated, as proposed by Skalomenos et al. [3], by the load corresponding to the elastic limit state of a column under eccentric axial load.

Keeping all other parameters constant, the magnitude of the eccentricity controls the values of T_y, K_i, K_s, and C'. An example of the influence of the eccentricity on the tensile response of BIEs is presented in Figure 4.3, which shows the force-deformation curves in tension of HSS 178×178×16 BIEs for increasing levels of eccentricity, as obtained from OpenSees [6] models. In these models, L was 5408 mm and the *eccentering* assemblies were represented by rigid links with length, L_{ea}, of 360 mm. The end connections were modelled as rectangular plates with thickness of 38.1 mm

and width of 360 mm, and a free length of 77 mm intended to yield in flexure under low levels of force, thus approximating the desired pin-like behaviour. The yield stress was taken as 345 MPa both for the plates and the HSS.

When subjected to cyclic loading, the contrast between the CCBs' and the BIEs' responses is also striking. Figure 4.4 shows the storey shear vs. storey drift plots for pairs of HSS 178×178×16 BIEs, with eccentricities of 120 and 180 mm acting together opposed against each other, on adjacent 6 m by 4 m braced bays under cyclic load with increasing displacement amplitude, as also obtained from OpenSees analyses. Although, evidently, the force opposed by the BIEs, and the net amount of energy they dissipate, is lower than for CCBs, it is noteworthy that BIEs exhibit a stable hysteretic response with significant positive secondary stiffness. The absence of peaks due to buckling would allow for avoiding the requirement of considering separate buckling and post-buckling cases when determining the capacity-based demands on the protected elements.

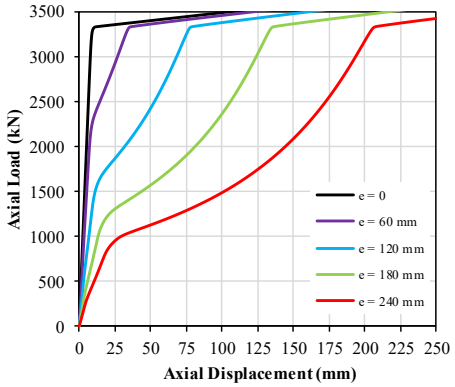

Figure 4.3: Influence of eccentricity in the tension force-displacement behaviour of 178×178×16 HSS BIEs

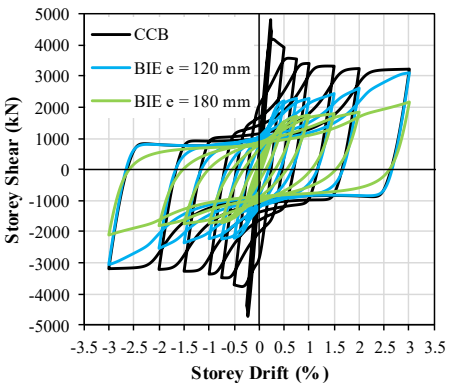

Figure 4.4: Storey shear vs. drift for 6 m by 4 m bays braced with 178×178×16 HSS BIEs and CCBs

4.3. PROPOSED DESIGN PROCEDURE FOR FIEBs

As can be implied from the previous section, force-based procedures, commonly employed following up-to-date code provisions, such as those provided in [4] for the design of MD-, LD-

and CC-CBFs, are not well suited for use in the design of FIEBs. Standard force-based design procedures, albeit implicitly, assume that the dissipating elements behave in an elastic-perfectly plastic manner, with small yield displacements or rotations. This allows for the dissipating elements to be dimensioned by leveling their capacity to the anticipated seismic force demands, scaled down in account of the ductility and overstrength of the system. In the case of BIEs, however, the maximum force level depends on the eccentricity, and the associated axial displacement can often be too large to be compatible with serviceability limit states, rendering inappropriate an approach based on said maximum force. Furthermore, their post-yielding stiffness is not negligible and, as stated earlier, will increase with the displacement (Figure 4.2-a); as such, their overall force-deformation response strays far from an elastic-perfectly plastic idealisation.

Considering the arguments above, and noting that for a given section and set of dimensions, the relevant properties of the BIEs' response for design effects (i.e. T_y, T_u K_i, K_s, and C'), can be easily obtained numerically for any eccentricity value, thus enabling to express the force developed as a function of the imposed displacement, the adoption of a displacement-based design procedure appears as an appropriate course of action for FIEBs. More precisely, a procedure based on the Direct Displacement-Based Design (DDBD) [7] is adopted in this research. In the available literature, several examples of the successful application of DDBD to the design of CBFs are available [8, 9]. A preliminary version of the design procedure, and its application to the design of FIEBs, was presented by the authors in [10]. In the following lines, a brief description of the steps constituting the proposed design procedure is presented.

1. *Selection of Target Storey Drift, θ_d, and definition of equivalent SDOF mass and displacement*

The normalised target displacement vector is calculated using Equation (4.1), which corresponds to inelastic mode shapes for low-rise and taller moment frames given in [7]. Although expressions

developed specifically for CBFs have been proposed [11], verifications performed by the authors indicate that the mode shapes given by Equation (4.1) are closer to the inelastic mode shape of FIEBs, presumably owing to their higher flexibility decreasing the contribution of the columns' deformation to the deformed shape. In Equation (4.1), n is the number of storeys, H_i and H_n are the elevations of the ith and top storeys, and δ_i is the normalised lateral displacement of the ith storey. The normalised target displacement vector is then scaled so that the maximum storey drift matches the Target Storey Drift, θ_d, which corresponds to the maximum storey drift that is intended to occur in the building under the Design Earthquake, and is defined as the starting point of the design process.

$$\begin{aligned} n \leq 4: &\qquad \delta_i = \frac{H_i}{H_n} \\ n > 4: &\qquad \delta_i = \frac{4H_i}{3H_n}\left(1 - \frac{H_i}{4H_n}\right) \end{aligned} \tag{4.1}$$

Having obtained and scaled the normalised displacement vector, the equivalent SDOF mass, M_{eq}, and displacement, Δ_{eq}, can be calculated with Equation (4.2) and Equation (4.3), where d_i and m_i are the target displacement and the mass of the ith storey.

$$\Delta_{eq} = \frac{\sum d_i^2 m_i}{\sum d_i m_i} \tag{4.2}$$

$$M_{eq} = \frac{\sum d_i m_i}{\Delta_{eq}} \tag{4.3}$$

2. *Determination of the Target Secant Period from the Damped Displacement Design Spectrum*

The target secant period, T_{eq}, corresponds to the ordinate of the point with abscissa Δ_{eq} in the Damped Displacement Design Spectrum. To avoid excessively flexible structures, however, the

authors recommend that T_{eq} should not be taken larger than 10 s. The 5% damped displacement spectrum, S_d, can be obtained directly from the design acceleration spectrum, S_a, using Equation (4.4), and the be scaled down to account for the equivalent viscous damping, ξ_{eq}. In this research, the equivalent damping reduction factor, R_ξ, recommended by Eurocode 8 [12], given by Equation (4.5), is adopted.

$$S_d = S_a \frac{T^2}{4\pi^2} \tag{4.4}$$

$$R_\xi = \sqrt{\frac{0.1}{0.05 + \xi_{eq}}} \tag{4.5}$$

The proper ξ_{eq} value to be used depends on the sections selected for the BIEs and on their anticipated ductility demand. As is explained in the companion paper [5], the model developed by Wijesundara et al. for CCBs [13], given in Equation (4.6), is used in this research. At the beginning of the design process, the BIEs' sections are not known and it is suggested to use ξ_{eq}= 0.15 as an initial estimate, to be corrected or verified later on. In Equation (4.6), μ is the ductility demand on the BIE, calculated with respect to its first yield point, r is the section's radius of gyration and E is the modulus of elasticity.

$$\begin{aligned} \mu \leq 2: &\qquad \xi_{eq} = 0.03 + \left(0.23 - \frac{\lambda}{15}\right)(\mu - 1) \\ \mu > 2: &\qquad \xi_{eq} = 0.03 + \left(0.23 - \frac{\lambda}{15}\right) \\ &\lambda = \frac{L}{r}\sqrt{\frac{F_Y}{\pi^2 E}} \end{aligned} \tag{4.6}$$

3. *Calculation of target "primary" secant stiffness, base shear, and equivalent static force vector*

Having determined T_{eq}, the target "primary" secant stiffness, K_{eq}, can be obtained from Equation (4.7). This stiffness, directly related to the target spectral displacement of the equivalent SDOF system, is dubbed "primary" to be put in contrast with additional, "auxiliary" stiffness that the FIEB may require to fulfill stability and regularity criteria, as will be explained. With K_{eq}, the equivalent "primary" base shear is obtained through Equation (4.8), and then distributed to each storey using Equation (4.9) and Equation (4.10), which are taken from [4].

$$K_{eq} = 4\pi^2 \frac{M_{eq}}{T_{eq}} \tag{4.7}$$

$$V_{eq} = K_{eq}\Delta_{eq} \tag{4.8}$$

$$F_{eq,i} = \left(V_{eq} - F_t\right)\frac{W_i h_i}{\sum_{i=1}^{n} W_i h_i} \tag{4.9}$$

$$F_t = 0.07 T_{eq} V_{eq} < 0.25 V_{eq} \quad \text{(for } T_{eq} > 0.7 \text{ s)} \tag{4.10}$$

4. *Selection of BIEs for each storey*

At each storey, the BIEs are selected in terms of section-eccentricity pairs, e.g. HSS 152×152×13 – e = 140 mm, such that the net lateral force they produce at the design displacement is equal to than the *design shear*, while complying with minimum stiffness, regularity, serviceability and fracture life criteria hereon discussed. The storey *design shear*, $v_{d,i}$, calculated with Equation (4.11) is defined as the sum of the equivalent "primary" storey shear $v_{eq,i}$ and the notional loads, $v_{n,i}$, (taken as 0.005 times the factored gravity loads as per [4]), amplified by the factor $U_{2,i}$ given by Equation (4.12). The $U_{2,i}$ factor, taken from CSA S16-14 [14], is used to

include the estimated P-Δ effects expected at the level of the design displacements. In Equation (4.12), $C_{f,i}$ are the cumulated factored gravity loads at the ith storey and v_i^* is the storey shear provided by the selected BIEs at the design displacement level.

$$v_{d,i} = U_{2,i}(v_{eq,i} + v_{n,i}) \tag{4.11}$$

$$U_{2,i} = 1 + \left(\frac{C_{f,i} d_i}{v_i^* h_i}\right) \tag{4.12}$$

Aiming to prevent potential instability issues, it is recommended that the ratio of secant lateral stiffness to geometric negative stiffness be larger than 1.5 at every storey. To further favour an adequate response of the structure, i.e. to avoid large concentrations of demands in particular storeys, the vertical stiffness regularity criterion of NBCC 2015 [4] is observed.

Recognizing that BIEs may have first yield points markedly lower than the yield strength of other, conventional, dissipating elements, and that premature yielding under frequent loading conditions is undesirable, the design procedure suggests that in each storey, the shear resistance that the selected BIEs can provide within the elastic range, i.e. that associated with axial forces equal to C' in both the tension and compression braces, be at least equal to the larger between the equivalent static storey shear calculated for a frequent, or service level, earthquake, which for the purposes of this research is determined using the acceleration spectra for a probability of exceedance of 40% in 50 years, and the factored wind shear. The elastic, or initial, period of the FIEB, T_i, used in the calculation of the considered frequent earthquake can be conservatively estimated using Equation (4.13).

$$T_i = 0.05 H_n \tag{4.13}$$

Finally, the fracture life of the selected BIEs shall be estimated in order to select section-eccentricity pairs that can indeed attain safely the intended displacement levels under cyclic loading. This can be performed using the proposed expression for the allowable drift ratio, θ_{md}, whose development is explained in the companion paper [5], and is given by Equation (4.14), where e_0 is the ratio of the eccentricity to the HSS outside height and $\lambda_0 = \frac{Lt}{rb_{el}}$ is a combined slenderness parameter (t is the HSS thickness and b_{el} is the effective width of its walls).

$$\theta_{md} = -0.4312 + 0.1943\lambda_0 + 0.6704e_0 - 0.001319\lambda_0^2 - 0.01833\lambda_0 e_0 + 0.241e_0^2 \quad (4.14)$$

To expedite the selection of the section-eccentricity pairs at each storey, is it suggested to assemble beforehand a database of BIE properties considering the available sections, a wide range of eccentricities, and the actual dimensions that the BIE would have when installed in the braced bay. This way, the forces that the BIEs develop as a function of the imposed displacement will be readily available and all the verifications included in the design procedure can be easily performed in a spreadsheet. The BIE properties can be easily gathered using fiber-based models in OpenSees, considering nominal material properties.

5. Design of the capacity-protected elements of the FIEB

In order to provide the conditions for the FIEBs to be able to develop their expected force-deformation hysteretic response at the design level, or eventually beyond, the non-dissipating elements of the FIEB are deemed protected members and designed according to Capacity-Based Design principles. Thus, the connections, beams, columns and foundations are dimensioned so that their response is elastic under the demands arising from the inelastic action of the braces. Acknowledging the unavoidable uncertainty in the prediction of the maximum storey drifts, it is proposed that the probable forces exerted by the braces on the protected elements of the FIEB be

taken as those corresponding to 1.25 times the design storey drift, considering probable material strength (i.e. $R_y F_y$). As discussed above, since the response of the BIEs in compression can be reasonably modelled as elastic-perfectly plastic, there is no need to distinguish between the buckling and post-buckling cases when determining the probable forces imposed in the non-dissipating elements of the FIEB.

6. *Assessment of the performance of the resulting design*

Considering the high degree of non-linearity of the BIEs' response, and that research on the structural system is still incipient, it is recommended that once the design has been completed, the performance of the building be assessed using a detailed analysis such as NLRHA to verify that the performance objectives are met.

4.4. SEISMIC PERFORMANCE OF FIEBs

To evaluate results obtained from the application of the proposed procedure, 12 buildings with FIEBs as their SFRS were designed. Two locations within Canada were selected to represent high and moderate seismic hazard: Vancouver, British Columbia, and Montréal, Québec. For each location, 12-, 8- and 4-storey FIEB buildings were designed for two values of θ_d: 2.5% and 1.5%. The 2.5% drift level corresponds to the maximum allowable drift ratio for buildings of the Normal Importance Category as per the NBCC [4], and the 1.5% target drift was selected as a moderate value to determine the effects of different target drift ratios on the performance and cost of the structures. All buildings were designed for identical dead and live loads, and for the snow and wind loads corresponding to their location. Class C (firm ground) site condition was assumed in all cases for the determination of the acceleration spectra. Square HSSs were considered for the bracing members and CSA G40.21–350W steel material was assumed for all components. A braced configuration consisting of pairs of single diagonals acting in opposite directions in

adjacent bays, as shown in Figure 4.5, which also presents the plan configuration of the buildings, was selected. The resulting structural design specific to any of the FIEBs along the E-W direction is included herein.

The connections of the braces to the frame consist of gusset- and knife-plate assemblies, connected by bolted angles. The introduction of the eccentricity is achieved by the use of side-plates linking rigidly the HSS to the knife plate, detailed using a clearance with a length of twice the plate's thickness, t_g, to allow for the unrestrained rotation of the BIE's ends. The knife plate is designed to yield in flexure at low levels of load. This configuration was selected because of its simplicity and cost-effectiveness, but also to produce in-plane bending of the frame, thus preventing the storey drifts from imposing flexural demands on the BIEs other than those produced by their eccentricity. The intent was to favour a more predictable force-deformation hysteretic response. A drawing of the typical considered *eccentering* assembly and connection configuration is presented in Figure 4.6.

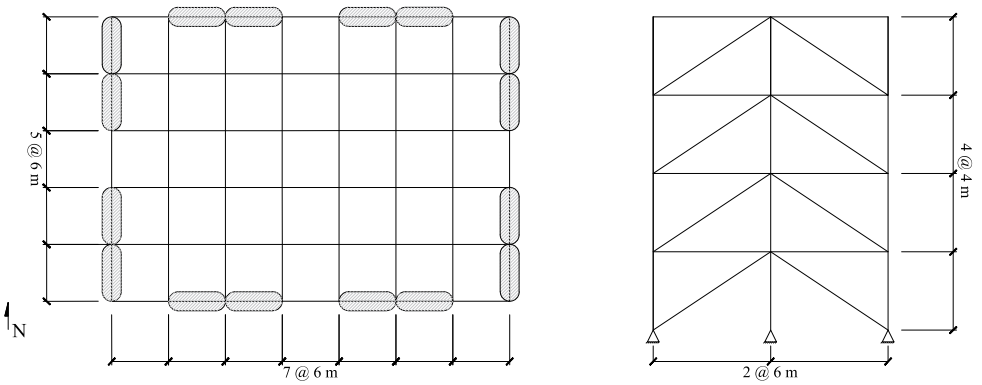

Figure 4.5 : Plan configuration of the buildings and elevation of the considered SFRS (4-storey frame shown)

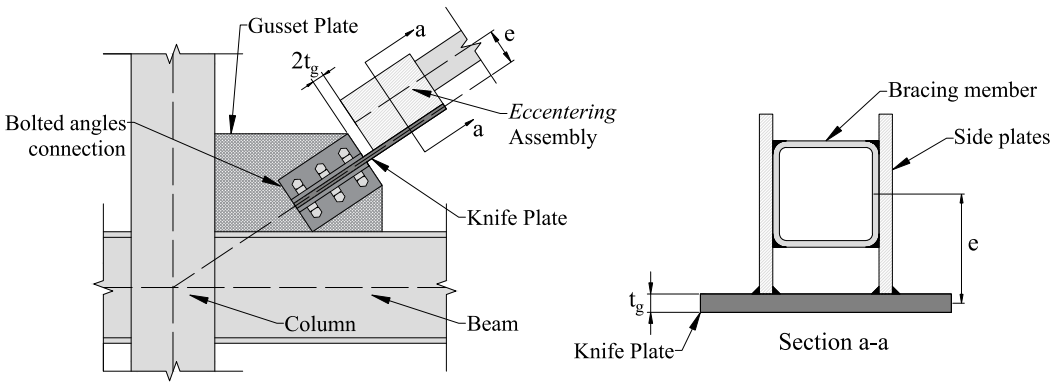

Figure 4.6: Example of the considered BIE to frame connection and *eccentering* assembly

Table 4.1 presents the target secant periods for the 12 designed buildings, as obtained from Step 2 of the design procedure, as well as the limit state which governed in the selection of the BIEs: Design Earthquake, Service Level Earthquake, or factored wind loading. It can be noted that for the location with moderate seismic hazard (Montréal), the 10 s limit on the target period governed for all buildings, as it did for the 12-Storey FIEB with θ_d= 2.5% located in Vancouver. It is also worth noting that, in most cases, the Service Level Earthquake equivalent static forces determined the BIE selection, and that in one case the wind loads governed. This implies that the chosen structure provided significantly more stiffness and resistance than that required to meet the intended displacements under the action of the Design Earthquake alone, therefore undermining the relevance of the target drift ratios. An example of the resultant designs is presented in Figure 4.7. As can be seen, only two HSS section sizes are used over the building's height, a result of varying the eccentricity introduced by the *eccentering* assembly. It has been found through iteration, that the most efficient design, considering cost and compliance with the design procedure's requirements, is often obtained by selecting one constant brace section for the lower three fourths to two thirds of the structure, and another one for the top storeys.

Table 4.1: Target secant period and limit state governing the design of the 12 buildings

	Vancouver		Montréal	
Building type	Target period	Governing limit state	Target period	Governing limit state
12-Storey, θ_d=2.5%	> 10 s	Service level earthquake	> 10 s	Design earthquake
12-Storey, θ_d=1.5%	4.98 s	Design earthquake	> 10 s	Design earthquake
8-Storey, θ_d=2.5%	6.97 s	Design earthquake	> 10 s	Wind
8-Storey, θ_d=1.5%	3.24 s	Service level earthquake	> 10 s	Service level earthquake
4-Storey, θ_d=1.5%	3.41 s	Service level earthquake	> 10 s	Service level earthquake
4-Storey, θ_d=1.5%	1.76 s	Service level earthquake	> 10 s	Service level earthquake

The seismic performance of the FIEB buildings was assessed through NLRHA of models based on fiber elements of the SFRSs in OpenSees. In the models, a yield strength of 460 MPa was considered for the HSSs and of 385 MPa for the beams, columns and connection elements, to represent probable material resistances. P-Δ effects were included in the models by incorporating a leaning column carrying the concomitant gravity loads tributary to the FIEB. For each location, a suite of ground motions specifically selected and scaled to be representative of the seismic hazard at the design level was selected, observing the provisions in [4]. In the case of Vancouver, three suites of five ground motion records were considered for the three seismic sources that contribute to the seismic hazard in that location: shallow crustal earthquakes, deep in-slab subduction earthquakes, and large interface subduction events [15]. For Montréal, a suite composed of 11 synthetic ground motions, developed by Atkinson [16], was selected. Only horizontal acceleration was considered in the analyses.

Additionally, to determine whether the BIEs remained in the elastic range during a service level earthquake, a second round of NLRHA was performed, with the ground motions scaled down accordingly. Scale factors with values of 0.23 and 0.12 were used for Vancouver's and Montréal's

ground motion suites, respectively, based on the maximum ratio between the spectral acceleration values of the spectra with 40% and 2% probability of exceedance in 50 years. Although this approach is an approximation that does not represent accurately the aggregated seismic hazard for the more frequent earthquakes, its use here to verify whether the BIEs comply with the proposed serviceability condition, may be considered acceptable.

In general, the NLRHA results show that the performance of the FIEBs was satisfactory, although the target drifts were not met: in all cases, the maximum storey drifts for any of the ground motions were significantly lower than the selected target drifts, owing both to the additional strength and stiffness provided to comply with the serviceability condition, and to the upper limit of 10 s applied to the target period. The building for which the maximum storey drifts were closer to the target drifts was the 12-storey Vancouver FIEB with θ_d=1.5%, seemingly because this was the only building located in the high seismic hazard region for which neither the design level earthquake nor the maximum target period governed the design. As shown in Figure 4.8, the 84th percentile value of its maximum storey drifts is close to 1.25%. As well, it was confirmed that the maximum storey shears were lower than the design probable storey shears used to design the capacity protected elements, which indicates that the related provision fulfills its purpose. An example of this is presented in Figure 4.9. From the results of the second round of NLRHA, it was confirmed both that the mean of the maximum storey drifts produced by the scaled-down ground motion suites were for all buildings lower than the storey drifts associated with the maximum storey capacity within the elastic range (elastic limit drifts), and that the residual storey drifts after the earthquake excitation were negligible, suggesting that the proposed design provision helps in assuring that the buildings will not likely be damaged by demands arising from frequent earthquakes or wind loads. The compared maximum storey drifts and elastic limit drifts are shown

for the 12-storey FIEB with θ_d=2.5% in Vancouver in Figure 4.10, and Figure 4.11 presents the residual storey drifts for the 12-storey FIEB with θ_d=1.5% in Vancouver. Note that a residual drift of 0.008% corresponds to an inter-storey displacement of 0.32 mm.

For all Vancouver buildings, it was observed that, for the design ground motion level, the interface subduction earthquakes invariably produced the largest responses, in terms of storey drifts and shears, even for the 4-storey buildings, as shown in Figure 4.12. Presumably, this is due to the larger effective periods of FIEBs, in comparison with other systems, such as CBFs. However, as Figure 4.11 shows, crustal earthquakes may govern the building's response at the service level earthquake. Furthermore, as can be noted from Figure 4.8, Figure 4.10, Figure 4.11, and Figure 4.12, the maximum storey drifts are concentrated in the higher storeys, showing the considerable contribution of the higher mode effects, likely related as well to the increased flexibility of the system. These results showcase one of the limitations of the design procedure as presented here that shall be addressed in future stages of the research through a formal calibration of a target displacement vector better suited for the system.

As shown in Figure 4.13, the characteristic force-deformation hysteretic behaviour is recognizable in the storey shear vs. drift history plots obtained under the effects of the imposed ground motions. Two distinct regimes, elastic (or initial) and post-yielding, are clearly marked in the plot and demonstrate the system's property of increasing its resistance and energy dissipation capacity as the displacement demands increase. Potentially, the significant post-yielding stiffness of BIEs and their increased fracture life, renders FIEBs more apt, in comparison to CCBs, to overcome seismic demands larger than those considered in design.

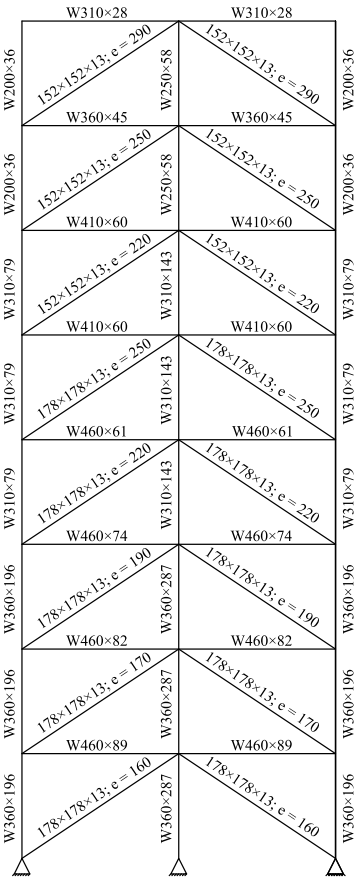

8 Storey FIEB, Vancouver

θ_d= 2.5 %,

Figure 4.7: Example of resulting FIEB design

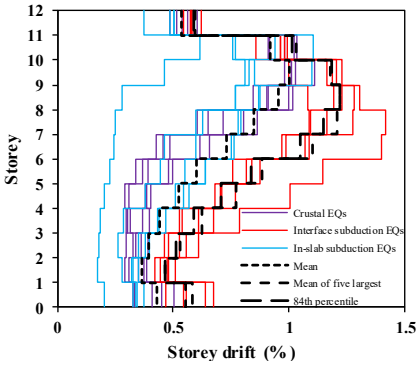

Figure 4.8: Maximum storey drifts for the 12-storey FIEB with θ_d=1.5% in Vancouver

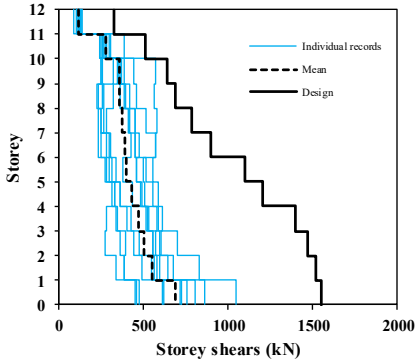

Figure 4.9: Maximum storey shears for the 12-storey FIEB with θ_d=1.5% in Montréal

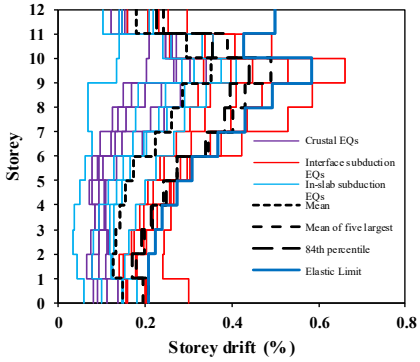

Figure 4.10: Maximum storey drifts for the 12-storey FIEB with θ_d=2.5% in Vancouver, for scaled-down ground motions

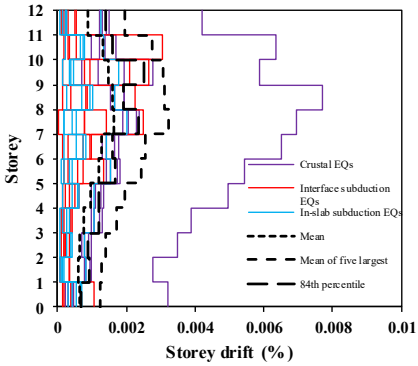

Figure 4.11: Residual storey drifts for the 12-storey FIEB with θ_d=1.5% in Vancouver, for scaled-down ground motions

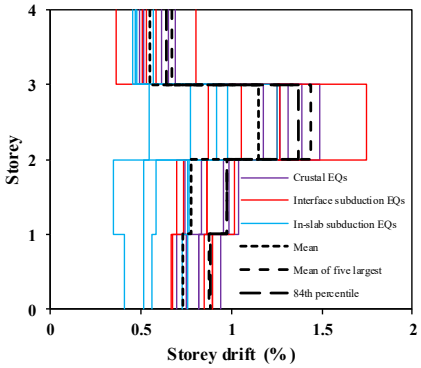

Figure 4.12: Maximum storey drifts for the 4-storey FIEB with θ_d=2.5% in Vancouver

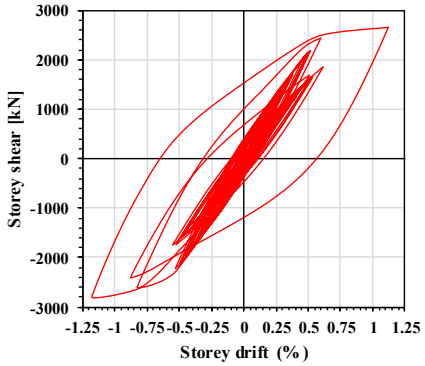

Figure 4.13: Example of first storey shear vs. drift history plot for the 12-storey FIEB with θ_d=2.5% in Vancouver, subjected to one of the interface subduction ground motions

To allow for a comparison, in terms of net tonnage, of the proposed FIEB system against traditional CBF buildings. Moderately Ductile (MD-) CBF and Limited Ductility (LD-) CBF versions of the buildings were also designed following the provisions from [4]. Although MD-CBFs taller than 40 m are not permitted by the NBCC 2015, the 12-storey CBFs with a height of 48 m, were designed nonetheless to obtain their hypothetical weight. The results of the tonnage comparison are given in Table 4.2. As the results show, FIEBs can require significantly less material that conventional CBFs, in particular for the larger building height considered and for the location with high seismic hazard. Although the net weight of the bracing members is greater in the FIEBs, this is compensated by a reduction of the material required for beams and columns due to the lower capacity-based design forces that determine their required dimensions. Had the foundations also been included in the comparison, the differences between the two systems would be more marked. The results also show that there is no recognizable difference between the costs of the FIEBs designed for θ_d=2.5% and those designed for θ_d=1.5%. Once more, this is a result of the proposed serviceability conditions and upper limit to the target period governing the selection of the BIEs. If these requirements were not applied, the FIEBs designed for θ_d=1.5% would have a tonnage approximately 25% higher, on average, than the ones designed for the larger target drift. However, it is arguably of greater benefit to guarantee that the flexibility of the system is not excessive, that minimum serviceability conditions are satisfied and that the building will respond adequately, i.e. elastically, to the factored wind loads.

Table 4.2: Steel tonnage for the resulting designs

	Vancouver			Montréal		
Building type	Beams and columns (ton)	Bracing members (ton)	Total weight (ton)	Beams and columns (ton)	Bracing members (ton)	Total weight (ton)
MD-CBF*	65.74	10.36	76.11	29.54	4.41	33.95
LD-CBF	76.69	10.80	90.49	22.76	4.43	27.19
12-Storey, θ_d=2.5%	41.53	12.43	53.96	21.92	8.52	30.44
12-Storey, θ_d=1.5%	43.75	12.09	55.84	21.89	6.95	28.84
MD-CBF	22.76	4.56	27.33	12.87	2.39	15.26
LD-CBF	30.69	6.63	37.31	12.83	3.18	16.01
8-Storey, θ_d=2.5%	18.69	6.93	25.62	11.34	3.01	14.35
8-Storey, θ_d=1.5%	19.02	7.23	26.24	11.63	3.00	14.63
MD-CBF	6.53	2.05	8.58	4.85	1.14	5.99
LD-CBF	7.26	2.43	9.70	4.84	1.52	6.35
4-Storey, θ_d=2.5%	5.92	3.08	8.99	4.63	1.49	6.12
4-Storey, θ_d=1.5%	6.44	3.14	9.58	4.15	1.26	5.41

4.5. CONCLUSIONS

The characteristics of the force-deformation response of BIEs allow them to overcome some of the most recognisable downsides of CCBs, in particular their invariably high stiffness and their propension to premature fracturing. Acknowledging the incompatibility of the traditional force-based design procedures with the BIEs' response, a seismic design procedure based on the DDBD method and the provisions from the National Building Code of Canada was formulated. It was found that buildings designed with said procedure offered a satisfactory performance, complying with all the selected target maximum drifts and performance objectives, both for the design ground motion and for demands closer to those expected for frequent earthquakes. The results also showed that the use of FIEBs can be advantageous in terms of cost compared to that of CBFs, specially for buildings with more than 8 storeys located in regions of high seismic hazard.

However, the design procedure failed to effectively produce buildings that would meet the intended target displacement levels as it required to provide the structures with additional stiffness and strength in order to fulfill the proposed minimum serviceability criteria. The current state of the design procedure also showed its limitations regarding the estimation of the contribution of the higher mode effects. These shortcomings of the design procedure will be addressed in future stages of the research program. The estimated fracture life of square HSS BIEs is also to be verified through physical testing under cyclic loading of full-scale specimens with *eccentering* assemblies such as those described above.

ACKNOWLEDGEMENTS

The authors would like to thank DPHV Structural Consultants, ADF Group Inc. and Constructions Proco for their generous technical and financial support, as well as the Natural Sciences and Engineering Research Council (NSERC) of Canada, the Fonds de Recherche du Québec – Nature et Technologies (FRQ-NT) and the Centre d'Études Interuniversitaire des Structures sous Charges Extrêmes (CEISCE). The first author also wishes to acknowledge Universidad de Costa Rica for financing the undertaking of his doctoral studies.

REFERENCES

[1] X. Tang and S. C. Goel, "Brace fractures and analysis of Phase I Structure," *Journal of Structural Engineering,* vol. 115, no. 8, pp. 1960-1976, 1989, doi: 10.1061/(ASCE)0733-9445(1989)115:8(1960).

[2] R. Tremblay, "Inelastic seismic response of steel bracing members," *Journal of Constructional Steel Research,* vol. 58, no. 5-8, pp. 665-701, 2002, doi: 10.1016/S0143-974X(01)00104-3.

[3] K. A. Skalomenos, H. Inamasu, H. Shimada, and M. Nakashima, "Development of a steel Brace with Intentional Eccentricity and experimental validation," *Journal of Structural Engineering,* vol. 143, no. 8, p. 04017072, 2017, doi: 10.1061/(ASCE)ST.1943-541X.0001809.

[4] *National Building Code of Canada 2015, 14th ed.* , National Research Council of Canada (NRCC), Ottawa, ON, 2015.

[5] A. González Ureña, R. Tremblay, and C. A. Rogers, "Numerical investigation of the seismic response of square HSS Braces with Intentional Eccentricity," Proceedings of the *17th World Conference on Earthquake Engineering*, Sendai, Japan, 2020. Paper no. C000832.

[6] F. T. McKenna, "Object-oriented finite element programming: Frameworks for analysis, algorithms and parallel computing," Ph.D. Thesis, Civil Engineering, University of California, Berkeley, 1997.

[7] M. J. N. Priestley, G. M. Calvi, and M. J. Kowalsky, *Displacement-based seismic design of structures*. Pavia, Italy: IUSS Press 2007, pp. xvii, 721 p.

[8] K. K. Wijesundara and P. Rajeev, "Direct displacement-based seismic design of steel concentric braced frame structures," *Australian Journal of Structural Engineering,* vol. 13, no. 3, pp. 243-257, 2012.

[9] G. O'Reilly, J. Goggins, and S. Mahin, "Performance-based design of a self-centering concentrically braced frame using the direct displacement-based design procedure," Proceedings of the *15th World Conference on Earthquake Engineering*, Lisbon, Portugal, 2012.

[10] A. González Ureña, R. Tremblay, and C. A. Rogers, "Design and seismic performance of multi-storey Frames with Intentionally Eccentric Braces," Proceedings of the *12th Canadian Conference on Earthquake Engineering*, Québec, Canada, 2019. Paper no. 192-coqm-119.

[11] M. Al-Mashaykhi, P. Rajeev, K. Wijesundara, and M. Hashemi, "Displacement profile for displacement based seismic design of concentric braced frames," *Journal of Constructional Steel Research,* vol. 155, pp. 233-248, 2019.

[12] *EN 1998-1:2004 Eurocode 8: Design of structures for earthquake resistance - Part 1: general rules, seimic action and rules for buildings*, European Committee for Standardization (CEN), Brussels, Belgium, 2004.

[13] K. Wijesundara, R. Nascimbene, and T. J. Sullivan, "Equivalent viscous damping for steel concentrically braced frame structures," *Bulletin of Earthquake Engineering,* vol. 9, no. 5, pp. 1535-1558, 2011, doi: 10.1007/s10518-011-9272-4.

[14] *CSA. S16-14: Design of steel structures*, Canadian Standards Association (CSA), Toronto, ON, 2014.

[15] R. Tremblay, G. M. Atkinson, N. Bouaanani, P. Daneshvar, P. Léger, and S. Koboevic, "Selection and scaling of ground motion time histories for seismic analysis using NBCC 2015," Proceedings of the *11th Canadian Conference on Earthquake Engineering (11CCEE)*, Victoria, BC, Canada, 2015, vol. 99060. Paper no. 99060.

[16] G. M. Atkinson, "Earthquake time histories compatible with the 2005 National Building Code of Canada uniform hazard spectrum," *Canadian Journal of Civil Engineering,* vol. 36, no. 6, pp. 991-1000, 2009.

FOREWORD TO CHAPTER 5

With BIEs being a novel brace type, great importance was given to testing physical specimens as part of this research, to shed light on failure modes not accounted for in the finite element models and to identify whether the promising results from the numerical studies presented in Chapters 2, 3, and 4 could be realized in practice. In Chapter 5, the experimental results from the physical testing of four full-scale square ASTM A1085 HSS Brace with Intentional Eccentricity specimens are presented, along with those from a reference traditional concentrically loaded brace. The experimental program herein presented corresponds to the first set of tests performed on BIE specimens other than those documented in the seminal paper by Skalomenos et al.. Moreover, it was the first time that full-scale square HSS BIE specimens were fabricated and tested. In addition to the results from the physical tests, supplementary data are provided by means of numerical analyses using models that were calibrated with the experimental results. The BIEs considered for these analyses were selected to complement the physical test specimens and to reflect the experience gathered from the studies on FIEBs. From those studies, it was learned that BIEs representative of the results of a cost-effectiveness- or performance-oriented design do not necessarily correspond to the specimens selected beforehand for testing.

CHAPTER 5: EXPERIMENTAL AND NUMERICAL STUDY OF SQUARE HSS BIEs UNDER CYCLIC LOADING

Submitted to *Engineering Structures*

Andrés González Ureña, Robert Tremblay, Colin A. Rogers

ABSTRACT

Braces with Intentional Eccentricity (BIEs) have recently been introduced as an alternative to traditional Concentrically Loaded Braces (CLBs) whose performance may overcome some of the shortcomings of the latter. It is postulated that the onset of local buckling in BIEs is delayed owing to a more even distribution of the strain demands under compression loading. Further, the significant post-yielding stiffness of the system can provide control over the predicted displacement levels under the action of the design earthquake. In this article, the results of the testing of four full-scale square ASTM A1085 HSS BIE specimens subjected to reversed cyclic loading are presented. The HSS members and eccentricities were selected with the intention of comparing the response of braces complying with and exceeding the CSA S16-14 global and local slenderness limits. The introduction of the eccentricity was achieved by means of side plates linking the HSS to bolted knife and gusset plate assembly connections. The experimental program is expanded and complemented with finite element analyses of additional BIE and CLB models. The experimental and numerical results show that the BIEs' response displays the purported benefits of the introduction of the eccentricity. However, it was also found that fracture due to the

rotational demand under tensile load at the bracing member's ends can govern the failure mode of BIEs that are more resistant to developing local buckling at mid-length. The implications of the results to the design of Frames with Intentionally Eccentric Braces (FIEBs) are discussed.

Keywords: Braces with Intentional Eccentricity; steel braces, earthquake-resistant design, physical testing, numerical modelling

5.1. INTRODUCTION

Although they are frequently employed as the Seismic-Force-Resisting System (SFRS) of low- and mid-rise buildings, Concentrically Braced Frames (CBFs) with HSS braces present a series of shortcomings that limit their benefits, of which three are addressed by the introduction of an intentional eccentricity to the bracing member's axis.

Due to the inherent stiffness of the cantilevered truss arrangement of CBFs, their fundamental period of vibration is naturally low; thus, the structure is constrained to high spectral acceleration demands. This results in large design forces which, combined with the significant overstrength that arises from the compression resistance governing the dimensioning of the bracing members, translate into considerable demands on the capacity-protected elements of the SFRS and its foundations, producing a notable impact on the material costs.

Moreover, CBFs are conceived to dissipate energy by the simultaneous yielding of the braces in tension and global buckling of the braces in compression. This behaviour implies a nearly null lateral stiffness in at least one storey which, if sustained, can prompt large drifts and potentially compromise stability if a soft-storey mechanism develops.

Finally, HSSs employed as Concentrically Loaded Braces (CLBs) are particularly prone to fracturing at the mid-length plastic hinge region shortly after the onset of local buckling, as has been reported extensively in research [1, 2], restricting the braced frame's energy dissipation capacity and ductility. To reduce the probability of this phenomenon and ensure that minimum ductility and energy dissipation are provided, modern seismic design provisions impose limits to the global and local slenderness ratios of bracing members. In the CSA S16-14 standard [3], a lower limit of 70 is established for the global slenderness ratio, KL/r, while the local slenderness

is restricted by an upper limit to the width-to-thickness ratio, b_{el}/t, that depends on the global slenderness. However, a side effect of these limits is that they can result in further overstrength in some storeys [4], consequently magnifying the drift demands in storeys with a lesser shear strength to demand ratio. KL is the effective length of the brace, r is the lesser radius of gyration of the section, b_{el} is the width of the wall within the corners of the HSS, and t is its thickness.

To overcome the listed disadvantages of CLBs, a group of researchers from Kyoto University [5] presented the concept of the Brace with Intentional Eccentricity (BIE). A BIE is an otherwise conventional brace with its axis offset from the line of action of the forces transmitted through it, which generally corresponds to the braced bent diagonal. As a consequence of the eccentric loading, the BIE is subjected to bending in addition to axial force, and therefore its initial stiffness is lower than that of CLBs. Moreover, yielding occurs initially along the exterior fibre, before progressing through the cross-section as the loading increases. Thus, the BIE retains a considerable post-yielding stiffness, whereas for a CLB the post-yielding stiffness is negligible as under tension the full cross-section yields uniformly. In BIEs, for a given section and effective length, the magnitude of both initial and post-yielding stiffnesses can be adjusted by varying the magnitude of the eccentricity, hence granting the designer greater control over the structure's response to loading. Furthermore, by adjusting the eccentricity of the BIEs of one storey, instead of choosing from a discrete set of sections, one can precisely provide the required strength and stiffness, favouring a smoother distribution of the drift demands over the building height.

Another effect of the combined axial force and bending is that, in compression, the BIE exhibits a smooth flexural response, rather than buckling under axial load alone, which induces a more even distribution of the strain demands over the brace length, instead of an earlier strain concentration

at mid-length as in CLBs. As such, the onset of local buckling is delayed, increasing the fracture life of the brace in terms of allowable displacement or drift ratio.

The authors of this article have investigated the application of BIEs to building structures, and have proposed the use of a procedure based on displacements for the seismic design of Frames with Intentionally Eccentric Braces (FIEBs) [6-8]. The building response, obtained from numerical models, shows that, in comparison with CBFs, FIEBs display an improved seismic performance in terms of maximum and residual storey drifts. Due to the enhanced control of overstrength, mid-rise FIEBs would require significantly less material than CBFs in regions with high seismic hazard, thus offering an economic advantage. The authors have also developed an expression to estimate the maximum equivalent drift ratio that BIEs can sustain under cyclic load before the onset of local buckling at mid-length based on the results of a parametric study incorporating finite element models of BIEs [9].

Other systems that take advantage of eccentric loading and combined axial and flexural response to offer improved seismic performance, presenting a behaviour similar to that of BIEs, such as the A-braced frame [10, 11], have recently been proposed. The effects of accentuating further the asymmetric nature of eccentric braces by using materials with different strength and ductility on opposed sides of the bracing member's cross-section have also been investigated [12, 13], producing promising results. Nevertheless, plain BIEs maintain, in the authors' opinion, a considerable potential which remains to be fully developed in research.

Skalomenos et al. [5] reported on the results of the testing of five half-scale BIE specimens with two eccentricity values and one CLB, all made from the same round HSS. Their results are consistent with the behaviour described above and showcase the potential of BIEs as an alternative

to CLBs with improved performance. To date, however, there are no published reports on the physical performance of full-scale nor square HSS BIE specimens.

In this article, the results of the laboratory testing of four full-scale square ASTM A1085 HSS BIE specimens subjected to reversed cyclic loading are presented, along with those from an additional CLB specimen. The sections and eccentricity levels were selected with the objective of studying the response of BIEs complying with and exceeding the CSA S16-14 limits for global and local slenderness. The accommodation of the eccentricity was achieved by employing assemblies consisting of two-side plates connecting the HSS to a knife plate detailed with a clearance intended to allow the unrestrained rotation of the BIE's ends. To complement and expand the experimental program, results from supplementary finite element models of BIEs and CLBs are also presented. The implications of the test specimen performance observations on the design of FIEBs are discussed.

5.2. BASIC CHARACTERISTICS OF BIEs

Before presenting the experimental program and results, a summary of the basic theoretical principles and behaviour of BIEs under monotonic loading is offered. For a more detailed report refer to [8].

5.2.1. Components of BIEs

The basic configuration and components of a BIE are presented in Figure 5.1. The eccentricity, e, is the initial parallel offset between the working points axis, or frame diagonal, and the axis of the bracing member. For simplicity, in this model the connections of the BIE to the rest of the structure are idealised as pins. In practice, a pin-like behaviour can be achieved by detailing the connections so that they yield in flexure at low levels of axial load and be able to sustain large reversed

rotations. One common way of accomplishing this is by using plate connections in which a clearance, with length L_k, is provided to allocate the rotations. A clearance with a length of twice the thickness of the plate has been shown to provide adequate ductility for the response under cyclic loading of CLBs [14]. Assumedly, such detailing would equally be adequate for BIEs. The total length of the BIE, L, is defined by the location of the hinges at the connections. Linking the connections and the bracing member itself, the *eccentering* assemblies accommodate the eccentricity. In general, the *eccentering* assemblies can be executed in many forms, provided that they attach rigidly the bracing member's ends to the connections at all anticipated displacement levels. The length of the *eccentering* assemblies, L_{ea}, is important to describe the kinematic behaviour of the BIE in tension, because it affects the brace stiffness and the rotational demand at the bracing member's ends.

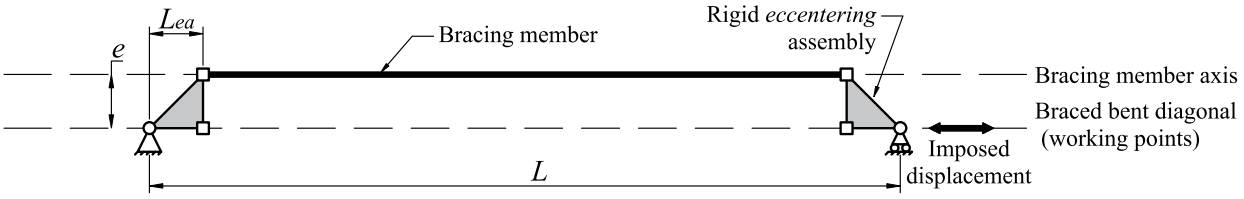

Figure 5.1: Components and dimensions of a BIE

5.2.2. Monotonic force-deformation behaviour of BIEs

The kinematic response of BIEs to tension and compression is presented in Figure 5.2 and Figure 5.3, respectively. When the BIE is subjected to tension, the *eccentering* assemblies rotate inward about the connections, and the bracing member bends toward the axis linking the working points, as illustrated in Figure 5.2 (a). As the outermost fibre in tension reaches the yielding stress, F_y, the BIE transitions from the elastic, or initial, stage to the post-yielding, or secondary, stage. This limit is denoted "First yield" point ($T_y - \delta_y$), as shown in Figure 5.4 (a). In the post-yielding stage, as the plasticisation of the cross-section progresses, the stiffness increases gradually since the

effective eccentricity decreases with the displacement, although remaining always lower than in the initial stage. For the BIE to develop its maximum tensile strength, T_u, equal to that of a CLB, the eccentricity must be annulled along the length of the brace to allow for the entire cross-section to yield in tension. Kinematically, this requires that plastic hinges form where the bracing member meets the *eccentering* assemblies, as presented schematically in Figure 5.2 (b). An approximation of the maximum theoretical rotation demand at these plastic hinges, θ_e is given by Equation (5.1), where H is the depth of the HSS.

$$\theta_e = tan^{-1}\left(\frac{e}{L_{ea} + \frac{H + L_k}{2}}\right) \tag{5.1}$$

As shown in Figure 5.4 (a), the force-deformation response of a BIE in tension can reasonably be approximated with a tri-linear model, composed of an elastic segment with initial stiffness K_i, followed by a post-yielding segment with stiffness K_s, and finally a fully-yielded segment with negligible stiffness. This response is markedly different from that of a CLB, which can be rather associated with an elastic-perfectly plastic model.

Under compression, the *eccentering* assemblies rotate outward about the connections and the BIE bends away from the working points axis, as represented in Figure 5.3 (a). In contrast with CLBs, BIEs show a smooth flexural response to compressive load, transitioning seamlessly from the elastic to the post-buckling regimes. Therefore, the force-deformation curve of BIEs under compression lacks the characteristic sharp peak due to buckling, as shown in Figure 5.4 (b). If the compressive loading carries on, a plastic hinge forms at mid-length where the deformation demands concentrate (Figure 5.3 (b)); however, this is expected to occur at larger displacement

levels than in CLBs since the strain demands prior to this stage are more evenly distributed along the brace length.

As proposed by Skalomenos et al. [5], the force-deformation response of BIEs in compression can be idealised as elastic-perfectly plastic with initial stiffness K_i, as suggested in Figure 5.4 (b). The maximum force developed in compression, C', can be approximated by the load corresponding to the elastic limit state of a column under eccentric axial load, using Equation (5.2), where P_{cr} is Euler's buckling load, A is the cross-section's area and S is the elastic section modulus.

$$C' = \frac{F_y A}{1 + \frac{eA}{S \cdot cos\left(\frac{\pi}{2}\sqrt{\frac{C'}{P_{cr}}}\right)}} \tag{5.2}$$

Given the cross-section, L, and L_{ea}, the magnitudes of K_i, K_s, T_y, and C' are functions of the applied eccentricity. As further expanded in [8] this constitutes one of the major advantages of BIEs, as they offer the designer significantly more control over the dynamic response of the structure than traditional braces.

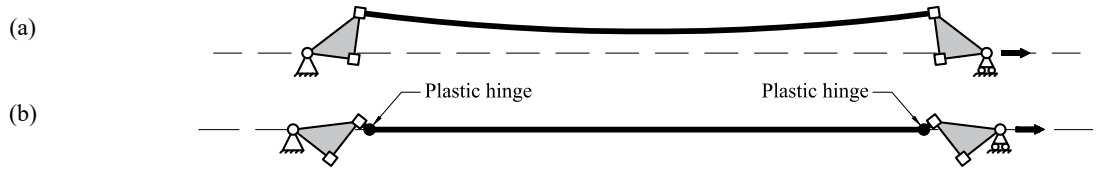

Figure 5.2: Deformed shape of a BIE under tension: small deformation (a) and large deformation (b)

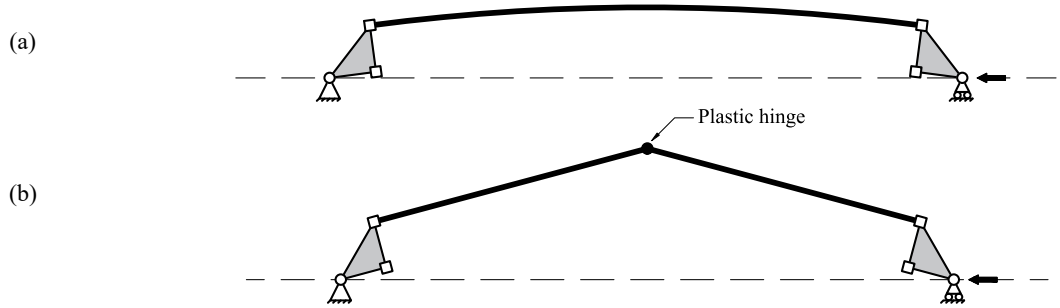

Figure 5.3: Deformed shape of a BIE under compression: small deformation (a) and large deformation (b)

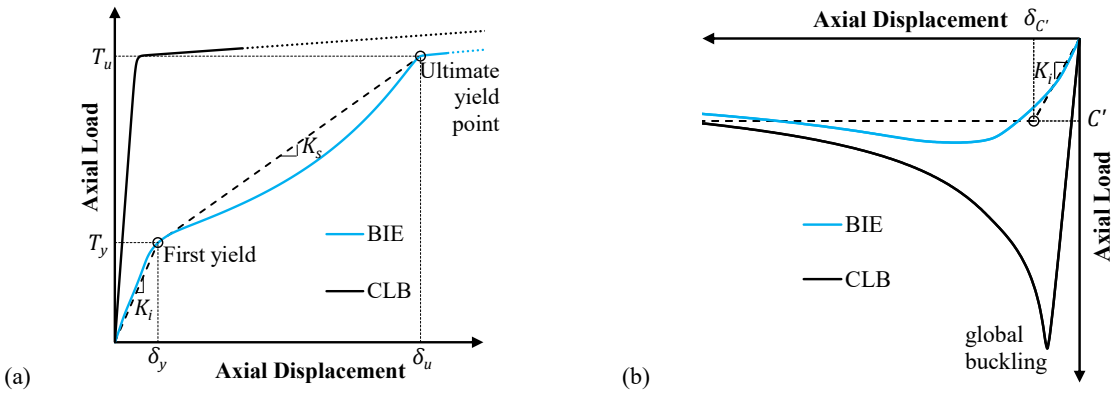

Figure 5.4: Compared BIE and CLB idealised monotonic force-deformation behaviour: tension (a) and compression (b) (not to scale)

5.3. EXPERIMENTAL PROGRAM

5.3.1. Specimen selection

As mentioned previously, the cross-sections of the specimens were selected with the intention of studying the response of BIEs complying with or exceeding the CSA S16-14 global and local slenderness limits for rectangular HSS CLBs. The length of the specimens was established based on the assumption of their use in a hypothetical 6 m wide by 4 m tall braced bent, considering realistic dimensions for the columns, beams, and connections involved. This assumption was embraced given its compatibility with the dimensions of the existing large-scale hydraulic press and associated brace-testing apparatus available at the Structures Laboratory of Polytechnique Montréal [15], where the testing took place. The sections, eccentricities, and global and local slenderness of the selected specimens are presented in Table 5.1.

Table 5.1: List of test specimens

Specimen	Section	Eccentricity, e (mm)	Global slenderness, KL/r	Local slenderness, $\frac{b_{el}}{t}$	Limit $\frac{b_{el}}{t}$
1	HSS 127×127×7.9	0	114	12.0	18.4
2	HSS 127×127×7.9	130	114	12.0	18.4
3	HSS 254×254×13	200	47.5	16.0	17.8
4	HSS 254×254×9.5	200	46.8	22.7	17.8
5	HSS 254×254×13	300	47.5	16.0	17.8

Specimen 1 was a traditional concentrically loaded brace made from an HSS 127×127×8. It was selected to provide data to contrast and compare the results from the eccentric braces. Both its global and local slenderness complied with the limits for seismic applications of rectangular HSS braces established in the CSA S16-14 standard. Specimen 2 was a BIE fabricated from the same section as Specimen 1, with an eccentricity of 130 mm such that its eccentricity ratio, e/H, was approximately 1.0.

For Specimens 3 and 5, an HSS 254×254×13 was selected to obtain a global slenderness ratio below the CSA S16-14 lower limit of 70. This limit being intended to preclude overly stocky braces, as low global slenderness is correlated with a higher probability of undesirable premature fracture [1, 2]. This CSA S16-14 limit was deliberately overridden to explore whether the introduction of the eccentricity could indeed offer an improvement to the brace's response by delaying the onset of local buckling. The local slenderness, however, was kept in compliance with the Standard's limit. The eccentricities of Specimens 3 and 5 were respectively 200 mm and 300 mm, thus, the only difference between Specimens 3 and 5 was that the former had an e/H ratio of approximately 0.8 while that of the latter was approximately 1.2.

Specimen 4 was identical to Specimen 3, except that the bracing member was an HSS 254×254×10, producing a local slenderness greater than that allowed by the CSA S16-14. As such, it was selected to investigate the impact of the variation of the local slenderness.

The conceptual arrangement considered in the design of the *eccentering* assemblies and the connections of Specimens 2 to 5 is presented in Figure 5.5. The eccentricity was introduced by means of two side plates connected with flare bevel welds to the corners of the HSS, linking the bracing member to a knife plate in which a clearance, L_k, was included to provide rotational capacity similar to that of a pinned connection, as explained in Section 5.2.1. The knife plate was then slotted perpendicularly into a gusset plate, to which it was connected by four bolted angles. In the hypothetical braced frame, this gusset plate would be connected with welds to the beam-column joints, as shown in Figure 5.5. In the case of the tests, the gussets were designed as T-stubs to be inserted in the grips of the hydraulic press to hold the specimen and apply the loading, as shown in Figure 5.6. This configuration was chosen for its simplicity and to allow for the re-use of the T-stubs: one pair was used for Specimens 1 and 2 and another, larger, pair was used for Specimens 3, 4 and 5. The specific arrangement of the *eccentering* assembly itself was designed with the objective of creating a cost-effective solution that could eventually be easily reproduced and applied by fabricators in the field. The final specimen design for Specimen 2 is presented in Figure 5.7.

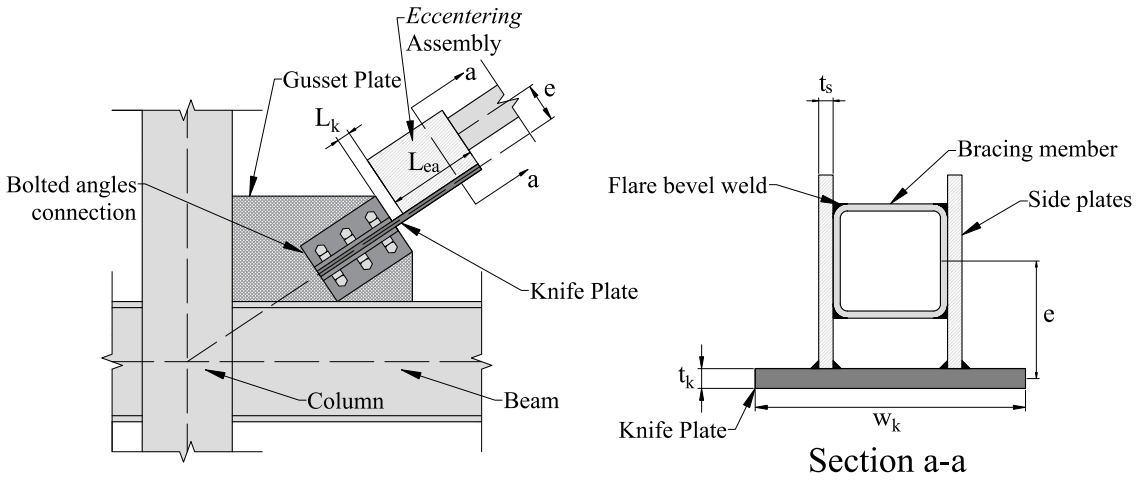

Figure 5.5: Design concept for *eccentering* assemblies and connections

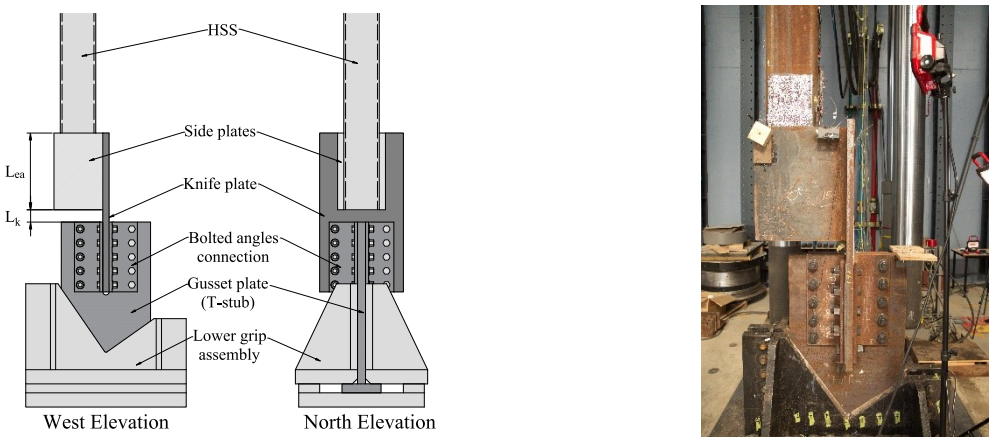

Figure 5.6: Detail of Specimen 5 attached to bottom T-stub inserted into press' grip, annotated drawing (a) and photograph of west side (b)

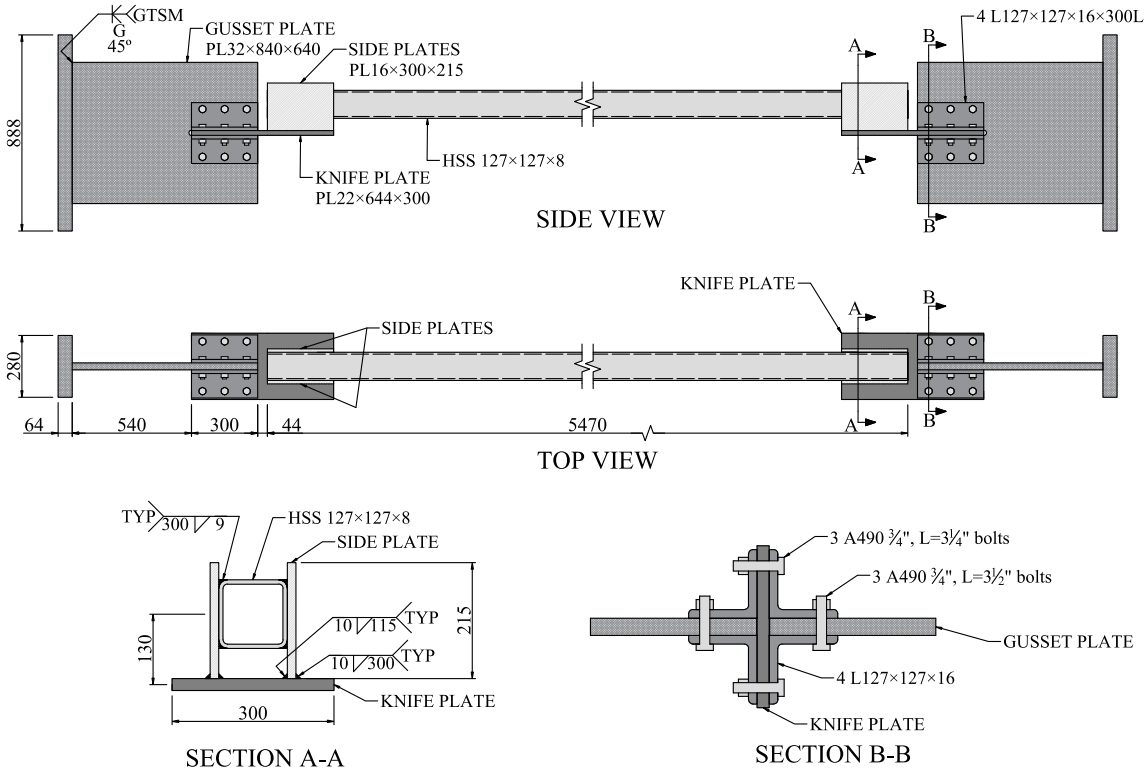

Figure 5.7: Specimen 2 – HSS 127×127×8, e =130 mm BIE (dimensions in mm)

In the case of Specimen 1, as no *eccentering* assemblies were required, the knife plate was directly slotted into the centre of the HSS and cover plates were used to reinforce the net section to prevent stress concentrations at that region and ensure that failure would occur due to fracture at the mid-span plastic hinge region. The final design for Specimen 1 is presented in Figure 5.8.

The detailed relevant dimensions of the CLB and BIE specimens are given in Table 5.2. As shown in Figure 5.5, t_k is the thickness of the knife plate, w_k its width, and L_k its clearance length; t_s is the thickness of the side plates that compose the *eccentering* assembly, and L_{ea} their length. L is the total, or hinge-to-hinge, length of the bracing member, H is the outside height of the HSS and t its wall thickness. In the case of Specimen 1, L_{ea} corresponds to the length of the slotted-in portion of the knife plate.

In all cases, all the elements composing the specimens' attachment to the test frame, i.e. bolted angles connection and T-stubs, were designed to withstand elastically the maximum probable force in tension that the HSS could develop. All bracing members were ASTM A1085 HSSs [16] and all plates were made from ASTM A572 grade 50 steel [17]. Both materials have nominal minimum yield stress, F_y, of 345 MPa and ultimate tensile stress, F_u, of 450 MPa. The actual values of F_y and F_u of the HSSs and the knife plates were obtained from tension tests on coupons extracted from the mother tubes or plates; these are listed in Table 5.3.

Table 5.2: Design dimensions of test specimens

Specimen	H (mm)	t (mm)	e (mm)	L (mm)	L_{ea} (mm)	w_k (mm)	L_k (mm)	t_s (mm)	t_k (mm)
1	127	7.94	0	5470	300	300	44	N/A	22
2	127	7.94	130	5470	300	300	44	16	22
3	254	12.7	200	4640	550	600	88	32	32
4	254	9.53	200	4640	550	600	88	32	32
5	254	12.7	300	4640	550	600	88	32	32

Table 5.3: Yield stress and ultimate tensile stress of HSSs and knife plates

Part	Specimens	F_y (MPa)	F_u (MPa)
HSS 127×127×8	1 and 2	436.7	487.0
HSS 254×254×13	3 and 5	434.3	503.0
HSS 254×254×9.5	4	413.0	487.7
22 mm knife plate	1 and 2	413.6	579.3
32 mm knife plate	3, 4, and 5	393.9	502.9

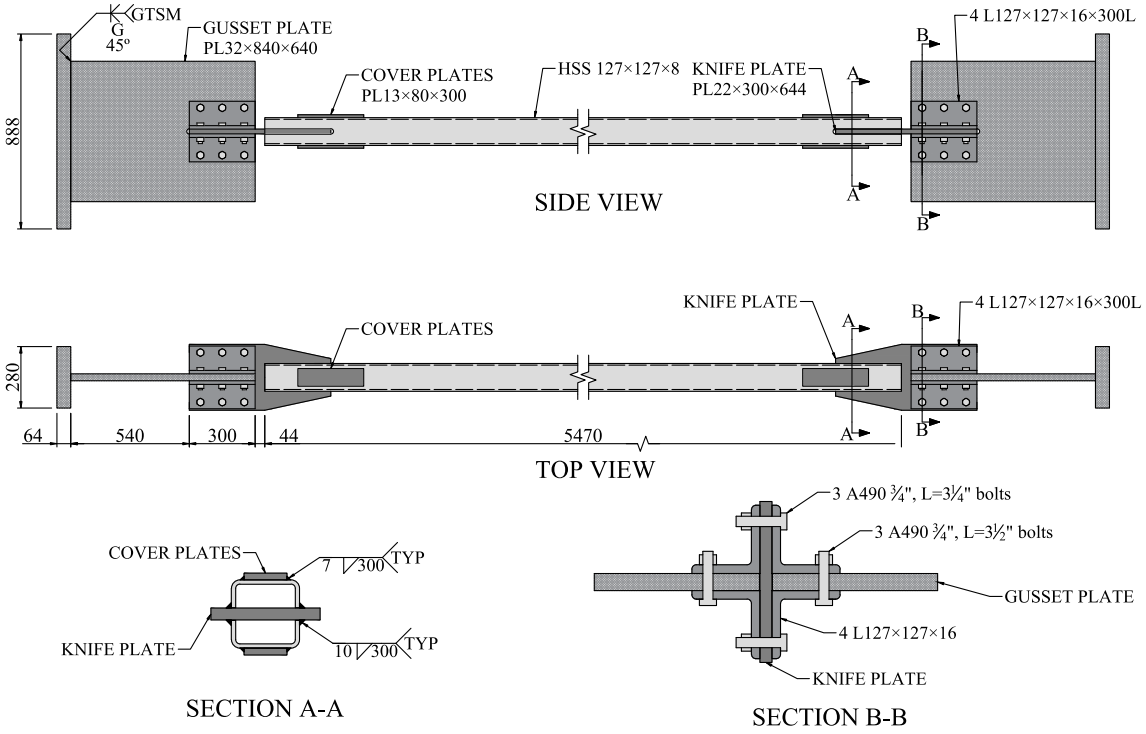

Figure 5.8: Specimen 1 – HSS 127×127×8 CLB (dimensions in mm)

5.3.2. Instrumentation

A common instrumentation arrangement was used with all five test specimens. To capture thoroughly the strain distribution along the braces' length and on the bottom knife plate hinge, six groups of strain gauges were placed as shown in Figure 5.9. Strain gauge group 1 was located at the centre of the clearance of the knife plate, groups 2 and 6 were placed near where the HSSs met the *eccentering* assemblies, groups 3 and 5 coincided with the quarter points of the total length of the bracing members and group 4 was placed at the centre of the bracing member's span. The distribution of the gauges around the cross section was intended to provide information on the extreme fibres and side faces of the HSS – bending was along the N-S direction. At the same positions of strain gauge groups 2 to 6, string potentiometers (string pots. 2 to 5) were placed to capture the in-plane deformed shape of the braces. Inclinometers were attached to the side plates of the top and bottom *eccentering* assemblies to record their rotation history during the tests. As described below, two string potentiometers (string pots. 1a and 1b) were employed to control the

application of displacement to the specimens. String potentiometer 6 was placed so that the net elongation of the bracing member in the vertical direction could be measured. Finally, a pair of linear potentiometers were employed to measure the slip of the knife plates vis-à-vis the gusset plates inserted in the press' grips. The typical distribution of the instruments and strain gauges employed in the testing of the five specimens is presented in Figure 5.9. The displacement and load of the 12 MN MTS test frame were captured with its internal LVDT and 12 MN load cell, and the MTS Series 793 and MTS TestSuite Multipurpose Elite software were used to control the actuator and implement the loading protocol, respectively. The measurements from the instruments were recorded with the Vishay System 6000 StrainSmart software, via a Vishay Model 6100 data acquisition system set up to perform 10 scans per second.

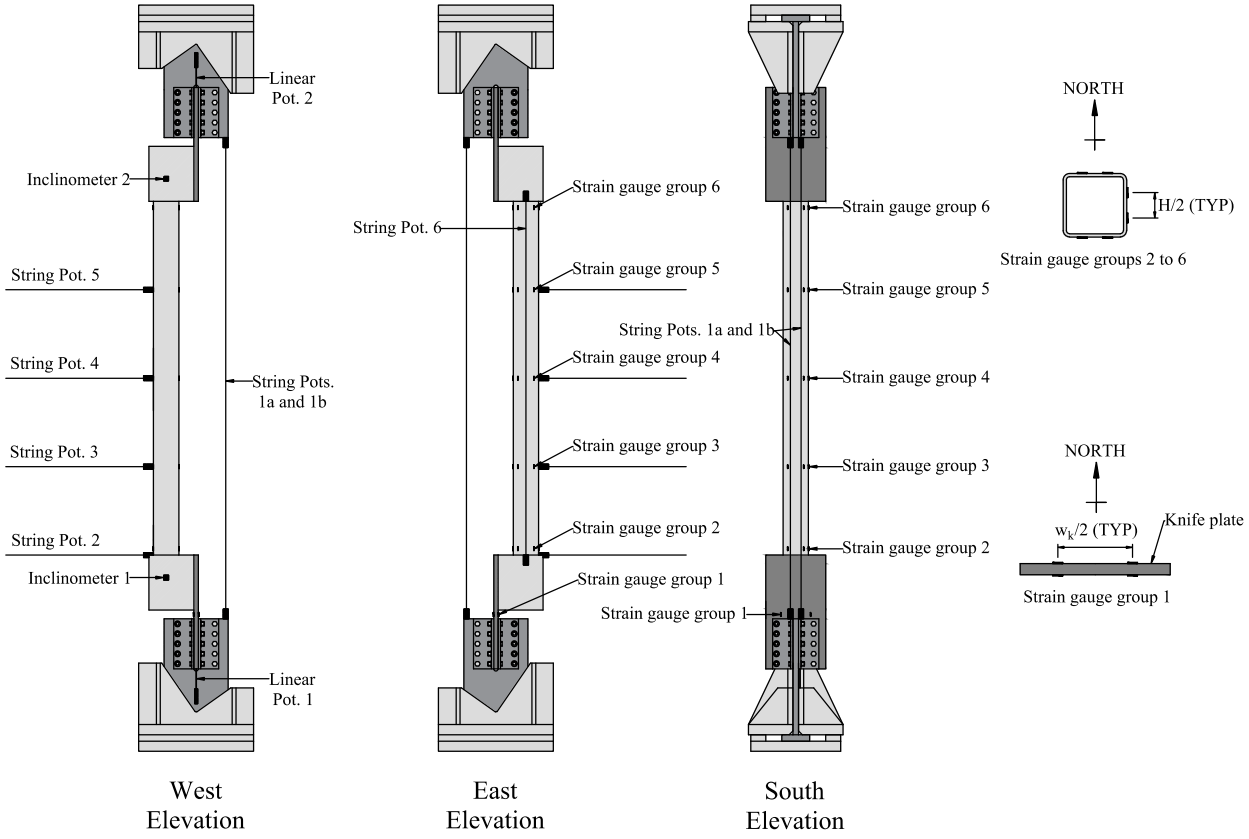

Figure 5.9: Typical arrangement of strain gauges and instruments (Specimen 5 shown)

5.3.3. Loading protocols

The five specimens were subjected to reversed cyclic loading following a protocol consisting of cycles of applied axial displacement with increasing amplitude, based on the equivalent inter-storey drift ratio (EDR) of the 4 m by 6 m braced bent on which the braces' design was based. Thus, 1% EDR corresponded to a brace axial displacement of 33.3 mm. As presented in Figure 5.10, for all specimens the loading history comprised initial cycles with amplitudes of 0.1 and 0.25% EDR, each repeated six times, followed by cycles of 0.5 and 0.75% EDR, each repeated twice. Following the 0.75% EDR cycles, the specimens were subjected to two cycles with 0.1% EDR amplitude but centred on + 0.1% EDR instead of 0. These cycles were included in the protocol to verify the capacity of the braces to retain their initial stiffness after withstanding moderate displacement demands, which could be associated with seismic events with an intensity lower than that of the Design Earthquake, but higher than that of a Service-Level Earthquake. After these offset small amplitude cycles, the protocol used with Specimens 1 and 2 comprised pairs of cycles with amplitudes of 1.0, 1.5, 2.0, 2.5, 3.0 and 4% EDR. In the case of Specimens 3, 4 and 5, the loading protocol was identical except that starting from the 1.0% EDR cycles, the increment in amplitude between pairs of cycles was fixed at 0.25% EDR. A constant displacement rate of 0.33 mm/s was employed throughout the five tests. This rate was selected to preclude any strain rate or dynamic effect. The tests were controlled using the average reading of the pair of string potentiometers attached to the top and bottom gusset plates (string pots. 1a and 1b), thus measuring the total elongation of the specimens, including any slippage within the bolted connections.

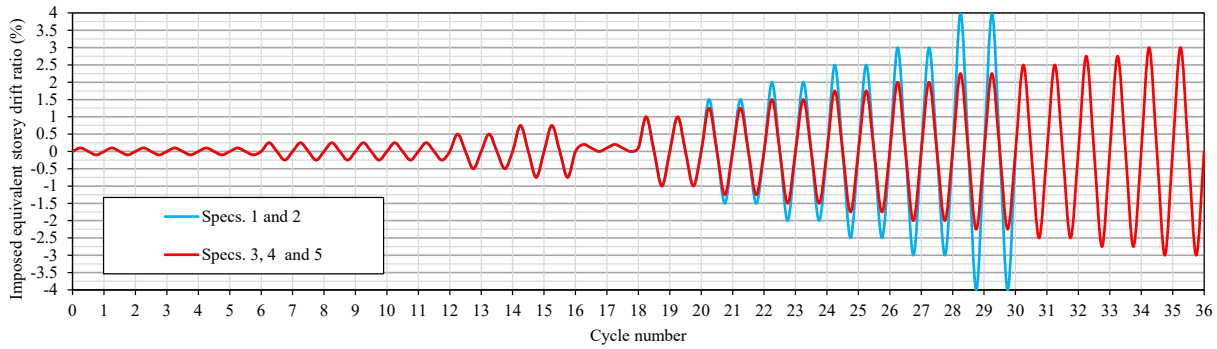

Figure 5.10: Loading protocols

5.4. RESULTS, COMPLEMENTARY FE ANALYSES, AND DISCUSSION

5.4.1. Overall behaviour

The axial force vs. equivalent storey drift hysteresis plots of the five specimens are presented in Figure 5.11. The peak forces in tension and compression, the cycles at which local buckling and fracture occurred, and the failure modes are reported in Table 5.4. To simplify the comparison of the performance of the different specimens, idealised backbone curves of the hysteretic response were constructed to obtain experimental values of T_y, C', K_i, and K_s. To do so, the envelopes of the response of the specimens in tension and in compression, before the onset of local buckling, were first obtained. Then, bilinear functions delimiting the same area as the envelopes were calculated to approximate those. In the case of the tension response, the initial stiffness was set equal to the initial elastic stiffness displayed by the specimens and the final point corresponds to the last peak in tension before fracture. For the compression side, an elastic-perfectly plastic model was selected with same initial stiffness as the tension backbone, as discussed in Section 5.2.2. The representative values of the so obtained simplified models are presented in Table 5.5. No simplified backbone curve in compression was calculated for Specimen 1 as its CLB response strayed far from the assumed model for BIEs due to the global buckling.

Specimen 1 displayed the behaviour typical of CLBs, with a clear transition between the elastic and post-yielding stages in tension, a nearly constant post-yielding maximum force, and a distinct peak force in compression before its strength deteriorated due to global buckling. Its post-yielding stiffness in tension was close to only 1% of the initial stiffness, as reported in Table 5.5. Local buckling developed near the centre of the brace length during the compression excursion of the first 3% EDR cycle and the low-cycle-fatigue-induced fracture occurred during the second 4% EDR cycle. As expected, due to its slenderness and stockiness, the fracture life of Specimen 1 was relatively long. Due to an unintentional fabrication misalignment of the bolt holes in the gusset plates, it was necessary to enlarge the bolt holes of the angles that connected the knife and gusset plates, to enable the installation in the press of Specimens 1 and 2. In the case of Specimen 1, this resulted in noticeable and frequent slippage in the connections with a magnitude of approximately ± 22 mm when the load neared the vicinity of ± 250 kN, as evident in Figure 5.11 (a). Although this prevented the application of the loading history onto the bracing member as intended, because part of the imposed displacement was buffered at the connections, the overall response and peak force values of the specimen were not affected.

Although Specimen 2 also required that the bolt holes of its angles be enlarged, it did not suffer from connection slippage issues as severely as Specimen 1. As shown in Figure 5.11 (b) and Table 5.5, Specimen 2 exhibited a significant post-yielding stiffness in tension, approximately 26% of the initial stiffness, and a smooth flexural response in compression, displaying neither global nor local buckling. The decrement in maximum compressive force as the cycles' amplitude increased, was due instead to the increment in the effective eccentricity as a result of the bending deformation. With a maximum tension force of 924 kN, Specimen 2 attained 58% of its theoretical T_u value, i.e. T_y of Specimen 1, assuming the bracing members had the same material properties. Before

attaining the first 2% EDR peak in tension, a fracture developed in the north face of the HSS at the interphase with the top *eccentering* assembly, as presented in Figure 5.12. The loading protocol was continued, and the fracture extended until complete separation occurred at a drift ratio of approximately 2.25% during the first 2.5% EDR cycle. The failure mode of Specimen 2 is discussed in more detail in Section 5.4.3.

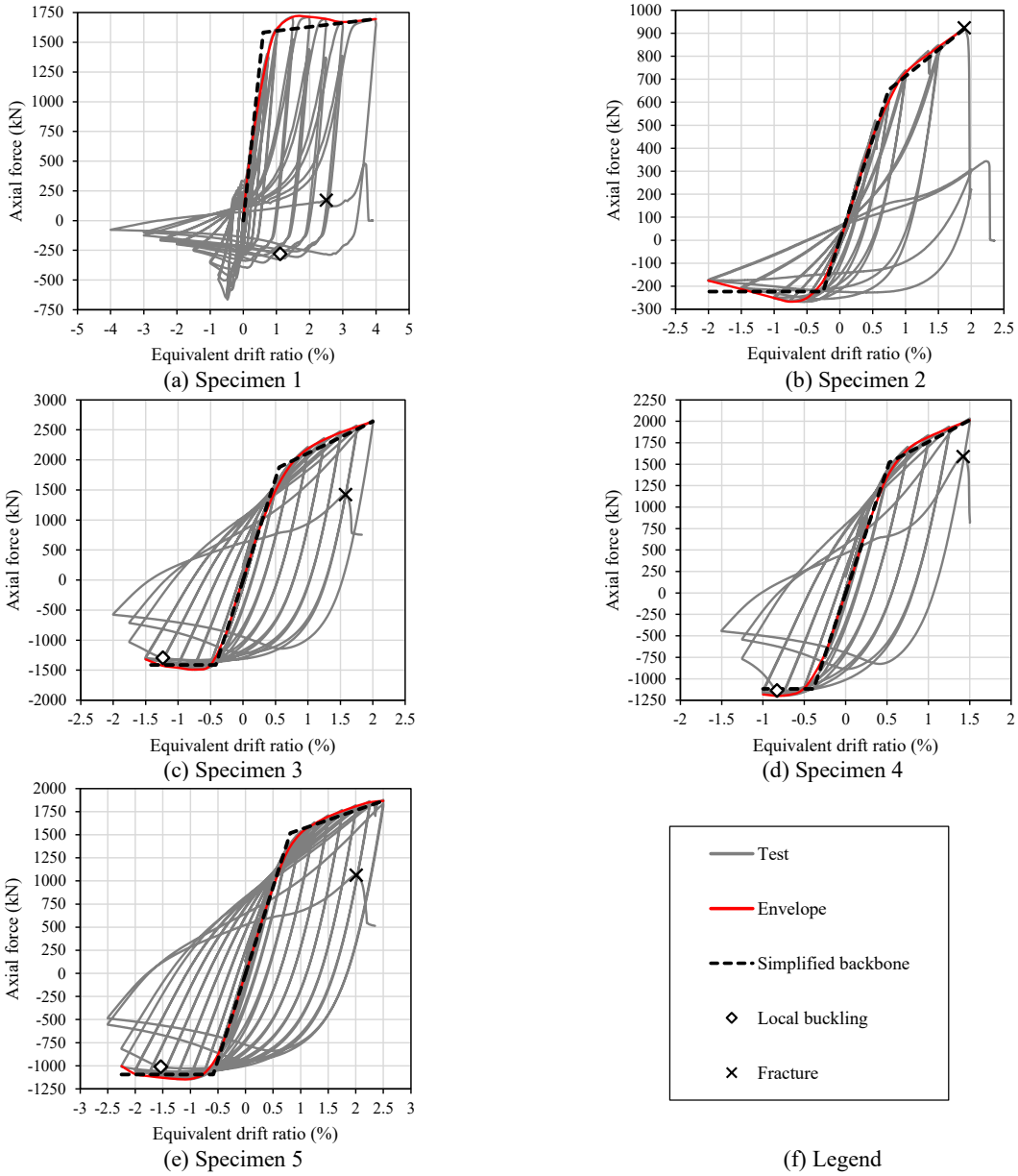

Figure 5.11: Axial force vs. equivalent storey drift, envelope, and simplified backbone curves of the five specimens

Table 5.4: Summary of specimen failure modes and peak forces

Specimen number and description	Peak force, tension (kN)	Peak force, compression (kN)	Failure mode	Onset of local buckling (EDR)	Fracture (EDR)
1. CLB – 127×127×7.9	1718	-691	local buckling and fracture at mid-length	1st 3% cycle	2nd 4% cycle
2. BIE – 127×127×7.9, e = 130 mm	924	-267	fracture at bracing member's end	N/A	1st 2% cycle
3. BIE – 254×254×13, e = 200 mm	2664	-1491	local buckling and fracture at mid-length	1st 1.75% cycle	2nd 2% cycle
4. BIE – 254×254×9.5, e = 200 mm	2032	-1198	local buckling and fracture at mid-length	1st 1.25% cycle	2nd 1.5% cycle
5. BIE – 254×254×13, e = 300 mm	1877	-1146	local buckling and fracture at mid-length	2nd 2.25% cycle	1st 2.75% cycle

Table 5.5: Simplified backbone parameters for the test specimens' response

Specimen	T_y (kN)	C' (kN)	δ_y (mm)	K_i (kN/mm)	K_s (kN/mm)	K_s/K_i
1	1584	N.A.	20.1 (0.60%)	78.9	0.99	0.01
2	653	-223	24.7 (0.74%)	26.4	6.91	0.26
3	1877	-1413	18.6 (0.56%)	100.9	15.8	0.16
4	1521	-1118	17.5 (0.53%)	86.7	15.2	0.17
5	1518	-1094	27.1 (0.81%)	56.1	6.18	0.11

Specimens 3, 4, and 5 displayed similar behaviours, with their failure mode consisting of low-cycle-fatigue-induced fracture at mid-length following the onset of local buckling. Comparing the results of Specimen 5 and Specimen 3, the significantly improved fracture life of the former can be explained by its larger eccentricity. However, it must be noted that this came at the expense of consequentially lower initial stiffness, post-yielding stiffness, and "first-yield" and maximum compression forces. The overall deformed shape of Specimen 5 when the local buckling became evident towards the compression peak of the 1st 2.25% EDR compression cycle is shown in Figure 5.13, and a detail of an early stage of the low-cycle fatigue fracture in the same specimen during the 1st 2.75% EDR cycle is presented in Figure 5.14. Specimen 4 exhibited the shortest fracture life among all specimens, which was attributed to its larger local slenderness. Comparing the

values of T_y, C', and K_i of Specimens 3 and 4, reported in Table 5.5, it can be noted that the ratios of these values in one specimen with respect to the other are of approximately 80%, which corresponds to the ratio of their respective nominal cross-sectional areas. The values obtained for K_s, however, were approximately the same.

Figure 5.12: Tension fracture in Specimen 2 (1st 2.0% EDR cycle)

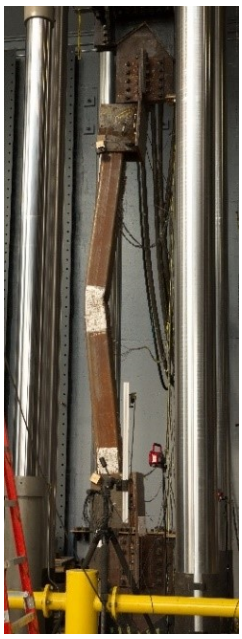

Figure 5.13: Onset of local buckling in Specimen 5 (1st 2.25% EDR cycle)

Figure 5.14: Low-cycle fatigue fracture in Specimen 5 (1st 2.75% EDR cycle)

5.4.2. Complementary FE Analyses

To provide supplementary data to further compare the performance of BIEs and CLBs, results of analyses of Finite Element (FE) models of CLBs based on the cross-sections of Specimens 3 and 5, and Specimen 4 are included in this study. These FE models are identified as Models 3' and 4' respectively. Additionally, models of the BIEs selected for the first level of the 12-storey FIEB designed for target drift ratios of 2.5% and 1.5% in [8], hereon referred to as Models 6 and 7, are also included. As the planning for the experimental program described in this article took place before the studies presented in [6-8] were conducted, the tested BIE specimens were not necessarily representative of BIEs resulting from the application of the design procedure. In

general, the outcome of said design procedure comprises BIEs with more compact HSSs than those of Specimens 2 to 5, and, in the case of the FIEBs designed for larger target drift ratios, larger e/H ratios. Thus, the inclusion of FE Models 6 and 7 intends to shed light on the performance under cyclic loading of BIEs akin to those which one would select for mid-rise FIEBs located in regions with high seismic hazard. The dimensions and global and local slenderness of the complementary BIE FE models are presented in Table 5.6. All FE analyses were performed with the Abaqus software [18].

Table 5.6: Design dimensions and slenderness of complementary FE models

Model	H (mm)	t (mm)	e (mm)	L (mm)	L_{ea} (mm)	w_k (mm)	L_k (mm)	t_s (mm)	t_k (mm)	KL/r	$\frac{b_{el}}{t}$	Limit $\frac{b_{el}}{t}$
3’	254	12.7	0	4640	550	600	88	-	32	47.5	16.0	17.8
4’	254	9.53	0	4640	550	600	88	-	32	46.8	22.7	17.8
6	177.8	15.88	230	5408	360	360	77	32	38	83.3	7.20	17.8
7	177.8	15.88	120	5408	360	360	77	32	38	83.3	7.20	17.8

5.4.2.1. Calibration of material model and modelling considerations

The results from Specimens 2 to 5 were used to calibrate an effective parametric stress-strain material model for HSSs for use in the FE models that would approximate satisfactorily the experimental behaviour. Although the material properties of the HSSs used in each specimen most likely vary, for simplicity a single material model was developed, aiming to result in good agreement with all four test results. Moreover, no distinction was made between the material properties of the HSS’ corners and flat walls to account for their expected differences in strength and ductility. Instead, it was sought to provide a material which reproduced globally the response of the section as a unit. As the objective of the study was to investigate the general performance under cyclic loading of square HSS BIEs, and compare it to that of CLBs, this approach was considered acceptable.

The parametric model to obtain the true stress-true strain curve for the material was based on the procedure described in [19] to approach the shape of the pre-necking and post-necking regions of the true stress-true strain curve, with the true stress as a function of the plastic strain. Through an iterative calibration process, a set of parameters was established to define a single true stress-true strain curve that reproduced as closely as possible the observed experimental behaviour of all specimens, when used in FE models of the same specimens. The so obtained true stress-true strain curve is presented in Figure 5.15. As a verification, the proposed material model was applied to the FE model of a standard tension coupon to obtain the engineering stress-strain curve of the material. In Figure 5.16, such curve is compared to stress-strain curves obtained from HSS walls [19] and corners [20]. As expected, the curve of the proposed material model lay in between the curves for the walls and the corners as it was intended to represent the whole section as a unit. As obtained from the tension coupon test FE model, the proposed material had a proportional limit of 350 MPa, a yield strength, F_y, of 383 MPa, and a ultimate tensile stress, F_u, of 534 MPa with a corresponding ultimate strain, ε_u, of 0.141.

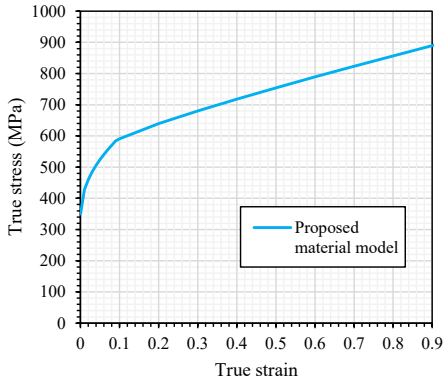

Figure 5.15: True stress-true strain curve of the proposed material model

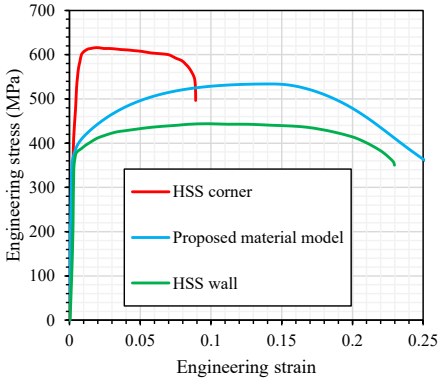

Figure 5.16: Engineering stress-strain curve of the proposed material and typical curves from HSS corners and walls

For the plates, an elastic-perfectly plastic material with F_y=385 MPa was used. The welds were modelled as elastic. The elastic modulus of elasticity, E, was taken as 200 GPa for all materials.

The results of the FE models of Specimens 2 to 5 using the material described above, superimposed over the experimental axial force vs. drift ratio curves of the same specimens, are shown in Figure 5.17. It can be noted that the models reproduced reasonably well the global shape of the hysteresis loops and the magnitude of the maximum and minimum force peaks. While the onset of local buckling was predicted accurately by the FE model of Specimen 4, in the models of Specimens 3 and 5 it occurred earlier than in the tests. In the case of the Specimen 3 model, local buckling occurred during the first 1.5% EDR cycle instead of the first 1.75% EDR cycle. For the Specimen 5 model, it occurred during the first 2.25% EDR cycle, instead of the second. Considering the onset of local buckling as an indicator of imminent failure, its earlier occurrence in the models can be accepted as conservative. Other differences between the experimental and numerical results can be attributed to various factors such as: (1) instead of modelling the gusset plates and bolted angles connections, the FE models were fully fixed at the end of the knife plate clearances, (2) the material property distribution over the cross-section was simplified as described and, (3) no residual stresses were considered. However, these simplifications in the models were accepted, as it has been determined in previous analyses that their effects on the overall response of the model were reasonably small [8].

In the models, the HSSs were represented using four node shell elements (S4) with 9 integration points through the thickness, and an element size of approximately 3 mm. The plates and welds were modelled with 8 node brick elements with reduced integration (C3D8R), with an average element size of 6 mm. A global bow imperfection equal to 1/500 times the hinge-to-hinge length, in the same direction as the eccentricity, was applied to the BIE models, as it corresponded, in average, to the observed out-of-straightness of the experimental BIE specimens. In the case of the CLB models, the applied out-of-straightness was of $L/1000$, which corresponds to half the

allowable deviation from straightness for HSSs as per CSA G40.20/G40.21 [21] and to the measured out-of-straightness of Specimen 1. No local imperfection was applied to the models as it was found that by not including it the results approached better the experimental data. To reduce the computational demand, only a quarter of the BIE was modelled taking advantage from the symmetry of the specimens.

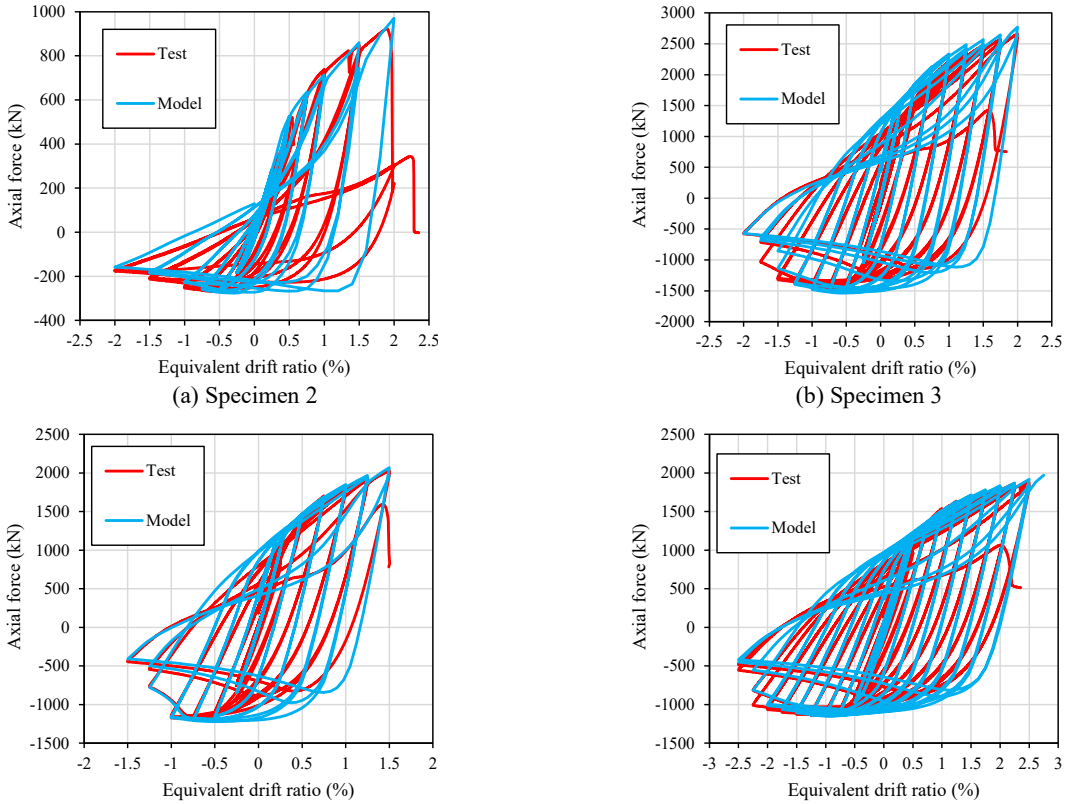

(a) Specimen 2 (b) Specimen 3

(c) Specimen 4 (d) Specimen 5

Figure 5.17: Results of the use of the calibrated material model on FE models of Specimens 2 to 5

The models were subjected to the same loading protocols as the physical specimens. As no failure criteria was explicitly included in the material model, two possible global failure conditions were considered, based on the observed failure modes of Specimens 1 to 5, i.e. local buckling and fracture at the brace mid-length, or fracture at the bracing member's end, with the latter being applicable only to the BIE models.

In the FE model of Specimen 2, as shown in Figure 5.18, it was observed that the longitudinal engineering (referred to as "nominal" in Abaqus) strain in the corner of the HSS, in the vicinity of the flare bevel weld, reached a maximum value of approximately 0.11 at the instant corresponding with fracture of the physical specimen (1.8% EDR during the tension excursion of the first 2.0% EDR cycle). Therefore, to attain a longitudinal strain of 0.11 in the region adjacent to the flare bevel weld in the interphase between the HSS and the *eccentering* assembly, was considered an indicator of failure by fracture at the bracing member's end in the FE models. Otherwise, if the maximum strain near the connection to the *eccentering* assembly remained under 0.11, it was considered that failure by fracture at mid-length occurred during the tension excursion of the third cycle after the onset of local buckling; this corresponds to what was observed experimentally for Specimens 1, 3, 4 and 5, as reported in Table 5.4. It was verified in the FE models of Specimens 3, 4 and 5 that the maximum strains in the concerned region were lower than 0.11: those had reached peak values between 0.072 and 0.078 when failure occurred at mid-length.

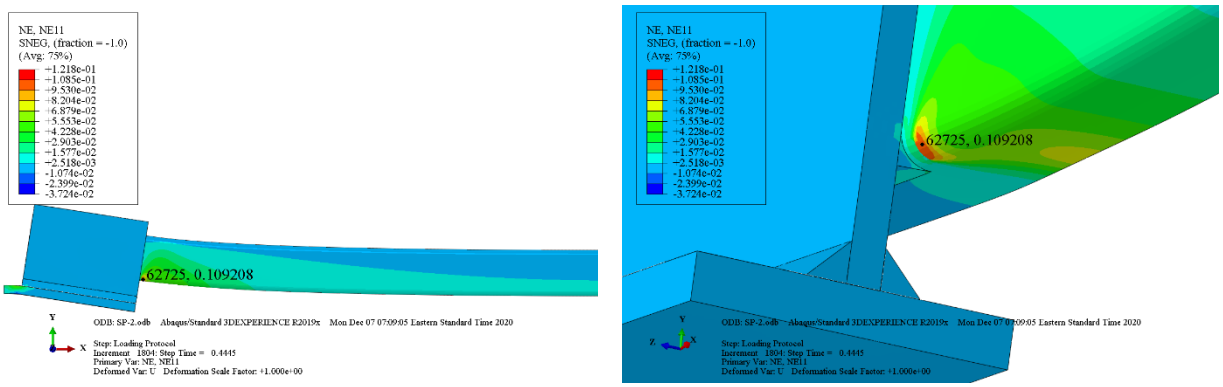

Figure 5.18: Specimen 2 FE model: maximum strain in HSS corner at fracture

5.4.2.2. Results

The axial force vs. equivalent storey drift plots of the four supplementary FE models, along with their envelopes and simplified backbone curves, obtained as discussed in Section 5.4.1 for the physical specimens' results, are presented in Figure 5.19. A summary of the numerical models'

peak forces and failure modes and the simplified backbone curve parameters are presented in Table 5.7 and Table 5.8, respectively. As can be observed in the figure and tables, the responses of Models 3'and 4' were consistent with the expected CLB behaviour, and markedly different from that of Specimens 3 and 5, and 4, which used the same HSSs for the bracing member. It is worth noting the relatively poor performance of these models, in particular that of Model 4', which showcases the known limitations of overly stocky and non-compact HSS bracing members to provide adequate ductility under reversed cyclic loading. As such, failure due to local buckling and fracture at mid-length occurred significantly earlier for both CLB FE models: the presumed fracture of Model 3' was during the 2nd 1.5% EDR cycle, while that of Model 4' occurred during the 1st 1% cycle. These data, compared to those of Table 5.4, clearly suggest that the introduction of the eccentricity can delay the onset of local buckling, even in the case of bracing members not complying with the CSA S16-14 limits on either or both global and local slenderness.

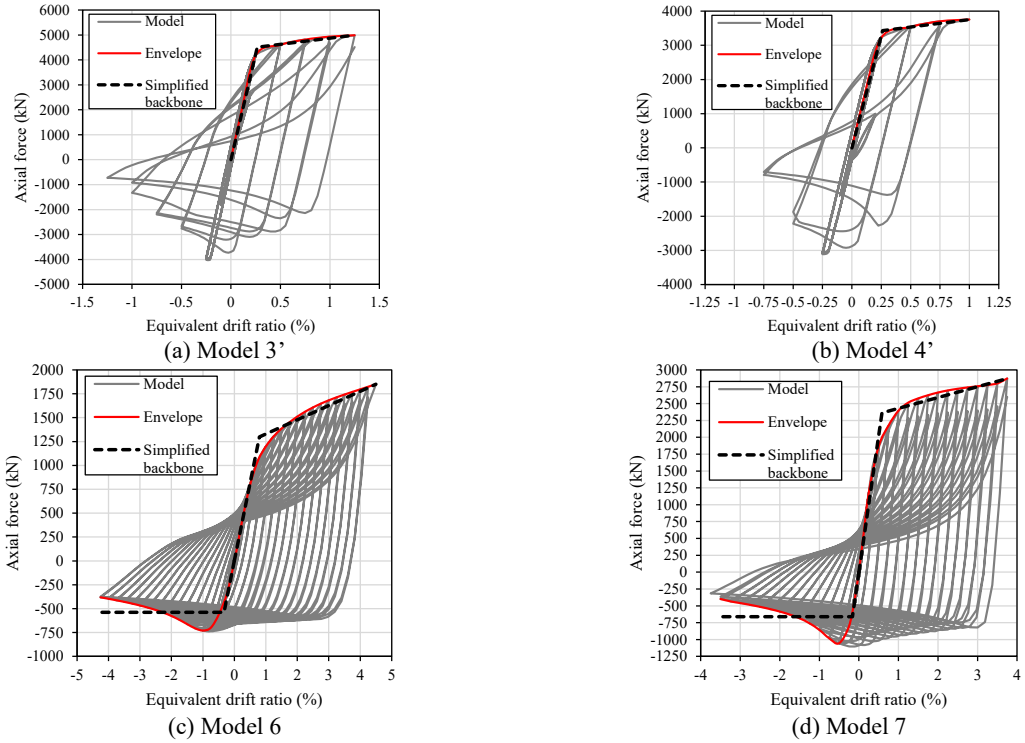

(a) Model 3' (b) Model 4'

(c) Model 6 (d) Model 7

Figure 5.19: Axial force vs. drift ratio plots, envelope, and simplified backbone curves for Models 3', 4', 6, and 7

Models 6 and 7 exhibited a significantly longer fracture life than the physical specimens, and a hysteretic response which remained stable as the cycles' amplitude increased. However, the pertinence of the elastic-perfectly plastic idealisation of the response in compression is questionable for these numerical BIEs. Given that the level of displacement is considerably larger than that attained by Specimens 2 to 5, the effects of the increased bending result in a marked reduction of the compression strength. According to the criterion discussed in Section 5.4.2.1, the presumed failure mode of Model 6 was fracture where the bracing member's end meets the *eccentering* assemblies, immediately before reaching the peak in tension of the first 4.5% EDR cycle. No sign of local buckling was observed before then. In the case of Model 7, the presumed failure mode was local buckling and fracture at the brace mid-length. The HSS buckled locally in the compression part of the first 3.5% EDR cycle, and fracture was assumed to occur in tension during the second 3.75% EDR cycle. Since the eccentricity ratio of Model 7 (0.67) was lower than those of Specimens 3 and 4, arguably the section's compactness is a factor that weighs more than the intentional eccentricity in the propensity of a bracing member to buckle locally.

Table 5.7: Summary of numerical models' presumed failure modes and peak forces

Model number and description	Peak force, tension (kN)	Peak force, compression (kN)	Presumed failure mode	Onset of local buckling (EDR)	Presumed fracture (EDR)
3'. CLB – 254×254×13	4990	-4093	local buckling and fracture at mid-length	1st 1% cycle	2nd 1.25% cycle
4'. CLB – 254×254×9.5	3752	-3111	local buckling and fracture at mid-length	2nd 0.5% cycle	1st 1% cycle
6. BIE – 178×178×16, e = 230 mm	1851	-738	fracture at bracing member's end	N/A	1st 4.5% cycle
7. BIE – 178×178×16, e = 120 mm	2871	-1104	local buckling and fracture at mid-length	1st 3.5% cycle	2nd 3.75% cycle

Table 5.8: Simplified backbone parameters for the numerical models' response

Model[o]	T_y (kN)	C' (kN)	δ_y (mm)/(EDR)	K_i (kN/mm)	K_s (kN/mm)	K_s/K_i
3'	4514	N.A.	8.9 (0.27%)	509	14.5	0.0285
4'	3430	N.A.	8.7 (0.26%)	394	13.1	0.0332
6	1299	-507	26.6 (0.80%)	48.9	4.50	0.0920
7	2361	-660	19.5 (0.58%)	121	4.84	0.0400

5.4.3. Fracture at bracing member's end

The failure mode exhibited by Specimen 2, which was also the presumed failure mode of Model 6, brings to light a significant weakness of BIEs in general, and particularly of the *eccentering* assembly employed in this study. When the BIE is under tension, the ends of the bracing member adjacent to the *eccentering* assemblies are subjected to the largest flexural demands over the length, while simultaneously being required to transmit the tensile load. In the case of the *eccentering* assembly configuration employed in this study, the issue is aggravated by the HSS being welded along its corners only This forces the load to be transferred through a portion of the HSS cross-section where the material ductility has been reduced by cold working, as can be clearly noted in Figure 5.16, and is further affected by heat during the welding process. Arguably, a configuration in which the entire perimeter of the HSS is connected would allow for a larger maximum strain prior to fracture. However, as observed in Skalomenos et al. [5] for one of their specimens, a brittle failure is still possible with such a connection.

If the magnitude of the intentional eccentricity is large enough, attaining the maximum tensile strength of the bracing member, T_u, necessitates the formation of plastic hinges at the bracing member's ends and, thus, implies requiring the bracing member to sustain at the same time its plastic bending moment, M_p; however, this is unlikely achievable given the limited ductility an HSS can provide. The axial force and bending moment history taken from a free body cut of the

HSS adjacent to the *eccentering* assembly in the FE model of Specimen 2, up to the moment of fracture is shown in Figure 5.20. It can be noted that at failure, the bending moment was equal to the plastic moment capacity (60.8 kN·m for a plastic section modulus, Z, of 159×10^3 mm^3 and F_y=383 MPa as discussed in Section 5.4.2.1.) while the axial force only reached 71% of T_u (1385 kN for A=3620 mm^2). Similarly, it was found that at the instant of presumed failure of Model 6, the HSS carried its full plastic moment capacity in conjunction with only 50.6% of T_u.

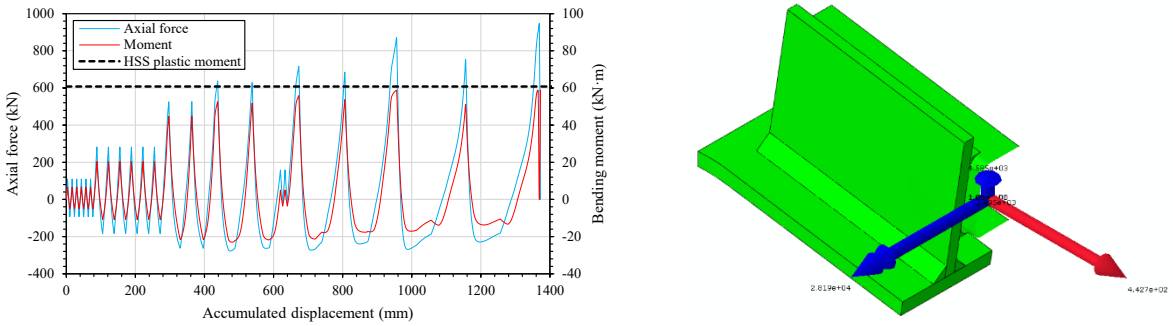

Figure 5.20: Axial force and bending moment history in critical section of Specimen 2 FE model

Presumably, for a BIE whose failure mode is not governed by local buckling at mid-length, the deformation capacity is determined by the maximum strain in tension that the corners of the section can withstand at the connection between the bracing member and the *eccentering* assembly. However, from a design perspective, it could be difficult to predict the maximum strain demands in the critical region of the HSS as a function of the target displacement levels, especially considering the variation of the material properties throughout the section and stress concentrations. A variable that could offer a reasonable level of correlation with the strain demand is the rotational demand of the *eccentering* assembly, which can be easily obtained from simplified numerical models of BIEs subjected to monotonic load under tension, such as those employed and discussed in [6-8]. In Figure 5.21, the rotation history of the bottom *eccentering* assembly of Specimen 2, as recorded in the test, is presented along with the strain history of the critical element in the HSS corner adjacent to the flare bevel weld, taken from the FE model of Specimen 2. The

rotation history predicted by the FE model is also included as a verification of the model's accuracy because there was concern that the rotation measurements in the test had been affected by shifts in the position of the inclinometer as a result of the shocks due to the connection slippage. As shown, the fracture occurred at a rotation of approximately 9.0º. For Model 6, fracture (strain in the corner of the HSS of 0.11) was presumed to occur at a rotation of approximately 11.2º, as shown in Figure 5.22; its higher rotation capacity was possibly related to its significantly lower local slenderness in comparison with Specimen 2. The strain and rotation history of Model 7 are also presented. For this specimen, note that prior to fracturing at mid-length, the rotation of its *eccentering* assemblies and the maximum strain in the HSS corners both remained below the levels associated with fracture at the bracing member's end. The rotation histories of Specimens 3, 4 and 5's *eccentering* assemblies are presented in Figure 5.23; for these as well, the observed rotations are smaller than those associated with the failure of Specimen 2 and Model 6.

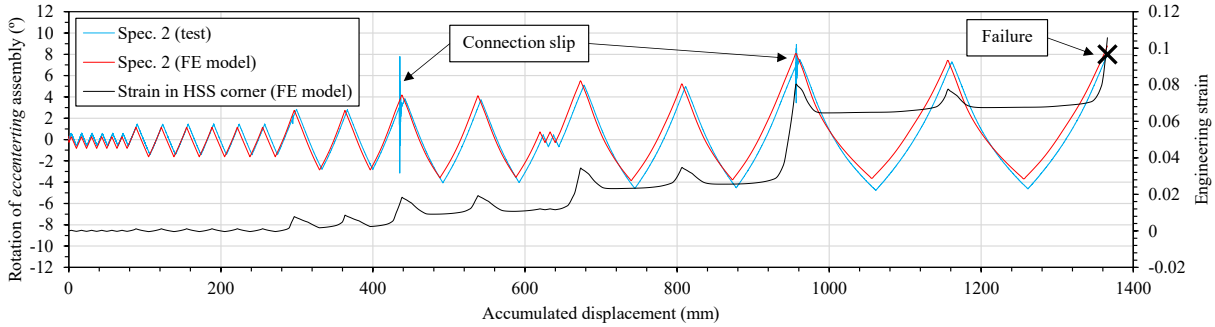

Figure 5.21: Histories of rotation of *eccentering* assembly and strain in critical HSS corner element: Specimen 2

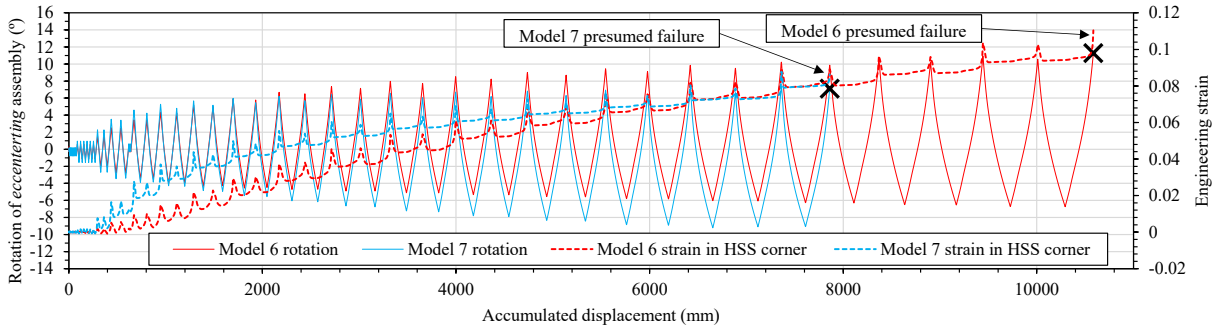

Figure 5.22: Histories of rotation of *eccentering* assemblies and strain in critical HSS corner element: Models 6 & 7

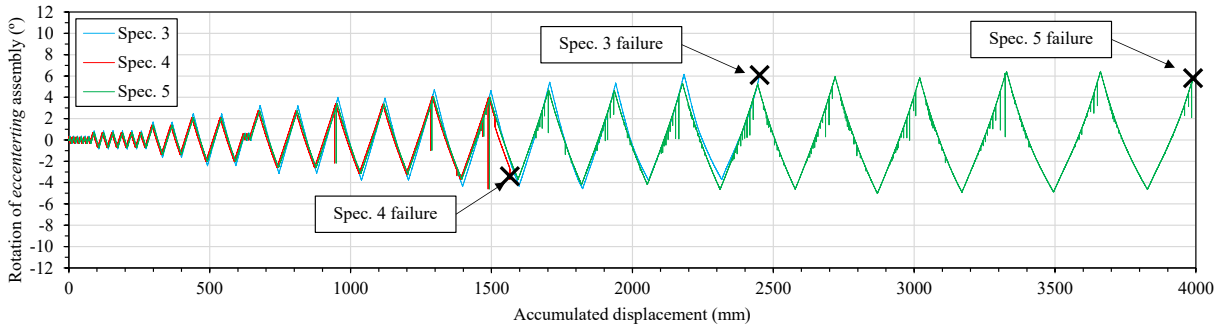

Figure 5.23: Rotation history of *eccentering* assemblies: Specimens 3, 4 and 5

Since published reports on the rotation capacity of HSSs under tensile loads are scarce, and as the data gathered in this study is limited as well, it is suggested that a conservative limit for the allowable rotation demand on HSS BIEs be considered in design. Based on the results presented here, and considering that the BIEs that typically result from the application of the design procedure developed by the authors have relatively compact cross-sections, a provisional design rotation limit, θ_d, of 10º is tentatively proposed for use with the simplified monotonic models used for design, if *eccentering* assemblies of the type used in this study are employed. As shown by the results of subjecting Model 6 to monotonic tensile loading, presented in Figure 5.24, the rotation of the *eccentering* assemblies varies linearly with the applied displacement. As such, to obtain the allowable displacement based on the allowable rotation criterion, δ_d, it suffices to multiply the displacement corresponding to T_u under monotonic load, δ_u, by the ratio $\frac{\theta_d}{\theta_e}$, with θ_e given by Equation (5.1). The allowable displacement derived from this approach is conservative as, under tensile load, θ_d is reached at smaller displacements than under reversed cyclic loading. For instance, for Model 6, θ_e=25.3º and δ_u= 214.2 mm, thus δ_d =84.7 mm, which corresponds to an equivalent drift ratio of 2.54%, significantly lower than the 4.5% EDR attained under cyclic loading.

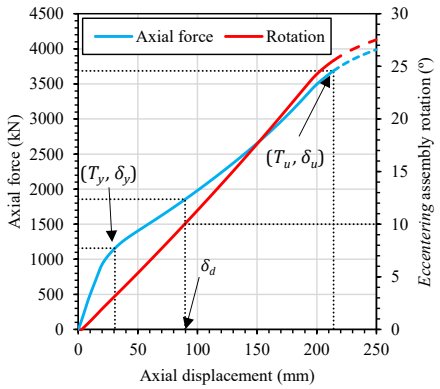

Figure 5.24: Response under monotonic tensile load and associated *eccentering* assembly rotation: Model 6

5.4.4. Strain distribution along the length of BIEs

One of the purported advantages of BIEs with respect to CLBs is that the onset of local buckling is delayed, owing to a more evenly distributed strain demand along the brace length in compression, as the brace deflected shape is governed by bending rather than by global buckling. To verify this hypothesis, the average measured strains along the flat width of the HSS south face during the peak in compression of the first 0.5% EDR cycle are plotted in Figure 5.25 for all specimens and models. The location of the strain gauges and orientation of the specimens is shown in Figure 5.9; the specimens deflected to the north under compression, thus bending resulted in compression along the south face. As such, the strains on the south face are those most directly related with local buckling The first 0.5% EDR cycle was selected as it corresponded with the largest displacement amplitude that any of the specimens or FE models could sustain before the onset of local buckling. Comparing the response of Model 3' to that of Specimens 3 and 5 in Figure 5.25 (b), it is clear that while the strain demand in the CLB concentrated at mid-length, the BIEs presented a more even distribution. The same observation applies to Specimen 4 and Model 4' in Figure 5.25 (c). Moreover, as the intentional eccentricity is increased, the overall magnitude of the strain demands in compression over the length decreases, as can be seen in Figure 5.25 (b), comparing Specimens 3 and 5, and in Figure 5.25 (d), comparing Models 6 and 7. In the case of Specimens 1 and 2, during the 0.5% EDR cycle peak in compression, the strain demands over the

length in Specimen 1 were lower than in Specimen 2; however, this is explained by Specimen 1 not having globally buckled yet, as can be seen in Figure 5.11 (a), presumably due to the effects of the connection slippage.

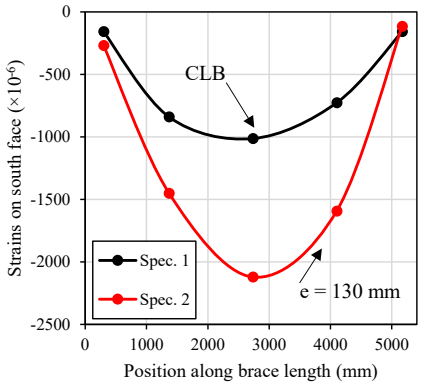

(a) Specimens 1 and 2 (HSS 127×127×7.9)

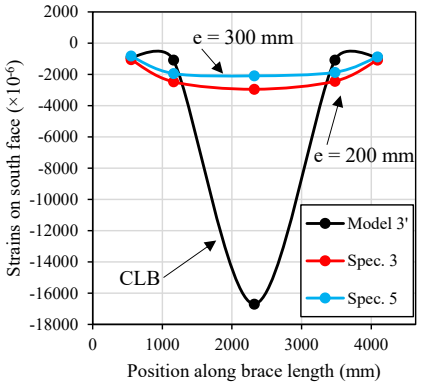

(b) Specimens 3 and 5 and Model 3' (HSS 254×254×13)

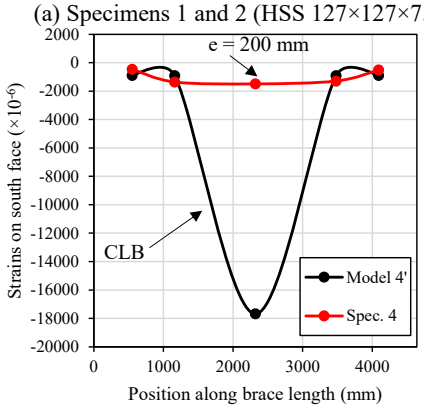

(c) Specimen 4 and Model 4' (HSS 254×254×9.5)

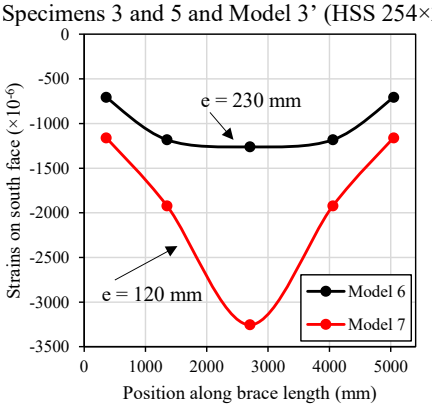

(d) Models 6 and 7 (HSS 178×178×16)

Figure 5.25: Measured strain along the length of the bracing members' south face during the first 0.5% EDR cycle peak (Data points correspond to average measured strains; solid lines are automatically generated trendlines)

As discussed in Section 5.4.3, the ends of the bracing member adjacent to the *eccentering* assemblies constitute the critical regions in BIEs whose failure mode is not governed by local buckling at mid-length. The strains along the south face of Specimen 2 during the displacement peaks in tension and compression, for the first cycle of each EDR amplitude increment, are respectively presented in Figure 5.26 (a) and (b). In Figure 5.26, the points marked with a square symbol indicate that the corresponding data were taken from the FE model of Specimen 2 and are not experimental readings; during the test of Specimen 2 the data acquisition system was configured to measure strains up to only ± 16000 $\times 10^{-6}$. This was corrected for the subsequent tests

of Specimens 3 to 5. Overall, the strain demands were significantly more severe in tension than in compression. As early as the first 0.5% EDR cycle, the south face of the HSS yielded at the ends of the bracing member, and the strain demands subsequently escalated as the cycles' amplitude increased. By the 1% EDR cycle, the strain demand exceeded 10 times the yield strain (20000×10^{-6}), and, as can be noted in Figure 5.26 (b), little of this strain demand was relieved during the subsequent compression cycles.

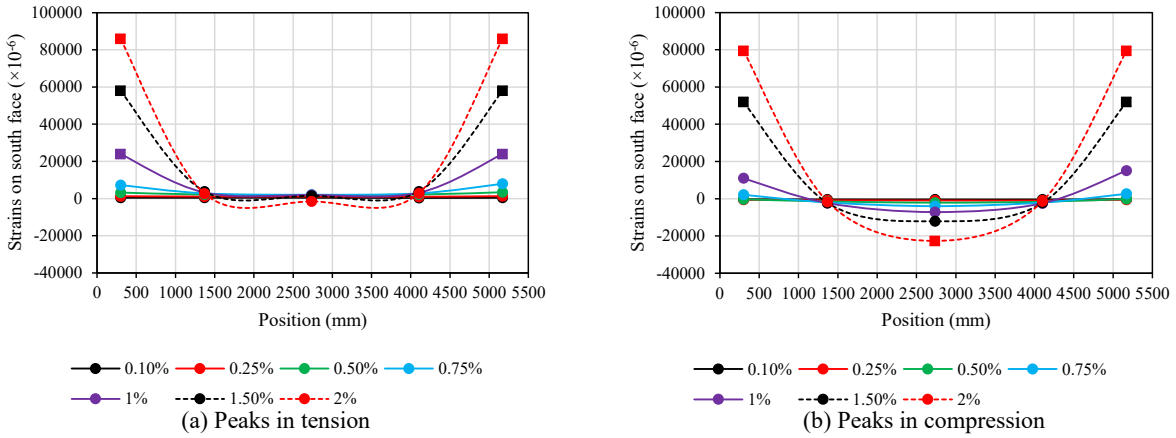

(a) Peaks in tension (b) Peaks in compression

Figure 5.26: Strain history along south face of Specimen 2 (square symbols indicate data from FE model; lines are automatically generated trendlines)

5.4.5. Energy dissipation

To compare the effects of the eccentricity on the energy dissipation capacity of braces with the same section, the dissipated energy during the first cycle of each applied EDR increment is presented in Figure 5.27 as a function of the EDR amplitude. The energy dissipated by the specimens and FE models was obtained by calculating the area enclosed by the corresponding hysteretic loop. Except for Figure 5.27 (a), because Specimen 2 had a shorter fracture life than Specimen 1, the plots show that the effect of the eccentricity was to increase the displacement levels at which the braces dissipated the most energy, while the magnitude of the maximum energy dissipated did not change significantly. Overall, as the eccentricity lengthened the fracture life of

the bracing members, the total energy dissipated during the loading history was greater for BIEs and increased with the eccentricity.

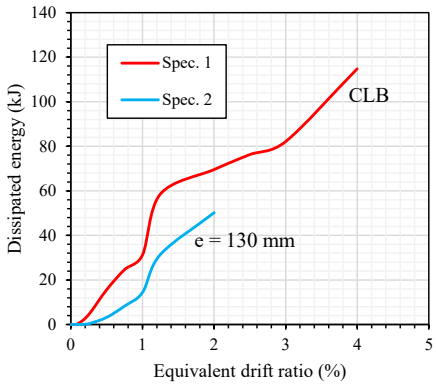

(a) Specimens 1 and 2 (HSS 127×127×7.9)

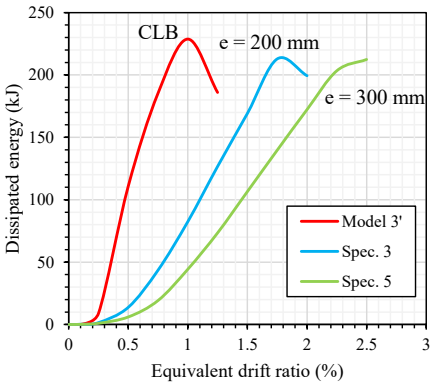

(b) Specimens 3 and 5 and Model 3' (HSS 254×254×13)

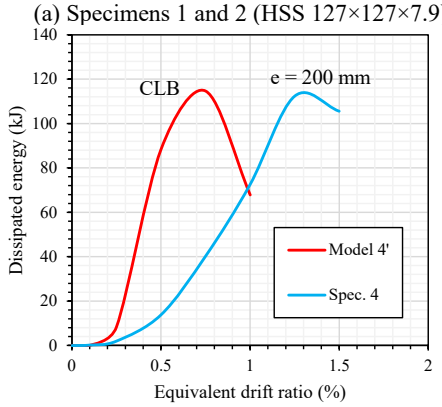

(c) Specimen 4 and Model 4' (HSS 254×254×9.5)

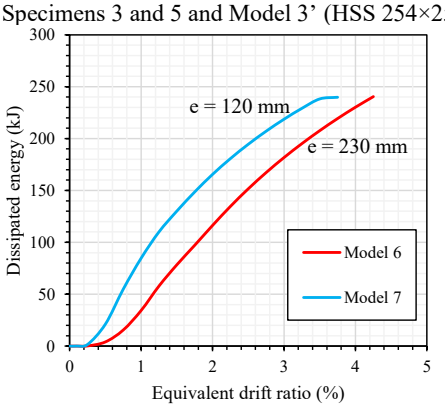

(d) Models 6 and 7 (HSS 178×178×16)

Figure 5.27: Dissipated energy during the first cycle of each equivalent drift ratio amplitude

As discussed in [8], it is proposed that the equivalent damping ratio be used in design to estimate the net damping capacity of BIEs at a given displacement level and adjust accordingly the design displacement spectrum. The equivalent damping ratio as a function of the ductility, taken as the cycle displacement amplitude divided by the estimated "first-yield" displacement, δ_y, (Table 5.5 and Table 5.8), for all specimens and FE models is presented in Figure 5.28. As observed, the maximum damping ratios were attained at ductility ratios between 2 and 3, regardless of the eccentricity, and their magnitude increased as an inverse function of the global slenderness. This confirms that the use in design of the models to estimate the equivalent damping ratio of HSS bracing members proposed by Wijesundara et al. [22] is adequate, as also suggested by the results in [7, 8]. It can also be noted that the braces with more compact sections exhibited much slower

deterioration of the damping capacity after reaching the peak, compared to the braces with more locally slender sections.

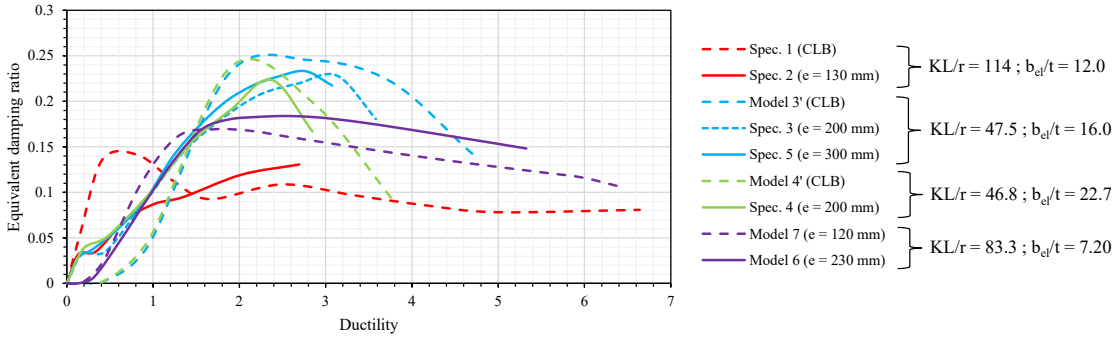

Figure 5.28: Equivalent damping ratio as a function of ductility

5.4.6. Degradation of initial stiffness

As mentioned in Section 5.3.3, between the cycles with EDR amplitudes of 0.75% and 1.0%, two supplemental cycles were included in the loading protocols with an amplitude of 0.1% EDR, as the first overall cycles, but centred at +0.1% EDR. These cycles were introduced to determine how much of the initial stiffness could be maintained after the specimens had been subjected to a loading history which could be associated with moderate seismic demand. As a reference, note that in the preliminary investigations by the authors on the application of BIEs to building structures [6-8], the design target storey drift ratios, associated with a seismic hazard with a probability of exceedance of 2% in 50 years, were set equal to 1.5% and 2.5%. To compare the initial stiffness with the residual stiffness in the 0.1% EDR supplemental cycles, the axial force vs. displacement responses for the corresponding cycles were plotted, and the trendlines, whose slope corresponds to the stiffness, were obtained with linear regression. An example of these plots is presented in Figure 5.29, which shows the results for Specimen 2. The residual stiffness the specimens displayed during the supplemental cycles, as a percentage of the initial stiffness, is presented in Table 5.9. The results show that, in comparison with the CLBs, the BIEs were able to retain significantly more of their initial stiffness after sustaining part of the loading history.

Moreover, for Specimens 3, 4 and 5, and for Model 6, the residual stiffness was identical to the initial stiffness. These results indicate that, in the hypothetical case of a structure being struck by aftershocks following a seismic event, BIEs could offer an advantage over CLBs as they can still provide a response closer to that of the undamaged structure.

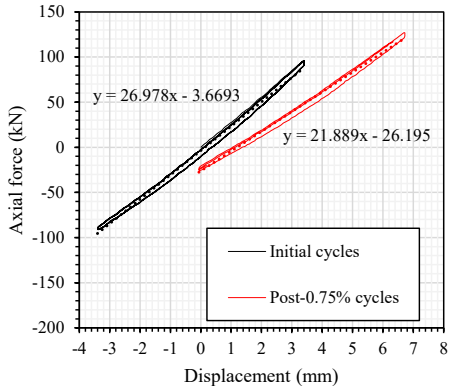

Figure 5.29: Initial stiffness and stiffness during supplemental cycles: Specimen 2

Table 5.9: Residual stiffness in 0.1% EDR supplemental cycles after 0.75% EDR cycles, as a percentage of initial stiffness

Specimen or Model	Residual Stiffness
1	63%
2	81%
3	100%
4	99%
5	100%
3’	72%
4’	46%
6	100%
7	89%

5.4.7. Demands in knife plate

In contrast with CLBs, which only bend in compression due to global buckling, the kinematic response of BIEs entails bending in tension as well. If connections with a knife or gusset plate intended to work as pins are used, this additional bending in tension must be accommodated. Part of the strain history recorded by the strain gauges located on the clearance of the knife plates of Specimens 1 and 2, as shown in Figure 5.9, is presented in Figure 5.30. While the south face of Specimen 1’s knife plate was only subjected to tension due to bending as the brace buckled, the knife plate of Specimen 2 experienced cycles of reversed tension and compression. Although this type of connection has been widely investigated in the context of CLBs, the more severe demands imposed by BIEs could potentially make a difference for the knife plate in terms of low cycle fatigue effects. As such, additional research is advocated to confirm whether this detailing of

gusset or knife plates can provide the ductility under reversed cyclic bending that BIEs in FIEBs designed for large target drift ratios would require.

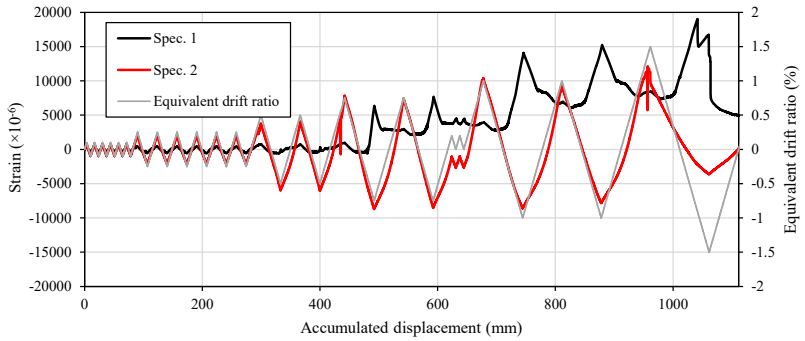

Figure 5.30: Strain history in south face of knife plate clearance: Specimens 1 and 2

5.4.8. Prediction of the onset of local buckling

The authors have developed an expression, for use in the design of FIEBs, to estimate the maximum drift ratio that BIEs can safely sustain under cyclic loading before developing local buckling at their mid-length, or the allowable design drift ratio, θ_{md}. As described in [9], the proposed formula, given in Equation (5.3), was obtained from a multiple regression analysis of the results of a parametric finite element study of BIE models. It expresses θ_{md} as a function of the eccentricity to height ratio, $e_0 = e/H$, and a combined slenderness ratio, $\lambda_0 = (KL/r)/(b_{el}t)$. The material properties considered in the study presented in [9], were based on coupon data of CSA G40-21 350W Class C HSSs, obtained from [19]. Specimens 1, 3, 4, and 5, as well as Models 3', 4', and 7, withstood loading cycles with amplitudes significantly larger than those predicted by Equation (5.3), which suggests that the use of the equation may be overly conservative for ASTM 1085 HSS members, especially in the case of CLBs or BIEs with low eccentricity ratios. The θ_{md} values, taken as the EDR of the cycle with largest amplitude that the specimens or models could withstand before local buckling were evident, are provided in Table 5.10 along with those estimated with Equation (5.3).

$$\theta_{md} = -0.4312 + 0.1943\lambda_0 + 0.6704e_0 - 0.001319\lambda_0^2 - 0.01833\lambda_0 e_0 + 0.241e_0^2 \quad (5.3)$$

Table 5.10: Experimental and numerical, and predicted values of θ_{md}

Specimen or Model	θ_{md}, experimental/FE model (EDR)	θ_{md}, Eq. (5.3) (EDR)
Specimen 1	2.5%	1.3%
Specimen 2	> 2.0%	2.06%
Specimen 3	1.5%	0.77%
Specimen 4	1.0%	0.61%
Specimen 5	2.0%	1.2%
Model 3'	0.75%	0.13%
Model 4'	0.5%	0%
Model 6	> 4.5%	2.64%
Model 7	3.25%	2.06%

5.5. CONCLUSIONS

Reversed cyclic loading tests were performed on 4 full scale square HSS BIE specimens designed with *eccentering* assemblies based on side plates connected to the HSS corners, and on one CLB specimen. Supplementary finite element analyses were carried out on two BIE and two CLB models calibrated using the physical test results, to expand upon and complement the experimental data. The studied specimens and models varied in the global and local slenderness of the bracing member and in the magnitude of the applied eccentricity. The objectives were to confirm whether so constructed BIEs would display the expected advantages of the introduction of an intentional eccentricity, namely a delay to the onset of local buckling and a markedly enhanced post-yielding stiffness, and verify if the addition of the eccentricity could mitigate the detrimental effects of excessive stockiness and section non-compactness in braces not complying with the CSA S16-14 limits to global and local slenderness. The overall force-deformation hysteretic response of the

specimens and models was examined, as well as their failure mode and fracture life, the strain distribution along their length, their energy dissipation and damping capacity, the degradation of their initial stiffness, and the flexural demands they imposed on their knife plate connections.

- The BIE specimens exhibited the expected overall behaviour and beneficial effects of the applied eccentricity, specifically substantial post-yielding stiffness and delayed onset of local buckling at the brace mid-length. Two types of failure were observed: low-cycle fatigue induced fracture at the brace mid-length (Specimens 3, 4, and 5), and tensile fracture at the bracing member's end (Specimen 2). The first failure mode occurred as expected. The unexpected fracture of Specimen 2 was a consequence of the plastic strain concentration at the end of the HSS induced by the large rotation demands.
- The analysis of the strain distribution along the bracing members length shed light on the magnitude of the rotation and strain demands to which the ends of the BIE HSS bracing members are subjected, and on the propensity of these regions to fracture determining the failure mode of BIEs for which local buckling does not govern.
- The addition of the eccentricity can substantially improve the fracture life of HSS braces not complying with the CSA S16-14 limits on global and local slenderness.
- The magnitude of the equivalent damping ratio provided by BIEs is not affected sensibly by the eccentricity. Instead, it depends primarily on the global slenderness of the bracing member and on the ductility demand. As such, the equations presented in [22] for the estimation of the equivalent damping ratio of BIEs for the displacement-based design of FIEBs is deemed adequate until a revised model, calibrated considering explicitly the response of FIEBs to ground motions, is formulated. Additionally, it was observed that an

increased section compactness grants the brace the ability to better sustain its maximum damping capacity as the ductility demand increases.

- BIEs can maintain more of their initial stiffness than CLBs after undergoing moderate displacement demands. After being subjected to EDR demands of 0.75%, the residual stiffness of the BIEs specimens was between 81% and 100% of their initial stiffness, while for the CLB specimens and FE models, the residual stiffness lay between 46% and 72% of their initial stiffness. Thus, BIEs could offer an advantage over CLBs with respect to the expected damage caused by moderately severe earthquakes and response to potential subsequent ground motions.
- In contrast with CLBs, the kinematic response of BIEs requires that their connections accommodate reversed cyclic rotation and therefore be subjected to higher cyclic strain demands. More research is required to verify whether this could pose a limitation to the use with BIEs of the traditional detail of a plate with a bending clearance long as twice its thickness, which is used ubiquitously with CLBs.
- In all brace specimens and all numerical models calibrated with the experimental results, local buckling occurred consistently at larger EDRs than those predicted by the use of Equation (5.3), previously developed by the authors [9]. The material properties considered in the development of Equation (5.3) were based on coupon data from the flat walls of HSSs. Therefore, the differences between the predicted and observed onsets of local buckling may be attributed to the omission of the effects of cold working at the HSS corners on the effective global stress-strain response of the cross-section.

The propensity of HSS BIEs to fracture at the ends of the bracing members, unbeknownst when initially developing the design procedure discussed in [6-8], limits the array of sections and

eccentricities combinations apt for use in FIEBs with large target drift ratios. While more research is required to reliably predict allowable cyclic displacement capacities for BIEs such as those considered in this study, considering both identified failure modes, it is the authors' opinion that the effort should be directed toward developing *eccentering* assemblies that would result in substantially alleviated rotation and strain demands at the bracing member's ends.

ACKNOWLEDGEMENTS

This work was made possible by the generous contribution of Atlas Tube and Constructions Proco, who donated the HSSs and fabricated the test specimens, respectively, and by the obliging collaboration of the technicians and engineers at the Polytechnique Montréal's structures laboratory, as well as undergraduate and graduate research assistants from Polytechnique Montréal and McGill University. The authors would also like to acknowledge DPHV Structural Consultants and ADF Group Inc. for their generous financial support and technical input, as well as the Natural Sciences and Engineering Research Council of Canada (NSERC), the Fonds de Recherche du Québec – Nature et Technologies (FRQ-NT) and the Centre d'Études Interuniversitaire des Structures sous Charges Extrêmes (CEISCE) for providing funding for this research project. The first author wishes to thank the Universidad de Costa Rica for financing the undertaking of his doctoral studies

REFERENCES

[1] X. Tang and S. C. Goel, "Brace fractures and analysis of Phase I Structure," *Journal of Structural Engineering,* vol. 115, no. 8, pp. 1960-1976, 1989, doi: 10.1061/(ASCE)0733-9445(1989)115:8(1960).

[2] R. Tremblay, "Inelastic seismic response of steel bracing members," *Journal of Constructional Steel Research,* vol. 58, no. 5-8, pp. 665-701, 2002, doi: 10.1016/S0143-974X(01)00104-3.

[3] *CSA. S16-14: Design of steel structures*, Canadian Standards Association (CSA), Toronto, ON, 2014.

[4] S. Costanzo, M. D'Aniello, and R. Landolfo, "Proposal of design rules for ductile X-CBFS in the framework of EUROCODE 8," *Earthquake Engineering & Structural Dynamics,* vol. 48, no. 1, pp. 124-151, 2019, doi: 10.1002/eqe.3128.

[5] K. A. Skalomenos, H. Inamasu, H. Shimada, and M. Nakashima, "Development of a steel Brace with Intentional Eccentricity and experimental validation," *Journal of Structural Engineering,* vol. 143, no. 8, p. 04017072, 2017, doi: 10.1061/(ASCE)ST.1943-541X.0001809.

[6] A. González Ureña, R. Tremblay, and C. A. Rogers, "Design and seismic performance of multi-storey Frames with Intentionally Eccentric Braces," Proceedings of the *12th Canadian Conference on Earthquake Engineering*, Québec, Canada, 2019. Paper no. 192-coqm-119.

[7] A. González Ureña, R. Tremblay, and C. A. Rogers, "Design and performance of Frames with Intentionally Eccentric Braces " Proceedings of the *17th World Conference on Earthquake Engineering*, Sendai, Japan, 2020. Paper no. C000830.

[8] A. González Ureña, R. Tremblay, and C. A. Rogers, "Earthquake-resistant design of steel Frames with Intentionally Eccentric Braces," *Journal of Constructional Steel Research,* vol. 178, p. 106483, 2021, doi: https://doi.org/10.1016/j.jcsr.2020.106483.

[9] A. González Ureña, R. Tremblay, and C. A. Rogers, "Numerical investigation of the seismic response of square HSS Braces with Intentional Eccentricity," Proceedings of the *17th World Conference on Earthquake Engineering*, Sendai, Japan, 2020. Paper no. C000832.

[10] H. L. Hsu and H. Halim, "Brace performance with steel curved dampers and amplified deformation mechanisms," *Engineering Structures,* vol. 175, pp. 628-644, 2018.

[11] H. Halim and H. L. Hsu, "Steel A-braced frame upgrade performance under various load characteristics," *Journal of Constructional Steel Research,* vol. 175, p. 106303, 2020.

[12] P. C. Hsiao, K. Hayashi, H. Inamasu, Y. B. Luo, and M. Nakashima, "Development and testing of naturally buckling steel braces," *Journal of Structural Engineering,* vol. 142, no. 1, p. 04015077, 2016, doi: 10.1061/(ASCE)ST.1943-541X.0001319.

[13] K. A. Skalomenos, M. Kurata, and M. Nishiyama, "Induction-heat treated steel Braces with Intentional Eccentricity," *Engineering Structures,* vol. 211, p. 110461, 2020.

[14] A. Astaneh-Asl, S. C. Goel, and R. D. Hanson, "Cyclic out-of-plane buckling of double-angle bracing," *Journal of structural Engineering,* vol. 111, no. 5, pp. 1135-1153, 1985.

[15] R. Tremblay, M. Haddad, G. Martínez, J. Richard, and K. Moffatt, "Inelastic cyclic testing of large size steel bracing members," Proceedings of the *14th World Conference on Earthquake Engineering*, Beijing, China, 2008. Paper no. 05-05-0071.

[16] *ASTM A1085/A1085M - 15 Standard specification for cold-formed welded carbon steel hollow structural sections (HSS)*, American Society for Testing and Materials (ASTM), West Conshohocken, Pennsylvania, USA, 2015.

[17] *ASTM A572/A572M - 18 Standard specification for high-strength low-alloy columbium-vanadium structural steel*, American Society for Testing and Materials (ASTM), West Conshohocken, Pennsylvania, USA, 2018.

[18] *Dassault Systèmes, Abaqus/CAE 2019*. (2018). Dassault Systèmes Simulia Corp., Providence, RI.

[19] R. Moreau, "Evaluation of the "Modified-Hidden-Gap" connection for square HSS brace members," M. Eng. Thesis, Civil Engineering and Applied Mechanics, McGill University 2014.

[20] R. K. Bubela, "An experimental and analytical study of chevron braced frames with vertical slotted connections," M. Eng. Thesis, Civil Engineering, University of British Columbia, 2003.

[21] *CSA. G40.20-13/G40.21-13: General requirements for rolled or welded structural quality steel/Structural quality steel*, Canadian Standards Association (CSA), Toronto, ON, 2014.

[22] K. Wijesundara, R. Nascimbene, and T. J. Sullivan, "Equivalent viscous damping for steel concentrically braced frame structures," *Bulletin of Earthquake Engineering,* vol. 9, no. 5, pp. 1535-1558, 2011, doi: 10.1007/s10518-011-9272-4.

CHAPTER 6: SUMMARY AND CONCLUSIONS

6.1. OVERVIEW

The general intent of this research was to generate information on the seismic performance of square HSS Braces with Intentional Eccentricity (BIEs), at the member level and as the principal component of the SFRS of buildings in regions with high seismic hazard. When this study was undertaken, BIEs had just been proposed as a novel type of brace showing great potential to overcome the main weaknesses of traditional concentrically loaded braces and Concentrically Braced Frames (CBFs). As such, the only published research on the subject was that of Skalomenos et al. [1, 2], which was limited to BIEs from a single circular HSS member. The application of BIEs to the design of buildings had yet to be addressed.

In this study, the response of square HSS BIEs to monotonic and reversed cyclic loading was examined through extensive numerical modelling and by means of the physical testing of full-scale BIE specimens. A preliminary displacement-based procedure for the earthquake-resistant design of Frames with Intentionally Eccentric Braces (FIEBs) was developed, aiming to accommodate both the performance objectives and the philosophy of modern design codes, and the load-deformation response of BIEs, distinct from that of traditional dissipating elements. Finally, the performance under the effects of ground motions of FIEBs resulting from the application of the proposed design methodology was assessed using numerical models and compared to that of traditional CBFs designed for the same conditions. An *eccentering* assembly consisting of side plates welded to the corners of the HSS bracing member, linking it to a knife plate detailed to yield in flexure and offer no restriction to the free rotation of the connection, was

considered throughout the numerical analyses, the physical testing and the design of model buildings.

6.2. SUMMARY AND CONCLUSIONS

6.2.1. Numerical study on BIEs

An extensive numerical study encompassing OpenSees and Abaqus models was undertaken to provide information on the response to monotonic and reversed cyclic loading of square HSS BIEs, and to clarify the relative influence of the variables involved. The effects and purported benefits of the introduction of the eccentricity, as reported by Skalomenos et al. [1, 2], were corroborated by the results and it was confirmed, numerically, that they translated to square HSSs.

The study shed light on a geometrical parameter not explicitly considered previously: the length of the *eccentering* assembly. The length of the *eccentering* assemblies, which can be assumed to be rigid in comparison to the rest of the BIE, is key in determining the elastic and post-yielding stiffness of the lateral system, and the rotation demands on the HSS. As such, this parameter plays a role in controlling the strain demands and thus, in some cases, the fracture life of the brace ends.

It was also found that although BIEs have a theoretically higher energy dissipation capacity than concentrically loaded braces under monotonic tension, as additional energy is required to straighten them and annul the eccentricity, under reversed cyclic loading the eccentricity tends not to alter significantly the equivalent damping ratio as a function of the ductility demand. For this reason, the use of an existing model developed for concentrically loaded braces [3] was considered acceptable in the preliminary version of the design procedure presented in this thesis.

The parametric study on the fracture life of BIEs confirmed that the onset of local buckling can be significantly delayed, in terms of applied displacement under cyclic loading, by the introduction

of the eccentricity. This effect is particularly marked in the case of braces with low global slenderness and/or highly non-compact sections. Thus, the use of BIEs could allow for the relaxation of the limits on global and local slenderness for rectangular HSSs in certain cases where the design target drift ratio is lower than the predicted fracture life of the brace. However, the exercise of designing prototype FIEBs with a focus on cost-effectiveness has shown that most often the use of sections with very low local slenderness ratios, and the choice of large design target drift ratios result in a more efficient outcome.

6.2.2. Laboratory testing of BIEs

To validate the results from the numerical analyses performed in this research, and to shed light on potential unforeseen characteristics of the BIEs' response not accounted for in the numerical models, a testing programme consisting of four full-scale square HSS BIE specimens, plus an additional concentrically loaded brace specimen, subject to reversed cyclic loading was undertaken. In general terms, the response of the specimens corresponded to what was expected based on the numerical studies, and the purported benefits of the introduction of the eccentricity, such as offering control over the stiffness and strength of the braces and delaying the onset of local buckling, were corroborated.

Moreover, it was confirmed that the implementation in fabrication of the proposed design for the *eccentering* assemblies posed no difficulties, and that the resulting assembly and the selected knife-to-gusset bolted connection performed as intended. Notwithstanding, it was noted that BIEs impose more severe demands in the plastic hinge in the for-this-purpose-specified clearance in the connection, in comparison to concentrically loaded braces.

Finally, the test results showcased a significant weak point of BIEs with fully rigid *eccentering* assemblies, which can result in premature fracture at the interphase of the HSS with the *eccentering* assemblies. Such fractures were also observed by Skalomenos et al. in [2] and [4], which were then attributed to damage in the heat affect zone adjacent to the full perimeter weld they used to attach the HSS to the end-plate *eccentering* assembly. Incidentally, in otherwise identical specimens they tested, but in which the critical region was reinforced with rib stiffeners to reduce the deformation demand on the heat-affected zone, this type of fracture was avoided.

The circumstance of this failure mode is implicit in the kinematic model of the response to tension loading of BIEs: to attain its tensile capacity, the eccentricity along the bracing member must be annulled and, for this to be accomplished, plastic hinges in the vicinity of the *eccentering* assemblies must accommodate the required rotation demand. Thus, the HSS at the bracing member's ends must in theory provide simultaneously its plastic moment and tensile strength capacities. In practical terms, this means that a BIE can only attain the tensile strength of the bracing member if its geometric dimensions are such that the rotation demand on its ends is compatible with the required tension force demand. Evidently, the reduced ductility due to welds weighs in to reduce the deformation capacity, depending on how the HSS is connected to the *eccentering* assembly; however, the predominant factor in this issue is presumably the rotation capacity under tension of HSSs.

6.2.3. Design procedure and seismic performance of FIEBs

A displacement-based procedure was developed for the seismic design of FIEBs, explicitly accounting for the particular force-displacement characteristics of BIEs. The use of the procedure resulted in buildings that, overall, displayed a satisfactory performance and complied with the selected target maximum drift ratios and performance objectives. What is more, the results showed

that for severe ground motions FIEBs presented a better performance than traditional CBFs, in terms of maximum and residual drift ratios. In addition to this, FIEBs were shown to be economically advantageous compared to CBFs, as the lower design forces and better control of the overstrength allowed for a reduction of the weight of the capacity-protected elements of the SFRS. The reduction in costs was more significant in the case of FIEBs designed for high target drift ratios in high seismic hazard settings.

The inclusion of design provisions related to serviceability criteria proved to be successful in that the so designed FIEBs exhibited virtually no damage when subjected to the ground motions scaled to represent a Service Level Earthquake. However, the additional strength and stiffness required by these provisions led to an undershooting of the targeted displacements at the Design Level Earthquake in most cases.

6.2.4. Conclusions

The main conclusions of the study presented in this thesis can be summarized as follows:

- The inherent characteristics of BIEs enable them to overcome the most prominent shortcomings of traditional concentrically loaded braces, namely those associated with their high initial stiffness, low post-yielding stiffness, and susceptibility to local buckling.
- The proposed displacement-based design procedure for FIEBs results in buildings that, according to numerical models, offer a satisfactory seismic performance, complying with modern codes' capacity-based design philosophy and performance objectives, both for design-level and service-level ground motions.
- FIEBs potentially offer better seismic performance and exhibit less damage than traditional CBFs, in terms of maximum and residual storey drifts, while requiring less overall material

owing to the better control of the structure's response and its overstrength that the possibility of adjusting the eccentricity provides.

- The introduction of the eccentricity improves the response and fracture life of overly stocky and non-compact bracing members, however performance- and efficiency-oriented designs tend to result naturally in the selection of BIEs with relatively slender and compact bracing members.
- The side plated *eccentering* assembly considered in this study is cost efficient and easily fabricated; however, as every rigid *eccentering* assembly is suspected to be, it is associated with the probability of the bracing member fracturing in tension under certain conditions which remain to be fully understood.
- The use of FIEBs with HSS bracing members to resist seismic loads in multi-storey buildings has the potential to become a competitive alternative to CBFs, considering both structural performance and cost. However, to fulfill this potential, more research is needed to either predict reliably the fracture life of BIEs with rigid *eccentering* assemblies considering the failure mode of fracture in tension at the bracing member's end, or to produce an effective *eccentering* assembly that can safely enable HSS BIEs to attain the required axial deformation levels by reducing strain concentrations under tension so that higher rotation can be achieved without fracture.

6.3. RECOMMENDATIONS FOR FUTURE RESEARCH

6.3.1. Design procedure for FIEBs

Although the preliminary design procedure for FIEBs presented in this thesis produced satisfactory results, several aspects that can be improved through further research were identified.

As discussed, the force-displacement model used to select the BIEs at each stage, is based on the simplification of their response in tension and compression considering tri-linear and elastic-perfectly plastic idealisations, respectively, with the former relying on OpenSees models and the latter on Equation (2.1). However, it could be more accurate to instead use models of the response of the opposed tension and compression braces acting in tandem. For BIEs with compact sections and large eccentricities, the use of the elastic-perfectly plastic model to approximate their response in compression can result in an underestimation of their strength for small drift ratios and an overestimation for large drift ratios. The use of tri-linear models based on the combined response of the pair of braces would circumvent this limitation without requiring additional effort.

Although the use of the inelastic displacement vector developed by Priestley et al. [5] for moment frames offered reasonably good results for the preliminary design procedure presented in this thesis, the distribution of the maximum storey drifts displayed by the taller FIEBs showed that the procedure failed to capture adequately the higher order effects. As such, the rational approach would be to determine by means of research a model to estimate a target displacement vector specially tailored for FIEBs for use in design.

The use of an equivalent damping model developed for concentrically loaded braces [3] was shown to work adequately with BIEs. However, it is advisable to invest time in the calibration of an equivalent damping model explicitly based on BIEs and corrected for the response of FIEBs to ground motions, as the question arises whether the similarities in the damping capacity of BIEs and concentrically loaded braces under controlled cyclic loading are conserved if realistic earthquake excitation is instead considered.

The results of the NLRHAs performed in Chapter 2, for structures designed as per the American standards, indicated that for some of the ground motions scaled to the MCE_R level, the storey

shears exceeded the forces used in the design of the capacity-protected elements of the SFRS. The implementation of fuse-like devices in the brace connections to pose a cap to the transmitted forces was then proposed as a possible solution to these occurrences. However, the idea was discarded as it was deemed that the effective loss of storey stiffness that would result from its enactment would conflict with one of the main perks of employing BIEs: their large post-yielding stiffness.

Moreover, it was reasoned that the observed overshoots of the storey shears in Chapter 2: are a consequence of evaluating the response of FIEBs using a method formulated for structures with different characteristics. The performance assessment following the requirements from ASCE/SEI 7-16 [6] requires that the ground motions used for the NLRHA be scaled at a level larger than which corresponds to the seismic hazard considered in the design (MCE_R and DBE, respectively). In the case of traditional SFRSs, this has no impact on the maximum storey shears since the force-deformation response of its dissipating elements is, for practical purposes, elastic-perfectly plastic. In contrast, for FIEBs, which have significant post-yielding stiffness, this results in irremediably higher storey shears, and thus in larger forces in the non-dissipating elements. The design procedure for FIEBs proposed in this thesis intended to account for ground motions producing displacement demands larger than those anticipated in design by requiring that the expected forces developed by the BIEs be calculated assuming brace displacements larger than the selected target. An increment of 25% was prescribed in the version of the design procedure adapted for use in Canada (Chapter 4:, while an increment of 50% was specified for the version adapted for use in the USA (Chapter 2:. For the designs and performance assessments of FIEBs performed according to Canadian standards, the 25% increment was adequate, as indicated by the results presented in Chapter 4:. For the adaptation of the design procedure to the American practice, however, it is

recommended that the corresponding amplification factor be revised acknowledging explicitly the seismic hazard which will be used to assess the performance of the structure.

The results from the physical testing suggested that the fracture lives predicted by the proposed equation (Equation (3.1)) can be overly conservative in the case of ASTM A1085 HSS BIEs, which is presumably due to differences between the effective stress-strain curve of the cross-sections of the test specimens and that considered in the study. When calibrating the material model for the numerical models complementary to the physical testing, it was noticed that the accurate reproduction of the onset of local buckling depends greatly on the slope of the effective true stress-true strain curve of the employed material after yielding. As such, to properly predict in models the onset of local buckling, reliable information on the yield stress, F_y, the tensile strength, F_u, and the strain at which the latter occurs, ε_u, is required. However, it is known that there exists great variability in these values, even for HSSs complying with a given standard. To account for this variability, a revised parametric study similar to the one included in this thesis should be performed, but considering material models statistically representative of the physical properties of HSSs fabricated under different standards of common use in North America, such as ASTM A1085, ASTM A500, and CSA G40.21 350W (Class C and Class H), in order to provide more robust fracture life prediction equations to use in the design of FIEBs. As a further potential improvement of the parametric study, it could also be explored whether the consideration of an alternative parameter to characterise the eccentricity results in a more accurate prediction. It could be determined if a non-dimensional parameter relating the eccentricity (e) with relevant properties of the cross-section, such as the area (A) and section modulus (S), eA/S, offers a better correlation with fracture life than the eccentricity to HSS depth ratio (e/H) used in obtaining Equation (3.1).

Finally, more research is required to shed light on the precise threshold in terms of strain demand that triggers tensile fracture at the interphase of the HSS with the *eccentering* assemblies for a given BIE geometry, and to establish a link with the associated demand, be it in terms of rotation demand under tension or of combined axial force and bending moment. It is known that the length of the *eccentering* assembly and the magnitude of the eccentricity are determinant in the rotation demands at the bracing member's end under tension, and presumably other variables such as the radius of gyration of the section play a role as well, although at the moment it has not yet been clearly identified. Further investigation must be undertaken to produce means to reliably predict the fracture life of BIEs, considering both this criterion and low-cycle fatigue-induced fracture at mid-length.

6.3.2. Alternative *eccentering* assembly design

In addition to developing models to predict fracture in the interphase between the HSS and a rigid *eccentering* assembly, the susceptibility of BIEs to tensile fracture at the bracing member end could be reduced by revising the design of the *eccentering* assembly and its connection to the bracing member so that the high strain concentrations in the HSS are reduced. A potential way of achieving this could be to use an *eccentering* assembly similar to the one described by Skalomenos et al. [1, 2]. By connecting the full perimeter of the HSS to an end plate, instead of connecting it by its corners alone, one would avoid concentrating the strain demands in the regions of the HSS that present the lowest ductility and, thus, its plastic rotation capacity would presumably be increased.

Another viable course of action, which could potentially enable even larger displacement capacity, is to substitute the HSS in the critical region by an element capable of attaining greater rotational deformations, such as a rectangular plate. By dimensioning the plate so that its plastic modulus be

equal to that of the HSS, its flexural stiffness and capacity would match that of the HSS but with a much higher capacity in tension. This would allow the plastic hinge to develop in a much more ductile medium without significantly altering the overall strength and stiffness properties of the BIEs. A concept drawing of the proposed *eccentering* assembly is presented in Figure 6.1. Although the connection of the rectangular plate to the HSS shown in the drawing is of the traditional slotted-in with cover-plate reinforcements of the net section, other alternatives such as Slotted Hidden-Gap connections or connections based on an end plate could be employed without altering significantly the expected behaviour of the system.

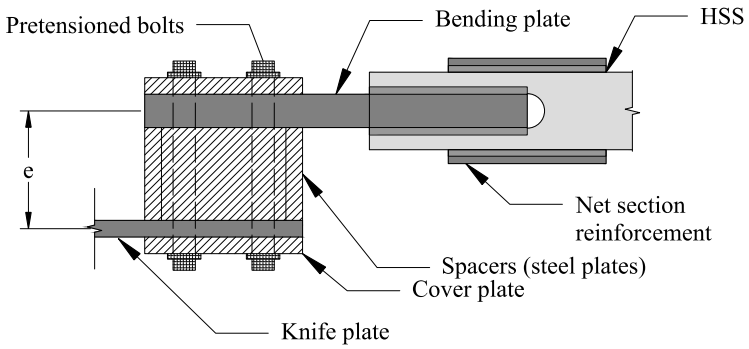

Figure 6.1: Proposed revised *eccentering* assembly

6.3.3. Inelastic rotation capacity under reversed cyclic loading of knife or gusset plate connections

It was noted that BIEs impose more severe demands in comparison to concentrically loaded braces in the clearance provided in the knife plate connection to accommodate the inelastic end rotations. This raises the concern whether this detail would still be appropriate to sustain the large displacements that BIEs with more compact sections and with larger eccentricities could require, and, as such, demands further research.

6.3.4. Effects of vertical acceleration from ground motions on FIEBs

Although the effects of the vertical component of ground motions on the response of braced frames are typically small in comparison to those of the horizontal components, it remains to be confirmed through research whether this is still the case for FIEBs. A rational and practical way of incorporating these effects in a revision of the displacement-based design procedure presented in this thesis must also be determined. An additional aspect to consider is that, as in FIEBs the braces are considerably less stiff than in other braced frame systems, presumably the additional forces produced by the vertical acceleration will have a comparatively more significant effect in the columns of the braced bents and the gravity columns than in the braces themselves.

6.3.5. Alternative braced bent configurations for FIEBs

In this thesis, a single configuration for the braced bents was considered for all designs and analyses: opposed braces in adjacent bays in a pseudo-chevron arrangement with connections producing in-plane bending of the braces. Research on whether alternative configurations for the braces result in benefits in terms of cost or structural performance is recommended. One such configuration is that of BIEs in a single bay in an unconnected X arrangement. If connections designed for out-of-plane bending are used, and sufficient eccentricity is provided so that the bracing members do not intersect at the centre of the X in their undeformed position, they will not come in contact with each other when the structure responds to lateral loading since the lateral storey displacements will result in the tension and compression braces deflecting in the same direction, and the magnitude of the deflection of the compression brace is larger than that of the tension brace. Other configurations to study include true chevron, i.e. without an intermediate column, and inverted chevron.

6.3.6. BIEs with bracing members other than square HSSs

Only square HSSs were considered for the bracing member of the BIEs studied in this thesis, however, the use of other types of sections, such as circular HSSs and W shapes could offer advantages and is therefore worthy of investigation.

Given that their fabrication process involves less cold working than that of rectangular HSSs, circular HSSs are likely to exhibit greater ductility when subjected to reversed cycles of combined flexure and axial load. As such, circular HSS BIEs are presumably less susceptible to tensile fracture at the bracing member ends than the BIEs considered in this thesis. Case in point, the BIEs tested by Skalomenos et al. [1, 2] were capable of developing the full tensile strength of their cross section before failure. Further research is thus recommended to determine if similar results can be achieved with other circular HSSs and different BIE geometries.

BIEs based on W shapes are also expected to present an enhanced plastic rotation capacity with respect to square HSS BIEs due to their relatively higher ductility. In these BIEs, the W shape should be oriented so that bending occurs about its minor axis to prevent the possibility of lateral torsional buckling. Also, this orientation would allow the use of an *eccentering* assembly based on side plates such as that considered in this thesis, with the advantage that a welded connection between the flanges of the W shape and the side plates should lead to a lesser stress concentration.

6.3.7. Equations to calculate design parameters of BIEs

The displacement-based design procedure described in the thesis relies on numerical models in OpenSees to obtain the needed BIE design parameters, i.e. “first yield” strength, initial stiffness, and post-yielding stiffness. From a practical point of view, it would be more convenient to rely instead on an established set of equations which allow one to calculate those parameters. The

determination of such equations, which has been left out of the scope of this thesis, requires the explicit consideration of geometric and material non-linearity, and the actual dimensions of the BIE, including the length of the *eccentering* assemblies, L_{ea}. The author recommends conducting research aiming for the development of such equations, as they would render the design of FIEBs significantly more accessible to practicing engineers and researchers.

REFERENCES

[1] K. A. Skalomenos, H. Inamasu, H. Shimada, M. Kurata, and M. Nakashima, "Experimental investigation of steel braces installed with intentional eccentricity using gusset plate connections," Proceedings of the *16th World Conference on Earthquake Engineering*, 2017, vol. 188.

[2] K. A. Skalomenos, H. Inamasu, H. Shimada, and M. Nakashima, "Development of a steel Brace with Intentional Eccentricity and experimental validation," *Journal of Structural Engineering,* vol. 143, no. 8, p. 04017072, 2017, doi: 10.1061/(ASCE)ST.1943-541X.0001809.

[3] K. Wijesundara, R. Nascimbene, and T. J. Sullivan, "Equivalent viscous damping for steel concentrically braced frame structures," *Bulletin of Earthquake Engineering,* vol. 9, no. 5, pp. 1535-1558, 2011, doi: 10.1007/s10518-011-9272-4.

[4] K. Skalomenos, M. Kurata, H. Shimada, and M. Nishiyama, "Braces with intentional eccentricity and partial cross-section strength enhancement," Proceedings of the *16th European Conference on Earthquake Engineering*, Thessaloniki, Greece, 2018.

[5] M. J. N. Priestley, G. M. Calvi, and M. J. Kowalsky, *Displacement-based seismic design of structures*. Pavia, Italy: IUSS Press 2007, pp. xvii, 721 p.

[6] *ASCE/SEI 7-16: Minimum design loads and associated criteria for buildings and other structures*, American Society of Civil Engineers (ASCE), Reston, VA, 2017. [Online]. Available: https://ascelibrary.org/doi/abs/10.1061/9780784414248

MASTER LIST OF REFERENCES

A. Agüero, C. Izvernari, and R. Tremblay, "Modelling of the seismic response of concentrically braced steel frames using the OpenSees analysis environment," *International Journal of Advanced Steel Construction,* vol. 2, no. 3, pp. 242-274, 2006.

M. Al-Mashaykhi, P. Rajeev, K. Wijesundara, and M. Hashemi, "Displacement profile for displacement based seismic design of concentric braced frames," *Journal of Constructional Steel Research,* vol. 155, pp. 233-248, 2019.

ANSI/AISC 360-16: Specification for structural steel buildings American Institute for Steel Construction (AISC), Chicago, IL, 2016.

ANSI/AISC 341-16: Seismic provisions for structural steel buildings, American Institute for Steel Construction (AISC), Chicago, IL, 2016.

ASTM A1085/A1085M - 15 Standard specification for cold-formed welded carbon steel hollow structural sections (HSS), American Society for Testing and Materials (ASTM), West Conshohocken, Pennsylvania, USA, 2015.

ASTM A572/A572M - 18 Standard specification for high-strength low-alloy columbium-vanadium structural steel, American Society for Testing and Materials (ASTM), West Conshohocken, Pennsylvania, USA, 2018.

ASCE/SEI 7-16: Minimum design loads and associated criteria for buildings and other structures, American Society of Civil Engineers (ASCE), Reston, VA, 2017. [Online]. Available: https://ascelibrary.org/doi/abs/10.1061/9780784414248

A. Astaneh-Asl, S. C. Goel, and R. D. Hanson, "Cyclic out-of-plane buckling of double-angle bracing," *Journal of structural Engineering,* vol. 111, no. 5, pp. 1135-1153, 1985.

G. M. Atkinson, "Earthquake time histories compatible with the 2005 National Building Code of Canada uniform hazard spectrum," *Canadian Journal of Civil Engineering,* vol. 36, no. 6, pp. 991-1000, 2009.

M. Bruneau, C. M. Uang, and R. Sabelli, *Ductile design of steel structures*, 2nd ed. New York: McGraw-Hill, 2011, pp. xxi, 905 p.

R. K. Bubela, "An experimental and analytical study of chevron braced frames with vertical slotted connections," M. Eng. Thesis, Civil Engineering, University of British Columbia, 2003.

CSA. S16-14: Design of steel structures, Canadian Standards Association (CSA), Toronto, ON, 2014.

CSA. G40.20-13/G40.21-13: General requirements for rolled or welded structural quality steel/Structural quality steel, Canadian Standards Association (CSA), Toronto, ON, 2014.

A. K. Chopra, *Dynamics of structures: theory and applications to earthquake engineering*, 4th ed. Upper Saddle River, N.J.: Prentice Hall, 2012, pp. xxxiii, 944 p.

S. Costanzo, M. D'Aniello, and R. Landolfo, "Proposal of design rules for ductile X-CBFS in the framework of EUROCODE 8," *Earthquake Engineering & Structural Dynamics,* vol. 48, no. 1, pp. 124-151, 2019, doi: 10.1002/eqe.3128.

EN 1998-1:2004 Eurocode 8: Design of structures for earthquake resistance - Part 1: general rules, seimic action and rules for buildings, European Committee for Standardization (CEN), Brussels, Belgium, 2004.

B. Fell, A. Kanvinde, and G. Deierlein, *Large-scale testing and simulation of earthquake-induced ultra low cycle fatigue in bracing members subjected to cyclic inelastic buckling*. Stanford, CA: John A. Blume Earthquake Engineering Center, 2010.

B. V. Fell, *Large-scale testing and simulation of earthquake-induced ultra low cycle fatigue in bracing members subjected to cyclic inelastic buckling*. University of California, Davis, 2008.

FEMA, "Quantification of building seismic performance factors, FEMA P695," Federal Emergency Management Agency (FEMA),, Redwood City, CA 2009.

A. González Ureña, R. Tremblay, and C. A. Rogers, "Design and seismic performance of multi-storey Frames with Intentionally Eccentric Braces," Proceedings of the *12th Canadian Conference on Earthquake Engineering*, Québec, Canada, 2019. Paper no. 192-coqm-119.

A. González Ureña, R. Tremblay, and C. A. Rogers, "Numerical investigation of the seismic response of square HSS Braces with Intentional Eccentricity," Proceedings of the *17th World Conference on Earthquake Engineering*, Sendai, Japan, 2020. Paper no. C000832.

A. González Ureña, R. Tremblay, and C. A. Rogers, "Design and performance of Frames with Intentionally Eccentric Braces " Proceedings of the *17th World Conference on Earthquake Engineering*, Sendai, Japan, 2020. Paper no. C000830.

A. González Ureña, R. Tremblay, and C. A. Rogers, "Earthquake-resistant design of steel Frames with Intentionally Eccentric Braces," *Journal of Constructional Steel Research,* vol. 178, p. 106483, 2021, doi: https://doi.org/10.1016/j.jcsr.2020.106483.

H. Halim and H. L. Hsu, "Steel A-braced frame upgrade performance under various load characteristics," *Journal of Constructional Steel Research,* vol. 175, p. 106303, 2020.

P. C. Hsiao, K. Hayashi, H. Inamasu, Y. B. Luo, and M. Nakashima, "Development and testing of naturally buckling steel braces," *Journal of Structural Engineering,* vol. 142, no. 1, p. 04015077, 2016, doi: 10.1061/(ASCE)ST.1943-541X.0001319.

H. L. Hsu and H. Halim, "Brace performance with steel curved dampers and amplified deformation mechanisms," *Engineering Structures,* vol. 175, pp. 628-644, 2018, doi: https://doi.org/10.1016/j.engstruct.2018.08.052.

H. Inamasu, K. A. Skalomenos, P. C. Hsiao, K. Hayashi, M. Kurata, and M. Nakashima, "Gusset plate connections for Naturally Buckling Braces," *Journal of Structural Engineering,* vol. 143, no. 8, p. 04017065, 2017, doi: 10.1061/(ASCE)ST.1943-541X.0001794.

H. Inamasu, K. A. Skalomenos, P. C. Hsiao, K. Hayashi, M. Kurata, and M. Nakashima, "Experimental investigation of bolt-configured naturally buckling braces with gusset plate connections," Proceedings of the *16th World Conference on Earthquake Engineering (16WCEE)*, 2017, vol. 619.

I. Koval, "Accounting for cold working and residual stress effects on the axial strength of HSS bracing members," M. Eng. Thesis, Civil, Geological, and Mining Engineering, École Polytechnique de Montréal, 2018.

K. Lee and M. Bruneau, "Energy dissipation of compression members in concentrically braced frames: Review of experimental data," *Journal of structural engineering,* vol. 131, no. 4, pp. 552-559, 2005.

F. T. McKenna, "Object-oriented finite element programming: Frameworks for analysis, algorithms and parallel computing," Ph.D. Thesis, Civil Engineering, University of California, Berkeley, 1997.

R. Moreau, "Evaluation of the "Modified-Hidden-Gap" connection for square HSS brace members," M. Eng. Thesis, Civil Engineering and Applied Mechanics, McGill University 2014.

National Building Code of Canada 2015, 14th ed. , National Research Council of Canada (NRCC), Ottawa, ON, 2015.

G. O'Reilly, J. Goggins, and S. Mahin, "Performance-based design of a self-centering concentrically braced frame using the direct displacement-based design procedure," Proceedings of the *15th World Conference on Earthquake Engineering*, Lisbon, Portugal, 2012.

PEER. The PEER ground motion selection web application [Online] Available: http://ngawest2.berkeley.edu/

M. J. N. Priestley, G. M. Calvi, and M. J. Kowalsky, *Displacement-based seismic design of structures*. Pavia, Italy: IUSS Press 2007, pp. xvii, 721 p.

S. Santagati, D. Bolognini, and R. Nascimbene, "Strain life analysis at low-cycle fatigue on concentrically braced steel structures with RHS shape braces," *Journal of earthquake engineering,* vol. 16, no. sup1, pp. 107-137, 2012.

K. Skalomenos, M. Kurata, H. Shimada, and M. Nishiyama, "Braces with intentional eccentricity and partial cross-section strength enhancement," Proceedings of the *16th European Conference on Earthquake Engineering*, Thessaloniki, Greece, 2018.

K. A. Skalomenos, H. Inamasu, H. Shimada, M. Kurata, and M. Nakashima, "Experimental investigation of steel braces installed with intentional eccentricity using gusset plate connections," Proceedings of the *16th World Conference on Earthquake Engineering*, 2017, vol. 188.

K. A. Skalomenos, H. Inamasu, H. Shimada, and M. Nakashima, "Development of a steel Brace with Intentional Eccentricity and experimental validation," *Journal of Structural Engineering,* vol. 143, no. 8, p. 04017072, 2017, doi: 10.1061/(ASCE)ST.1943-541X.0001809.

K. A. Skalomenos, M. Kurata, and M. Nishiyama, "Induction-heat treated steel Braces with Intentional Eccentricity," *Engineering Structures,* vol. 211, p. 110461, 2020.

K. A. Skalomenos, M. Kurata, H. Shimada, and M. Nishiyama, "Use of induction-heating in steel structures: material properties and novel brace design," *Journal of Constructional Steel Research,* vol. 148, pp. 112-123, 2018, doi: https://doi.org/10.1016/j.jcsr.2018.05.016.

Dassault Systèmes, Abaqus/CAE 2019. (2018). Dassault Systèmes Simulia Corp., Providence, RI.

X. Tang and S. C. Goel, "Brace fractures and analysis of Phase I Structure," *Journal of Structural Engineering,* vol. 115, no. 8, pp. 1960-1976, 1989, doi: 10.1061/(ASCE)0733-9445(1989)115:8(1960).

R. Tremblay, "Inelastic seismic response of steel bracing members," *Journal of Constructional Steel Research,* vol. 58, no. 5-8, pp. 665-701, 2002, doi: 10.1016/S0143-974X(01)00104-3.

R. Tremblay, "Achieving a stable inelastic seismic response for concentrically braced steel frames," *Engineering Journal, AISC,* vol. 40(2), pp. 111-129, 2003.

R. Tremblay, M. H. Archambault, and A. Filiatrault, "Seismic response of concentrically braced steel frames made with rectangular hollow bracing members," *Journal of Structural Engineering,* vol. 129, no. 12, pp. 1626-1636, 2003.

R. Tremblay, G. M. Atkinson, N. Bouaanani, P. Daneshvar, P. Léger, and S. Koboevic, "Selection and scaling of ground motion time histories for seismic analysis using NBCC 2015," Proceedings of the *11th Canadian Conference on Earthquake Engineering (11CCEE)*, Victoria, BC, Canada, 2015, vol. 99060. Paper no. 99060.

R. Tremblay, M. Haddad, G. Martínez, J. Richard, and K. Moffatt, "Inelastic cyclic testing of large size steel bracing members," Proceedings of the *14th World Conference on Earthquake Engineering*, Beijing, China, 2008. Paper no. 05-05-0071.

P. Uriz, F. C. Filippou, and S. A. Mahin, "Model for cyclic inelastic buckling of steel braces," *Journal of structural engineering,* vol. 134, no. 4, pp. 619-628, 2008.

P. Uriz and S. A. Mahin, "Toward earthquake-resistant design of concentrically braced steel-frame structures," Pacific Earthquake Engineering Research Center (PEER), University of California, Berkeley, 2008.

K. Wijesundara, R. Nascimbene, and T. J. Sullivan, "Equivalent viscous damping for steel concentrically braced frame structures," *Bulletin of Earthquake Engineering,* vol. 9, no. 5, pp. 1535-1558, 2011, doi: 10.1007/s10518-011-9272-4.

K. K. Wijesundara and P. Rajeev, "Direct displacement-based seismic design of steel concentric braced frame structures," *Australian Journal of Structural Engineering,* vol. 13, no. 3, pp. 243-257, 2012.

Z. Zhou, B. Ye, and Y. Chen, "Experimental investigation on monotonic performance of steel curved knee braces for weld-free beam-to-column connections," Proceedings of the *2017 World Congress on Advances in Structural Engineering and Mechanics (ASEM17)*, Ilsan, South Korea, 2017.

Z. Zhou, B. Ye, and Y. Chen, "Experimental investigation of curved steel knee braces with adjustable yield displacements," *Journal of Constructional Steel Research,* vol. 161, pp. 17-30, 2019, doi: https://doi.org/10.1016/j.jcsr.2019.06.011.

APPENDIX A: OPENSEES CODE SAMPLES

This appendix contains samples of the OpenSees codes used for the models of individual BIEs and complete FIEBs used throughout the thesis, for reference purposes only. The codes were written for use with OpenSees Version 2.5.0. Code is ready to copy and paste into a dedicated text editor such as Notepad++.

MONOTONIC LOADING OF ISOLATED BIE

```
#Monotonic Test of Square HSS Brace with Intentional Eccentricity -- Out-of-
Plane Bending Gusset Plate and Side-Plated Connection
#Units: kN;mm;s
model Basic Builder -ndm 2 -ndf 3
#
file mkdir "design properties";#directory where results are saved

#Global Geometry
set hf 4000.0;#storey height
set bf 6000.0;#bay width
set D [expr pow(pow($hf,2)+pow($bf,2),0.5)];#frame diagonal length
set L [expr $D*0.75];#Assumed hinge-to-hinge length of BIE, considering real
dimensions of beams and columns and connection from knife plate to frame
set imp 0.005; #Out of plane imperfection of brace, fraction of L

#BIE Geometry
set H 177.8; #Square HSS height
set t 12.7; #HSS wall thickness
set Lp 360.0; #Length of side-plate eccentering assembly
set ts 25.4; #Side-plate thickness
set bg 360.0; #Knife-plate width
set tg 38.1; #Knife-plate thickness
set Lg 77.0; #Knife-plate clearance length
set e 130.0; #eccentriciy
set Hs [expr $e+0.75*$H]; # side plates height

set name $H-$H-$t-$e-Tension


#Material Definition (toggle on option desired)
#1. If no residual stresses nor Fy gradation is considered
set Fy 0.345; # Yield stress for HSS
set Fyg 0.345; #Yield stress for plates
set E0 200;  # Elasticity Modulus
set b [expr (0.1*$Fy/0.04)/$E0]; # Strain Hardening ratio
set R0 20; # Parameter that controls transition form elastic to plastic
branches, recommended value between 10 and 20
set CR1 0.925; # Parameter that controls transition form elastic to plastic
branches, recommended value 0.925
```

```
set CR2 0.15; # Parameter that controls transition form elastic to plastic
branches, recommended value 0.15
uniaxialMaterial Steel02 1 $Fy $E0 $b $R0 $CR1 $CR2; #HSS section steel
uniaxialMaterial Steel02 2 $Fyg $E0 $b $R0 $CR1 $CR2; #Plates steel
#2. If residual stresses (through thickness) and Fy gradation are to be
considered according to Koval's model
# set E 200.0;#Young's modulus
# set Fy 0.291827; #Nominal yield stress of HSS; If set equal to 0.389103,
the equivalent resultant max stress is equal to 0.46; If set to 0.291827
resultant max stress is equal to 0.345
# set Ehb [expr (0.1*$Fy/0.04)/$E];#Brace sections strain-hardening ratio
# set Fyc [expr $Fy*1.6]; #Yield stress of HSS corners
# set Fyf [expr $Fy*1.2]; #Yield stress where flats meet corners
# set Rs 0.6; #Multiplier for through thickness residual stresses
# set Fyw 0.38;#Plates yield stress
# set Ehw [expr (0.1*$Fyw/0.04)/$E];#Plates strain-hardening slope
# set R0 30.0;# Parameter that controls transition form elastic to plastic
branches, recommended value between 10 and 20. Value of 30 for HSSs is used
as recommended by Prof. Tremblay.
# set CR1 0.925;# Parameter that controls transition form elastic to plastic
branches, recommended value 0.925
# set CR2 0.15;# Parameter that controls transition form elastic to plastic
branches, recommended value 0.15
# set a1 0.4;#isotropic hardening parameter, increase of compression yield
envelope as proportion of yield strength after a plastic strain of
$a2*($Fy/E0);
# set a2 22.0;#isotropic hardening parameter;
# set a3 0.4;#isotropic hardening parameter, increase of tension yield
envelope as proportion of yield strength after a plastic strain of
$a4*($Fy/E0);
# set a4 22.0;#isotropic hardening parameter;
# uniaxialMaterial Steel02 1 $Fy $E $Ehb $R0 $CR1 $CR2 $a1 $a2 $a3 $a4; #HSS
sections steel
# uniaxialMaterial Steel02 2 $Fyw $E $Ehw $R0 $CR1 $CR2 $a1 $a2 $a3 $a4;
#Plates steel


#Sections Definition

# Use if residual stress distribution is to be neglected
set ns 21; #number of fibers along flat edges of HSS
set nc 15; #number of fibers along round corners of HSS
set nt 21; #number of fibers across thickness of HSS
set ng 34; #number of fibers across thickness of plates
set nb 1; #number of fibers along plates width
set c [expr $H*0.5-$t*2]; # y and z absolute coordinates of center of round
coordinates

section fiberSec 1 {
patch circ 1 $nc $nt $c $c $t [expr 2*$t] 0.0 90.0
patch circ 1 $nc $nt -$c $c $t [expr 2*$t] 90.0 180.0
patch circ 1 $nc $nt -$c -$c $t [expr 2*$t] 180.0 270.0
patch circ 1 $nc $nt $c -$c $t [expr 2*$t] 270.0 360.0
patch quad 1 $nt $ns [expr $H/2-$t] [expr -$H/2+2*$t] [expr $H/2] [expr -
$H/2+2*$t] [expr $H/2] [expr +$H/2-2*$t] [expr $H/2-$t] [expr +$H/2-2*$t]
patch quad 1 $nt $ns -[expr $H/2] [expr -$H/2+2*$t] -[expr $H/2-$t] [expr -
$H/2+2*$t] -[expr $H/2-$t] [expr +$H/2-2*$t] -[expr $H/2] [expr +$H/2-2*$t]
```

```
patch quad 1 $ns $nt [expr -$H/2+2*$t] [expr $H/2-$t] [expr $H/2-2*$t] [expr
$H/2-$t] [expr $H/2-2*$t] [expr $H/2] [expr -$H/2+2*$t] [expr $H/2]
patch quad 1 $ns $nt [expr -$H/2+2*$t] -[expr $H/2] [expr $H/2-2*$t] -[expr
$H/2] [expr $H/2-2*$t] -[expr $H/2-$t] [expr -$H/2+2*$t] -[expr $H/2-$t]
}

#Use if residual stresses are to be considered

# set ns 21 ; #number of fibres along flats of HSS -- MAX=99
# set nc 15 ; #number of fibres along corners of HSS -- MAX=99
# set nt 21 ; #number of fibres accross thickness of HSS - Needs to be a
number divisible by 3 -- MAX=99

# for {set k 1} {$k<=1} {incr k} {
# set c [expr $H*0.5-$t*2]; # y and z absolute coordinates of center of round
coordinates
# #Creating materials loops for yield stress gradation and residual stress
(Ihor Koval's thesis--but corners corrected)
# #Flats
# for {set i 1} { $i <= $ns} { incr i} {
# for {set j 1} { $j <= [expr $nt/3]} { incr j} {
# puts $k
# puts $i
# puts $j
# puts [expr 10000*$k+($i-1)*100+$j]
# uniaxialMaterial Steel02 [expr 10000*$k+($i-1)*100+$j] [expr $Fy+($Fyf-
$Fy)/(int($ns-$ns*0.5))*int(abs($i-0.5-$ns*0.5))] $E $Ehb $R0 $CR1 $CR2 $a1
$a2 $a3 $a4 [expr -($Fy*$Rs)]
# #uniaxialMaterial Fatigue [expr 10000+($i-1)*100+$j] [expr ($i-1)*100+$j]
$E0 $m -1e16 1e16;
# }
# for {set j [expr $nt/3+1]} { $j <= [expr 2*$nt/3]} { incr j} {
# uniaxialMaterial Steel02 [expr 10000*$k+($i-1)*100+$j] [expr $Fy+($Fyf-
$Fy)/(int($ns-$ns*0.5))*int(abs($i-0.5-$ns*0.5))] $E $Ehb $R0 $CR1 $CR2 $a1
$a2 $a3 $a4 [expr -($Fy*$Rs)+2*($Fy*$Rs)/($nt/3)*($j-0.5-$nt/3)]
# #uniaxialMaterial Fatigue [expr 10000+($i-1)*100+$j] [expr ($i-1)*100+$j]
$E0 $m -1e16 1e16;
# }
# for {set j [expr 2*$nt/3+1]} { $j <= $nt} { incr j} {
# uniaxialMaterial Steel02 [expr 10000*$k+($i-1)*100+$j] [expr $Fy+($Fyf-
$Fy)/(int($ns-$ns*0.5))*int(abs($i-0.5-$ns*0.5))] $E $Ehb $R0 $CR1 $CR2 $a1
$a2 $a3 $a4 [expr $Fy*$Rs]
# #uniaxialMaterial Fatigue [expr 10000+($i-1)*100+$j] [expr ($i-1)*100+$j]
$E0 $m -1e16 1e16;
# }
# }
# #Corners
# for {set i 1} { $i <= [expr $nt/3]} { incr i} {
# uniaxialMaterial Steel02 [expr 10000*$k+($ns-1)*1000+$nt+$i] [expr $Fyc] $E
$Ehb $R0 $CR1 $CR2 $a1 $a2 $a3 $a4 [expr -($Fy*$Rs)*(pow(2*$t,2)-
pow($t,2))/$nt*1/(pow(($t+$i*1.0/$nt*$t),2)-pow(($t+($i-1)*1.0/$nt*$t),2))]
# #uniaxialMaterial Fatigue [expr 10000+($ns-1)*1000+$nt+$i] [expr ($ns-
1)*1000+$nt+$i] $E0 $m -1e16 1e16;
# }
# for {set i [expr $nt/3+1]} { $i <= [expr 2*$nt/3]} { incr i} {
# uniaxialMaterial Steel02 [expr 10000*$k+($ns-1)*1000+$nt+$i] [expr $Fyc] $E
$Ehb $R0 $CR1 $CR2 $a1 $a2 $a3 $a4 [expr (-($Fy*$Rs)+2*($Fy*$Rs)/($nt/3)*($i-
```

```
0.5-$nt/3))*(pow(2*$t,2)-pow($t,2))/$nt*1/(pow(($t+$i*1.0/$nt*$t),2)-
pow(($t+($i-1)*1.0/$nt*$t),2))]
# #uniaxialMaterial Fatigue [expr 10000+($ns-1)*1000+$nt+$i] [expr ($ns-
1)*1000+$nt+$i] $E0 $m -1e16 1e16;
# }
# for {set i [expr 2*$nt/3+1]} { $i <= $nt} { incr i} {
# uniaxialMaterial Steel02 [expr 10000*$k+($ns-1)*1000+$nt+$i] [expr $Fyc] $E
$Ehb $R0 $CR1 $CR2 $a1 $a2 $a3 $a4 [expr ($Fy*$Rs)*(pow(2*$t,2)-
pow($t,2))/$nt*1/(pow(($t+$i*1.0/$nt*$t),2)-pow(($t+($i-1)*1.0/$nt*$t),2))]
# #uniaxialMaterial Fatigue [expr 10000+($ns-1)*1000+$nt+$i] [expr ($ns-
1)*1000+$nt+$i] $E0 $m -1e16 1e16;
# }
# #Build the HSS
# section fiberSec $k {
# for {set j 1} { $j <= $nt} { incr j} {
# for {set i 1} { $i <= $ns} { incr i} {
# fiber [expr $H/2.0-$t+($j*1.0-0.5)*$t/$nt] [expr $H/2.0-2*$t-($i*1.0-
0.5)*($H-4*$t)/$ns] [expr ($H-4.0*$t)*$t/($ns*$nt)] [expr 10000*$k+($j-
1)*100+$i]
# fiber [expr -$H/2.0+2*$t+($i*1.0-0.5)*($H-4*$t)/$ns] [expr $H/2.0-
$t+($i*1.0-0.5)*$t/$nt] [expr ($H-4.0*$t)*$t/($ns*$nt)] [expr  10000*$k+($j-
1)*100+$i]
# fiber [expr -($H/2.0-$t+($j*1.0-0.5)*$t/$nt)] [expr -($H/2.0-2*$t-($i*1.0-
0.5)*($H-4*$t)/$ns)] [expr ($H-4.0*$t)*$t/($ns*$nt)] [expr  10000*$k+($j-
1)*100+$i]
# fiber [expr -(-$H/2.0+2*$t+($i*1.0-0.5)*($H-4*$t)/$ns)] [expr -($H/2.0-
$t+($i*1.0-0.5)*$t/$nt)] [expr ($H-4.0*$t)*$t/($ns*$nt)] [expr 10000*$k+($j-
1)*100+$i]
# #puts "[expr $H/2.0-$t+($j*1.0-0.5)*$t/$nt] [expr $H/2.0-2*$t-($i*1.0-
0.5)*($H-4*$t)/$ns] [expr -($H/2.0-$t+($j*1.0-0.5)*$t/$nt)] [expr -($H/2.0-
2*$t-($i*1.0-0.5)*($H-4*$t)/$ns)] [expr -$H/2.0+2*$t+($i*1.0-0.5)*($H-
4*$t)/$ns] [expr $H/2.0-$t+($i*1.0-0.5)*$t/$nt] [expr -(-$H/2.0+2*$t+($i*1.0-
0.5)*($H-4*$t)/$ns)] [expr -($H/2.0-$t+($i*1.0-0.5)*$t/$nt)]"
# }
# patch circ [expr 10000*$k+($ns-1)*1000+$nt+$j] $nc 1 [expr $H/2-2*$t] [expr
$H/2-2*$t] [expr $t+($j*1.0-1.0)*$t/$nt] [expr $t+($j*1.0)*$t/$nt] 0.0 90.0
# patch circ [expr 10000*$k+($ns-1)*1000+$nt+$j] $nc 1 [expr -($H/2-2*$t)]
[expr $H/2-2*$t] [expr $t+($j*1.0-1.0)*$t/$nt] [expr $t+($j*1.0)*$t/$nt] 90.0
180.0
# patch circ [expr 10000*$k+($ns-1)*1000+$nt+$j] $nc 1 [expr -($H/2-2*$t)]
[expr -($H/2-2*$t)] [expr $t+($j*1.0-1.0)*$t/$nt] [expr $t+($j*1.0)*$t/$nt]
180.0 270.0
# patch circ [expr 10000*$k+($ns-1)*1000+$nt+$j] $nc 1 [expr $H/2-2*$t] [expr
-($H/2-2*$t)] [expr $t+($j*1.0-1.0)*$t/$nt] [expr $t+($j*1.0)*$t/$nt] 270.0
360.0
# }
# }
# }
section fiberSec 2 {
patch rect 2 $ng $nb [expr -$tg/2] [expr -$bg/2] [expr $tg/2] [expr $bg/2]
}
section fiberSec 3 {
patch rect 2 $ng $nb [expr -$e-$tg/2] [expr -$bg/2] [expr -$e+$tg/2] [expr
$bg/2]
patch rect 2 $nb $ng [expr -$e+$tg/2] [expr -$H/2-$ts] [expr -$e+$tg/2+$Hs]
[expr -$H/2]
```

```
patch rect 2 $nb $ng [expr -$e+$tg/2] [expr $H/2] [expr -$e+$tg/2+$Hs] [expr
$H/2+$ts]
patch circ 2 $nc $nt $c $c $t [expr 2*$t] 0.0 90.0
patch circ 1 $nc $nt -$c $c $t [expr 2*$t] 90.0 180.0
patch circ 1 $nc $nt -$c -$c $t [expr 2*$t] 180.0 270.0
patch circ 1 $nc $nt $c -$c $t [expr 2*$t] 270.0 360.0
patch quad 1 $nt $ns [expr $H/2-$t] [expr -$H/2+2*$t] [expr $H/2] [expr -
$H/2+2*$t] [expr $H/2] [expr +$H/2-2*$t] [expr $H/2-$t] [expr +$H/2-2*$t]
patch quad 1 $nt $ns -[expr $H/2] [expr -$H/2+2*$t] -[expr $H/2-$t] [expr -
$H/2+2*$t] -[expr $H/2-$t] [expr +$H/2-2*$t] -[expr $H/2] [expr +$H/2-2*$t]
patch quad 1 $ns $nt [expr -$H/2+2*$t] [expr $H/2-$t] [expr $H/2-2*$t] [expr
$H/2-$t] [expr $H/2-2*$t] [expr $H/2] [expr -$H/2+2*$t] [expr $H/2]
patch quad 1 $ns $nt [expr -$H/2+2*$t] -[expr $H/2] [expr $H/2-2*$t] -[expr
$H/2] [expr $H/2-2*$t] -[expr $H/2-$t] [expr -$H/2+2*$t] -[expr $H/2-$t]
}

#Geometric Transformation
geomTransf Corotational 1
set pi 3.14159265359;
#Nodes and elements definition
set elb 20; #number of elements along brace, use even number
set elg 10; #number of elements along free gusset, use even number
set elp 2; #number of elements along plated connection, use even number
set ip 6; #number of integration points along elements

set Lb [expr $L-2*$Lp]

node 1 0 0
for {set i 1 } { $i <= [expr $elg] } {incr i } {
node [expr $i+1] [expr $i*$Lg/$elg] 0
}
node [expr $elg+2] [expr $Lg] $e
for {set i 1 } { $i <= [expr $elp] } {incr i } {
node [expr $elg+2+$i] [expr $i*$Lp/$elp+$Lg] $e
}
for {set i 1 } { $i <= [expr $elb] } {incr i } {
node [expr 2+$elg+$elp+$i] [expr $Lg+$Lp+$i*$Lb/$elb] [expr
$e+sin($pi*$i/$elb)*$imp*$Lb]
}
for {set i 1 } { $i <= [expr $elp] } {incr i } {
node [expr $elg+$elp+$elb+2+$i] [expr $i*$Lp/$elp+$Lg+$Lp+$Lb] $e
}
node [expr $elg+$elp+$elb+$elp+3] [expr $Lg+$Lp+$Lb+$Lp] 0
for {set i 1 } { $i <= [expr $elg] } {incr i } {
node [expr $elg+$elp+$elb+$elp+3+$i] [expr ($i)*$Lg/$elg+$Lg+$Lp+$Lb+$Lp] 0
}
fix 1 0 1 1; #moveable in x for applying displacement
fix [expr 2*($elp+$elg)+$elb+3] 1 1 1;#encastrement

for {set i 1 } { $i <= $elg} {incr i } {
element forceBeamColumn [expr $i] [expr $i] [expr $i+1] 1 Lobatto 2 $ip
}
rigidLink beam [expr $elg+1] [expr $elg+2]
for {set i 1 } { $i <= $elp } {incr i } {
element forceBeamColumn [expr $elg+$i] [expr $elg+1+$i] [expr $elg+2+$i] 1
Lobatto 3 $ip
}
```

```
for {set i 1 } { $i <= $elb } {incr i } {
element forceBeamColumn [expr $elg+$elp+$i] [expr $elg+$elp+1+$i] [expr
$elg+$elp+2+$i] 1 Lobatto 1 $ip
}
for {set i 1 } { $i <= $elp } {incr i } {
element forceBeamColumn [expr $elg+$elp+$elb+$i] [expr $elg+$elp+$elb+1+$i]
[expr $elg+$elp+$elb+2+$i] 1 Lobatto 3 $ip
}
rigidLink beam [expr $elg+$elp+$elb+$elp+2] [expr $elg+$elp+$elb+$elp+3]
for {set i 1 } { $i <= $elg } {incr i } {
element forceBeamColumn [expr $elg+$elp+$elb+$elp+$i] [expr
$elg+$elp+$elb+$elp+2+$i] [expr $elg+$elp+$elb+$elp+3+$i] 1 Lobatto 2 $ip
}
pattern Plain [expr 1] Linear {load 1 1.0 0.0 0.0}
#
#Recorders
#
#Global Response Recorder
recorder Node -file [format "design properties/$name-globaldisp.dat"] -node 1
-dof 1 disp
recorder Node -file [format "design properties/$name.dat"] -node [expr
$elg+$elp+$elb+$elp+$elg+3] -dof 1 reaction
system UmfPack
numberer RCM
constraints Transformation
test EnergyIncr 1.0e-8 30 0
algorithm Newton
analysis Static

#Loading Protocol - monotonic - can be modified for cyclic
set peaks [ list 0.0 -200]; #negative produces tension
for {set i 1 } { $i <= 1 } {incr i } {
set dU [expr ([lindex $peaks $i ]-[lindex $peaks [expr $i-1]])/200.0 ]
integrator DisplacementControl 1 1 $dU 1 $dU $dU
analyze 200
}
wipe
```

NLRHA OF 12-STOREY FIEB

```
# 2-D Multi-Storey Pseudo-Chevron Braced Frame with square BIE HSS Braces -
In-Plane Buckling - Non Linear Response History Analysis -
#Design following modified DDBD procedure. 10 % increase in accelerograms due
to accidental eccentricity
# |/|\|
# |/|\|
# |/|\|
# |/|\|
# |/|\|
# |/|\|
# |/|\|
# |/|\|
# |/|\|
# |/|\|
```

```
# Vancouver, BC  Site Class C - NBCC 2015
#
# Andrés González Ureña, DEC 2019 - REVISED JUL 2021
# units: kN,mm,s
# ------------------------------------------------
wipe
model Basic Builder -ndm 2 -ndf 3
source DisplayModel2D.tcl;#For animation during analysis (available online)

set pi 3.14159265
set g 9806.55
set ip 7;#number of integration points for forceBeamColumn elements
set record CC5; #Ground motion file, in format .tcl, must be saved in same
folder.
set duration 45.005; #Ground motion duration (s)
set step 0.005; #Ground motion data step (s)
set scale 1.0; #Scale Factor (1.0 if ground motion is already properly
scaled)
file mkdir $record-results;
# -------------------------
# General Frame Information
# -------------------------

set n 12;#number of storeys
set H(1) 4000.0;#First storey height
for {set i 2} {$i<=$n} {incr i} {
set H($i) 4000.0;#Typical storey height
}
set L 6000.0;#Bay width
set imp 0.001;#out-of-straightness of frame members, fraction of free length
set damping 0.03;#equivalent damping ratio
# -------------------------
# Masses and Gravity Loads
# -------------------------
set masses [list 1547.6563 1547.6563 1547.6563 1547.6563 1547.6563 1547.6563
1547.6563 1547.6563 1547.6563 1547.6563 1547.6563 1547.6563 679.85];#Storey Seismic
Masses (as weight in kN) from bottom to top storey
set columnloadsend [list 60.73 60.862 61.016 61.2 61.426 61.71 62.086 62.615
63.442 65.25 74.55 31.035 ];#Point loads on end columns in kN, from bottom to
top (tributary area is supposed equal on exterior and interior columns, loads
are such that combined with the beam loads and leaning frame loads produce
same amount as factored gravity load as considered in design)
set columnloadscenter [list -13.82 -13.688 -13.534 -13.35 -13.124 -12.840 -
12.464 -11.935 -11.108 -9.3 0.0 0.0 ];#Point loads on center columns in kN,
from bottom to top ()
set beamloads [list 0.02485 0.02485 0.02485 0.02485 0.02485 0.02485 0.02485
0.02485 0.02485 0.02485 0.02485 0.010345 ];#Distributed gravity loads on
beams in kN/mm, from bottom to top
set leaningframeloads [list 1425.73 1425.60 1425.45 1425.28 1425.06 1424.79
1424.42 1423.92 1423.12 1420.96 1412.86 655.67];#Point loads in kN to be
applied in leaning column for P-delta effects consideration
# -------------------------
# Braces Information
# -------------------------
#Storey 12 braces
set brace12 [list 152.40    12.70   4798.33 305.00  25.40   38.10   305.00
77.00   13360.00    42000000.00]
```

```
set B(12) [expr [lindex $brace12 0]];#width
set t(12) [expr [lindex $brace12 1]];#wall thickness
set e(12) 290.0;#eccentricity
set Lb(12) [expr [lindex $brace12 2]];#free length
set Lp(12) [expr [lindex $brace12 3]];#connection to gusset length (side
plates)
set Hs(12) [expr $e(12)+$B(12)/2+20];#side plates height
set ts(12) [expr [lindex $brace12 4]];#side plates thickness
set tg(12) [expr [lindex $brace12 5]];#gusset plate thickness
set bg(12) [expr [lindex $brace12 6]];#gusset width
set Lg(12) [expr [lindex $brace12 7]]; #Length of gusset plate clearing for
rotation
set Ai(12) [expr [lindex $brace12 8]]; #Cross-section area of knife-gusset-
angles assembly
set Ii(12) [expr [lindex $brace12 9]]; #Moment of Inertia of knife-gusset-
angles assembly
#Storey 11 braces
set brace11 [list 152.40    12.70   4798.33 305.00  25.40   38.10   305.00
77.00   13360.00    42000000.00]
set B(11) [expr [lindex $brace11 0]];#width
set t(11) [expr [lindex $brace11 1]];#wall thickness
set e(11) 260.0;#eccentricity
set Lb(11) [expr [lindex $brace11 2]];#free length
set Lp(11) [expr [lindex $brace11 3]];#connection to gusset length (side
plates)
set Hs(11) [expr $e(11)+$B(11)/2+20];#side plates height
set ts(11) [expr [lindex $brace11 4]];#side plates thickness
set tg(11) [expr [lindex $brace11 5]];#gusset plate thickness
set bg(11) [expr [lindex $brace11 6]];#gusset width
set Lg(11) [expr [lindex $brace11 7]]; #Length of gusset plate clearing for
rotation
set Ai(11) [expr [lindex $brace11 8]]; #Cross-section area of knife-gusset-
angles assembly
set Ii(11) [expr [lindex $brace11 9]]; #Moment of Inertia of knife-gusset-
angles assembly
#Storey 10 braces
set brace10 [list 177.80    15.88   4688.33 360.00  31.80   44.50   360.00
89.00   19280.00    81200000.00]
set B(10) [expr [lindex $brace10 0]];#width
set t(10) [expr [lindex $brace10 1]];#wall thickness
set e(10) 350.0;#eccentricity
set Lb(10) [expr [lindex $brace10 2]];#free length
set Lp(10) [expr [lindex $brace10 3]];#connection to gusset length (side
plates)
set Hs(10) [expr $e(10)+$B(10)/2+20];#side plates height
set ts(10) [expr [lindex $brace10 4]];#side plates thickness
set tg(10) [expr [lindex $brace10 5]];#gusset plate thickness
set bg(10) [expr [lindex $brace10 6]];#gusset width
set Lg(10) [expr [lindex $brace10 7]]; #Length of gusset plate clearing for
rotation
set Ai(10) [expr [lindex $brace10 8]]; #Cross-section area of knife-gusset-
angles assembly
set Ii(10) [expr [lindex $brace10 9]]; #Moment of Inertia of knife-gusset-
angles assembly
#Storey 9 braces
set brace9 [list 177.80 15.88   4688.33 360.00  31.80   44.50   360.00  89.00
19280.00    81200000.00]
```

```
set B(9) [expr [lindex $brace9 0]];#width
set t(9) [expr [lindex $brace9 1]];#wall thickness
set e(9) 310.0;#eccentricity
set Lb(9) [expr [lindex $brace9 2]];#free length
set Lp(9) [expr [lindex $brace9 3]];#connection to gusset length (side
plates)
set Hs(9) [expr $e(9)+$B(9)/2+20];#side plates height
set ts(9) [expr [lindex $brace9 4]];#side plates thickness
set tg(9) [expr [lindex $brace9 5]];#gusset plate thickness
set bg(9) [expr [lindex $brace9 6]];#gusset width
set Lg(9) [expr [lindex $brace9 7]]; #Length of gusset plate clearing for
rotation
set Ai(9) [expr [lindex $brace9 8]]; #Cross-section area of knife-gusset-
angles assembly
set Ii(9) [expr [lindex $brace9 9]]; #Moment of Inertia of knife-gusset-
angles assembly
#Storey 8 braces
set brace8 [list 177.80 15.88   4688.33 360.00  31.80   44.50   360.00  89.00
19280.00    81200000.00]
set B(8) [expr [lindex $brace8 0]];#width
set t(8) [expr [lindex $brace8 1]];#wall thickness
set e(8) 280.0;#eccentricity
set Lb(8) [expr [lindex $brace8 2]];#free length
set Lp(8) [expr [lindex $brace8 3]];#connection to gusset length (side
plates)
set Hs(8) [expr $e(8)+$B(8)/2+20];#side plates height
set ts(8) [expr [lindex $brace8 4]];#side plates thickness
set tg(8) [expr [lindex $brace8 5]];#gusset plate thickness
set bg(8) [expr [lindex $brace8 6]];#gusset width
set Lg(8) [expr [lindex $brace8 7]]; #Length of gusset plate clearing for
rotation
set Ai(8) [expr [lindex $brace8 8]]; #Cross-section area of knife-gusset-
angles assembly
set Ii(8) [expr [lindex $brace8 9]]; #Moment of Inertia of knife-gusset-
angles assembly
#Storey 7 braces
set brace7 [list 177.80 15.88   4688.33 360.00  31.80   44.50   360.00  89.00
19280.00    81200000.00]
set B(7) [expr [lindex $brace7 0]];#width
set t(7) [expr [lindex $brace7 1]];#wall thickness
set e(7) 250.0;#eccentricity
set Lb(7) [expr [lindex $brace7 2]];#free length
set Lp(7) [expr [lindex $brace7 3]];#connection to gusset length (side
plates)
set Hs(7) [expr $e(7)+$B(7)/2+20];#side plates height
set ts(7) [expr [lindex $brace7 4]];#side plates thickness
set tg(7) [expr [lindex $brace7 5]];#gusset plate thickness
set bg(7) [expr [lindex $brace7 6]];#gusset width
set Lg(7) [expr [lindex $brace7 7]]; #Length of gusset plate clearing for
rotation
set Ai(7) [expr [lindex $brace7 8]]; #Cross-section area of knife-gusset-
angles assembly
set Ii(7) [expr [lindex $brace7 9]]; #Moment of Inertia of knife-gusset-
angles assembly
#Storey 6 braces
set brace6 [list 177.80 15.88   4688.33 360.00  31.80   44.50   360.00  89.00
19280.00    81200000.00]
```

```
set B(6) [expr [lindex $brace6 0]];#width
set t(6) [expr [lindex $brace6 1]];#wall thickness
set e(6) 220.0;#eccentricity
set Lb(6) [expr [lindex $brace6 2]];#free length
set Lp(6) [expr [lindex $brace6 3]];#connection to gusset length (side
plates)
set Hs(6) [expr $e(6)+$B(6)/2+20];#side plates height
set ts(6) [expr [lindex $brace6 4]];#side plates thickness
set tg(6) [expr [lindex $brace6 5]];#gusset plate thickness
set bg(6) [expr [lindex $brace6 6]];#gusset width
set Lg(6) [expr [lindex $brace6 7]]; #Length of gusset plate clearing for
rotation
set Ai(6) [expr [lindex $brace6 8]]; #Cross-section area of knife-gusset-
angles assembly
set Ii(6) [expr [lindex $brace6 9]]; #Moment of Inertia of knife-gusset-
angles assembly
#Storey 5 braces
set brace5 [list 177.80 15.88   4688.33 360.00  31.80   44.50   360.00  89.00
19280.00    81200000.00]
set B(5) [expr [lindex $brace5 0]];#width
set t(5) [expr [lindex $brace5 1]];#wall thickness
set e(5) 200.0;#eccentricity
set Lb(5) [expr [lindex $brace5 2]];#free length
set Lp(5) [expr [lindex $brace5 3]];#connection to gusset length (side
plates)
set Hs(5) [expr $e(5)+$B(5)/2+20];#side plates height
set ts(5) [expr [lindex $brace5 4]];#side plates thickness
set tg(5) [expr [lindex $brace5 5]];#gusset plate thickness
set bg(5) [expr [lindex $brace5 6]];#gusset width
set Lg(5) [expr [lindex $brace5 7]]; #Length of gusset plate clearing for
rotation
set Ai(5) [expr [lindex $brace5 8]]; #Cross-section area of knife-gusset-
angles assembly
set Ii(5) [expr [lindex $brace5 9]]; #Moment of Inertia of knife-gusset-
angles assembly
#Storey 4 braces
set brace4 [list 177.80 15.88   4688.33 360.00  31.80   44.50   360.00  89.00
19280.00    81200000.00]
set B(4) [expr [lindex $brace4 0]];#width
set t(4) [expr [lindex $brace4 1]];#wall thickness
set e(4) 180.0;#eccentricity
set Lb(4) [expr [lindex $brace4 2]];#free length
set Lp(4) [expr [lindex $brace4 3]];#connection to gusset length (side
plates)
set Hs(4) [expr $e(4)+$B(4)/2+20];#side plates height
set ts(4) [expr [lindex $brace4 4]];#side plates thickness
set tg(4) [expr [lindex $brace4 5]];#gusset plate thickness
set bg(4) [expr [lindex $brace4 6]];#gusset width
set Lg(4) [expr [lindex $brace4 7]]; #Length of gusset plate clearing for
rotation
set Ai(4) [expr [lindex $brace4 8]]; #Cross-section area of knife-gusset-
angles assembly
set Ii(4) [expr [lindex $brace4 9]]; #Moment of Inertia of knife-gusset-
angles assembly
#Storey 3 braces
set brace3 [list 177.80 15.88   4688.33 360.00  31.80   44.50   360.00  89.00
19280.00    81200000.00]
```

```
set B(3) [expr [lindex $brace3 0]];#width
set t(3) [expr [lindex $brace3 1]];#wall thickness
set e(3) 170.0;#eccentricity
set Lb(3) [expr [lindex $brace3 2]];#free length
set Lp(3) [expr [lindex $brace3 3]];#connection to gusset length (side
plates)
set Hs(3) [expr $e(3)+$B(3)/2+20];#side plates height
set ts(3) [expr [lindex $brace3 4]];#side plates thickness
set tg(3) [expr [lindex $brace3 5]];#gusset plate thickness
set bg(3) [expr [lindex $brace3 6]];#gusset width
set Lg(3) [expr [lindex $brace3 7]]; #Length of gusset plate clearing for
rotation
set Ai(3) [expr [lindex $brace3 8]]; #Cross-section area of knife-gusset-
angles assembly
set Ii(3) [expr [lindex $brace3 9]]; #Moment of Inertia of knife-gusset-
angles assembly
#Storey 2 braces
set brace2 [list 177.80 15.88   4688.33 360.00  31.80   44.50   360.00  89.00
19280.00    81200000.00]
set B(2) [expr [lindex $brace2 0]];#width
set t(2) [expr [lindex $brace2 1]];#wall thickness
set e(2) 160.0;#eccentricity
set Lb(2) [expr [lindex $brace2 2]];#free length
set Lp(2) [expr [lindex $brace2 3]];#connection to gusset length (side
plates)
set Hs(2) [expr $e(2)+$B(2)/2+20];#side plates height
set ts(2) [expr [lindex $brace2 4]];#side plates thickness
set tg(2) [expr [lindex $brace2 5]];#gusset plate thickness
set bg(2) [expr [lindex $brace2 6]];#gusset width
set Lg(2) [expr [lindex $brace2 7]]; #Length of gusset plate clearing for
rotation
set Ai(2) [expr [lindex $brace2 8]]; #Cross-section area of knife-gusset-
angles assembly
set Ii(2) [expr [lindex $brace2 9]]; #Moment of Inertia of knife-gusset-
angles assembly
#Storey 1 braces
set brace1 [list 177.80 15.88   4688.33 360.00  31.80   44.50   360.00  89.00
19280.00    81200000.00]
set B(1) [expr [lindex $brace1 0]];#width
set t(1) [expr [lindex $brace1 1]];#wall thickness
set e(1) 160.0;#eccentricity
set Lb(1) [expr [lindex $brace1 2]];#free length
set Lp(1) [expr [lindex $brace1 3]];#connection to gusset length (side
plates)
set Hs(1) [expr $e(1)+$B(1)/2+20];#side plates height
set ts(1) [expr [lindex $brace1 4]];#side plates thickness
set tg(1) [expr [lindex $brace1 5]];#gusset plate thickness
set bg(1) [expr [lindex $brace1 6]];#gusset width
set Lg(1) [expr [lindex $brace1 7]]; #Length of gusset plate clearing for
rotation
set Ai(1) [expr [lindex $brace1 8]]; #Cross-section area of knife-gusset-
angles assembly
set Ii(1) [expr [lindex $brace1 9]]; #Moment of Inertia of knife-gusset-
angles assembly
# -------------------------
# Columns Information
# -------------------------
```

```
#Storey 12 External Columns
set welist12 [list 204.00   12.60   206.00  7.90]
set we(12) [expr [lindex $welist12 0]];#flange width
set fte(12) [expr [lindex $welist12 1]];#flange thickness
set de(12) [expr [lindex $welist12 2]];#outside height
set twe(12) [expr [lindex $welist12 3]];#web thickness
#Storey 12 Internal Column
set wilist12 [list 254.00   14.20   253.00  8.60]
set wi(12) [expr [lindex $wilist12 0]];#flange width
set fti(12) [expr [lindex $wilist12 1]];#flange thickness
set di(12) [expr [lindex $wilist12 2]];#outside height
set twi(12) [expr [lindex $wilist12 3]];#web thickness
#Storey 11 External Columns
set we(11) $we(12);#flange width
set fte(11) $fte(12);#flange thickness
set de(11) $de(12);#outside height
set twe(11) $twe(12);#web thickness
#Storey 11 Internal Column
set wi(11) $wi(12);#flange width
set fti(11) $fti(12);#flange thickness
set di(11) $di(12);#outside height
set twi(11) $twi(12);#web thickness
#Storey 10 External Columns
set we(10) $we(12);#flange width
set fte(10) $fte(12);#flange thickness
set de(10) $de(12);#outside height
set twe(10) $twe(12);#web thickness
#Storey 10 Internal Column
set wi(10) $wi(12);#flange width
set fti(10) $fti(12);#flange thickness
set di(10) $di(12);#outside height
set twi(10) $twi(12);#web thickness
#Storey 9 External Columns
set welist9 [list 257.00    19.60   264.00  11.90]
set we(9) [expr [lindex $welist9 0]];#flange width
set fte(9) [expr [lindex $welist9 1]];#flange thickness
set de(9) [expr [lindex $welist9 2]];#outside height
set twe(9) [expr [lindex $welist9 3]];#web thickness
#Storey 9 Internal Column
set wilist9 [list 371.00    21.80   364.00  13.30]
set wi(9) [expr [lindex $wilist9 0]];#flange width
set fti(9) [expr [lindex $wilist9 1]];#flange thickness
set di(9) [expr [lindex $wilist9 2]];#outside height
set twi(9) [expr [lindex $wilist9 3]];#web thickness
#Storey 8 External Columns
set we(8) $we(9);#flange width
set fte(8) $fte(9);#flange thickness
set de(8) $de(9);#outside height
set twe(8) $twe(9);#web thickness
#Storey 8 Internal Column
set wi(8) $wi(9);#flange width
set fti(8) $fti(9);#flange thickness
set di(8) $di(9);#outside height
set twi(8) $twi(9);#web thickness
#Storey 7 External Columns
set we(7) $we(9);#flange width
set fte(7) $fte(9);#flange thickness
```

```
set de(7) $de(9);#outside height
set twe(7) $twe(9);#web thickness
#Storey 7 Internal Column
set wi(7) $wi(9);#flange width
set fti(7) $fti(9);#flange thickness
set di(7) $di(9);#outside height
set twi(7) $twi(9);#web thickness
#Storey 6 External Columns
set welist6 [list 394.00    27.70   375.00  17.30]
set we(6) [expr [lindex $welist6 0]];#flange width
set fte(6) [expr [lindex $welist6 1]];#flange thickness
set de(6) [expr [lindex $welist6 2]];#outside height
set twe(6) [expr [lindex $welist6 3]];#web thickness
#Storey 6 Internal Column
set wilist6 [list 399.00    36.60   393.00  22.60]
set wi(6) [expr [lindex $wilist6 0]];#flange width
set fti(6) [expr [lindex $wilist6 1]];#flange thickness
set di(6) [expr [lindex $wilist6 2]];#outside height
set twi(6) [expr [lindex $wilist6 3]];#web thickness
#Storey 5 External Columns
set we(5) $we(6);#flange width
set fte(5) $fte(6);#flange thickness
set de(5) $de(6);#outside height
set twe(5) $twe(6);#web thickness
#Storey 5 Internal Column
set wi(5) $wi(6);#flange width
set fti(5) $fti(6);#flange thickness
set di(5) $di(6);#outside height
set twi(5) $twi(6);#web thickness
#Storey 4 External Columns
set we(4) $we(6);#flange width
set fte(4) $fte(6);#flange thickness
set de(4) $de(6);#outside height
set twe(4) $twe(6);#web thickness
#Storey 4 Internal Column
set wi(4) $wi(6);#flange width
set fti(4) $fti(6);#flange thickness
set di(4) $di(6);#outside height
set twi(4) $twi(6);#web thickness
#Storey 3 External Columns
set welist3 [list 302.00    63.50   555.00  35.60]
set we(3) [expr [lindex $welist3 0]];#flange width
set fte(3) [expr [lindex $welist3 1]];#flange thickness
set de(3) [expr [lindex $welist3 2]];#outside height
set twe(3) [expr [lindex $welist3 3]];#web thickness
#Storey 3 Internal Column
set wilist3 [list 416.00    62.70   446.00  39.10]
set wi(3) [expr [lindex $wilist3 0]];#flange width
set fti(3) [expr [lindex $wilist3 1]];#flange thickness
set di(3) [expr [lindex $wilist3 2]];#outside height
set twi(3) [expr [lindex $wilist3 3]];#web thickness
#Storey 2 External Columns
set we(2) $we(3);#flange width
set fte(2) $fte(3);#flange thickness
set de(2) $de(3);#outside height
set twe(2) $twe(3);#web thickness
#Storey 2 Internal Column
```

```
set wi(2) $wi(3);#flange width
set fti(2) $fti(3);#flange thickness
set di(2) $di(3);#outside height
set twi(2) $twi(3);#web thickness
#Storey 1 External Columns
set we(1) $we(3);#flange width
set fte(1) $fte(3);#flange thickness
set de(1) $de(3);#outside height
set twe(1) $twe(3);#web thickness
#Storey 1 Internal Column
set wi(1) $wi(3);#flange width
set fti(1) $fti(3);#flange thickness
set di(1) $di(3);#outside height
set twi(1) $twi(3);#web thickness
# -------------------------
# Beams Information
# -------------------------
#Storey 12 Beam
set beam12list [list 102.00 8.90    309.00  6.00]
set web(12) [expr [lindex $beam12list 0]];#flange width
set fteb(12) [expr [lindex $beam12list 1]];#flange thickness
set deb(12) [expr [lindex $beam12list 2]];#outside height
set tweb(12) [expr [lindex $beam12list 3]];#web thickness
#Storey 11 Beam
set beam11list [list 171.00 9.80    352.00  6.90]
set web(11) [expr [lindex $beam11list 0]];#flange width
set fteb(11) [expr [lindex $beam11list 1]];#flange thickness
set deb(11) [expr [lindex $beam11list 2]];#outside height
set tweb(11) [expr [lindex $beam11list 3]];#web thickness
#Storey 10 Beam
set beam10list [list 140.00 11.20   403.00  7.00]
set web(10) [expr [lindex $beam10list 0]];#flange width
set fteb(10) [expr [lindex $beam10list 1]];#flange thickness
set deb(10) [expr [lindex $beam10list 2]];#outside height
set tweb(10) [expr [lindex $beam10list 3]];#web thickness
#Storey 9 Beam
set beam9list [list 152.00  10.80   450.00  7.60]
set web(9) [expr [lindex $beam9list 0]];#flange width
set fteb(9) [expr [lindex $beam9list 1]];#flange thickness
set deb(9) [expr [lindex $beam9list 2]];#outside height
set tweb(9) [expr [lindex $beam9list 3]];#web thickness
#Storey 8 Beam
set beam8list [list 178.00  12.80   407.00  7.70]
set web(8) [expr [lindex $beam8list 0]];#flange width
set fteb(8) [expr [lindex $beam8list 1]];#flange thickness
set deb(8) [expr [lindex $beam8list 2]];#outside height
set tweb(8) [expr [lindex $beam8list 3]];#web thickness
#Storey 7 Beam
set beam7list [list 189.00  10.80   450.00  8.10]
set web(7) [expr [lindex $beam7list 0]];#flange width
set fteb(7) [expr [lindex $beam7list 1]];#flange thickness
set deb(7) [expr [lindex $beam7list 2]];#outside height
set tweb(7) [expr [lindex $beam7list 3]];#web thickness
#Storey 6 Beam
set beam6list [list 154.00  15.40   459.00  9.10]
set web(6) [expr [lindex $beam6list 0]];#flange width
set fteb(6) [expr [lindex $beam6list 1]];#flange thickness
```

```
set deb(6) [expr [lindex $beam6list 2]];#outside height
set tweb(6) [expr [lindex $beam6list 3]];#web thickness
#Storey 5 Beam
set beam5list [list 191.00  16.00   460.00  9.90]
set web(5) [expr [lindex $beam5list 0]];#flange width
set fteb(5) [expr [lindex $beam5list 1]];#flange thickness
set deb(5) [expr [lindex $beam5list 2]];#outside height
set tweb(5) [expr [lindex $beam5list 3]];#web thickness
#Storey 4 Beam
set beam4list [list 192.00  17.70   463.00  10.50]
set web(4) [expr [lindex $beam4list 0]];#flange width
set fteb(4) [expr [lindex $beam4list 1]];#flange thickness
set deb(4) [expr [lindex $beam4list 2]];#outside height
set tweb(4) [expr [lindex $beam4list 3]];#web thickness
#Storey 3 Beam
set beam3list [list 193.00  19.00   466.00  11.40]
set web(3) [expr [lindex $beam3list 0]];#flange width
set fteb(3) [expr [lindex $beam3list 1]];#flange thickness
set deb(3) [expr [lindex $beam3list 2]];#outside height
set tweb(3) [expr [lindex $beam3list 3]];#web thickness
#Storey 2 Beam
set beam2list [list 194.00  20.60   469.00  12.60]
set web(2) [expr [lindex $beam2list 0]];#flange width
set fteb(2) [expr [lindex $beam2list 1]];#flange thickness
set deb(2) [expr [lindex $beam2list 2]];#outside height
set tweb(2) [expr [lindex $beam2list 3]];#web thickness
#Storey 1 Beam
set beam1list [list 280.00  17.30   463.00  10.80]
set web(1) [expr [lindex $beam1list 0]];#flange width
set fteb(1) [expr [lindex $beam1list 1]];#flange thickness
set deb(1) [expr [lindex $beam1list 2]];#outside height
set tweb(1) [expr [lindex $beam1list 3]];#web thickness
# -------------------------
#Material Properties
# -------------------------

#USE LINES 434 and 449 IF RESIDUAL STRESSES AND VARIATION OF Fy in THE HSSs
ARE TO BE NEGLECTED; USE LINES 435 TO 437 AND 450 IF THOSE ARE TO BE
CONSIDERED

set E 200.0;#Young's modulus
set Fyb 0.46;#Brace sections yield stress
#set Fyb 0.389103; #Nominal yield stress of HSS; If set equal to 0.389103,
the equivalent resultant max stress is equal to 0.46
#set Fyc [expr $Fyb*1.6]; #Yield stress of HSS corners
#set Fyf [expr $Fyb*1.2]; #Yield stress where flats meet corners
set Rs 0.6; #Multiplier for through thickness residuall stresses
set Ehb [expr (0.1*$Fyb/0.04)/$E];#Brace sections strain-hardening ratio
set Fyw 0.38;#W shapes yield stress
set Ehw [expr (0.1*$Fyw/0.04)/$E];#W shapes strain-hardening slope
set R0 30.0;# Parameter that controls transition form elastic to plastic
branches, recommended value between 10 and 20. Value of 30 is used as
recommended by Prof. Tremblay for HSS
set CR1 0.925;# Parameter that controls transition form elastic to plastic
branches, recommended value 0.925
set CR2 0.15;# Parameter that controls transition form elastic to plastic
branches, recommended value 0.15
```

```
set a1 0.4;#isotropic hardening parameter, increase of compression yield
envelope as proportion of yield strength after a plastic strain of
$a2*($Fy/E0);
set a2 22.0;#isotropic hardening parameter;
set a3 0.4;#isotropic hardening parameter, increase of tension yield envelope
as proportion of yield strength after a plastic strain of $a4*($Fy/E0);
set a4 22.0;#isotropic hardening parameter;
uniaxialMaterial Steel02 1 $Fyb $E $Ehb $R0 $CR1 $CR2 $a1 $a2 $a3 $a4; #HSS
sections steel (no residual stresses)
#uniaxialMaterial Steel02 1 $Fyb $E $Ehb $R0 $CR1 $CR2 $a1 $a2 $a3 $a4; #HSS
sections steel (with residual stresses)
uniaxialMaterial Steel02 2 $Fyw $E $Ehw $R0 $CR1 $CR2 $a1 $a2 $a3 $a4; #W
shapes steel
#
#
#
# ------------------------------------------------------------------------
-------------------------------------------
#
#
# END OF DATA INPUT BY USER
#
#
# ------------------------------------------------------------------------
-------------------------------------------
#
# -------------------------
#Geometric Transformation
# -------------------------
geomTransf Corotational 1;#For braces, columns and leaning frame
geomTransf PDelta 2;#For beams, as corotational transformation is not
compatible with element loads
# -------------------------
#Section Definition
# -------------------------
# ----- Braces ------------

#USE LINES 475 to 490 IF RESIDUAL STRESSES AND AND VARIATION OF Fy in THE
HSSs ARE TO BE NEGLECTED; USE LINES 492 TO 536 IF THOSE ARE TO BE CONSIDERED

set ns 12; #number of fibers along flat edges of HSS
set nc 6; #number of fibers along round corners of HSS
set nt 1; #number of fibers across thickness of HSS
for {set i 1} {$i<=$n} {incr i} {
set c [expr $B($i)*0.5-$t($i)*2]; # y and z absolute coordinates of center of
round coordinates
section fiberSec $i {;#integer tags for brace section from 1 to $n
patch circ 1 $nc $nt $c $c $t($i) [expr 2*$t($i)] 0.0 90.0
patch circ 1 $nc $nt -$c $c $t($i) [expr 2*$t($i)] 90.0 180.0
patch circ 1 $nc $nt -$c -$c $t($i) [expr 2*$t($i)] 180.0 270.0
patch circ 1 $nc $nt $c -$c $t($i) [expr 2*$t($i)] 270.0 360.0
patch quad 1 $ns $nt [expr $B($i)/2-$t($i)] [expr -$B($i)/2+2*$t($i)] [expr
$B($i)/2] [expr -$B($i)/2+2*$t($i)] [expr $B($i)/2] [expr +$B($i)/2-2*$t($i)]
[expr $B($i)/2-$t($i)] [expr +$B($i)/2-2*$t($i)]
patch quad 1 $ns $nt -[expr $B($i)/2] [expr -$B($i)/2+2*$t($i)] -[expr
$B($i)/2-$t($i)] [expr -$B($i)/2+2*$t($i)] -[expr $B($i)/2-$t($i)] [expr
+$B($i)/2-2*$t($i)] -[expr $B($i)/2] [expr +$B($i)/2-2*$t($i)]
```

```
patch quad 1 $ns $nt [expr -$B($i)/2+2*$t($i)] [expr $B($i)/2-$t($i)] [expr
$B($i)/2-2*$t($i)] [expr $B($i)/2-$t($i)] [expr $B($i)/2-2*$t($i)] [expr
$B($i)/2] [expr -$B($i)/2+2*$t($i)] [expr $B($i)/2]
patch quad 1 $ns $nt [expr -$B($i)/2+2*$t($i)] -[expr $B($i)/2] [expr
$B($i)/2-2*$t($i)] -[expr $B($i)/2] [expr $B($i)/2-2*$t($i)] -[expr $B($i)/2-
$t($i)] [expr -$B($i)/2+2*$t($i)] -[expr $B($i)/2-$t($i)]
}
}

# set ns 21 ; #number of fibres along flats of HSS -- MAX=99
# set nc 15 ; #number of fibres along corners of HSS -- MAX=99
# set nt 21 ; #number of fibres accross thickness of HSS - Needs to be a
number divisible by 3 -- MAX=99

 # for {set k 1} {$k<=$n} {incr k} {
# set c [expr $B($k)*0.5-$t($k)*2]; # y and z absolute coordinates of center
of round coordinates
# #Creating materials loops for yield stress gradation and residual stress
(Ihor Koval's thesis--but corners corrected)
# #Flats
# for {set i 1} { $i <= $ns} { incr i} {
# for {set j 1} { $j <= [expr $nt/3]} { incr j} {
# uniaxialMaterial Steel02 [expr 10000*$k+($i-1)*100+$j] [expr $Fyb+($Fyf-
$Fyb)/(int($ns-$ns*0.5))*int(abs($i-0.5-$ns*0.5))] $E $Ehb $R0 $CR1 $CR2 $a1
$a2 $a3 $a4 [expr -($Fyb*$Rs)]
# }
# for {set j [expr $nt/3+1]} { $j <= [expr 2*$nt/3]} { incr j} {
# uniaxialMaterial Steel02 [expr 10000*$k+($i-1)*100+$j] [expr $Fyb+($Fyf-
$Fyb)/(int($ns-$ns*0.5))*int(abs($i-0.5-$ns*0.5))] $E $Ehb $R0 $CR1 $CR2 $a1
$a2 $a3 $a4 [expr -($Fyb*$Rs)+2*($Fyb*$Rs)/($nt/3)*($j-0.5-$nt/3)]
# }
# for {set j [expr 2*$nt/3+1]} { $j <= $nt} { incr j} {
# uniaxialMaterial Steel02 [expr 10000*$k+($i-1)*100+$j] [expr $Fyb+($Fyf-
$Fyb)/(int($ns-$ns*0.5))*int(abs($i-0.5-$ns*0.5))] $E $Ehb $R0 $CR1 $CR2 $a1
$a2 $a3 $a4 [expr $Fyb*$Rs]
# }
# }
# #Corners
# for {set i 1} { $i <= [expr $nt/3]} { incr i} {
# uniaxialMaterial Steel02 [expr 10000*$k+($ns-1)*1000+$nt+$i] [expr $Fyc] $E
$Ehb $R0 $CR1 $CR2 $a1 $a2 $a3 $a4 [expr -($Fyb*$Rs)*(pow(2*$t($k),2)-
pow($t($k),2))/$nt*1/(pow(($t($k)+$i*1.0/$nt*$t($k)),2)-pow(($t($k)+($i-
1)*1.0/$nt*$t($k)),2))]
# }
# for {set i [expr $nt/3+1]} { $i <= [expr 2*$nt/3]} { incr i} {
# uniaxialMaterial Steel02 [expr 10000*$k+($ns-1)*1000+$nt+$i] [expr $Fyc] $E
$Ehb $R0 $CR1 $CR2 $a1 $a2 $a3 $a4 [expr (-
($Fyb*$Rs)+2*($Fyb*$Rs)/($nt/3)*($i-0.5-$nt/3))*(pow(2*$t($k),2)-
pow($t($k),2))/$nt*1/(pow(($t($k)+$i*1.0/$nt*$t($k)),2)-pow(($t($k)+($i-
1)*1.0/$nt*$t($k)),2))]
# }
# for {set i [expr 2*$nt/3+1]} { $i <= $nt} { incr i} {
# uniaxialMaterial Steel02 [expr 10000*$k+($ns-1)*1000+$nt+$i] [expr $Fyc] $E
$Ehb $R0 $CR1 $CR2 $a1 $a2 $a3 $a4 [expr ($Fyb*$Rs)*(pow(2*$t($k),2)-
pow($t($k),2))/$nt*1/(pow(($t($k)+$i*1.0/$nt*$t($k)),2)-pow(($t($k)+($i-
1)*1.0/$nt*$t($k)),2))]
# }
```

```
# #Build the HSS
# section fiberSec $k {
# for {set j 1} { $j <= $nt} { incr j} {
# for {set i 1} { $i <= $ns} { incr i} {
# fiber [expr $B($k)/2.0-$t($k)+($j*1.0-0.5)*$t($k)/$nt] [expr $B($k)/2.0-
2*$t($k)-($i*1.0-0.5)*($B($k)-4*$t($k))/$ns] [expr ($B($k)-
4.0*$t($k))*$t($k)/($ns*$nt)] [expr 10000*$k+($j-1)*100+$i]
# fiber [expr -$B($k)/2.0+2*$t($k)+($i*1.0-0.5)*($B($k)-4*$t($k))/$ns] [expr
$B($k)/2.0-$t($k)+($i*1.0-0.5)*$t($k)/$nt] [expr ($B($k)-
4.0*$t($k))*$t($k)/($ns*$nt)] [expr  10000*$k+($j-1)*100+$i]
# fiber [expr -($B($k)/2.0-$t($k)+($j*1.0-0.5)*$t($k)/$nt)] [expr -
($B($k)/2.0-2*$t($k)-($i*1.0-0.5)*($B($k)-4*$t($k))/$ns)] [expr ($B($k)-
4.0*$t($k))*$t($k)/($ns*$nt)] [expr  10000*$k+($j-1)*100+$i]
# fiber [expr -(-$B($k)/2.0+2*$t($k)+($i*1.0-0.5)*($B($k)-4*$t($k))/$ns)]
[expr -($B($k)/2.0-$t($k)+($i*1.0-0.5)*$t($k)/$nt)] [expr ($B($k)-
4.0*$t($k))*$t($k)/($ns*$nt)] [expr 10000*$k+($j-1)*100+$i]
# }
# patch circ [expr 10000*$k+($ns-1)*1000+$nt+$j] $nc 1 [expr $B($k)/2-
2*$t($k)] [expr $B($k)/2-2*$t($k)] [expr $t($k)+($j*1.0-1.0)*$t($k)/$nt]
[expr $t($k)+($j*1.0)*$t($k)/$nt] 0.0 90.0
# patch circ [expr 10000*$k+($ns-1)*1000+$nt+$j] $nc 1 [expr -($B($k)/2-
2*$t($k))] [expr $B($k)/2-2*$t($k)] [expr $t($k)+($j*1.0-1.0)*$t($k)/$nt]
[expr $t($k)+($j*1.0)*$t($k)/$nt] 90.0 180.0
# patch circ [expr 10000*$k+($ns-1)*1000+$nt+$j] $nc 1 [expr -($B($k)/2-
2*$t($k))] [expr -($B($k)/2-2*$t($k))] [expr $t($k)+($j*1.0-1.0)*$t($k)/$nt]
[expr $t($k)+($j*1.0)*$t($k)/$nt] 180.0 270.0
# patch circ [expr 10000*$k+($ns-1)*1000+$nt+$j] $nc 1 [expr $B($k)/2-
2*$t($k)] [expr -($B($k)/2-2*$t($k))] [expr $t($k)+($j*1.0-1.0)*$t($k)/$nt]
[expr $t($k)+($j*1.0)*$t($k)/$nt] 270.0 360.0
# }
# }
# }
```

```
# ----- Brace Side plates connection------------
set ng 20; #number of fibers across thickness of plates
set nb 1; #number of fibers along plates width
for {set i 1} {$i<=$n} {incr i} {
section fiberSec [expr 20+$i] {
patch rect 2 $ng $nb [expr -$tg($i)/2] [expr -$bg($i)/2] [expr $tg($i)/2]
[expr $bg($i)/2]
}
section fiberSec [expr 40+$i] {
patch rect 2 $ng $nb [expr -$tg($i)/2] [expr -$bg($i)/2] [expr $tg($i)/2]
[expr $bg($i)/2]
patch circ 1 $nc $nt $c $c $t($i) [expr 2*$t($i)] 0.0 90.0
patch circ 1 $nc $nt -$c $c $t($i) [expr 2*$t($i)] 90.0 180.0
patch circ 1 $nc $nt -$c -$c $t($i) [expr 2*$t($i)] 180.0 270.0
patch circ 1 $nc $nt $c -$c $t($i) [expr 2*$t($i)] 270.0 360.0
patch quad 1 $ns $nt [expr $B($i)/2-$t($i)] [expr -$B($i)/2+2*$t($i)] [expr
$B($i)/2] [expr -$B($i)/2+2*$t($i)] [expr $B($i)/2] [expr +$B($i)/2-2*$t($i)]
[expr $B($i)/2-$t($i)] [expr +$B($i)/2-2*$t($i)]
patch quad 1 $ns $nt -[expr $B($i)/2] [expr -$B($i)/2+2*$t($i)] -[expr
$B($i)/2-$t($i)] [expr -$B($i)/2+2*$t($i)] -[expr $B($i)/2-$t($i)] [expr
+$B($i)/2-2*$t($i)] -[expr $B($i)/2] [expr +$B($i)/2-2*$t($i)]
```

```
patch quad 1 $ns $nt [expr -$B($i)/2+2*$t($i)] [expr $B($i)/2-$t($i)] [expr
$B($i)/2-2*$t($i)] [expr $B($i)/2-$t($i)] [expr $B($i)/2-2*$t($i)] [expr
$B($i)/2] [expr -$B($i)/2+2*$t($i)] [expr $B($i)/2]
patch quad 1 $ns $nt [expr -$B($i)/2+2*$t($i)] -[expr $B($i)/2] [expr
$B($i)/2-2*$t($i)] -[expr $B($i)/2] [expr $B($i)/2-2*$t($i)] -[expr $B($i)/2-
$t($i)] [expr -$B($i)/2+2*$t($i)] -[expr $B($i)/2-$t($i)]
}

}
# -------------------------
# ----- Columns and Beams -
set nf 20;#number of fibers along flange width (for bending about weak axis)
set nw 20;#number of fibers along web height (for bending about strong axis)
set nt 20;#number of fibers across flange or web thickness (for bending about
strong axis)
for {set i 1} {$i<=$n} {incr i} {

section fiberSec [expr 100+$i] {;#integer tags for external columns section
from 101 to (100+$n)
patch rect 2 $nt 1 [expr -$we($i)/2] [expr $de($i)/2-$fte($i)] [expr
$we($i)/2] [expr $de($i)/2]
patch rect 2 $nt 1 [expr -$we($i)/2] [expr -$de($i)/2] [expr $we($i)/2] [expr
-$de($i)/2+$fte($i)]
patch rect 2 $nw 1 [expr -$twe($i)/2] [expr -$de($i)/2+$fte($i)] [expr
$twe($i)/2] [expr $de($i)/2-$fte($i)]
}
section fiberSec [expr 200+$i] {;#integer tags for internal columns section
from 201 to (200+$n)
patch rect 2 $nt 1 [expr -$wi($i)/2] [expr $di($i)/2-$fti($i)] [expr
$wi($i)/2] [expr $di($i)/2]
patch rect 2 $nt 1 [expr -$wi($i)/2] [expr -$di($i)/2] [expr $wi($i)/2] [expr
-$di($i)/2+$fti($i)]
patch rect 2 $nw 1 [expr -$twi($i)/2] [expr -$di($i)/2+$fti($i)] [expr
$twi($i)/2] [expr $di($i)/2-$fti($i)]
}
section fiberSec [expr 300+$i] {;#integer tags for beams sections from 301 to
(300+$n)
patch rect 2 $nt 1 [expr $deb($i)/2-$fteb($i)] [expr -$web($i)/2] [expr
$deb($i)/2] [expr $web($i)/2]
patch rect 2 $nt 1 [expr -$deb($i)/2] [expr -$web($i)/2] [expr -
$deb($i)/2+$fteb($i)] [expr $web($i)/2]
patch rect 2 $nw 1 [expr -$deb($i)/2+$fteb($i)] [expr -$tweb($i)/2] [expr
$deb($i)/2-$fteb($i)] [expr $tweb($i)/2]
}
}
# -------------------------
#Node Definition
# -------------------------
#Note that nodes at the ends of columns/beams/braces are duplicated,
continuity must be enforced by use of constraints
# -----Nodes for Columns and Beams---
set noc 8;#number of column/beam elements
for {set i 1} {$i<=$n} {incr i} {
for {set j 1} {$j<=[expr $noc+1]} {incr j} {
node [expr 2000+$i*100+$j] [expr 0+$imp*sin(($i-1)*$pi-$pi*($j-
1)/$noc)*$H($n)] [expr ($j-1)*$H($i)/$noc+$i*($H($i))-$H(1)];#Left Columns
```

```
node [expr 4000+$i*100+$j] [expr $L+$imp*sin(($i-1)*$pi-$pi*($j-
1)/$noc)*$H($n)] [expr ($j-1)*$H($i)/$noc+$i*($H($i))-$H(1)];#Center Columns
node [expr 6000+$i*100+$j] [expr 2*$L+$imp*sin(($i-1)*$pi-$pi*($j-
1)/$noc)*$H($n)] [expr ($j-1)*$H($i)/$noc+$i*($H($i))-$H(1)];#Right Columns
node [expr 10000+$i*100+$j] [expr ($j-1)*$L/$noc] [expr $i*($H($i))-
sin($pi*($j-1)/$noc)*$L*$imp];#Left Bay Beams
node [expr 20000+$i*100+$j] [expr ($j-1)*$L/$noc+$L] [expr $i*($H($i))-
sin($pi*($j-1)/$noc)*$L*$imp];#Right Bay Beams
}
}
# -----Nodes for Braces---
set nob 8;#number of brace elements
for {set i 1} {$i<=$n} {incr i} {
set ang [expr atan2($H($i),$L)]
set offset [expr (sqrt($H($i)*$H($i)+$L*$L)-
($Lb($i)+2*$Lp($i)+2*$Lg($i)))/2];#"offset" accounts for actual distance
between column/beam node to brace hinge (gusset), it is idealised as
perfectly rigid
# Left Bay
node [expr $i*200000+1] [expr $offset*cos($ang)] [expr
$offset*sin($ang)+$i*($H($i))-$H(1)]
node [expr $i*200000+2] [expr ($offset+$Lg($i))*cos($ang)] [expr
($offset+$Lg($i))*sin($ang)+$i*($H($i))-$H(1)]
node [expr $i*200000+3] [expr ($offset+$Lg($i)+$Lp($i))*cos($ang)] [expr
($offset+$Lg($i)+$Lp($i))*sin($ang)+$i*($H($i))-$H(1)]
node [expr $i*200000+4] [expr ($offset+$Lg($i)+$Lp($i))*cos($ang)-
$e($i)*sin($ang)] [expr
($offset+$Lg($i)+$Lp($i))*sin($ang)+$e($i)*cos($ang)+$i*($H($i))-$H(1)]
for {set j 1} {$j<=$nob} {incr j} {
node [expr $i*200000+4+$j] [expr
($offset+$Lg($i)+$Lp($i)+$j*$Lb($i)/$nob)*cos($ang)-
($e($i)+$imp*sin($pi*$j/$nob)*$Lb($i))*sin($ang)] [expr
($offset+$Lg($i)+$Lp($i)+$j*$Lb($i)/$nob)*sin($ang)+($e($i)+$imp*sin($pi*$j/$
nob)*$Lb($i))*cos($ang)+$i*($H($i))-$H(1)]
}
node [expr $i*200000+4+$nob+1] [expr
($offset+$Lg($i)+$Lp($i)+$Lb($i))*cos($ang)] [expr
($offset+$Lg($i)+$Lp($i)+$Lb($i))*sin($ang)+$i*($H($i))-$H(1)]
node [expr $i*200000+4+$nob+2] [expr
($offset+$Lg($i)+2*$Lp($i)+$Lb($i))*cos($ang)] [expr
($offset+$Lg($i)+2*$Lp($i)+$Lb($i))*sin($ang)+$i*($H($i))-$H(1)]
node [expr $i*200000+4+$nob+3] [expr
($offset+2*$Lg($i)+2*$Lp($i)+$Lb($i))*cos($ang)] [expr
($offset+2*$Lg($i)+2*$Lp($i)+$Lb($i))*sin($ang)+$i*($H($i))-$H(1)]
# Right Bay
node [expr $i*405000+1] [expr $L+$offset*cos($ang)] [expr -
$offset*sin($ang)+$i*($H($i))]
node [expr $i*405000+2] [expr $L+($offset+$Lg($i))*cos($ang)] [expr -
($offset+$Lg($i))*sin($ang)+$i*($H($i))]
node [expr $i*405000+3] [expr $L+($offset+$Lg($i)+$Lp($i))*cos($ang)] [expr -
($offset+$Lg($i)+$Lp($i))*sin($ang)+$i*($H($i))]
node [expr $i*405000+4] [expr
$L+($offset+$Lg($i)+$Lp($i))*cos($ang)+$e($i)*sin($ang)] [expr -
($offset+$Lg($i)+$Lp($i))*sin($ang)+$e($i)*cos($ang)+$i*($H($i))]
for {set j 1} {$j<=$nob} {incr j} {
node [expr $i*405000+4+$j] [expr
$L+($offset+$Lg($i)+$Lp($i)+$j*$Lb($i)/$nob)*cos($ang)+($e($i)+$imp*sin($pi*$
```

```
j/$nob)*$Lb($i))*sin($ang)] [expr -
($offset+$Lg($i)+$Lp($i)+$j*$Lb($i)/$nob)*sin($ang)+($e($i)+$imp*sin($pi*$j/$
nob)*$Lb($i))*cos($ang)+$i*($H($i))]
}
node [expr $i*405000+4+$nob+1] [expr
$L+($offset+$Lg($i)+$Lp($i)+$Lb($i))*cos($ang)] [expr -
($offset+$Lg($i)+$Lp($i)+$Lb($i))*sin($ang)+$i*($H($i))]
node [expr $i*405000+4+$nob+2] [expr
$L+($offset+$Lg($i)+2*$Lp($i)+$Lb($i))*cos($ang)] [expr -
($offset+$Lg($i)+2*$Lp($i)+$Lb($i))*sin($ang)+$i*($H($i))]
node [expr $i*405000+4+$nob+3] [expr
$L+($offset+2*$Lg($i)+2*$Lp($i)+$Lb($i))*cos($ang)] [expr -
($offset+2*$Lg($i)+2*$Lp($i)+$Lb($i))*sin($ang)+$i*($H($i))]
}
# -----Nodes for Leaning Frame---
node 1 [expr 3*$L] 0
for {set i 1} {$i<=[expr $n]} {incr i} {
node [expr $i+1] [expr 3*$L] [expr ($i)*$H($i)]
}
# -------------------------
#Element Definition
# -------------------------
# -----Column Elements-----
for {set i 1} {$i<=$n} {incr i} {
for {set j 1} {$j<=$noc} {incr j} {
element forceBeamColumn [expr 2000+$i*100+$j] [expr 2000+$i*100+$j] [expr
2000+$i*100+$j+1] 1 Lobatto [expr 100+$i] $ip
element forceBeamColumn [expr 4000+$i*100+$j] [expr 4000+$i*100+$j] [expr
4000+$i*100+$j+1] 1 Lobatto [expr 200+$i] $ip
element forceBeamColumn [expr 6000+$i*100+$j] [expr 6000+$i*100+$j] [expr
6000+$i*100+$j+1] 1 Lobatto [expr 100+$i] $ip
}
}
# -----Beam Elements-----
for {set i 1} {$i<=$n} {incr i} {
for {set j 1} {$j<=$noc} {incr j} {
element forceBeamColumn [expr 10000+$i*100+$j] [expr 10000+$i*100+$j] [expr
10000+$i*100+$j+1] 1 Lobatto [expr 300+$i] $ip
element forceBeamColumn [expr 20000+$i*100+$j] [expr 20000+$i*100+$j] [expr
20000+$i*100+$j+1] 1 Lobatto [expr 300+$i] $ip
}
}
# -----Brace Elements-----
for {set i 1} {$i<=$n} {incr i} {
element elasticBeamColumn [expr $i*10+3] [expr 2000+$i*100+1] [expr
$i*200000+1] $Ai($i) $E $Ii($i) 1
element forceBeamColumn [expr $i*10+4] [expr $i*200000+1] [expr $i*200000+2]
1 Lobatto [expr 20+$i] $ip
element forceBeamColumn [expr $i*10+5] [expr $i*200000+2] [expr $i*200000+3]
1 Lobatto [expr 40+$i] $ip
element elasticBeamColumn [expr $i*10+6] [expr $i*200000+3] [expr
$i*200000+4] [expr 2*$Lp($i)*$ts($i)] $E [expr
2*($Lp($i)*$Lp($i)*$Lp($i)*$ts($i)/12)] 1
element elasticBeamColumn [expr $i*10+7] [expr 4000+$i*100+1+$noc] [expr
$i*405000+1] $Ai($i) $E $Ii($i) 1
element forceBeamColumn [expr $i*10+8] [expr $i*405000+1] [expr $i*405000+2]
1 Lobatto [expr 20+$i] $ip
```

```
element forceBeamColumn [expr $i*10+9] [expr $i*405000+2] [expr $i*405000+3]
1 Lobatto [expr 40+$i] $ip
element elasticBeamColumn [expr $i*10+10] [expr $i*405000+3] [expr
$i*405000+4] [expr 2*$Lp($i)*$ts($i)] $E [expr
2*($Lp($i)*$Lp($i)*$Lp($i)*$ts($i)/12)] 1
for {set j 1} {$j<=$nob} {incr j} {
element forceBeamColumn [expr $i*200000+$j] [expr $i*200000+4+$j-1] [expr
$i*200000+4+$j] 1 Lobatto [expr $i] $ip
element forceBeamColumn [expr $i*405000+$j] [expr $i*405000+4+$j-1] [expr
$i*405000+4+$j] 1 Lobatto [expr $i] $ip
}
element elasticBeamColumn [expr ($i+12)*10+3] [expr $i*200000+4+$nob] [expr
$i*200000+4+$nob+1] [expr 2*$Lp($i)*$ts($i)] $E [expr
2*($Lp($i)*$Lp($i)*$Lp($i)*$ts($i)/12)] 1
element forceBeamColumn [expr ($i+12)*20+4] [expr $i*200000+4+$nob+1] [expr
$i*200000+4+$nob+2] 1 Lobatto [expr 40+$i] $ip
element forceBeamColumn [expr ($i+12)*30+5] [expr $i*200000+4+$nob+2] [expr
$i*200000+4+$nob+3] 1 Lobatto [expr 20+$i] $ip
element elasticBeamColumn [expr ($i+12)*40+6] [expr $i*200000+4+$nob+3] [expr
4000+$i*100+$noc+1] $Ai($i) $E $Ii($i) 1
element elasticBeamColumn [expr ($i+12)*50+7] [expr $i*405000+4+$nob] [expr
$i*405000+4+$nob+1] [expr 2*$Lp($i)*$ts($i)] $E [expr
2*($Lp($i)*$Lp($i)*$Lp($i)*$ts($i)/12)] 1
element forceBeamColumn [expr ($i+12)*60+8] [expr $i*405000+4+$nob+1] [expr
$i*405000+4+$nob+2] 1 Lobatto [expr 40+$i] $ip
element forceBeamColumn [expr ($i+12)*70+9] [expr $i*405000+4+$nob+2] [expr
$i*405000+4+$nob+3] 1 Lobatto [expr 20+$i] $ip
element elasticBeamColumn [expr ($i+12)*80+10] [expr $i*405000+4+$nob+3]
[expr 6000+$i*100+1] $Ai($i) $E $Ii($i) 1
}
# -----Leaning Frames-----
for {set i 1} {$i<=[expr $n]} {incr i} {
element elasticBeamColumn $i [expr $i] [expr $i+1] 59213412.19 200 [expr
0.0001*18115147.65] 2;# area is 10000 times area of bottom brace, I is 0.0001
times I of bottom frame
element truss [expr 1000*$i-1] [expr 6000+$i*100+1+$noc] [expr $i+1]
59213412.19 1
}
# -------------------------
#Constraints and supports
# -------------------------
# -----Ground supports
fix 1 1 1 0
for {set i 1} {$i<=3} {incr i} {
fix [expr $i*2000+101] 1 1 0
}
# -----Inter-Storey Column Continuity (full restraint)
for {set i 1} {$i<=($n-1)} {incr i} {
for {set j 1} {$j<=3} {incr j} {
equalDOF [expr $j*2000+$i*100+$noc+1] [expr $j*2000+($i+1)*100+1] 1 2 3
}
}
# -----Beam-Column Continuity (shear connection)
for {set i 1} {$i<=$n} {incr i} {
equalDOF [expr 2000+$i*100+$noc+1] [expr 10000+$i*100+1] 1 2 3;#left colum-
left beam
```

```
equalDOF [expr 4000+$i*100+$noc+1] [expr 10000+$i*100+$noc+1] 1 2 3;#Center
colum-left beam
equalDOF [expr 4000+$i*100+$noc+1] [expr 20000+$i*100+1] 1 2 3;#Center colum-
right beam
equalDOF [expr 6000+$i*100+$noc+1] [expr 20000+$i*100+$noc+1] 1 2 3;#Right
colum-right beam
}

# -----Floor Diaphragms
for {set i 1} {$i<=$n} {incr i} {
equalDOF [expr 4000+$i*100+$noc+1] [expr 2000+$i*100+$noc+1] 1
equalDOF [expr 4000+$i*100+$noc+1] [expr 6000+$i*100+$noc+1] 1
}
# -------------------------
#Apply masses
# -------------------------
for {set i 1} {$i<=$n} {incr i} {
mass [expr 4000+$i*100+$noc+1] [expr [lindex $masses [expr $i-1]]/$g] 0. 0.
}
# -------------------------
#Calculate Periods
# -------------------------
constraints Plain
system UmfPack
set omega1 [expr pow( [lindex [eigen 2] 0], 0.5)]; # frequency 1
set omega2 [expr pow( [lindex [eigen 2] 1], 0.5)]; # frequency 2

set T1 [expr 2 * 3.1416 / $omega1]
set T2 [expr 2 * 3.1416 / $omega2]

puts " Period = $T1 s (mode 1)"
puts " Period = $T2 s (mode 2)"

# -------------------------
#Rayleigh Damping
# -------------------------
rayleigh [expr $damping*2*$omega1*$omega2/($omega1+$omega2)] 0.0 [expr
$damping*2/($omega1+$omega2)] 0.0; # In models with distributed plasticity,
response is not affected due to spurious damping forces related to Rayleigh
Damping (Chopra & McKenna, 2015)
# -------------------------
#Apply gravitational loads
# -------------------------
pattern Plain 1 Linear {
for {set i 1} {$i<=$n} {incr i} {
# -----Point loads on SFRS
load [expr 2000+$i*100+$noc+1] 0 -[expr [lindex $columnloadsend [expr $i-1]]]
0
load [expr 4000+$i*100+$noc+1] 0 [expr [lindex $columnloadscenter [expr $i-
1]]*-1.0] 0
load [expr 6000+$i*100+$noc+1] 0 -[expr [lindex $columnloadsend [expr $i-1]]]
0

# -----Point loads on leaning columns
load [expr $i+1] 0 -[expr [lindex $leaningframeloads [expr $i-1]]] 0
# -----Element loads on beams
for {set k 1} {$k<=$noc} {incr k} {
```

```
eleLoad -ele [expr 10000+$i*100+$k] [expr 20000+$i*100+$k] -type -beamUniform
-[expr [lindex $beamloads [expr $i-1]]]
}
}
}
recorder display "try" 10 10 500 500 -file -wipe
prp 6000 10000 1
vup 0 1 0
vpn 0 0 1
display 1 1 1
test EnergyIncr 1.0e-8 30 0
algorithm Newton
analysis Static
integrator LoadControl 0.01
analyze 100
loadConst -time 0.0



#Storey Displacement Recorders

recorder Node -file [format "$record-results/-displacements.dat"] -node [expr
4000+12*100+$noc+1] [expr 4000+11*100+$noc+1] [expr 4000+10*100+$noc+1] [expr
4000+9*100+$noc+1] [expr 4000+8*100+$noc+1] [expr 4000+7*100+$noc+1] [expr
4000+6*100+$noc+1] [expr 4000+5*100+$noc+1] [expr 4000+4*100+$noc+1] [expr
4000+3*100+$noc+1] [expr 4000+2*100+$noc+1] [expr 4000+1*100+$noc+1] -dof 1
disp

#Storey Drifts Recorders

recorder Drift -file [format "$record-results/-allstoreysdrift.dat"] -iNode
[expr 4000+12*100+$noc+1] [expr 4000+11*100+$noc+1] [expr 4000+10*100+$noc+1]
[expr 4000+9*100+$noc+1] [expr 4000+8*100+$noc+1] [expr 4000+7*100+$noc+1]
[expr 4000+6*100+$noc+1] [expr 4000+5*100+$noc+1] [expr 4000+4*100+$noc+1]
[expr 4000+3*100+$noc+1] [expr 4000+2*100+$noc+1] [expr 4000+1*100+$noc+1] -
jNode [expr 4000+11*100+$noc+1] [expr 4000+10*100+$noc+1] [expr
4000+9*100+$noc+1] [expr 4000+8*100+$noc+1] [expr 4000+7*100+$noc+1] [expr
4000+6*100+$noc+1] [expr 4000+5*100+$noc+1] [expr 4000+4*100+$noc+1] [expr
4000+3*100+$noc+1] [expr 4000+2*100+$noc+1] [expr 4000+1*100+$noc+1] [expr
4000+1*100+1] -dof 1 -perpDirn 2

#Braces Forces Recorders
recorder Element -file [format "$record-results/-storey12braces.dat"] -ele
[expr 12*200000+1] [expr 12*405000+1] globalForce
recorder Element -file [format "$record-results/-storey11braces.dat"] -ele
[expr 11*200000+1] [expr 11*405000+1] globalForce
recorder Element -file [format "$record-results/-storey10braces.dat"] -ele
[expr 10*200000+1] [expr 10*405000+1] globalForce
recorder Element -file [format "$record-results/-storey9braces.dat"] -ele
[expr 9*200000+1] [expr 9*405000+1] globalForce
recorder Element -file [format "$record-results/-storey8braces.dat"] -ele
[expr 8*200000+1] [expr 8*405000+1] globalForce
recorder Element -file [format "$record-results/-storey7braces.dat"] -ele
[expr 7*200000+1] [expr 7*405000+1] globalForce
recorder Element -file [format "$record-results/-storey6braces.dat"] -ele
[expr 6*200000+1] [expr 6*405000+1] globalForce
```

```
recorder Element -file [format "$record-results/-storey5braces.dat"] -ele
[expr 5*200000+1] [expr 5*405000+1] globalForce
recorder Element -file [format "$record-results/-storey4braces.dat"] -ele
[expr 4*200000+1] [expr 4*405000+1] globalForce
recorder Element -file [format "$record-results/-storey3braces.dat"] -ele
[expr 3*200000+1] [expr 3*405000+1] globalForce
recorder Element -file [format "$record-results/-storey2braces.dat"] -ele
[expr 2*200000+1] [expr 2*405000+1] globalForce
recorder Element -file [format "$record-results/-storey1braces.dat"] -ele
[expr 1*200000+1] [expr 1*405000+1] globalForce

#Columns Forces Recorders

recorder Element -file [format "$record-results/-storey12columns.dat"] -ele
[expr 2000+12*100+1] [expr 4000+12*100+1] [expr 6000+12*100+1] globalForce
recorder Element -file [format "$record-results/-storey11columns.dat"] -ele
[expr 2000+11*100+1] [expr 4000+11*100+1] [expr 6000+11*100+1] globalForce
recorder Element -file [format "$record-results/-storey10columns.dat"] -ele
[expr 2000+10*100+1] [expr 4000+10*100+1] [expr 6000+10*100+1] globalForce
recorder Element -file [format "$record-results/-storey9columns.dat"] -ele
[expr 2000+9*100+1] [expr 4000+9*100+1] [expr 6000+9*100+1] globalForce
recorder Element -file [format "$record-results/-storey8columns.dat"] -ele
[expr 2000+8*100+1] [expr 4000+8*100+1] [expr 6000+8*100+1] globalForce
recorder Element -file [format "$record-results/-storey7columns.dat"] -ele
[expr 2000+7*100+1] [expr 4000+7*100+1] [expr 6000+7*100+1] globalForce
recorder Element -file [format "$record-results/-storey6columns.dat"] -ele
[expr 2000+6*100+1] [expr 4000+6*100+1] [expr 6000+6*100+1] globalForce
recorder Element -file [format "$record-results/-storey5columns.dat"] -ele
[expr 2000+5*100+1] [expr 4000+5*100+1] [expr 6000+5*100+1] globalForce
recorder Element -file [format "$record-results/-storey4columns.dat"] -ele
[expr 2000+4*100+1] [expr 4000+4*100+1] [expr 6000+4*100+1] globalForce
recorder Element -file [format "$record-results/-storey3columns.dat"] -ele
[expr 2000+3*100+1] [expr 4000+3*100+1] [expr 6000+3*100+1] globalForce
recorder Element -file [format "$record-results/-storey2columns.dat"] -ele
[expr 2000+2*100+1] [expr 4000+2*100+1] [expr 6000+2*100+1] globalForce
recorder Element -file [format "$record-results/-storey1columns.dat"] -ele
[expr 2000+1*100+$noc] [expr 4000+1*100+$noc] [expr 6000+1*100+$noc]
globalForce
recorder Element -file [format "$record-results/-storey1leaningframe.dat"] -
ele 1 globalForce

timeSeries Path 1 -dt $step -filePath $record.tcl -factor [expr
$g*1.1*$scale];#1.1 factor to account for 10% accidental eccentricity
increment
pattern UniformExcitation 3 1 -accel 1
set dursism $duration
set tol 0.001
set maxNumIter 50
numberer    RCM
system UmfPack
constraints Plain
test EnergyIncr $tol $maxNumIter
algorithm   NewtonLineSearch        0.8
integrator  Newmark 0.5 0.25
analysis    Transient

        set dt0 [expr $step/ 2.0]
```

```
        set steps 50.;                                  # Number of steps to
divide $NTINCR
        puts "Progress 0%..."
        puts ""

        for {set i 1} {$i <= $steps} {incr i} {
            set ok 0
            set controlTime [getTime]
            while {$controlTime < [expr $i / $steps * $dursism] && $ok == 0}
{
                set controlTime [getTime]
                set ok [analyze 1 $dt0]
                if {$ok != 0} {
                    set dt1 [expr $dt0 / 2.]
                    puts ""
                    puts "Fail to converge @ $controlTime s, trying 2x
smaller time step $dt1 s"
                    puts ""
                    set ok [analyze 1 $dt1]
                    if {$ok == 0} {
                        puts "It converged! Back to a time step of $dt0 s"
                        puts ""
                    }
                }
                if {$ok != 0} {
                    set dt2 [expr $dt0 / 5.]
                    puts ""
                    puts "Fail to converge @ $controlTime s, trying 5x
smaller time step $dt2 s"
                    puts ""
                    set ok [analyze 1 $dt2]
                    if {$ok == 0} {
                        puts "It converged! Back to a time step of $dt0 s"
                        puts ""
                    }
                }
                if {$ok != 0} {
                    set dt3 [expr $dt0 / 10.]
                    puts ""
                    puts "Fail to converge @ $controlTime s, trying 10x
smaller time step $dt3 s"
                    puts ""
                    set ok [analyze 1 $dt3]
                    if {$ok == 0} {
                        puts "It converged! Back to a time step of $dt0 s"
                        puts ""
                    }
                }
                if {$ok != 0} {
                    set dt4 [expr $dt0 / 20.]
                    puts ""
                    puts "Fail to converge @ $controlTime s, trying 20x
smaller time step $dt4 s"
                    puts ""
                    set ok [analyze 1 $dt4]
                    if {$ok == 0} {
                        puts "It converged! Back to a time step of $dt0 s"
```

```
                    puts ""
                }
            }
            if {$ok != 0} {
                set dt5 [expr $dt0 / 50.]
                puts ""
                puts "Fail to converge @ $controlTime s, trying 50x
smaller time step $dt5 s"
                puts ""
                set ok [analyze 1 $dt5]
                if {$ok == 0} {
                    puts "It converged! Back to a time step of $dt0 s"
                    puts ""
                }
            }

#               for {set ii 1} {$ii <= 2} {incr ii 1} {
#                   set disp$ii [nodeDisp [expr $ii * 1000 + 101 +
$Column_nel] 1]
#               }
#               set Drift1 $disp1
#               set Drift2 [expr $disp2 - $disp1]

#               if {$peakDrift1 < abs($Drift1)} {set peakDrift1 [expr
abs($Drift1)]}
#               if {$peakDrift2 < abs($Drift2)} {set peakDrift2 [expr
abs($Drift2)]}
#           }

            if {$ok != 0} {
                set controlTime [getTime]
                puts "Analysis Stopped @ $controlTime s"
                puts "Record duration is $dursism s"
                puts ""
                puts "Dynamic analysis FAILED"
                puts ""
                return -1
            } else {
                puts "Progress [format %.0f [expr $i / $steps * 100]]%..."
                puts ""
            }
        }

        set controlTime [getTime]
        if {$controlTime >= $dursism } {
            puts ""
            puts "Dynamic analysis completed SUCCESSFULLY"
            puts ""
        }

        # Set time to zero and wipe analysis
        loadConst -time 0.0
        #wipeAnalysis

        puts " *-* *-* *-* *-* *-* *-* Dynamic Analysis is Done! *-* *-* *-*
*-* *-* *-* "
        puts ""
```

```
wipe all        set dt0 [expr $step/ 2.0]
        set steps 50.;                                  # Number of steps to
divide $NTINCR
        puts "Progress 0%..."
        puts ""

        for {set i 1} {$i <= $steps} {incr i} {
            set ok 0
            set controlTime [getTime]
            while {$controlTime < [expr $i / $steps * $dursism] && $ok == 0}
{
                set controlTime [getTime]
                set ok [analyze 1 $dt0]
                if {$ok != 0} {
                    set dt1 [expr $dt0 / 2.]
                    puts ""
                    puts "Fail to converge @ $controlTime s, trying 2x
smaller time step $dt1 s"
                    puts ""
                    set ok [analyze 1 $dt1]
                    if {$ok == 0} {
                        puts "It converged! Back to a time step of $dt0 s"
                        puts ""
                    }
                }
                if {$ok != 0} {
                    set dt2 [expr $dt0 / 5.]
                    puts ""
                    puts "Fail to converge @ $controlTime s, trying 5x
smaller time step $dt2 s"
                    puts ""
                    set ok [analyze 1 $dt2]
                    if {$ok == 0} {
                        puts "It converged! Back to a time step of $dt0 s"
                        puts ""
                    }
                }
                if {$ok != 0} {
                    set dt3 [expr $dt0 / 10.]
                    puts ""
                    puts "Fail to converge @ $controlTime s, trying 10x
smaller time step $dt3 s"
                    puts ""
                    set ok [analyze 1 $dt3]
                    if {$ok == 0} {
                        puts "It converged! Back to a time step of $dt0 s"
                        puts ""
                    }
                }
                if {$ok != 0} {
                    set dt4 [expr $dt0 / 20.]
                    puts ""
                    puts "Fail to converge @ $controlTime s, trying 20x
smaller time step $dt4 s"
                    puts ""
                    set ok [analyze 1 $dt4]
                    if {$ok == 0} {
```

```
                    puts "It converged! Back to a time step of $dt0 s"
                    puts ""
                }
            }
            if {$ok != 0} {
                set dt5 [expr $dt0 / 50.]
                puts ""
                puts "Fail to converge @ $controlTime s, trying 50x
smaller time step $dt5 s"
                puts ""
                set ok [analyze 1 $dt5]
                if {$ok == 0} {
                    puts "It converged! Back to a time step of $dt0 s"
                    puts ""
                }
            }



        if {$ok != 0} {
            set controlTime [getTime]
            puts "Analysis Stopped @ $controlTime s"
            puts "Record duration is $dursism s"
            puts ""
            puts "Dynamic analysis FAILED"
            puts ""
            return -1
        } else {
            puts "Progress [format %.0f [expr $i / $steps * 100]]%..."
            puts ""
        }
    }

    set controlTime [getTime]
    if {$controlTime >= $dursism } {
        puts ""
        puts "Dynamic analysis completed SUCCESSFULLY"
        puts ""
    }

    # Set time to zero and wipe analysis
    loadConst -time 0.0
    #wipeAnalysis

    puts " *-* *-* *-* *-* *-* *-* Dynamic Analysis is Done! *-* *-* *-*
*-* *-* *-* "
    puts ""
wipe all
```